SYNTHESIS OF CARVACROL DERIVATIVES AND THEIR POTENTIAL AS CARDIOPROTECTIVE AGENTS AGAINST DOXORUBICIN -INDUCED CARDIOTOXICITY

RINI RETNOSARI

UNIVERSITI KEBANGSAAN MALAYSIA

SYNTHESIS OF CARVACROL DERIVATIVES AND THEIR POTENTIAL AS CARDIOPROTECTIVE AGENTS AGAINST DOXORUBICIN-INDUCED CARDIOTOXICITY

RINI RETNOSARI

THESIS SUBMITTED IN FULFILMENT FOR THE DEGREE OF DOCTOR OF PHILOSOPHY

FACULTY SCIENCE AND TECHNOLOGY
UNIVERSITI KEBANGSAAN MALAYSIA
BANGI

2025

SINTESIS TERBITAN KARVAKROL DAN POTENSINYA SEBAGAI AGEN KARDIOPROTEKTIF TERHADAP KARDIOTOKSIK YANG DIARUH DOKSORUBISIN

RINI RETNOSARI

TESIS YANG DIKEMUKAKAN UNTUK MEMPEROLEH
IJAZAH DOKTOR FALSAFAH

FAKULTI SAINS DAN TEKNOLOGI
UNIVERSITI KEBANGSAAN MALAYSIA
BANGI
2025

DECLARATION

I hereby declare that the work in this thesis is my own except for quotations and summaries which have been duly acknowledged.

06 February 2025

RINI RETNOSARI
P116079

PERAKUAN TESIS SARJANA / DOKTOR FALSAFAH
(DECLARATION OF MASTER / DOCTOR OF PHILOSOPHY THESIS)

A. MAKLUMAT PELAJAR/*STUDENT DETAILS*

B. PERAKUAN / *DECLARATION*

	RAHSIA *CONFIDENTIAL*	Mengandungi maklumat yang berdarjah keselamatan sebagaimana yang termaktub di dalam AKTA RAHSIA RASMI 1972 *Consisting of classified information as specified by the OFFICIAL SECRETS ACT 1972*
	TERHAD *RESTRICTED*	Mengandungi maklumat TERHAD yang telah ditentukan oleh organisasi/ badan di mana penyelidikan dijalankan *Consisting of RESTRICTED information which has been determined by the organisation/body where the research was conducted*
√	AKSES TERBUKA/ TIDAK TERHAD *OPEN ACCESS/ NON-RESTRICTED*	Saya membenarkan tesis ini diterbitkan secara akses terbuka (boleh perpustakaan atau dibuat salinan untuk tujuan pengajian, pembelajaran & penyelidikan sahaja

Tandatangan Pelajar
Student's Signature

Tarikh: Disember 2025

ASSOC. PROF. DR. HALIPAH ALI
Department of Chemical Sciences
Faculty of Science and Technology
Universiti Kebangsaan Malaysia

C. PENGESAHAN FAKULTI/INSTITUT | *VERIFICATION OF FACULTY/INSTITUTE*

Tandatangan: *Signature*
Nama: *Name*
Tarikh: *Date*
Cop Rasmi: *Official Stamp*

PROF. MADYA DR. ABDUL MUNIR AB MURAD
Timbalan Dekan
Siswazah
Fakulti Sains dan Teknologi
Universiti Kebangsaan Malaysia

**Kuatkuasa 15 Julai 2021

ACKNOWLEDGEMENT

With profound sincerity, I express my heartfelt gratitude to my God, Allah Subhanahu wa ta'ala, for bestowing me the strength, ease, and sustenance needed to complete this work. Without Allah's boundless generosity, guidance, grace, and unwavering support, I am certain I could not have completed this PhD program.

With profound gratitude, I extend my heartfelt thanks to my tireless and dedicated supervisors, Assoc. Prof. Dr. Jalifah Latip (UKM), Prof. Natsuhisa Oka (GifuUniversity), Assoc. Prof. Dr. Satirah Zainalabidin (UKM), and Assoc. Prof. Dr. Azizah Ugusman (UKM). These academic giants have provided unwavering support and guidance throughout my journey. Their exceptional supervision and steadfast mentorship during my Doctoral studies have been invaluable, and I deeply appreciate their significant contributions to my success. Thank you all for your patience, wisdom, and encouragement, which have been instrumental in helping me achieve this milestone.

I would like to extend my heartfelt thanks to Prof. Kentaro Oh-hashi for his invaluable help and guidance during the cardioprotective evaluation of hybrid compounds at the Department of Chemistry and Biomolecular Sciences, Faculty of Engineering at Gifu University.

Additionally, I would like to express my profound gratitude to all the professors who educated and encouraged me during my coursework. I extend my heartfelt thanks to all the teachers, laboratory assistants, and staff members from the Department of Chemistry, Faculty of Science and Technology at UKM, and the Department of Chemistry and Biomolecular Sciences, Faculty of Engineering at Gifu University for their unwavering support throughout my Doctoral studies.

I gratefully acknowledge the financial support provided by Universitas Negeri Malang, and Gifu University, which allowed me to undertake a research attachment under the Joint Degree Program between UKM and Gifu University. Additionally, I extend my sincere thanks to Universiti Kebangsaan Malaysia for their generous funding (Grant no: DIP-2020-020).

I wish to express my profound appreciation to my husband, daughter, and family members for their unwavering support throughout my graduation period. Their encouragement and love have been a constant source of strength for me. Additionally, I extend my heartfelt thanks to my wonderful friends, including the Oka Lab members, the postgraduate students of UKM and Gifu University, Chemistry Department members in UM, for their steadfast encouragement and support throughout this journey. Your companionship and motivation have been invaluable to my success.

ABSTRAK

Kanser merupakan salah satu ancaman global yang membunuh ribuan manusia setiap tahun, dengan lebih 10 juta kematian direkodkan dalam tahun 2020. Walaupun rawatan kanser telah berkembang dari masa ke masa, pesakit yang menjalani kemoterapi berisiko terdedah kepada penyakit kardiovaskular disebabkan oleh kesan kardiotoksik beberapa ubatan, termasuk doksorubisin (DOX). Karvakrol (CA) dengan nama IUPAC 5-isopropil-2-metilfenol merupakan monoterpena fenolik terkenal dengan manfaat farmakologi, terutamanya sifat kardioprotektif. Pada masa yang sama, asid fenolik (PA) menunjukkan potensi melawan kardiotoksik yang diaruh DOX (DIC). Penyelidikan menyeluruh terhadap hibrid karvakrol asid fenolik (CPAH) yang dijalankan ini dijangka mampu menghasilkan sebatian yang berpotensi memerangi DIC secara efektif. Dua puluh satu CPAH (**1–21**) telah disintesis dengan peratusan hasil yang sederhana hingga tinggi melalui pengikatan kovalen yang mengikat perancah CA dan PA termasuk penghubung asil dan alkil. Struktur CPAH yang disintesis telah dicirikan menggunakan spektroskopi resonans magnet nuklear (NMR) dan spektrometri jisim beresolusi tinggi (HRMS). Selanjutnya, potensi kardioprotektif CPAH terhadap kematian sel H9c2 yang diaruh oleh DOX telah diterokai melalui ujian kebolehhidupan sel MTT. Kebolehidupan sel kardiomiosit berkurang secara signifikan dalam kehadiran DOX pada kepekatan 3 μM dan 10 μM. Hal yang berbeza bagi CPAH dan sebatian induknya; yang didapati tidak toksik terhadap kardiomiosit. Menariknya, pada dos 0.01 μg/mL, **1–6** didapati melindungi sel H9c2 daripada DIC, lebih baik daripada CA dan asid 3,4-dihidroksibenzoik; maka CPAH daripada hibrid CA dan asid hidroksibenzoik mempamerkan aktiviti kardioprotektif yang ketara. Aktiviti ini pada dasarnya memerlukan kehadiran kumpulan hidroksil pada moieti asid benzoik bagi PA; tetapi bilangan dan/atau kedudukan kumpulan hidroksil pada struktur PA tidak mempengaruhi potensi aktiviti secara signifikan. Sementara itu, CPAH yang diterbitkan daripada CA dan analog asid sinamik (**7–10**) mempamerkan bahawa hanya sebatian **8**, dengan kumpulan hidroksil pada kedudukan para, menunjukkan aktiviti kardioprotektif yang positif pada kepekatan 0.01 μg/mL terhadap kerosakan sel H9c2 yang diaruh DOX. Adalah ketara bahawa pengurangan kumpulan hidroksil, penggantian dengan kumpulan kloro, atau penambahan kumpulan hidroksil pada gelang sinamik terbukti mengurangkan aktiviti. Maka, kehadiran satu kumpulan hidroksil adalah penting bagi aktiviti pelindungan CPAH terhadap kematian sel yang diaruh DOX. Seterusnya, kesan jenis penghubung yang berbeza (**11–15**) dan kesan pengenalan kumpulan CH_2OH di kedudukan para pada CA (**16–21**) juga telah diterokai. Hasil penerokaan mendapati hanya **15** (10 μM), yang mengandungi penghubung eter empat karbon menunjukkan keberkesanan kardioprotektif optimum, berdasarkan peningkatan ketara peratus kebolehidupan sel berbanding kumpulan DOX ($p < 0.05$). Sebaliknya, **16–21** gagal mengurangkan kerosakan sel yang diaruh DOX berdasarkan ketoksikan yang ketara, yang dibuktikan melalui pengurangan kebolehidupan sel berbanding dengan kumpulan rawatan DOX. Hasil kajian ini mencadangkan kehadiran CA mewakili perancah farmakofor dengan hubungan aktiviti-struktur (SAR) yang paling optimum bagi aktiviti kardioprotektif. Kesimpulannya, sintesis CPAH telah memperkenalkan entiti kimia baharu dengan aktiviti kardioprotektif yang berpotensi terhadap DIC, dan berpotensi meningkatkan kualiti hidup untuk bekas pesakit kanser.

ABSTRACT

Cancer, a pervasive global threat, is killing millions of people each year, with over 10 million deaths in 2020. While cancer treatments have advanced over time, chemotherapy patients are at risk of developing cardiovascular disease due to the cardiotoxic effects of certain drugs, including doxorubicin (DOX). Carvacrol (CA) with an IUPAC name 5-isopropyl-2-methylphenol is a phenolic monoterpene known for its pharmacological benefits, particularly cardioprotective properties. Concurrently, phenolic acids (PA) have shown promising effects against DOX-induced cardiotoxicity (DIC). Thorough research on carvacrol phenolic acid hybrids (CPAH) in this present study is expected to supplement the potential drug candidates for combating the alarming DIC. Twenty-one CPAHs (**1–21**) were synthesized with moderate to high yield by covalently linking the scaffolds of CA and PA *via* acyl or alkyl linkers. The structures of CPAHs were characterized using nuclear magnetic resonance (NMR) spectroscopy and high-resolution mass spectrometry (HRMS). Subsequently, the CPAH's cardioprotective potential against DOX-induced H9c2 cell death was explored *via* MTT cell viability assay. The cardiomyocytes H9c2 cell viability was significantly reduced in the presence of 3 μM and 10 μM DOX. In contrast, the CPAHs and their parent compounds were non-toxic to cardiomyocytes. Interestingly, at 0.01 μg/mL, **1–6** protected H9c2 cells during DIC, better than CA and 3,4-dihydroxybenzoic acid; therefore, revealed that the CPAHs from the hybrids of CA and hydroxylated-benzoic acid demonstrated notable cardioprotective activity. The cardioprotective activity essentially necessitates the presence of a hydroxy group on the benzoic acid moiety of PA; however, the numbers and/or positions of substituted hydroxy groups on PA do not show any significant changes in its potency. Meanwhile, the CPAHs derived from CA and cinnamic acid analogs (**7–10**) revealed only **8**, with *p*-hydroxycinnamic acid moiety, demonstrated positive cardioprotective activity at 0.01 μg/mL concentration against DOX-induced H9c2 cell damages. It was notable that diminishing the hydroxy group, replacing the hydroxy group with a chloro group, or substituting an additional hydroxy group on the cinnamic ring were proven to decrease the activity. Therefore, the presence of only one hydroxy substituent is vital for the protective effect of CPAH against DOX-induced cell death. Furthermore, the effect of different types of linkers (**11–15**) and an introduction of CH_2OH group at the para position of CA (**16–21**) were explored. It is revealed that only **15** (10 μM), with an ether linkage containing four carbons possessed an optimal cardioprotective efficacy based on a notable increase in the percentage of viable cells compared to the DOX group ($p<0.05$). Conversely, **16–21**, failed to attenuate DOX-induced cell damage based on notable toxicity, as evidenced by the reduced cell viability compared to the DOX-treated group. This suggested that the presence of CA represented as the pharmacophore scaffold with the most optimal SAR for cardioprotective activity. In conclusion, the synthesis of CPAHs introduces new chemical entities with potential cardioprotection against DIC and potentially improves the quality of life for cancer survivors.

TABLE OF CONTENTS

LIST OF TABLES

LIST OF ILLUSTRATIONS

Schemes No. **Page**

LIST OF ABBREVIATIONS

AST	Aspartate aminotransferase
α-SMA	alpha-Smooth muscle actin
BAD	Bcl-2-associated death
CA	Carvacrol
CK	Creatine kinase
COX-2	Cyclooxygenase-2
CPAH	Carvacrol phenolic acid hybrid
CVD	Cardiovascular disease
DCC	*N*,*N*′-Dicyclohexylcarbodiimide
DCM	Dichloromethane
DIC	Doxorubicin-induced cardiotoxicity
DMAP	4-Dimethylaminopyridine
DMF	Dimethylformamide
DNA	Deoxyribonucleic acid
DNS	Daunosamine
DOX	Doxorubicin
EDC.HCl	1-Ethyl-3-(3-dimethylaminopropyl)carbodiimide hydrochloride
EMA	European medicines agency
FIC	Fractional inhibitory concentration
GPx	Glutathione peroxidase
GSH	Glutathione
HBA	Hydroxylated benzoic acids
HCA	Hydroxylated cinnamic acids
HDI	Human development index
HF-pyridine	Hydrogen fluoride-pyridine
HRMS	High-resolution mass spectrometry
IL-6	Interleukin-6

IL-10	Interleukin-10
iNOS	inducible Nitric oxide synthase
KI	Potassium iodide
KOH	Potassium hydroxide
K_2CO_3	Potassium carbonate
LDH	Lactate dehydrogenase
LMIC	Low- and Middle-Income Countries
LV	Left ventricular
MDA	Malondialdehyde
MIC	Minimum inhibitory concentration
MRSA	Methicillin-resistant *Staphylococcus aureus*
NADP	Nicotinamide adenine dinucleotide phosphate
NaOH	Sodium hydroxide
$NaHCO_3$	Sodium bicarbonate
NCDs	Non-communicable diseases
NF-κB	Nuclear factor kappa-light-chain-enhancer of activated B cells
NMR	Nuclear magnetic resonance
NO	Nitric oxide
NOS	Nitric oxide synthase
Nox	NADPH oxidase
Nrf2	Nuclear factor erythroid 2-related factor
PA	Phenolic acid
ROS	Reactive oxygen species
SAR	Structure-activity relationship
SOD	Superoxide dismutase
TBS	*tert*-butyldimethylsilyl
TBAF	Tetrabutylammonium fluoride
TEA	Triethylamine
THF	Tetrahydrofuran

TNF-α	Tumor necrosis factor-alpha
Top2	Topoisomerase II
Top IIβ	Topoisomerase II beta
USFDA	US food and drug administration
WHO	World health organization
3HA	3-Hydroxybenzoic acid
3,4-HB	3,4-Dihydroxybenzoic acid

CHAPTER I

INTRODUCTION

1.1 RESEARCH BACKGROUND

Cancer is a leading global cause of mortality, with 19.3 million new cases and 10 million deaths in 2020, projected to rise to 28.4 million cases by 2040—a 47% increase (Sung et al. 2021). Malaysia mirrors this trend, driven by urbanization and lifestyle changes, increasing non-communicable diseases (NCDs), including cancer (Department of Statistics Malaysia 2023). Between 2007–2011, 103 507 cancer cases were recorded, increasing to 48 639 in 2020 (Azizah et al. 2015; WHO 2022). Cancer remains Malaysia's second leading cause of premature death, highlighting its growing health burden.

Advances in surgery, chemotherapy, radiotherapy, and immunotherapy have significantly improved cancer survival rates. Chemotherapy, particularly doxorubicin (DOX), effectively targets tumors by disrupting their metabolic and mitotic processes (Sawicki et al. 2021). However, antitumor therapies, including DOX, often harm sensitive tissues, with DOX-induced cardiotoxicity (DIC) being a major concern (Huang et al. 2022; Meng et al. 2024). DOX damages the heart through mechanisms such as topoisomerase inhibition, oxidative stress, inflammation, and calcium overload, leading to heart failure and irreversible damage (Abdelgawad et al. 2021; Pecoraro et al. 2016; Wenningmann et al. 2019; Zhao et al. 2018). Acute cardiotoxicity, occurring in 11% of cases within days of treatment, contrasts with the rarer chronic effects (1.7%), which may emerge years later (Chatterjee et al. 2010). Despite extensive studies on chronic toxicity, acute cardiotoxicity remains underexplored, demanding urgent mitigation efforts (Dulf et al. 2023).

Reducing the risk of DIC in cancer patients through current clinical approaches can be achieved by lowering the dosage of DOX. However, this approach fails to achieve the desired clinical efficacy and significantly reduces the effectiveness of the DOX (Oliveira et al. 2014). Additionally, using cardioprotective agents such as dexrazoxane, glutathione, coenzyme Q10, leucovorin, antioxidants, and iron chelators has highly controversial safety and efficacy. As a result, no practical measures are currently available to prevent DIC, making the prevention of cardiotoxicity a focus and challenge of research in recent years (van Dalen et al. 2011).

Exploring and developing new drug candidates with potent pharmacological efficacy is crucial to addressing DIC effectively. There is a rising scientific interest in researching the possible cardioprotective properties of natural substances against DIC. Carvacrol (CA), is a phenolic monoterpene found in the essential oils of various aromatic plants in the Lamiaceae family. Its pharmacological prowess spans a spectrum, boasting anticancer, antidiabetic properties, hepatoprotective, and antioxidant effects (Ali et al. 2024). CA's potential in combating cardiovascular disease (CVD) is particularly intriguing. It has garnered widespread acclaim for its influence on various facets of cardiovascular health. By targeting oxidative stress, inflammation, and cell death processes, CA demonstrates promise in mitigating the development and progression of CVD (Imran et al. 2022). Despite CA's potential, challenges abound. Its low water solubility requires high doses for therapeutic plasma concentrations, as Marinelli et al. (2019) highlighted, limiting its clinical utility. Furthermore, Jamhiri et al. (2019) observed a decrease in the heart rate of normal animals treated with CA, and El-Sayed et al. (2016) proposed that combining CA with its isomer, thymol could enhance its cardioprotective effects, indicating room for improvement.

To address these limitations, the potential of hybridizing CA with phenolic acid (PA) to enhance CA's cardioprotective activity was investigated. Diets rich in natural phenolic acids have been linked to reduced risk of oxidative stress-related diseases, including cancer, diabetes, and CVD (Kumar & Goel 2019). Therefore, the phenolic hydroxy group of CA was selected as a critical modification to find the best way to introduce PA into the CA structure. Consequently, twenty-one carvacrol-

phenolic acid hybrids (CPAH) (**1–21**) were synthesized, combining the therapeutic capabilities of both molecules to provide superior cardioprotection. Furthermore, the efficacy of these CPAHs in mitigating DIC in H9c2 cells *in vitro* has been investigated to establish a structure-activity relationship (SAR) and better understand their therapeutic potential. These findings could inform the development of CPAHs as adjunct therapies to counteract the progression of heart failure induced by DOX.

1.2 PROBLEM STATEMENT

According to the World Health Organization (WHO), cancer was responsible for around 10 million fatalities worldwide in 2022, accounting for nearly one in every six deaths. In the same year, Malaysia reported 51 650 new cancer cases and the numbers are expected to double by 2040. Cancer treatments have evolved dramatically over the years, resulting in a better likelihood of recovery for cancer patients. However, the long-term use of anticancer drugs causes side effects and risks to the patients. For example, some medications may raise the risk of CVD (Adhikari et al. 2021). DOX is one such medicine that is particularly successful in treating solid tumors. Nonetheless, it can result in cardiotoxicity, a potentially fatal condition that causes heart failure. Scientists have studied a variety of pharmacological drugs and natural products to reduce DIC. However, dexrazoxane is currently the only cardioprotective agent approved by the US Food and Drug Administration (USFDA) and the European Medicines Agency (EMA) (Bansal et al. 2019; Kong et al. 2022). As a result, there is an urgent need for the development of effective medicines to reduce the risk of CVD in cancer patients undergoing chemotherapy.

Previous studies have shown that CA and PA are cardioprotective (Abdul Ghani et al. 2023; Liu et al. 2022). Jafarinezhad et al. (2019) demonstrated that oral administration of 50 mg/kg CA over six weeks mitigated DOX-induced cardiac damage in rats. Similarly, El-Sayed et al. (2016) reported that 25 mg/kg CA administered for 14 days reduced DOX cardiotoxicity by alleviating oxidative stress, inflammation, and apoptosis. However, CA's clinical utility is hindered by poor water solubility and low bioavailability, necessitating large doses. Furthermore, CA reduces heart rate in normal animals, highlighting the need for further modifications to

enhance its effectiveness. Chemical modifications, such as the development of CPAHs, have been explored to address these limitations. These hybrids aim to provide superior cardioprotection by combining the therapeutic capabilities of both molecules. This study focuses on synthesizing CPAHs and investigating their efficacy in mitigating DIC in H9c2 cells *in vitro*, followed by establishing a SAR.

1.3 OBJECTIVES OF RESEARCH

This study embarks on the following objectives:

1. To synthesize CA derivatives by hybridizing CA with various phenolic acids.
2. To evaluate the *in vitro* cardioprotective effect of CA derivatives on DIC in cardiomyocytes.
3. To establish the SAR of CA derivatives as the cardioprotective agent based on *in vitro* experimental data.

1.4 SCOPE OF WORKS

CPAHs (**1–10**) were synthesized in a two-step reaction. First, CA reacted with chloroacetyl chloride in the presence of triethylamine (TEA) and dichloromethane (DCM) *via* esterification to form an intermediate. In the second step, the intermediate underwent nucleophilic substitution with hydroxylated benzoic or cinnamic acids, using TEA and potassium iodide (KI) as promoters, yielding the final compounds. Compound **12** was synthesized similarly, with chloroacetyl chloride replaced by 4-chlorobutyril chloride. A distinct method was applied for the synthesis of compound **11**, where the intermediate served as a nucleophilic source in a condensation reaction with 3-hydroxybenzoic acid (3HA), employing 1-ethyl-3-(3-dimethylaminopropyl)carbodiimide hydrochloride (EDC.HCl) and 4-dimethylaminopyridine (DMAP) as coupling agents. The synthesis of compounds **13–15** involved nucleophilic substitution reaction between CA and appropriate alkyl dihalide linker in the presence of potassium hydroxide (KOH), followed by hybridization with 3HA in the presence of sodium bicarbonate ($NaHCO_3$). Compounds **16–21** were synthesized using a method similar to that employed for compounds **1** and **11–15**, with 4-hydroxycarvacrol serving as the starting material in place of CA. A final step involved *tert*-butyldimethylsilyl (TBS) group removal using

tetrabutylammonium fluoride (TBAF) or hydrogen fluoride-pyridine (HF-pyridine). All the products were purified by silica gel column chromatography using hexane and ethyl acetate as eluents, and their structures were confirmed by nuclear magnetic resonance (NMR) spectroscopy and high-resolution mass spectrometry (HRMS). All synthesized compounds were evaluated for their ability to alleviate DIC in H9c2 cells *in vitro*. The protective activity of their parent compounds (CA, 3,4-hydroxybenzoic acid, 3-hydroxybenzoic acid) was also investigated for comparison. The H9c2 cell line (passages 4–6), cultured in Dulbecco's modified eagle medium (DMEM) with 10% fetal bovine serum (FBS) and 1% penicillin, was used for the assays. In Stage 1, cells were treated with tested compounds for 48 hours to assess their cytotoxicity on H9c2 cells. In Stage 2, cells were pre-treated with non-toxic compounds for 24 hours, followed by co-treatment with DOX for 24 hours to evaluate their cardioprotective activity. With successful synthesis and *in vitro* cardioprotective evaluation of compounds **1–21** and their parent compounds, SAR analysis was conducted to identify structural features—such as functional groups and chain lengths—that influence biological activity. This analysis establishes a correlation between structural modifications and efficacy.

CHAPTER II

LITERATURE REVIEW

2.1 CANCER INCIDENCE WORLDWIDE AND IN MALAYSIA

Cancer is a multifaceted disease characterized by genomic and molecular changes that result in uncontrolled cell growth and proliferation, leading to rapid increases in tissue mass in affected areas. Under normal conditions, cells undergo programmed death, allowing new, healthy cells to be replaced. However, cancer cells bypass these signals, consuming the body's oxygen and nutrients, and depriving other cells of essential resources. They manipulate their microenvironment, evade the immune system, and exploit the physiology of nearby cells to support their growth and survival. This uncontrolled proliferation produces aggressive malignancies, leading to millions of deaths annually (Anand et al. 2023).

Cancer is a major challenge in the 21st century, causing nearly one in six deaths globally and one in four deaths from NCDs. It also accounts for three in ten premature deaths from NCDs worldwide (Bray et al. 2021). In 2022, approximately 20 million new cancer cases were reported globally, resulting in 9.7 million deaths. Lung cancer emerged as the most frequently diagnosed cancer, with nearly 2.5 million new cases, representing 12.4% of all global cases. Following lung cancer, the most common diagnoses were breast cancer in females (11.6%), colorectal cancer (9.6%), prostate cancer (7.3%), and stomach cancer (4.9%). Demographic forecasts predict that the annual incidence of new cancer cases will rise to 35 million by 2050, marking a 77% increase from the 2022 levels (Bray et al. 2024; Ferlay et al. 2024).

Currently, two-thirds of all cancer deaths occur in countries undergoing societal, economic, and lifestyle changes due to globalization and rising disposable incomes. Nearly half of all cancer cases and most cancer-related deaths are anticipated to occur in Asia, which accounts for 59.2% of the global population. As low- and middle-income countries (LMICs) in Asia continue to experience improvements in their Human Development Index (HDI) levels, cancer is expected to become an increasingly significant medical and public health concern (Rajappa et al. 2023).

In Malaysia, an LMIC with a population of 33.2 million, approximately 0.469% of the population has been diagnosed with or cured of cancer. In 2022, there were 51 650 new cancer cases and 31 633 deaths recorded. Breast cancer was the most prevalent, accounting for 16.2% of cases, followed by colorectal cancer (13.8%) and lung cancer (10.7%) (WHO 2022). Cancer incidence is projected to double by 2040. A significant factor contributing to the rise in cancer cases in Malaysia is the changing lifestyle. Malaysians are increasingly adopting behaviors associated with Western lifestyles, which are linked to a higher cancer risk. These behaviors include high consumption of saturated fatty acids, sugar, sweetened condensed milk, and local sweets, resulting in over 50% of Malaysians being overweight or obese. Furthermore, over 40% of Malaysian men were smokers, and their unhealthy dietary habits also contribute to the risk factors for cancer (Schliemann et al. 2020). The intersection of these demographic shifts with lifestyle changes will likely intensify the burden of cancer in the region, necessitating comprehensive health strategies to address this growing challenge.

2.2 CHEMOTHERAPY IN CANCER TREATMENT

Recent progress in medical treatments has enhanced survival rates for children and adults with cancer, due to the efficacy of therapies such as chemotherapy, radiation therapy, gene therapy, and immunotherapy. Among these options, chemotherapy is particularly effective, especially for cancers that have metastasized. This treatment utilizes powerful drugs or molecules specifically designed to target and destroy cancer cells, offering a crucial strategy in managing and combating advanced stages of the disease (Behranvand et al. 2022). Chemotherapy is often combined with radiation

therapy and surgery to enhance cancer treatment outcomes. Neoadjuvant chemotherapy, administered before surgery or radiation, aims to shrink the tumor, making subsequent treatments more effective and less invasive. Conversely, adjuvant chemotherapy, given after surgery or radiation, targets any remaining cancerous cells, reducing the risk of recurrence and improving long-term survival rates (Malik et al. 2021).

The metabolic processes of cancer cells often overlap with those of the host cells, making cancer treatment particularly challenging. The primary goal in designing drugs or therapeutics is to achieve selectivity, targeting and killing cancerous cells while sparing healthy ones (Kalyanaraman 2017). According to the latest review by (Anand et al. 2023), approximately 50 anticancer drugs are currently in use for cancer treatment. A significant category of these drugs comprises alkylating agents, which disrupt the formation and linkage of deoxyribonucleic acid (DNA) double strands (Kondo et al. 2010). As primary chemotherapeutic agents for various cancer types, alkylating drugs function by attaching an alkyl group to the guanine base in DNA. This leads to the cross-linking of nucleic acids with proteins or peptides, altering DNA geometry and causing incorrect base pairing and DNA strand breakage. Ultimately, this process halts cell division and induces irreversible cell senescence (Qin & Wang 2009).

Anthracyclines are considered some of the most effective chemotherapeutic agents for treating cancer. Anthracyclines are a class of natural antibiotics and among the most potent antineoplastic agents, with minimal resistance from most cancer types. The pioneering compounds, daunorubicin and DOX, were isolated from a mutant strain of *Streptomyces peucetius*. Daunorubicin was discovered in 1964, followed by DOX in 1969, originally named “daunomycin” and “Adriamycin”. These glycoside drugs consist of the amino sugar daunosamine (DNS) attached to a hydroxyanthraquinone aglycone, as shown in Figure 2.1 (Martins-Teixeira & Carvalho 2020). DOX is one of the most frequently utilized and effective chemotherapeutic agents. Compared to daunorubicin, DOX demonstrates a wider range of anti-cancer properties, particularly in the treatment of solid tumors (van der Zanden et al. 2021).

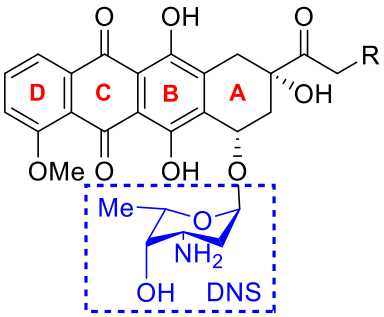

Figure 2.1 The initial generation of anthracyclines: daunorubicin (R = H) and doxorubicin (R = OH)

Anthracyclines act as potent anticancer agents through multiple mechanisms, including the induction of oxidative stress, intercalation into DNA, and, most critically, the inhibition of the topoisomerase II enzyme (Top2) (Marinello et al. 2018; Minotti et al. 2004). They generate reactive oxygen species (ROS) by undergoing one-electron reductions, transforming chelated ferric ions into ferrous ions or quinones into semiquinones. These intermediates then react with oxygen to produce superoxide anions, which are subsequently neutralized by superoxide dismutase into less harmful hydrogen peroxide. This process initiates redox cycles that generate highly reactive hydroxy radicals, causing protein alkylation, lipid peroxidation, and direct DNA damage. These molecular events trigger cellular cascades culminating in cell death (Angsutararux et al. 2015; Stěrba et al. 2013).

The polyaromatic planar structure of anthracyclines, specifically their aglycone component, allows these compounds to intercalate into DNA. Rings B and C of the anthraquinone segment slide between neighboring base pairs, causing separation and resulting in bidirectional positive torsion of the DNA double helix. Ring D situates itself in the major groove, while ring A and the daunosamine sugar moiety extend into the minor groove. This complex interaction disrupts the DNA structure, affecting its stability and function (Howerton et al. 2003; Martins-Teixeira & Carvalho 2020).

Topoisomerase II, a critical nuclear enzyme, alleviates DNA supercoiling tension during replication and transcription by creating temporary breaks in both DNA strands, passing an intact helix through the gap, and resealing the strands. Anthracyclines stabilize the cleavable complex formed between Top2 and DNA, trapping the covalent intermediate within a ternary drug-DNA-enzyme complex. This

inhibition prevents topoisomerase from repairing the broken phosphodiester bonds effectively. Consequently, anthracyclines disrupt the enzyme's normal functions, converting topoisomerase into a DNA-breaking nuclease, which leads to genomic instability and triggers apoptotic cell death (Hanušová et al. 2011; Li & Liu 2001; Nitiss 2009).

While anthracycline treatments are highly effective, they have significant limitations. In addition, the success of advanced cancer therapies depends on the accessibility of cancer drugs. Unfortunately, unequal distribution of these medications is a global issue, particularly challenging in LMICs in Asia, including Malaysia. Various factors, such as high costs and lengthy approval processes for government formularies, contribute to the lack of access. These issues make innovative cancer treatments cost-ineffective, restricting patient access to essential drugs. Despite these challenges, the use of anthracyclines remains prevalent (Tan et al. 2023).

2.3 THE SIDE EFFECT OF DOXORUBICIN: CARDIOTOXICITY

Despite DOX's pivotal role in cancer therapy for nearly fifty years, its use is significantly constrained by severe and limiting side effects. Chief among these is cardiotoxicity, which has consequently become the most extensively studied adverse effect of DOX. DIC can manifest as ventricular dysfunction, cardiomyopathy, arrhythmias, or pericarditis-myocarditis syndrome. This condition is dose-dependent and irreversible, presenting a significant challenge in the management of patients undergoing treatment with this potent chemotherapeutic agent (Jones et al. 2006). Swain et al. (2003) established that the cumulative dose of DOX should be limited to 400–450 mg/m² to mitigate the risk of dose-dependent cardiotoxicity. Furthermore, research by Leger et al. (2015) revealed that even lower doses of DOX (≤100 mg/m²) administered to childhood cancer survivors can cause abnormalities in the left ventricular structure of the cardiovascular system.

DIC can manifest in acute, subacute, or chronic forms, each with distinct clinical features and timelines. Acute cardiotoxicity typically appears within 2-3 days post-administration, with an incidence rate of approximately 11%. Histopathological examination of acute cardiac injury caused by DOX often reveals cytoplasmic

vacuolation, sparsity, and disruption of myofibrils (Kong et al. 2022). These acute changes can set the stage for more prolonged cardiac issues if not promptly addressed. Chronic cardiotoxicity, though less common, occurs in about 1.7% of cases. This form of cardiotoxicity generally manifests within 30 days of the final DOX dose but can also present itself 6–10 years later. The likelihood of developing DIC is significantly dose-dependent. It occurs in approximately 4% of patients receiving 500–550 mg/m², and 18% receiving 551–600 mg/m². It escalates to 36% in patients whose doses exceed 600 mg/m² (Chatterjee et al. 2010). Despite extensive research into chronic DOX toxicity, the manifestations and mechanisms of acute cardiotoxicity remain comparatively underexplored. Dulf et al. (2023) emphasized the need for further investigation into acute cardiotoxic effects, as understanding these early manifestations could lead to improved prevention and treatment strategies.

The exact mechanism underlying DIC remains controversial, as clinical and experimental data often diverge. Multiple pathways and factors contribute to the development of this cardiotoxicity (Mobaraki et al. 2017). Songbo et al. (2019) highlighted that oxidative stress and an imbalance in redox reactions are pivotal factors in DIC. The accumulation of DOX in the body can result in cellular iron overload, promoting the Fenton reaction, which generates substantial amounts of ROS. These ROS can inflict damage on lipids, nucleic acids, and enzymes within cardiomyocytes. Moreover, DOX's interaction with nitric oxide synthase (NOS) and NADPH oxidase (Nox) diminishes the activity of critical antioxidant enzymes, such as peroxidase, superoxide dismutase (SOD), and catalase, while concurrently increasing peroxide levels. On the other hand, DOX also induces inflammation and apoptosis (Alkreathy et al. 2012; Bagchi et al. 2021; Chen et al. 2007) and forms complexes with DNA and topoisomerase II, leading to substantial DNA damage (Sheibani et al. 2022).

2.4 RECENT ADVANCES IN MITIGATING DIC

Currently, dexrazoxane stands as the only FDA-approved cardioprotective drug proven to prevent DIC effectively. By binding to iron, dexrazoxane neutralizes the pro-oxidants generated by DOX, which are major contributors to oxidative stress and

mitochondrial dysfunction. This iron-chelation mechanism significantly reduces the cardiotoxic side effects associated with DOX therapy (Sangweni et al. 2022). Dexrazoxane modifies topoisomerase II beta (Top IIβ), preventing DOX from causing DNA damage and apoptosis. Its extensive cardioprotective effects benefit both adult and pediatric cancer patients (Lipshultz et al. 2010; Wenningmann et al. 2019). Dexrazoxane effectively protects heart function, improving left ventricular (LV) ejection fraction in advanced breast cancer patients and long-term heart health in pediatric cancer patients, including LV fractional shortening and wall thickness (Lipshultz et al. 2013; Marty et al. 2006).

The use of dexrazoxane is restricted due to controversy. It is FDA-approved solely for women with metastatic breast cancer requiring further DOX after receiving a minimum of 300 mg/m² of chemotherapy (Vejpongsa & Yeh 2014). Moreover, clinical trials in adult cancer patients indicated a higher risk of secondary malignant neoplasms with dexrazoxane use (Shaikh et al. 2015). Additional limitations of dexrazoxane include claims of providing greater cardioprotection to females than males and its high costs, which restrict its use in poorer communities (Friedman et al. 2010). These factors strongly advocate for the investigation of alternative therapies.

Various pharmaceutical agents have been investigated for treating DIC, including cilostazol, which improves symptoms through anti-inflammatory, antifibrotic, and antioxidative effects (Koh et al. 2015); fidarestat, which reduces inflammation and serum troponin I (Sonowal et al. 2017); rosuvastatin, known for its anti-inflammatory effects (Dong-Hyuk et al. 2020); and thiamine, which minimizes DIC through antioxidative and anti-apoptotic properties (Rankovic et al. 2021). However, the relevance of these findings is limited by the use of non-cancer rat models, which may not accurately reflect the effects in cancer-bearing rats receiving DOX treatment (Kabir et al. 2022). The chemical structure of these pharmaceuticals can be found in Figure 2.2.

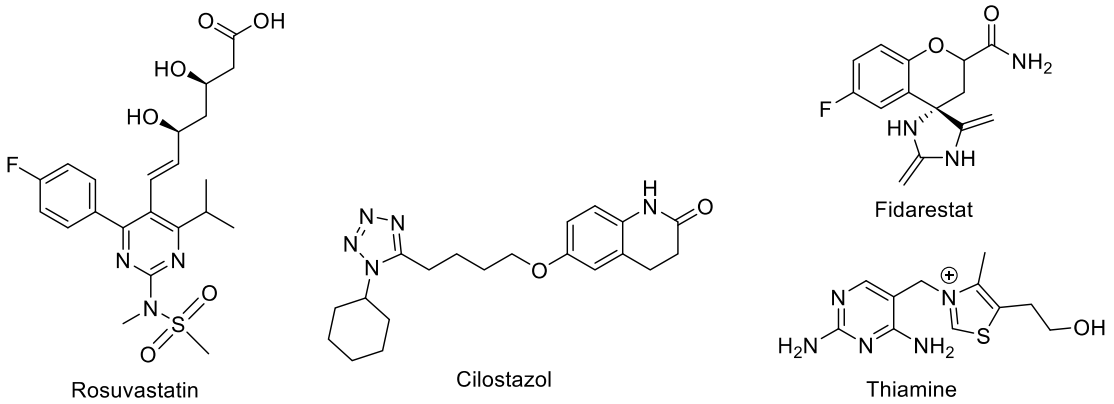

Figure 2.2 The structural features of pharmaceuticals with cardioprotective activity against DIC

Researchers continue to investigate phytochemicals to prevent and treat DIC due to their availability in natural foods. Numerous studies have explored natural compounds that can mitigate DOX's side effects on the heart. These compounds have shown potential to counteract the toxic effects of DOX through their antioxidant, antiapoptotic, and anti-inflammatory properties (Rai et al. 2016). Phytochemical compounds can alleviate oxidative stress by reducing ROS production, improving DOX-induced lipid peroxidation, and enhancing cellular antioxidant mechanisms. This is achieved by increasing the concentrations of nicotinamide adenine dinucleotide phosphate (NADP) and glutathione (GSH), boosting the activity of catalase, SOD, and glutathione reductase enzymes, and upregulating the expression of Nrf2. Moreover, phytochemicals exhibit anti-inflammatory activities by reducing the synthesis of proinflammatory mediators. They achieve this by inhibiting lipo-oxygenase and cyclooxygenase-II enzymes, downregulating tumor necrosis factor-alpha (TNF-α) expression, and decreasing neutrophil adhesion molecules on vascular endothelium (Abushouk et al. 2017). Additionally, the antiapoptotic mechanisms of phytochemicals as cardioprotectors include the attenuation of jun N-terminal kinase phosphorylation (Chang et al. 2011), inhibition of poly-ADP-ribose, caspases (-3, -7, -9) (Choi et al. 2008), extracellular signal-regulated kinases, and DOX-induced overexpression of p53 (Psotová et al. 2005).

2.5 CARDIOPROTECTIVE ACTIVITY OF PHENOLIC ACIDS

PAs, a subgroup of secondary plant metabolites within the polyphenol family, are extensively found in a diverse range of plant sources, including vegetables, fruits,

spices, grains, and beverages. Generally, "PAs" refer to phenolic compounds with a single carboxylic acid group. They are categorized into hydroxylated benzoic acids (HBA) and hydroxylated cinnamic acids (HCA)based on their unique carbon frameworks and the specific positioning and number of hydroxygroups on the aromatic ring (Białecka-Florjańczyk et al. 2018; Stuper-Szablewska & Perkowski 2019).

HBAs are benzoic acid derivatives with a seven-carbon C6-C1 framework. The main HBAs include 3-hydroxybenzoic acid (3HA), 4-hydroxybenzoic acid, salicylic acid, gallic acid, protocatechuic acid (3,4-dihydroxybenzoic acid), gentisic acid, vanillic acid, and syringic acid, which differ from each other based on modifications to the aromatic ring, as shown in Figure 2.3. HCAs are derivatives of cinnamic acid, characterized by a C6-C3 structure. The most common HCAs and their derivatives include cinnamic acid, *p*-coumaric acid, caffeic acid, sinapic acid, and ferulic acid as shown in Figure 2.4 (Rashmi & Negi 2020).

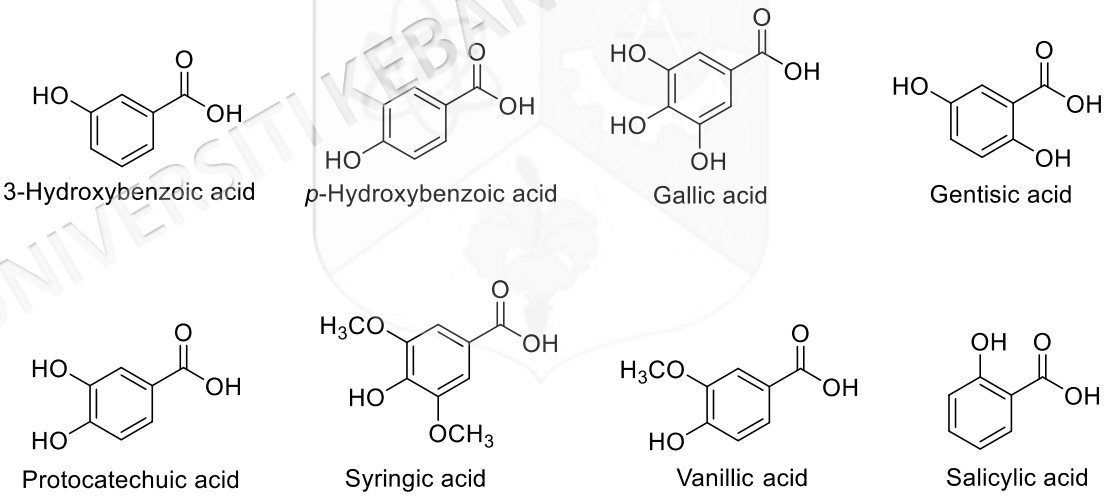

Figure 2.3 Structures of HBA derivatives

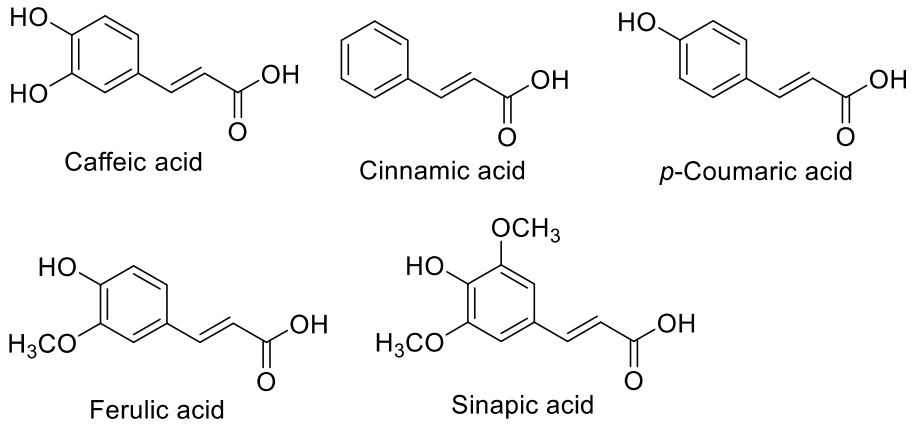

Figure 2.4 Structures of HCA derivatives

PAs exhibit a wide range of biological activities, significantly contributing to overall health improvement. Both HBA and HCA are particularly beneficial due to their antioxidant, anti-inflammatory, antimicrobial, anti-mutagenic, hypoglycaemic, and anti-platelet aggregating properties (Saxena et al. 2012). Diets rich in natural phenolic acids have been linked to a reduced risk of oxidative stress-related diseases, including diabetes, cancer, and CVD (Kumar and Goel 2019). Previous research has underscored the cardioprotective potential of phenolic acids, highlighting their anti-inflammatory, antioxidant, and anti-apoptotic properties (Liu et al. 2022).

In a literature review, gallic acid demonstrated cardioprotective activities in isoproterenol (ISO)-induced myocardial infarction (heart attack) as reported by Priscilla and Prince (2009). Yan et al. (2019) found that gallic acid also promotes autophagy to treat myocardial dysfunction and hypertrophy. Additionally, Vijaya Padma et al. (2013) highlighted that gallic acid alleviated lindane-induced myocardial damage through its antioxidant activity. Similarly, protocatechuic acid has been shown to prevent myocardial ischemia/reperfusion injury (Tang et al. 2014) and exhibit cardioprotective properties in type 1 diabetic rats (Semaming et al. 2014). Moreover, research by Koczurkiewicz-Adamczyk et al. (2021) indicated that derivatives of cinnamic acid also possess cardioprotective.

Furthermore, recent evidence highlights the significant potential of certain PAs in preventing DIC. Notably, gallic acid can substantially mitigate this cardiotoxicity in rats by enhancing the activities of key antioxidants such as GSH, SOD, catalase, and

glutathione peroxidase (GPx). Simultaneously, it lowers malondialdehyde (MDA) levels and reduces the expression of pro-inflammatory markers, TNF-α and cyclooxygenase-2 (COX-2). These combined effects underscore gallic acid's protective role against oxidative stress and inflammatory responses (Ekinci Akdemir et al. 2021; Omóbòwálé et al. 2018). Additionally, Ahmed et al. (2021) found that methyl gallate, an ester derivative of gallic acid, protects against DOX-induced cardiac injury by reducing levels of creatine kinase (CK), aspartate aminotransferase (AST), lactate dehydrogenase (LDH), and MDA while increasing GSH levels in rat serum.

Sinapic acid, a derivative of cinnamic acid with 3,5-dimethoxy and 4-hydroxy substitutions, effectively counteracts DIC. An *in vivo* study showed that sinapic acid significantly lowers serum CK-MB and LDH levels in rats treated with DOX. Additionally, it reduces the expression of Bax, Caspase-3, and NF-κB, while increasing Bcl-2 activity, suggesting it protects against oxidative stress, inflammation, and apoptosis (Bin Jardan et al. 2020). Additionally, recent research highlights the potent protective effects of *p*-coumaric acid against DIC. It ameliorates biochemical abnormalities by enhancing SOD, CAT, and GSH activities while reducing MDA and LDH levels in treated rats. Furthermore, *p*-coumaric acid improves mitochondrial membrane potential and intracellular calcium levels. It plays a crucial role in regulating oxidative stress, apoptosis, and autophagy, further solidifying its cardioprotective properties (Chacko et al. 2015; Shiromwar and Chidrawar 2011; Sunitha et al. 2018). Moreover, ferulic acid (4-hydroxy-3-methoxycinnamic acid), another cinnamic acid derivative, exhibits cardioprotective effects against DIC by attenuating oxidative stress and maintaining calcium homeostasis (Aswar et al. 2019). Collectively, these studies underscore the significant therapeutic potential of PAs in preventing DIC.

2.6 CARDIOPROTECTIVE ACTIVITY OF CARVACROL

Among aromatic monoterpenoids, CA has gained significant attention from researchers in organic synthesis and medicinal chemistry as a building block for developing new drugs. CA is naturally found in various plants such as *Origanum*

vulgare, *Origanum onites*, *Thymus vulgaris*, *Stellera chamaejasme*, *Carum copticum* L., and *Zataria multiflora* (Fachini-Queiroz et al. 2012; Hao et al. 2021). Additionally, CA can be synthesized chemically through the alkylation of o-cresol with isopropyl alcohol (Yadav and Kamble 2019).

The popularity of CA is based on its wide range of biological activities, including antiacetylcholinesterase (AChE) properties (Jukic et al. 2007), antioxidant activity (Llana-Ruiz-Cabello et al. 2015), anticancer effects (Günes-Bayir et al. 2017; Heidarian and Keloushadi 2019), antinociceptive properties (Guimarães et al. 2010), anxiolytic-like effects (Melo et al. 2010), antidepressant-like activity (Melo et al. 2011), anti-inflammatory effects (Li et al. 2016), antibacterial activity (De Souza et al. 2021), and antiviral activity (Pilau et al. 2011). Moreover, CA has been recommended for treating osteoarthritis (Xiao et al. 2018), human cystic echinococcosis (Fabbri et al. 2016), and diabetes mellitus (Cicalău et al. 2021).

CA's potential in combating CVD is particularly compelling. It has received widespread recognition for its beneficial effects on various aspects of cardiovascular health, such as improving lipid profiles, enhancing cardiac function, lowering blood pressure, and preventing myocardial infarction and ischemic reperfusion injury. By targeting mechanisms such as oxidative stress, inflammation, and cell death, CA shows significant promise in mitigating the onset and progression of CVD. Despite these promising findings, there have been no clinical trials conducted to assess CA's potential in reducing CVD risk. CVDs continue to be the leading cause of death worldwide, responsible for approximately 17.8 million deaths, with this number projected to rise to around 20.5 million by 2021 (Khazdair et al. 2024).

Recently, researchers have shown a strong interest in investigating the potential of CA in alleviating DIC. Studies by El-Sayed et al. (2016) and Khajavi Rad and Mohebbati (2019) reported significant improvements in cardiac function and oxidative stress parameters in rats pretreated with CA before receiving a single dose of DOX. These beneficial effects are attributed to CA's diverse properties, including its antioxidant, anti-inflammatory, and anti-apoptotic activities. Supporting these

findings, Jafarinezhad et al. (2019) demonstrated CA's effectiveness in enhancing heart function and reducing structural damage after 24 days of DOX treatment in rats.

Jamhiri et al. (2019) and Sadeghzadeh et al. (2018) have also demonstrated that CA administration effectively prevents aortic banding-induced left ventricular hypertrophy in rats. In hypertrophied left ventricles, an increase in cardiomyocyte apoptosis is evident, as indicated by elevated mRNA levels of the pro-apoptotic protein Bcl-2-associated death (BAD) promoter and the anti-apoptotic protein Bcl-2. CA demonstrated a notable capacity to decrease the expression of the pro-apoptotic factor BAD while simultaneously enhancing the levels of anti-apoptotic factors, specifically Bcl-2 and Bcl-xL, within the left ventricular tissue. This dual effect suggests a promising role for CA in modulating apoptotic processes associated with ventricular hypertrophy. Furthermore, the anti-apoptotic properties of CA were corroborated by Yu et al. (2013), who found that CA downregulated caspase-3 and Bax activity while increasing Bcl-2 expression at the protein level in cases of acute myocardial infarction.

Furthermore, Jamhiri et al. (2019) demonstrated CA's notable ability to reduce cardiac fibrosis. The proposed mechanisms behind CA's anti-fibrotic effects on DIC suggest that CA exerts its protective influence by inhibiting inflammatory cytokines, specifically TNF-α and interleukin-6 (IL-6) (El-Sayed et al. 2016). In another study, CA showed promising potential in reducing ethanol-induced hepatic fibrosis. The study highlighted a multifaceted mechanism where CA exerted therapeutic effects by reducing oxidative stress, downregulating the pro-fibrotic growth factor TGF-β1, increasing the anti-inflammatory cytokine interleukin-10 (IL-10), inhibiting collagen synthesis as evidenced by reduced 4-hydroxyproline levels, and attenuating hepatic stellate cell activation, indicated by decreased alpha-smooth muscle actin (α-SMA) expression in hepatocytes. These findings emphasize CA's significant antioxidant, anti-inflammatory, and anti-fibrotic properties, offering valuable insights into its potential therapeutic utility (Abu-Risha et al. 2023).

However, CA's poor water solubility requires large doses to reach therapeutic plasma levels, as noted by Marinelli et al. (2019), which restricts its clinical use.

Research by Ali et al. (2024) has shown that a large portion of orally taken CA remains in the gastrointestinal (GI) tract, with much of it excreted in the urine and only a small amount absorbed into the body's tissues, highlighting its low bioavailability. Additionally, Jamhiri et al. (2019) reported a reduction in heart rate in normal animals treated with CA. El-Sayed et al. (2016) showed that the cardioprotective activity of CA was lower compared to the combination of CA with its isomer, thymol.

These findings emphasize the necessity for modifications to CA to improve its clinical effectiveness and utility. Efforts are underway to transform or chemically modify CA and its derivatives to enhance their biological activities by reducing toxicity, increasing membrane permeability, and improving water solubility. Such modifications of natural compounds have been widely applied in drug development to create new compounds with better activities (Butler et al. 2014).

2.7 METHOD FOR THE SYNTHESIS OF CARVACROL DERIVATIVES

The development of new methods for synthesizing CA derivatives has increased significantly over the years. This section showcases examples of CA derivative synthesis, emphasizing esterification and *O*-alkylation reactions, which are fundamental for attaching linkers to the CA scaffold. Furthermore, detailed discussions cover modifications to the benzene ring of CA as a precursor for hybrid synthesis, alongside the creation of hybrid CA derivatives that integrate other pharmacophores.

2.7.1 Synthesis of Carvacryl Ester Containing Simple Alkyl or Aryl Moiety

The synthesis of various carvacryl esters containing a simple alkyl or aryl moiety has been reported in the literature. Generally, the purpose of CA's transformation into its ester derivatives was to enhance their hydrophobicity, making the derivatives easily penetrate the cell membrane, or to decrease their toxicity. The carvacryl esters were commonly synthesized by reacting CA with the appropriate acid chlorides or acid anhydrides in the presence of a base. Figures 2.5 and 2.6 show the structural diversity

of carvacryl esters containing a simple alkyl or aryl moiety, and their synthesis methods can be seen in Table 2.1.

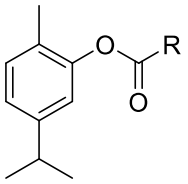

(**38**) R = CH_3
(**39**) R = CH_2CH_3
(**40**) R = $CH(CH_3)_2$
(**41**) R = $CH_2CH(CH_3)_2$
(**42**) R = $(CH_2)_4CH_3$
(**43**) R = $(CH_2)_{10}CH_3$
(**44**) R = CH_2Cl
(**45**) R = CCl_3
(**46**) R = $CH=C(CH_3)_2$
(**47**) R = $CH=CHCH_3$
(**48**) R = $=CH=C(CH_3)(CH_2)_2CH=C(CH_3)_2$
(**49**) R = $CH_2CH(CH_3)(CH_2)_2CH=C(CH_3)_2$
(**50**) R = $CH=CHC_6H_5$
(**51**) R = $CH_2C_6H_5$

Figure 2.5 CA ester derivatives with an alkyl moiety

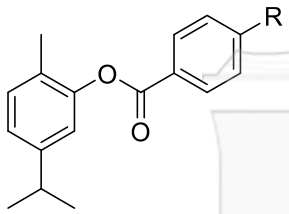

(**52**) R = H
(**53**) R = OCH_3
(**54**) R = Cl
(**55**) R = Br
(**56**) R = F
(**57**) R = NO_2
(**58**) R = CH_3

Figure 2.6 CA ester derivatives with an aryl moiety

The first attempt at converting CA to ester derivatives was carried out by Nikumbh et al. (2003) using acid chlorides as an acylating agent and sodium hydroxide (NaOH) solution (10%) as both a base and solvent. This method successfully synthesized **38**, **50**, **51**, and **52** with a high yield (85–92%). Another attempt was made to obtain **38** (yielding 86%) by using TEA as a base in a different solvent, such as DCM or tetrahydrofuran (THF) (Alokam et al. 2014; Mathela et al. 2010; Wang et al. 2019). The basicity of NaOH is higher than that of TEA, whereas the yield of the resulting ester, as well as the reaction time, were similar. The other method of synthesizing **38** (76% yield) was conducted by using acetic anhydride as an acylating agent and sodium acetate or pyridine as a base. These methods necessitated a longer reaction time and higher temperature than acetyl chloride (Andre et al. 2016; Ben Arfa et al. 2006; Damasceno et al. 2014; De Moraes et al. 2013; Pires et al. 2013; Pires et al. 2014).

Furthermore, De Mesquita et al. (2018) treated CA with acetic anhydride using DMAP and TEA as bases to obtain compound **38**. Unfortunately, the reaction time was still long, and the yield of the compound was low. A different result was obtained

when a 10% solution of NaOH was used as a base. The completion reaction was only reached in 15 minutes at room temperature (Konig et al. 2019). It can be concluded that the esterification reaction of CA may be affected by the acylating agent and the basicity of the base. The acid chlorides were more reactive than acid anhydrides, and TEA, commonly used as a base, tended to result in high yield.

Moreover, more advanced and greener methods have been developed by using support and microwave irradiation to obtain compounds **38**, **39**, and **52**. More et al. (2007) used solid resins, i.e., Amberlite IRA 400, Indion 820, and Amberlyst A 26, to support the CA anion. The CA-supported resin was then mixed with the appropriate acid chlorides to form carvacryl ester. The mixture was stirred at room temperature until the reaction was completed within 10–20 minutes. The yield and purity of products are higher in comparison with conventional methods. Besides that, the resins were reusable by regenerating their activity, which is in line with green chemistry principles. Besides, Narkhede et al. (2008) have continuously developed greener, simpler, and more rapid methods with higher yield and purity to obtain carvacryl ester. The method was assisted by microwave irradiation and solid supports such as alumina, silica gel, and fly ash. The solid supports absorbed the CA using aqueous sodium hydroxide, and then it was further reacted with acid chlorides under microwave irradiation. The reaction time ranged from 1 to 5 minutes. This method was also used to successfully synthesize CA dimeric esters (**59** and **60**) from CA-supported alumina, silica gel, or fly ash and the appropriate diacid chloride. The structures of **59** and **60** can be seen in Figure 2.7.

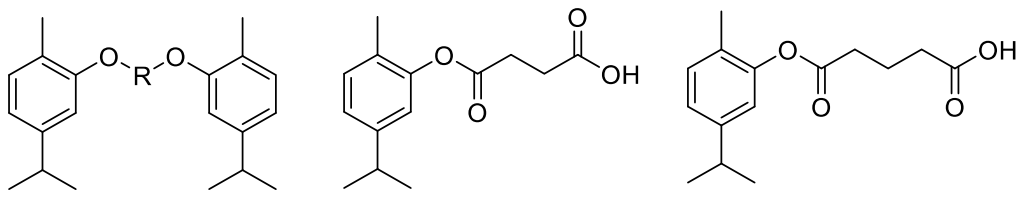

R = -COCO- (**59**)
R = -CO(CH$_2$)$_4$CO- (**60**)

(**61**) (**62**)

Figure 2.7 The structures of compounds **59**–**62**

Unfortunately, this greener method with many advantages was only adopted by Nesterkina et al. (2020), and the other researchers still focus on conventional

methods, i.e., the synthesis of **39**; **40**; **41**; **47**; **50**; **58** (Mathela et al. 2010), **39** (De Santana et al. 2014), **44**; **45** (Silva et al. 2017), **42** (De Mesquita et al. 2018), and **46** (Marinelli et al. 2019). Besides, **43**, containing a longer alkyl chain, has been obtained by treating CA with fatty acid in the presence of inorganic acid. This method used different acylating agents and acids as catalysts. It was the first attempt to make carvacryl ester using fatty acid and an inorganic acid. Moreover, the yield was low, the time was long, and the temperature was also high (Bassanetti et al. 2016). On the other hand, the other longer alkyl derivatives (**48** and **49**) have been obtained with a higher yield by reacting CA with the appropriate acid chlorides in the presence of TEA as a base. This method was more effective than organic acids based on yield, time, and reaction temperature. Ester derivatives with a carboxylic acid moiety in the terminal alkyl group have also been successfully synthesized by stirring a mixture of CA and succinic/glutaric anhydride overnight to yield **61** and **62** (Figure 2.7). However, dicyclohexylamine catalyzed this reaction, and the yield was still low (Marinelli et al. 2019).

Furthermore, the ester derivatives containing a benzoyl moiety (**51–56**) were also successfully synthesized using substituted benzoic acids as acylating agents. The success of this method was supported using *N*,*N*'-dicyclohexylcarbodiimide (DCC) and DMAP as a condensing agent and a base, respectively. This reaction was also affected by the substituted benzoic acid derivatives. The strong electron withdrawing group ($-NO_2$) in the para position can increase the yield of the reaction, whereas the electron donating group ($-OCH_3$ and CH_3) decreases the yield of the reaction (De Mesquita et al. 2018). Mbese et al. (2022) continuously developed CA derivatives utilizing DCC and DMAP as catalysts, demonstrating their effectiveness in facilitating direct esterification reactions between phenolic compounds and carboxylic acid derivatives.

Table 2.1 The synthesis methods of ester derivatives of CA containing alkyl and aryl moieties

No	The carvacryl esters	Reagent	Catalyst, activating agent/method	Solvent	Temperature	Time	Yield (%)	References
1	**38**; **50**; **51**; **52**	Sodium salt of CA and acid chloride	NaOH	N/A	r.t	2-3 h	85 – 92	Nikumbh et al. 2003
2	**38**	CA and the corresponding acid chlorides	TEA	DCM	0 °C	1 h	78	Mathela et al. 2010
	39				r.t	10 h	75	
	40						85	
	41						75	
	47						78	
	51						82	
	52						78	
3	**38**	CA and acetyl chloride	TEA	DCM	r.t	3 h	75	Alokam et al. 2014
4	**38**	CA and acetyl chloride	TEA	THF	0 °C r.t	15 min 3 h	86	Wang et al. 2018
5	**38**	CA and acetic anhydride	Sodium acetate	N/A	110 °C	24 h	76	Ben Arfa et al. 2006; Silva et al. 2017

To be continued…

…continuation

6	**38**	CA and acetic anhydride	Pyridine	N/A	Refluxed	24 h	76	Damasceno et al. 2014; De Moraes et al. 2013; Pires et al. 2013
7	**38**	CA and acetic anhydride	Pyridine	N/A	r.t	48 h	N/A	Novato et al. 2018
8	**38** **54** **52**	CA and acid anhydride	DMAP and TEA	DCM	r.t	24 h	59 91 46	De Mesquita et al. 2018
9	**38**	CA and acetic anhydride	Sodium hydroxide	N/A	r.t	15 min	N/A	Konig et al. 2019
10	**38** **39** **52**	CA-supported Amberlite IRA 400 and acid chloride	Polymer-supported reactions (Amberlite IRA 400 (chloride form) as supporting)	Acetone	r.t	10 min	93 92 92	More et al. 2007
11	**38** **39** **52**	CA-supported alumina and the appropriate acid halide	Microwave irradiation	N/A	N/A	1-5 min	94 91 90	Narkhede et al. 2008

To be continued…

…continuation

12	39	CA and propionyl chloride	TEA	THF	r.t	2 h	75	De Santana et al. 2014
13	44	CA and chloroacetyl chloride	TEA	THF	N/A	r.t	78	Silva et al. 2017
14	**45**	CA and trichloroacetyl chloride	TEA	THF	N/A	r.t	84	Silva et al. 2017
15	**43**	CA and lauric acid	Phosphoric acid	N/A	150 °C	12 h	51	Bassanetti et al. 2016
16	**53**	CA and benzoic acid derivatives	DCC and DMAP	DCM	r.t	4 h	45	De Mesquita et al. 2018
	54						67	
	55						64	
	56						96	
	57						55	
	58						41	
17	**46**	CA and the suitable acid chlorides	TEA	DCM	r.t	4-5 h	90	Marinelli et al. 2019
	48						82	
	49						75	

2.7.2 Synthesis of Carvacryl Ether Containing Simple Alkyl or Aryl Moiety

Alkyl/benzyl carvacryl ether was another CA derivative based on hydroxy group functionalization. The various ether derivatives of CA reported in the literature can be shown in Figures 2.8 and 2.9. On the other hand, the variety of synthesis methods can be seen in Table 2.2.

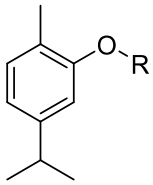

(**63**) R = CH_3
(**64**) R = CH_2CH_3
(**65**) R = $CH_2CH_2CH_3$
(**66**) R = $CH(CH_3)_2$
(**67**) R = $CH_2(CH)_2CH_3$
(**68**) R = $CH(CH_3)CH_2CH_3$
(**69**) R = $(CH_2)_4CH_3$
(**70**) R = $(CH_2)_7CH_3$
(**71**) R = $(CH_2)_{11}CH_3$
(**72**) R = Geranyl
(**73**) R = Farnesyl
(**74**) R = $CH_2CH{=}CH_2$
(**75**) R = $CH_2CH{=}CHCH_3$
(**76**) R = $CH_2CH{=}C(CH_3)_2$
(**77**) R = CH_2CCH
(**78**) R = $CH_2CH{=}C(CH_3)(CH_2)_2CH{=}C(CH_3)_2$
(**79**) CH_2CN
(**80**) CH_2COOCH_3
(**81**) CH_2COOH

Figure 2.8 The ether derivatives of CA contain alkyl moiety

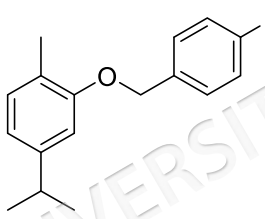

(**82**) R = H
(**83**) R = CH_3
(**84**) R = Cl
(**85**) R = Br
(**86**) R = CF_3
(**87**) R = C_6H_5
(**88**) R = CN
(**107**) R = NO_2

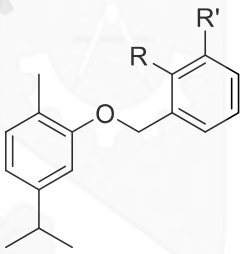

(**89**) R = CH_3 ; R' = H
(**90**) R = CF_3 ; R' = H
(**91**) R = Br ; R' = H
(**92**) R = NO_2 ; R' = H
(**93**) R = H ; R' = CH_3
(**94**) R = H ; R' = CF_3
(**95**) R = H ; R' = F
(**96**) R = H ; R' = OCH_3
(**97**) R = H ; R' = NO_2

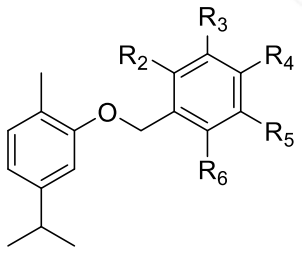

(**98**) R_3, R_5 = CH_3; R_2, R_4, R_6 = H
(**99**) R_3, R_5 = F; R_2, R_4, R_6 = H
(**100**) R_3, R_5 = CF_3; R_2, R_4, R_6 = H
(**101**) R_2, R_6 = F; R_3, R_4, R_5 = H
(**102**) R_2 = Cl; R_4 = OCH_3; R_3, R_5, R_6 = H
(**103**) R_3, R_4 = Cl; R_2, R_5, R_6 = H

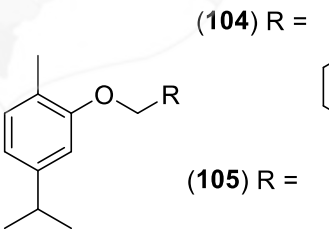

(**104**) R =

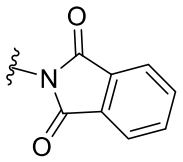

(**105**) R =

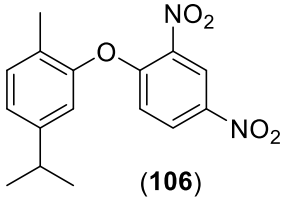

(**106**)

Figure 2.9 The ether derivatives of CA containing benzyl/aryl moiety

The initial work to convert CA into its ether derivatives has been carried out by Lupo et al. (2000). The allyl carvacryl ether (**74**) has already been synthesized by refluxing overnight the mixture of CA in acetone, potassium carbonate (K_2CO_3), and KI. By replacing KI and K_2CO_3 with NaOH solution (10%), Nikumbh et al. (2003) successfully synthesized **74** and other derivatives (**63**,**64**,**67**,**81**, and **82**) using CA and the appropriate alkyl halide as an alkylating agent. This method was modified by Pinheiro et al. (2018) by adding acetone as a solvent to shorten the reaction time. However, in the continuous study, Ben Arfa et al. (2006) and Concepción et al. (2013) obtained **63** using dimethyl sulfate as an alkylating agent and acetone as a solvent in the presence of K_2CO_3 as a base. This method needed a higher temperature and longer reaction time than that of Nikumbh et al. (2003).

Similar to the development of ester derivatives, More et al. (2007) and Narkhede et al. (2008) have demonstrated simpler, greener, and faster methods to obtain ether derivatives of CA (**63–68**, **74**, **81**, **82**, and **106**) using solid support and microwave irradiation. In these methods, alkyl halide was used as an alkylating agent, and the reaction time was shortened. The dimeric ether of CA was also successfully synthesized by using microwave irradiation. To obtain **108** and **109**, the CA must be supported by alumina, silica gel, or fly ash and then reacted with the corresponding dihaloalkanes for 1–5 minutes with microwave irradiation (Figure 2.10). Furthermore, Patil et al. (2010) has continuously developed ether derivatives under microwave irradiation conditions without the use of solid supports. CA has been reacted with a variety of substituted chloroacetanilides to produce a variety of carvacryl ethers with an amide moiety. This reaction was assisted by microwave irradiation for 1–3 minutes in the presence of NaOH as base and acetone as a solvent to give **110–115** (Figure 2.10) with a better yield and purity in mild conditions. Microwave irradiation has several advantages over traditional methods, including a shorter reaction time, ease of isolating and purifying products, and a simpler experimental procedure.

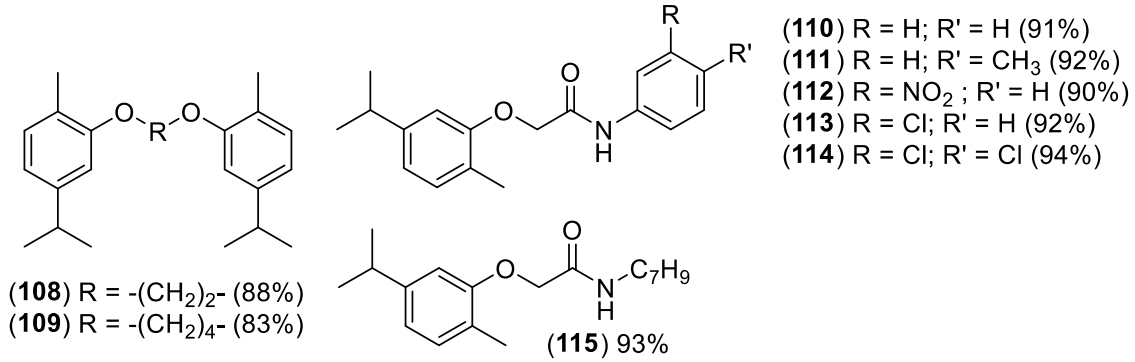

Figure 2.10 The structure of compounds **108**–**115**

Unfortunately, this beneficial method was only imitated by Bonfim et al. (2014) and Nesterkina et al. (2020), and the other researchers still prefer conventional methods to develop carvacryl ether. For example, **63** has been obtained by the reaction of CA with methyl iodide in the presence of K_2CO_3 as a base and acetone as a solvent. The reaction mixture is stirred and heated at 60 °C for 2 h (Alokam et al. 2014) or refluxed overnight (Silva et al. 2017). Besides, **64** was also synthesized using either iodoethane or bromoethane as alkylating agents under refluxed or stirred conditions. A variety of bases, including K_2CO_3 and sodium methoxide, as well as solvents (acetone, dimethylformamide (DMF), and acetonitrile), were used. These conventional methods were used to develop the other ether derivatives (Aneja et al. 2018; Natal et al. 2021; Silva et al. 2017; Wang et al. 2018). The use of various alkylating agents, bases, and solvents has affected the yield of reactions. Interestingly, Natal et al. (2021) prefer cesium carbonate as a base over previously used base to synthesize **65**, **70**, and **71**. However, the performance of this base was lower than that of those previously used.

2.7.3 The Modification of CA Based-functionalization of Benzene Ring

CA derivatives with functionalized phenyl rings, as illustrated in Figure 2.11, have been reported. This modification facilitates the formation of CA hybrids with other pharmacophores. The derivatization of the CA structure was started by Lupo et al. (2000). The continued heating of allyl carvacryl ether (**74**) in a nitrogen atmosphere at 200 °C gave ortho/para-allylcarvacrol (**116**) with a high yield.

Table 2.2 The synthesis methods of ether derivatives of CA containing alkyl and benzyl/aryl moieties

No	The ethers of CA	Reagent	Base/Activating Agent	Solvent	Temperature	Time	Yield (%)	References
1	**74**	CA	K_2CO_3 and KI	Acetone	Refluxed	24 h	90	Lupo et al. (2000)
2	**63**, **64**, **67**, **74**, **81**, **82**	CA and alkyl halide	NaOH 10 %	-	Refluxed	5 – 6 h	83 – 90	Nikumbh et al. (2003)
3	**63**	CA, and dimethyl sulfate	K_2CO_3	Acetone	Refluxed	24 h	88	Ben Arfa et al. (2006) Concepción et al. (2013)
4	**63**	CA-supported Amberlite IRA 400 and the corresponding alkyl halide	Polymer-supported reactions (Amberlite IRA 400 (chloride form) as supporting)	Acetone	r.t	20 – 35 min	92	More et al. (2007)
	64						96	
	65						78	
	66						86	
	67						88	
	68						90	
	81						94	
	106						86	

To be continued…

… continuation

5	**63**	CA- supported alumina and the appropriate alkyl halide	Alumina as solid support	-	Microwave irradiation	1-5 min	92	Narkhede et al. (2008)
	64						94	Nesterkina et al. (2020)
	65						90	
	66						91	
	67						89	
	68						90	
	81						79	
	103						87	
	74						84	
	82						85	
6	**63**	CA and methyl iodide	K_2CO_3	Acetone	60 °C	2 h	81	Alokam et al. (2014)
7	**81**	CA and chloroacetic acid	NaOH	Water	Refluxed	24 h	77	Silva et al. (2017)
8	**63**	CA and the corresponding alkyl iodide	K_2CO_3	Acetone	Refluxed	24 h	75	Silva et al. (2017)
	64						61	
9	**64**	CA and bromoethane	K_2CO_3	DMF	r.t	10 h	90	Wang et al. (2018)
10	**74**	CA and allyl bromide	NaOH aqueous	Acetone	50 – 60 °C	2 h	N/A	Pinheiro et al. (2018)

To be continued…

30

… continuation

11	**64**	CA and bromoethane	Sodium methoxide	Anhydrous acetonitrile	Refluxed	22 h	60	Brotzman et al. (2019)
12	**76**	CA and the suitable alkyl chlorides	K_2CO_3	Dry acetone	80 °C	4 h	95	Marinelli et al. (2019)
	72						91	
	73						83	
13	**64**	CA and the proper (substituted) benzyl, diarylmethyl, heteroaryl methyl or alkyl bromide	Anhydrous K_2CO_3	Dry DMF	r.t	30 min	66	Sisto et al. (2020)
	66						56	
	74						70	
	77						74	
	67						78	
	75						69	
	76						71	
	69						78	
	78						74	
	79						79	
	80						80	
	82						88	
	89						86	
	93						85	
	83						73	
	98						63	

To be continued…

31

… continuation

	94						78	
	86						84	
	100						80	
	95						82	
	99						80	
	101						89	
	96						80	
	84						79	
	102						82	
	103						92	
	91						61	
	85						66	
	92						91	
	97						72	
	88						79	
	87						90	
	104						98	
	105						88	
	107						95	
14	**65**, **70**, **71**	CA and the corresponding alkyl halide	Cesium carbonate	Acetonitrile	65 °C	24 h	54 – 62	Natal et al. (2021)

Furthermore, **117** was synthesized by hydrogenating **116** in the presence of Pd/C as a catalyst using the Parr hydrogenation apparatus. The methods carried out to synthesize **188–125** can also be seen in Table 2.3. Furthermore, Mastelić et al. (2008) modified the CA structure by inserting a hydroxymethyl moiety into its benzene ring to obtain **126–127**. The modification aimed to improve the polarity and solubility of CA in water and its antioxidant activity. CA has been reacted with methanal in the presence of NaOH as the base to obtain **126–127.** The formation of **126** occurs through the nucleophilic addition of methanal by the phenolate ion of CA. The role of a base (NaOH) is to promote the formation of phenolate ions by deprotonation of the hydroxy group in the phenolic ring. The formed hydroxymethylphenol (**126**) can undergo a further reaction with the parent CA through an electrophilic aromatic substitution reaction to give **127**. Moreover, De Oliveria et al. (2016) have already synthesized **128** by reacting CA with chlorosulfonic acid at 0 °C. Compound **126** demonstrated increased antioxidant activity compared to CA alone, making it a suitable candidate for developing hybrids with enhanced antioxidant properties.

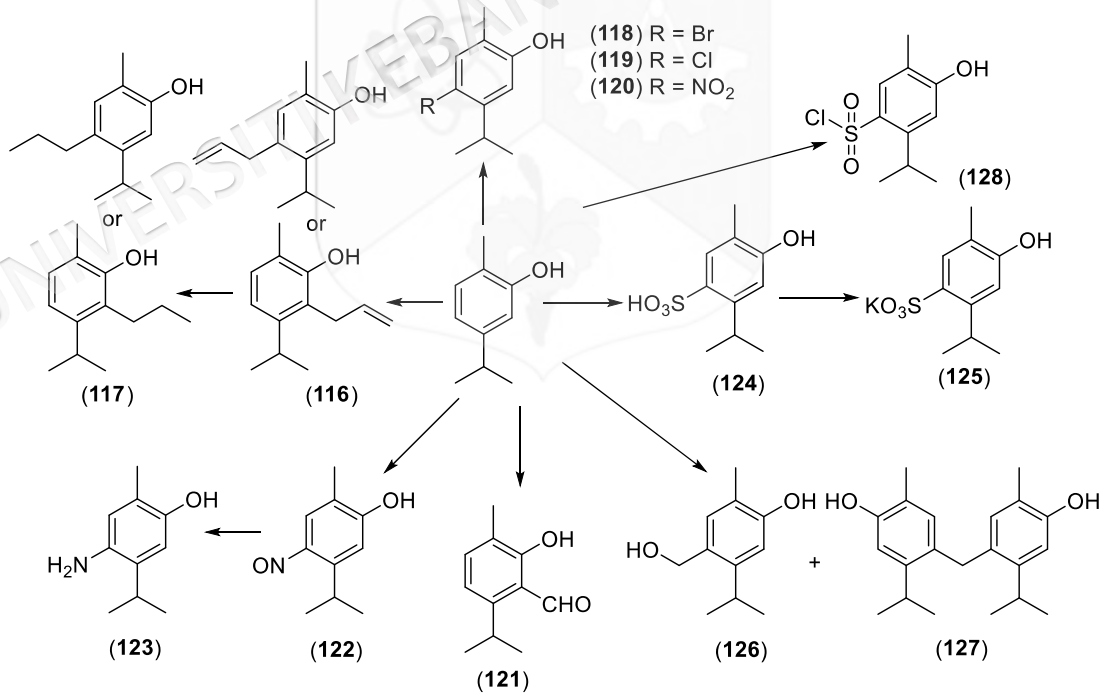

Figure 2.11 The structural diversity of CA derivatives derived from the functionalization of the benzene ring

Table 2.3 The synthesis methods of CA derivatives based-functionalization of benzene ring

No	The CA derivatives	Reagent	Catalyst /Base/Acid	Solvent	The synthesis method	Tempe-rature	Time	Yield (%)	References
1	**116**	Allyl CA ether	-	-	Heated under nitrogen atmosphere	200 °C	4 h	97	Lupo et al. (2000)
2	**117**	Allyl CA + hydrogen gas (40 psi)	Pd/C (5%) (Catalyst)	10% ethanol in ethyl acetate	Parr hydrogenat-ion apparatus	N/A	3 h	98	Lupo (20 ,
3	**118**	CA and bromine	-	Acetic acid	Stirred	r.t	N/A	47	Alokam et al. (2014)
	118	CA and bromine	-	Glacial acetic acid	Cooled	0 °C	20 min	N/A	Wang et al. (2019)
					Stirred	r.t	3 h		
4	**119**	CA and SO_2Cl_2	-	CCl_4	Stirred	r.t	45 min	81	Alokam et al. (2014)
	119	CA and LiCl	Copper catalyst ($CuCl_2$)	Acetic acid	Agitated under oxygen atmosphere	80 °C	6 h	N/A	Pinheiro et al. (2018)
5	**120**	CA and nitric acid	-	Acetic acid	Stirred	r.t	N/A	33	Alokam et al. (2014)
6	**120**	CA	NaOH (base)	Water	Heated	60–70 °C	N/A	N/A	Silva et al. (2017)
					Added chloroform				

To be continued…

… continuation

	120	CA and paraformaldehyde	TEA and $SnCl_2$	Toluene	Refluxed	50 – 60 °C	2 – 3 h	N/A	Bansal et al. (2022)
7	**121**	CA	Concentrated HCl (acid)	Ethyl alcohol (95%)	Cooled Added sodium nitrite	0 – 5 °C	N/A	75	Pete et al. (2012) Rajput et al. (2017)
8	**122**	4-nitrosocarvacrol	Aqueous ammonia (28%) (base)	Water	N/A	N/A	N/A	82	Pete et al. (2012) Rajput et al. (2017)
9	**123**	CA and sulfuric acid 96%w	-	-	Mixed under vacuum	30 °C	2 h	N/A	Bassanetti et al. (2017)
10	**124**	CA sulfonate	-	Methanol	Neutralized with a saturated KOH (pH 7)	N/A	N/A	95	Bassanetti et al. (2017)

2.7.4 Synthesis of CA Hybrids with Diverse Pharmacophores

Several CA hybrids have been developed to enhance the biological activity of the parent compound. For example, Pete et al. (2012) have already developed a hybrid of CA and benzoyl phenyl urea/thiourea derivatives by incorporating benzoyl phenyl urea/thiourea moiety into CA (**129–140**). Their well-established insecticidal properties informed the choice of benzoyl phenyl urea/thiourea linkages, while CA had previously exhibited antifungal efficacy in studies. This strategic fusion aimed to produce hybrid molecules with dual functionality capable of combating fungal infections and insect pests, thus presenting a promising prospect for the agricultural sector. The synthesis began with the reaction of compound **123** with substituted benzoyl chloride in the presence of ammonium thiocyanate and dry acetone, yielding benzoyl CA thiourea derivatives (**129–134**). Furthermore, the benzoyl CA thiourea has been oxidized to obtain benzoyl CA urea derivatives (**135–140**) using formic acid, hydrogen peroxide, and DMF, as shown in Scheme 2.1. Although the antifungal activity against phytopathogenic fungi was lower than that of CA, some derivatives exhibited enhanced antifungal activity against human fungal pathogens compared to the parent compound.

128 also underwent further reactions to obtain sulfonamide derivatives of CA (De Oliveira et al. 2016). **128** was subjected to various amines using dichloromethane as a solvent to obtain **141–152,** as shown in Scheme 2.2. These hybrids exhibited superior antibacterial activity against methicillin-resistant *Staphylococcus aureus* (MRSA) compared to the parent compound. Notably, among these derivatives, those containing the 4-methylaniline moiety (**141**) displayed the most potent antibacterial activity against MRSA, with minimum inhibitory concentration (MIC) values ranging from 3.9 to 15.62 ppm. Another potential derivative was a sulfonamide derivative containing a 4-fluoro aniline moiety (**143**), which exhibited a synergistic effect with tetracycline and a partial synergistic effect with ampicillin with the fractional inhibitory concentration (FIC) indices of 0.50 and 0.75, respectively. SAR demonstrated that phenyl sulfonamide moiety plays a crucial role in antibacterial movement. Additionally, the methyl group appended to the phenyl ring enhanced the antibacterial activity significantly. Substituting the -CH_3 group with either an electron-

withdrawing group (-NO_2 or -F) or another electron-donating group (-OH or -OCH_3) decreased anti-MRSA efficacy.

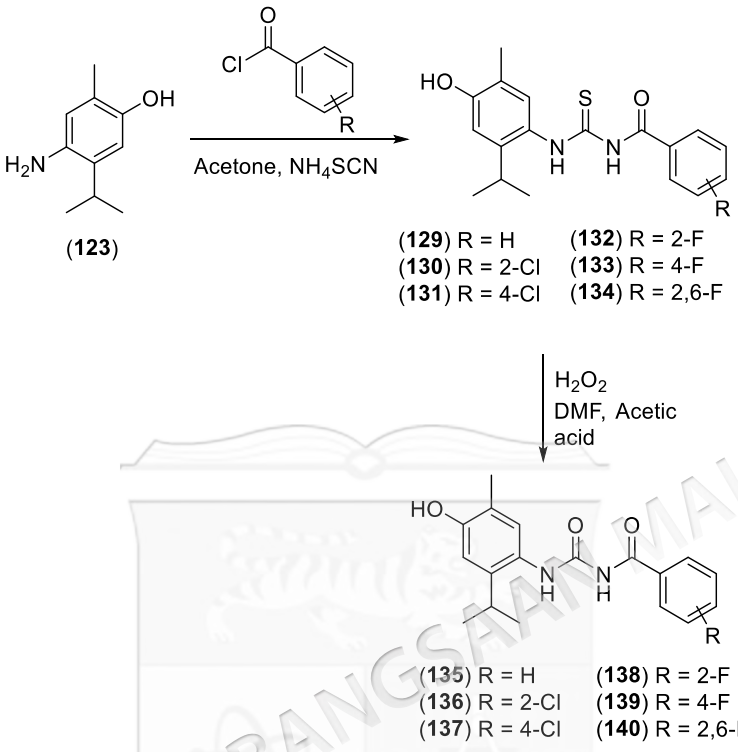

Scheme 2.1 The synthetic pathway of compounds **129**–**140**

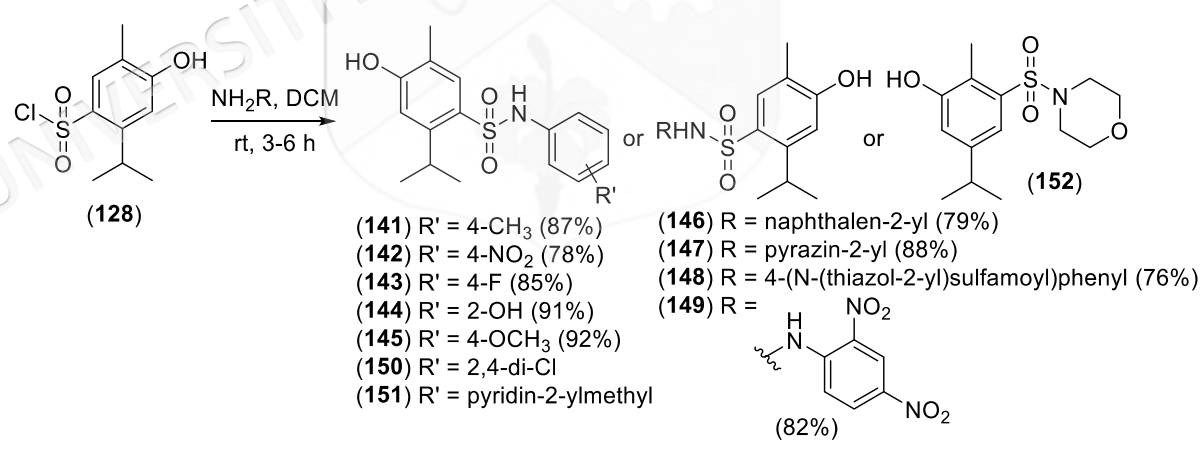

Scheme 2.2 The synthetic pathway of compounds **141**–**152**

In 2017, Ashraf et al. reported a synthesis method for hybrids combining CA with phenolic acids through an ester bond. This study introduced a novel tyrosinase inhibitor derived from CA, highlighting its potential applications in addressing melanin-related skin disorders and fruit oxidation. The synthesis began with an

esterification reaction between CA and chloroacetyl chloride in the presence of TEA and DCM as solvents. The mixture was then stirred for 4 hours at room temperature. A nucleophilic substitution reaction was conducted in the second, incorporating benzoic acid or cinnamic acid derivatives. The deprotonated carboxy group of benzoic acid derivatives nucleophilically attacked the terminal chloromethyl group. The presence of TEA will assist benzoic/cinnamic acid derivatives in undergoing deprotonation reactions. The method included stirring the mixture of benzoic/cinnamic acid derivatives, TEA, potassium iodide, intermediate, and dimethyl formamide for 24 h at room temperature. The various hybrids of CA and hydroxy-substituted benzoic/cinnamic acid (**1–10)** can be shown in Scheme 2.3. Most of CA derivatives demonstrated robust tyrosinase inhibition except for **5-6**, with IC_{50} values ranging from 0.0167 to 15.9 µM, although slightly below the benchmark set by kojic acid (IC_{50} of 16.69 µM). **10** emerged as the most potent inhibitor, boasting an IC_{50} of 0.0167 µM. Generally, compounds featuring a hydroxy-substituted cinnamic acid residue exhibited superior activity compared to those with a hydroxy-substituted benzoic acid moiety.

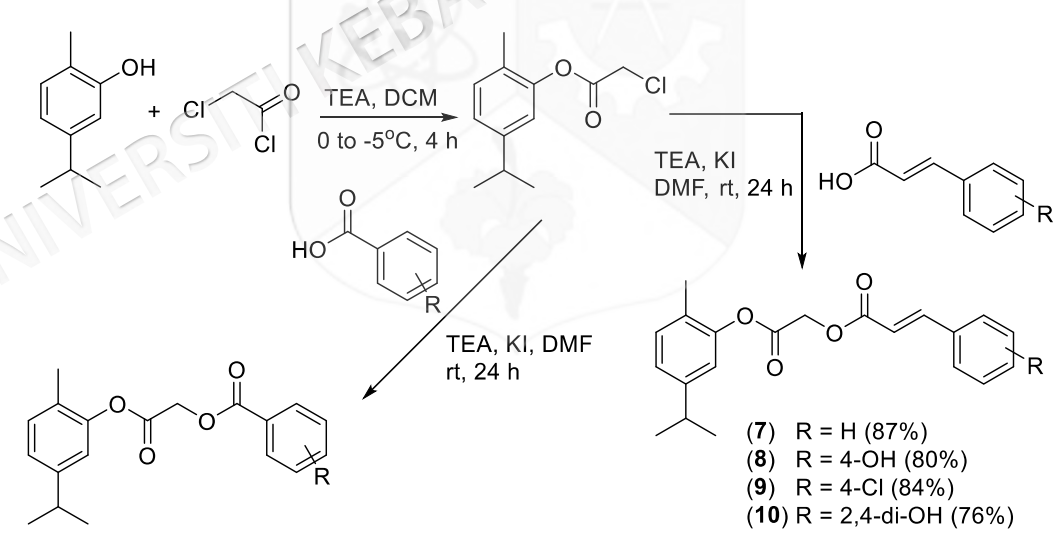

(**1**) R = 3-OH (85%)
(**2**) R = 4-OH (84%)
(**3**) R = 3,4-di-OH (78%)
(**4**) R = 2,4-di-OH (81%)
(**5**) R = 3,5-di-OH (86%)
(**6**) R = 3,4,5-tri-OH (87%)

Scheme 2.3 The synthetic pathway of compounds **1**–**10**

Bkhaitan et al. (2018) synthesized two hybrids of CA and metronidazole to evaluate the influence of the linker on the biological activity of the resulting hybrids. Metronidazole, a key therapeutic agent for treating *Helicobacter pylori*-induced

gastric ulcers, faces limitations due to bacterial resistance and safety concerns, creating a need for new derivatives with comparable or improved efficacy. The development of hybrid drugs, such as the combination of metronidazole with CA, which possesses a broad biological activity spectrum, represents a potential strategy to overcome these challenges. The synthesis of compound **153** involved an esterification reaction between CA and the oxidized form of metronidazole. To oxidize the metronidazole, the mixture of metronidazole, potassium dichromate, and sulfuric acid in water was stirred overnight. The carboxylic acid moiety product was subjected to an esterification reaction with CA. The reaction was allowed in the presence of DMAP and DCC in DMF and DCM. After 50 hours at room temperature, the reaction mixture yielded **153**, as shown in Scheme 2.4.

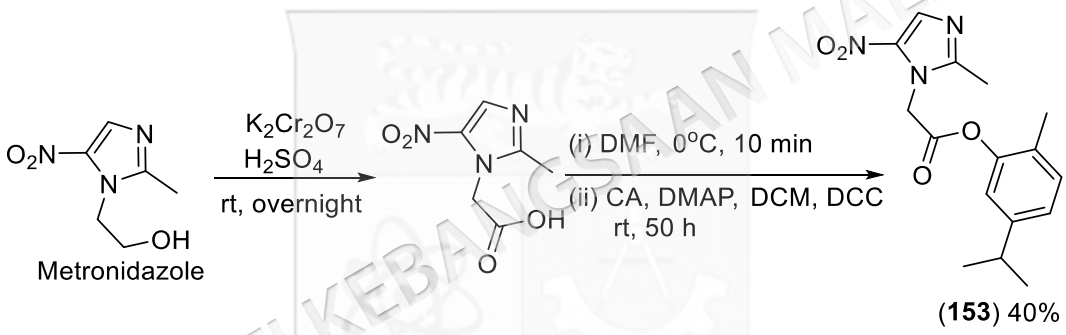

Scheme 2.4 The synthetic pathway of compound **153**

To synthesize compound **154** containing an ether linkage, the hydroxy group of metronidazole was first converted into a tosylate group to serve as an effective leaving group. This was achieved by reacting metronidazole with 4-methylbenzenesulfonyl chloride in the presence of TEA and DCM (solvent) to obtain the metronidazole tosylate. This compound was subjected to the etherification reaction with CA using K_2CO_3 and DMF. The mixture was stirred for 14–16 h at 70–80 °C to produce **154** (51%) as shown in Scheme 2.5.

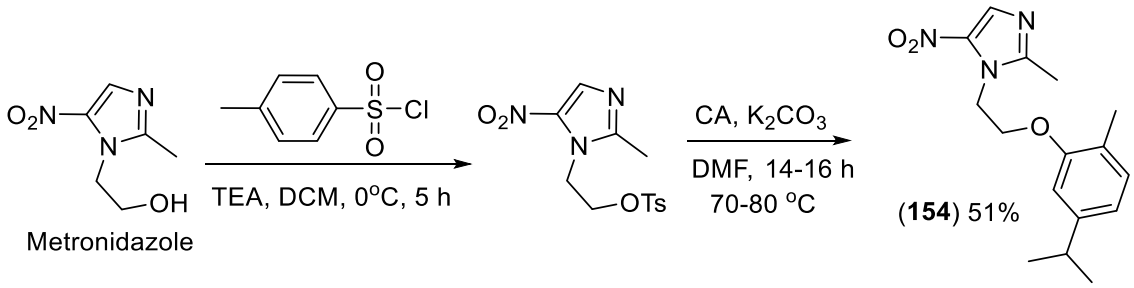

Scheme 2.5 The synthetic pathway of compound **154**

The resulting hybrids (**153**&**154**) exhibited potent activity against *Clostridium perfringens*. Notably, the ether-linked hybrid (**154**) displayed superior antibacterial potency compared to the ester-linked counterpart (**153**), particularly demonstrating strong efficacy against *H. pylori* strains. Encouragingly, the ether derivatives showed reduced toxicity towards normal human fetal lung fibroblasts compared to metronidazole, suggesting their potential for managing gastric ulcers effectively in the future. These findings highlight the critical role of the linker in influencing the biological activity of hybrid compounds.

Aneja et al. (2018) created a potential candidate for antimicrobial activity by adding a 1,2,3-triazole moiety and sulfonate to CA. **234–241** has been synthesized in three steps. CA was modified into its ether derivatives containing an alkyne moiety in the first step. CA was mixed with propargyl bromide in the presence of K_2CO_3 and DMF as a solvent. The mixture was stirred continuously for 24 hours. Secondly, the substituted anilines were converted to their azide derivatives via a diazotization reaction followed by treatment with sodium azide. The aniline derivatives were dissolved in ethyl acetate at 0 °C, HCl and sodium nitrite were added, and stirred continuously for 1 h. After that, the sodium azide solution was added to the mixture. After stirring the mixture at room temperature, the azide was obtained until the completion reaction was reached. Finally, alkyne and azide undergo a [3+2] cycloaddition reaction catalyzed by Cu(I) from $CuSO_4.5H_2O$ in sodium ascorbate's presence to obtain a CA-triazole hybrid. This cycloaddition reaction used a tetrahydrofuran (THF)/H_2O (1:2) mixture as a solvent to obtain **155–162**, as shown in Scheme 2.6.

Compound **159** emerged as a standout, displaying enhanced efficacy against *S. pneumoniae*, *E. faecalis*, and *E. coli*, with improved IC_{50} values (15–62 μg/mL). Studies illustrated its bacteriostatic effect on *S. pneumoniae* and *E. coli*, potent biofilm inhibition, and moderate activity against resistant *E. coli*. Additionally, *in vitro* assays revealed no hemolysis or cytotoxicity, while *in vivo* trials on *G. mellonella* confirmed its safety. These findings highlight **159** as a promising avenue for further research in developing potent antibacterial agents. The SAR analysis revealed that introducing a phenyl-1,2,3-triazole moiety did not significantly alter CA's antibacterial activity against the tested bacteria. Notably, within the series **155–162**, only the hybrid with a carboxyl substituent at the *para* position of the phenyl ring exhibited greater potency than CA. Substituting the -COOH group with other electron-withdrawing or electron-donating groups resulted in reduced activity compared to the parent compound.

The development of CA derivatives incorporating a thiazole moiety was further explored by Uddin et al. (2020). Computational studies, including molecular docking and molecular dynamic simulations, identified a potential antimalarial candidate capable of inhibiting *Plasmodium falciparum* growth without exhibiting toxicity toward human cells. Among these candidates, CA derivatives containing a triazole moiety were highlighted. To validate the antimalarial potential and conduct SAR analysis, the synthesis of these CA derivatives was adapted from the method reported by Aneja et al. (2018), resulting in compounds **161** and **163–174**, as depicted in Scheme 2.6. Of these, only compound **161** exhibited significant antimalarial activity. SAR analysis indicated that substituting the *p*-methoxy ($-OCH_3$) group with substituents in the ortho- or meta-positions led to a gradual reduction in activity, while optimal activity was achieved when the methoxy group was retained at the *para* position of the aromatic ring. These findings underscore the critical influence of substituent position and type on the biological activity of these derivatives.

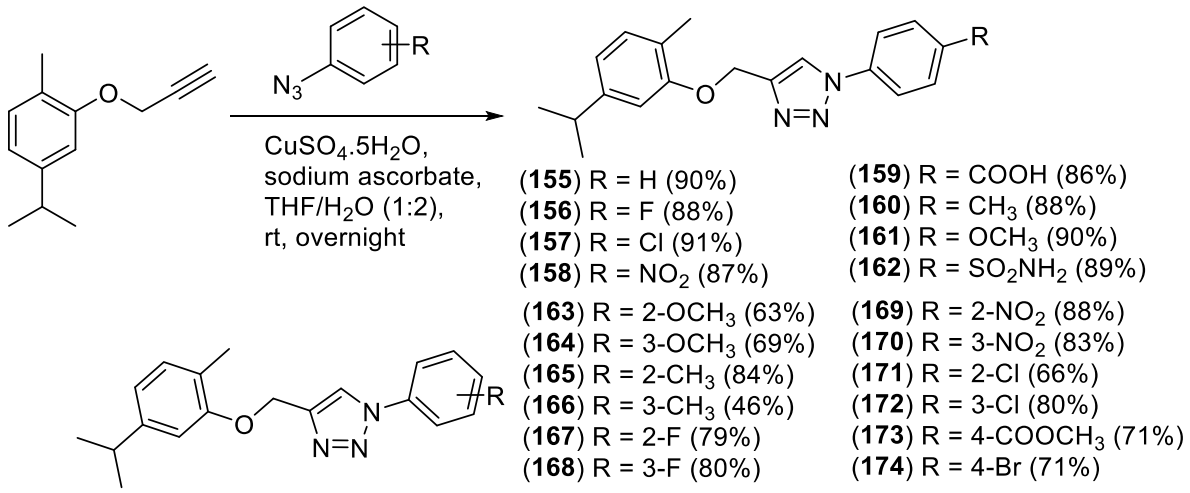

Scheme 2.6 The synthetic pathway of compounds **155**–**174**

2.8 METHOD FOR THE SYNTHESIS OF CARVACROL PHENOLIC ACID HYBRIDS

Building on previous findings highlighting the cardioprotective properties of CA and PA (Imran et al. 2022; Liu et al. 2022), this study examines the cardioprotective potential of CPAHs. Molecular hybridization, a pivotal strategy in medicinal chemistry, involves combining molecular fragments known as pharmacophores to enhance bioactivity or create novel properties do not present in the parent molecules alone (De Castro et al. 2020). Research suggests that this approach often yields significant therapeutic benefits, as hybrid compounds typically exhibit increased affinity and effectiveness compared to their parent compounds (Nepali et al. 2014). Additionally, hybridization can enhance physicochemical characteristics, drug delivery mechanisms, and biopharmaceutical properties (Das et al. 2010).

Forming CA derivatives, such as CPAH, may improve cardioprotective effects through synergistic or additive mechanisms while overcoming the limitations of CA. The formation of CA derivatives, such as CPAH, has the potential to enhance cardioprotective effects through synergistic or additive mechanisms while addressing the limitations of CA. According to the reported literature, hybridizing CA with diverse pharmacophores can be achieved by introducing linkers. Common linkers used include ester, ether, and thiazole linkers. In this study, ester and ether linkers were selected to provide the physicochemical properties necessary for optimal

activity. Additionally, alkyl linkers, being more flexible, may facilitate easier binding of the hybrids to various targets, as suggested by Dong et al. (2022).

Ashraf et al. (2017) previously synthesized ten CPAHs using an ester linker through a two-step reaction process. In the first step, CA was reacted with chloroacetyl chloride in the presence of TEA and dry DCM for four hours, yielding an intermediate. This intermediate was subsequently subjected to a nucleophilic substitution reaction with various HBA or cinnamic acid derivatives over 24 hours at room temperature, as depicted in Scheme 2.3. Expanding on this work, the CPAHs were re-synthesized (**1–10**), and eleven novel CPAHs (**11–21**) were developed. Their cardioprotective effects against DIC were systematically evaluated to investigate the SAR within this series and enhance the understanding of their therapeutic potential.

2.9 *IN VITRO* CARDIOPROTECTOR ACTIVITY AGAINST DIC

The H9c2 cell line, originating from embryonic BD1X rat heart tissue, is widely used in *in vitro* studies because it closely mimics the morphology of immature cardiomyocytes and exhibits strong proliferative abilities. Despite their immature state, H9c2 cells retain essential signalling components required for maturation into cardiac muscle cells. This line is particularly valuable for studying cardiotoxicity, especially of anticancer drugs such as DOX (Branco et al. 2012; Witek et al. 2016). Supporting this, research by Dallons et al (2020), demonstrates that the H9c2 cell line serves as an excellent model for investigating DIC and the protective effects of cardioprotectant. H9c2 cells accurately mimic key mechanisms of DIC, including oxidative stress, cell death, apoptosis, sarcoplasmic reticulum stress, and topoisomerase inhibition. In their evaluation of DOX toxicity on H9c2 cells *in vitro*, prolonged exposure to DOX for at least 24 hours resulted in a dose-dependent reduction in cell viability. Conversely, short-term exposure to DOX for just 4 hours did not negatively impact the viability of H9c2 cells. These findings underscore the utility of the H9c2 cell line in modeling DIC and testing cardioprotective interventions.

Currently, the primary strategy for managing DIC involves the concurrent administration of a cardioprotective agent (Chung and Youn 2016). To evaluate the cardioprotective activity of specific compounds *in vitro*, H9c2 cells were pre-incubated with the cardioprotectant before DOX exposure. The standard prophylactic treatment recommends administering the cardioprotectant 3 hours before DOX exposure. However, longer-term prophylactic delivery, administered 24 hours before DOX in an H9c2 model of DIC, demonstrated superior cardioprotective effects in preventing cardiomyocyte toxicity compared to the shorter-term approach. For instance, resveratrol showed significant cardioprotective activity against DOX-induced H9c2 cell death when administered 24 hours before DOX exposure, compared to a 3-hour pretreatment (Monahan et al. 2021). This finding underscores the critical importance of optimizing the timing of cardioprotectant delivery to maximize its effectiveness in preventing cardiomyocyte toxicity. Consequently, in this study, we employed a longer-term prophylactic delivery, administering the CPAHs 24 hours before DOX exposure for an additional 24 h in H9c2 cells, to assess the effectiveness of CPAHs in preventing DIC.

The effects of drugs on cardiomyocytes are assessed by measuring compound cytotoxicity, determining the percentage of necrotic cells, observing changes in cardiomyocyte morphology, and evaluating the impact on cell proliferation (Tan et al. 2010). To evaluate cytotoxic effects, cell viability analyses are commonly performed. Researchers calculate the number of surviving cells compared to an untreated control group to effectively gauge the cytotoxicity of the compounds. By comparing the cell viability of groups treated with both a cardioprotectant and DOX to those treated with DOX alone, the effectiveness of the cardioprotectant in reducing DIC can be determined (Sangweni et al. 2020; Sirangelo et al. 2020; Zhou et al. 2022). This comprehensive approach enables a thorough understanding of how cardioprotective agents can counteract the adverse effects of DOX on cardiomyocytes.

Several methods are available to determine cell survival in cell viability analysis. Among these, the MTT assay (3-(4,5-dimethylthiazol-2-yl)-2,5-diphenyl-2H-tetrazolium bromide) has been widely used for nearly four decades. It is a common and reliable tool for measuring cell proliferation, viability, drug cytotoxicity,

and mitochondrial/metabolic activity. The MTT reagent is a mono-tetrazolium salt composed of a positively charged quaternary tetrazole ring core, which contains four nitrogen atoms and is flanked by three aromatic rings, including two phenyl groups and one thiazolyl ring (Berridge et al. 2005). The MTT reagent can cross both the cell membrane and the mitochondrial inner membrane of viable cells, probably because of its positive charge and lipophilic nature (Stockert et al. 2018). The MTT assay results generally correlate with the number of viable cells in culture. Viable cells reduce MTT, disrupting the core tetrazole ring and forming a violet-blue, water-insoluble molecule called formazan. The formazan is then solubilized with a solvent such as DMSO, and the optical density (OD) is measured by a microplate reader at around 570 nm. The OD values represent formazan concentration and, consequently, MTT reduction (Ghasemi et al. 2021).

Recently, several water-soluble tetrazolium (WST) dyes have been developed and utilized for cell viability analysis. These WST dyes offer a more straightforward application, eliminating the need to dissolve formazan crystals in organic solvents, thereby simplifying the procedure and reducing potential complications associated with traditional assays (Berridge et al. 2005). Enhanced sensitivity WST dyes, including WST-1, WST-5, and WST-8 [2-(2-methoxy-4-nitrophenyl)-3-(4-nitrophenyl)-5-(2,4-disulfophenyl)-2H-tetrazolium], have been developed for cell proliferation and cytotoxicity assays. Among these, WST-8 stands out for its superior stability and sensitivity, making it more effective in these applications (Tiwari et al. 2015). The WST-8 assay operates on the principle of converting tetrazolium dye into yellow formazan crystals via mitochondrial NAD-dependent succinate dehydrogenase. These crystals are then dissolved in an aqueous solution and analyzed with a spectrophotometer to measure absorbance values, which correlate with cell metabolic activity or viability. This method enables precise measurement of cell proliferation and cytotoxicity. Additionally, some WST dyes, like WST-8, are now offered as commercial kits with ready-to-use reagents for various bioassays, streamlining the procedure and ensuring consistent outcomes (Präbst et al. 2017). In this study, both the MTT and the WST-8 assay were utilized to determine cell viability and evaluate the cardioprotective activity of CPAH to prevent DIC.

2.10 STRUCTURE-ACTIVITY RELATIONSHIP STUDY

SAR examines the correlation between a drug's chemical structure and biological activity. It is pivotal in drug candidates' design, optimization, and refinement. SAR strategies focus on systematic structural modifications, such as altering substituents, adjusting chain lengths, and modifying ring systems. These modifications enhance pharmacokinetic and pharmacodynamic properties, improve target binding affinity, and reduce toxicity (Andricopulo and Montanari 2005).

To establish a SAR, the process begins with the systematic collection of data on compounds with similar structural features that demonstrate comparable biological activities. This approach facilitates the identification of key structural elements, such as functional groups, ring systems, and chain lengths, that significantly influence the compound's biological activity. By methodically tracking how alterations in these structural components correlate with changes in biological efficacy, researchers can establish a qualitative SAR. This process identifies structural features that enhance or diminish the compound's activity. The SAR methodology is widely applied in medicinal chemistry and drug design. As an example, Kollárová-Brázdová et al. (2020) conducted a detailed investigation into the SAR of dexrazoxane derivatives, the only approved drug for preventing DIC. They synthesized six analogs (**175–180**) by modifying the dioxopiperazine rings and evaluated their cardioprotective efficacy, as illustrated in Figure 2.12. Despite these structural alterations, none of the analogs showed improved cardioprotective activity, emphasizing the rigid structural constraints of bisdioxopiperazines in cardioprotective applications. Further pharmacokinetic studies confirmed that the lack of efficacy was not due to differences in absorption, distribution, metabolism, or excretion but attributed to changes in pharmacodynamic interactions. Additional studies by Hasinoff et al. (2020) demonstrated that the linker connecting the two bisdioxopiperazine rings is essential for the cardioprotective activity of dexrazoxane. This was strongly linked to the compounds' ability to inhibit the catalytic activity of topoisomerase II.

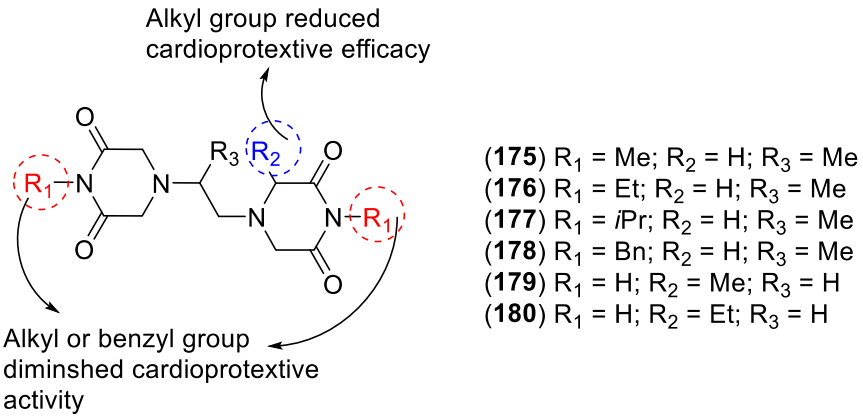

Figure 2.12 Dexrazoxane analogs (**175**–**180**) showed weak cardioprotective activity against DIC

Cuadrado and colleagues (2022) synthesized a series of labdane conjugates (**181**–**187**) to identify more potent cardioprotective agents against DIC, as depicted in Figure 2.13. These conjugates combined diterpene labdanodiol with various anti-inflammatory privileged structures, such as naphthalimide, furanonaphthoquinone, and naphthoquinone, to explore their SAR. Among the labdane conjugates with a triazole linker, only the compound containing a naphthalimide moiety (**183**) demonstrated significant cardioprotective activity. This suggests that the naphthalimide group plays a key role in enhancing the cardioprotective effects of these compounds. Additionally, in the series of labdane–furanonaphthoquinone conjugates, the nature of the substituent attached to the nitrogen atom significantly influenced the biological activity. Specifically, the labdane–furanonaphthoquinone conjugate with an *N*-cyclohexyl (**184**) group was the most effective, showing superior cardioprotective properties. These findings emphasize the importance of the nitrogen-linked moiety in interacting with specific residues of the biological target, thereby modulating the compound's activity. The study highlights that the size, shape, and flexibility of the nitrogen-substituent play a critical role in optimizing the compound's interaction with the target.

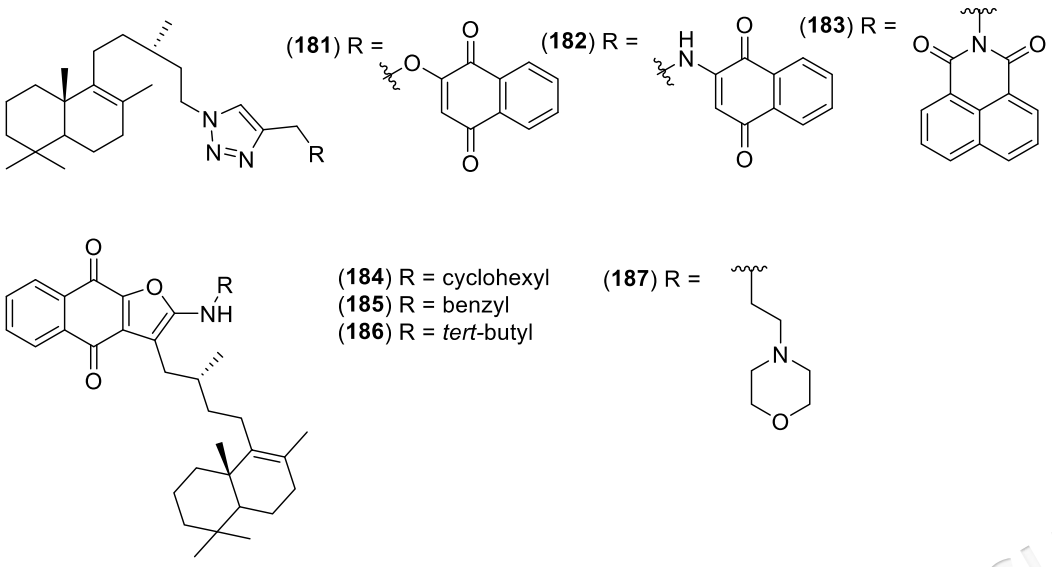

Figure 2.13 Labdane conjugates (**181**–**187**) showed weak to good cardioprotective activity against DIC

2.11 CONCLUSION

In conclusion, CA and PA are promising phytochemicals for the treatment of CVD. Their straightforward chemistry, ease of synthesis, and broad biological activity, both in natural and synthetic forms, position these scaffolds as valuable candidates for therapeutic applications, particularly in cardioprotection. Given their potent cardioprotective effects against DIC, hybrids combining both pharmacophores have been developed. Previous studies have highlighted the contribution of substituents on the ring and the linker to specific biological activities. As such, varying the number and position of substituents on the ring, as well as modifying the linker, was explored to identify the most effective hybrids for cardioprotective activity. This study focused on synthesizing twenty-one CPAHs (**1**–**21**) as potential cardioprotective agents by covalently linking CA with various PA scaffolds through acyl or alkyl linkers. The *in vitro* cardioprotective efficacy of these hybrids was evaluated against DOX-induced H9c2 cell death, providing insights into the SAR of the compounds.

CHAPTER III

METHODOLOGY

3.1 INTRODUCTION

This chapter discusses the general information, and methods used for the synthesis of CPAHs and *in vitro* study methods.

3.2 GENERAL INFORMATION

Commercially available reagents were used without further purification. Dry organic solvents were carefully prepared using appropriate methods before use. Other organic solvents met reagent grade standards and were used without further modification. To prevent unwanted reactions, reactions in dry solvents were meticulously controlled under an argon atmosphere throughout the experiment. Merck TLC plates (No. 5715) precoated with silica gel 60 F254 were used for analytical thin-layer chromatography (TLC). Kanto silica gel 60N, known for its spherical, neutral properties and particle sizes ranging from 40–50 or 63–210 μm, was used for column chromatography. Spectroscopic analyses, including ^{1}H (400 MHz) and ^{13}C NMR (100 MHz) spectra, were performed on a Bruker Avance III NMR spectrometer at i-CRIM laboratory UKM and JNM-ECS-400 spectrometer (JEOL) at Gifu University. For ^{1}H NMR measurements, tetramethylsilane (TMS; 0.0 ppm) was utilized as the internal standard, while $CDCl_3$ (δ = 77.0 ppm) was used for ^{13}C NMR measurements. ^{1}H NMR spectroscopic data is presented in a standardized format: chemical shift (multiplicity, coupling constants, integration), with multiplicity designations such as s (singlet), br. s. (broad singlet), d (doublet), dd (doublet of doublets), t (triplet), q (quartet), quin (quintet), spt (septet), and m (multiplet). The GC-MS in the instrumental laboratory, Faculty of Science and Technology, Universiti Kebangsaan Malaysia (UKM) is used to analyze the molecular weight of intermediate (**22**). High-resolution mass spectra

were meticulously recorded with a Waters Xevo Q-Tof mass spectrometer (ESI-TOF) at Gifu University.

3.3 GENERAL PROCEDURE TO SYNTHESIZE COMPOUNDS 1 – 10

Compounds **1-10** were synthesized following the protocols established by our research team, as detailed in previously published literature (Ashraf et al. 2017). The synthesis method involves a two-step reaction process, described below.

3.3.1 Synthesis of 5-Isopropyl-2-methylphenyl 2-chloroacetate (22)

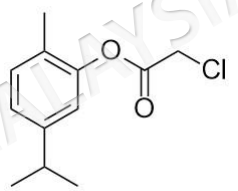

22

The synthesis of compound **22** employed the previously reported methods (Ashraf et al. 2017). TEA (5.0 mmol, 0.70 mL) and CA (5.0 mmol, 0.77 mL) are mixed in DCM (25 mL) at 0°C. The chloroacetyl chloride (5.0 mmol, 0.40 mL) in DCM is added dropwise to the reaction mixture under constant stirring for 1h. The reaction mixture is stirred at room temperature for 3 h. The reaction mixture is washed with water and dried over anhydrous $MgSO_4$. The $MgSO_4$ was removed using a filtration technique followed by solvent removal under reduced pressure. The reaction product is analyzed using GC-MS. The silica gel column chromatography is used to purify crude product using n-hexane: ethyl acetate (95:5) as eluent to afford compound **22** (colorless oil, 0.78 g, 3.5 mmol, 70%). ^{1}H NMR (400 MHz, $CDCl_3$) δ 1.21 (d, J = 6.8 Hz, 6H), 2.13 (s, 3H), 2.89 (m, 1H), 4.55 (s, 2H), 6.98 (d, J = 1.6 Hz, 1H), 7.08 (dd, J = 1.6, 7.6 Hz, 1H), 7.19 (d, J = 7.6 Hz, 1H). ESI-MS: m/z 226.1 [M^+].

3.3.2 Synthesis of compounds 1-10

The appropriate hydroxy-benzoic/cinnamic acid (2.5 mmol), potassium iodide (2.5 mmol, 0.42 g), TEA (2.5 mmol, 0.35 mL), and compound **22** (2.5 mmol, 0.55g) in dimethyl formamide (25.0 mL) were mixed and stirred at room temperature for 24 hours. The mixture was poured into ice and continually stirred after the completion of the reaction was reached. The product was extracted with ethyl acetate (3x25 mL). The crude product was obtained after removing the solvent under reduced pressure.

Then, the product was purified by silica gel column chromatography (n-hexane: ethyl acetate 4:1). This procedure was performed to prepare compounds **1-10**.

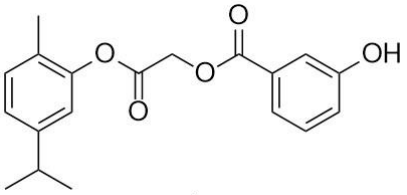

1

2-[(5-isopropyl-2-methyl)phenoxy]-2-oxoethyl 3-hydroxybenzoate (1) white solid (0.66 g, 2.0 mmol, 81%), ^{1}H NMR (400 MHz, Acetone-d_6) δ 1.20 (d, J = 6.8 Hz, 6H), 2.17 (s, 3H), 2.88 (sept, J = 6.8 Hz, 1H), 5.19 (s, 2H), 7.00 (d, J = 1.6 Hz, 1H), 7.05 (dd, J = 1.6, 7.6 Hz, 1H), 7.17 (d, J = 7.6 Hz, 1H), 7.19 (ddd, J = 1.2, 2.4, 8.0 Hz, 1H), 7.38 (dd, J = 7.6, 8.0 Hz, 1H), 7.66 (ddd, J = 1.2, 1.6, 7.6 Hz, 1H), 7.68 (dd, J = 1.6, 2.4 Hz, 1H), 8.84 (s, OH).^{13}C NMR (100 MHz, Acetone-d_6) δ 15.84, 24.20, 34.14, 61.82, 117.06, 120.37, 121.57, 121.74, 125.05, 128.02, 130.60, 131.38, 131.73, 148.84, 149.72, 158.33, 166.48, 167.05.HRMS (ESI-TOF) *m/z*: $[M+Na]^+$ calcd for $C_{19}H_{20}NaO_5^+$ requires: 351.1203; found 351.1202.

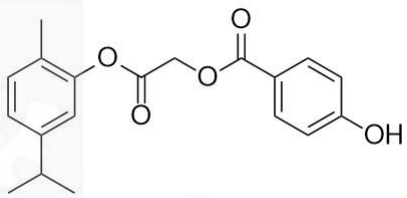

2

2-[(5-isopropyl-2-methyl)phenoxy]-2-oxoethyl 4-hydroxybenzoate (2) white solid (0.64 g, 1.9 mmol, 78%), ^{1}H NMR (400 MHz, Acetone-d_6) δ 1.20 (d, J = 6.8 Hz, 6H), 2.16 (s, 3H), 2.86 (sept, J = 6.8 Hz, 1H), 5.14 (s, 2H), 6.95 (d, J = 2.0 Hz, 1H), 6.97 (dd, J =2.8, 9.6 Hz, 2H), 7.06 (dd, J =2.0, 8.0 Hz, 1H), 7.18 (d, J = 8.0 Hz, 1H), 8.00 (dd, J =2.8, 9.6 Hz, 1H), 9.30(s, OH).^{13}C NMR (100 MHz, Acetone-d_6) δ 15.84, 24.26, 34.30, 61.64, 116.32, 120.57, 121.40, 125.13, 128.25, 132.89, 131.82, 148.99, 149.95, 163.32, 166.34, 167.38. HRMS (ESI-TOF) *m/z*: $[M+Na]^+$ calcd for $C_{19}H_{20}NaO_5^+$ requires: 351.1203; found 351.1212.

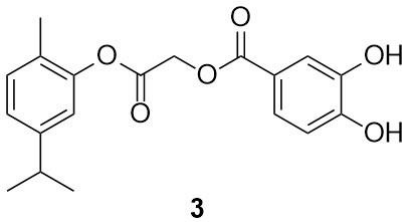

3

2-[(5-isopropyl-2-methyl)phenoxy]-2-oxoethyl 3,4-dihydroxybenzoate (3) white solid (0.67 g, 1.9 mmol, 78%), ^{1}H NMR (400 MHz, Acetone-d_6) δ 1.22 (d, J = 7.2 Hz, 6H), 2.17 (s, 3H), 2.93 (sept, J = 7.2 Hz, 1H), 5.16 (s, 2H), 7.00 (d, J = 1.6 Hz, 1H), 7.06 (dd, J =1.6, 8.0 Hz, 1H), 7.01 (d, J = 8.4 Hz, 1H), 7.19 (d, J = 8.0 Hz, 1H), 7.64 (dd, J =2.0, 8.4Hz, 1H), 7.69 (d, J = 2.0 Hz, 1H), 8.61 (s, 2OH).^{13}C NMR (100 MHz, Acetone-d_6) δ 15.82, 24.21, 34.17,

61.59, 117.46, 119.95, 120.42, 121.76, 123.94, 125.04, 128.06, 131.74, 145.67, 148.86, 149.79, 151.35, 166.37, 167.32.HRMS (ESI-TOF) *m/z*: $[M+Na]^+$ calcd for $C_{19}H_{20}NaO_6^+$ requires: 367.1152; found 367.1163.

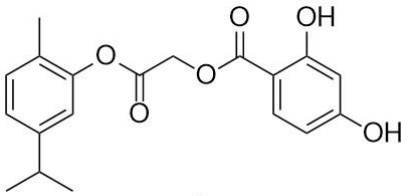

4

2-[(5-isopropyl-2-methyl)phenoxy]-2-oxoethyl 2,4-dihydroxybenzoate (4) white solid (0.689 g, 1.97 mmol, 81%), ^{1}H NMR (400 MHz, Acetone-d_6) δ 1.20 (d, *J* = 6.8 Hz, 6H), 2.14 (s, 3H), 2.91 (sept, *J* = 6.8 Hz, 1H), 5.22 (s, 2H), 6.44 (d, *J* = 2.0 Hz, 1H), 6.50 (dd, *J* =2.0, 8.8Hz, 1H), 6.99 (d, *J* = 2.0 Hz, 1H), 7.07 (dd, *J* =2.0, 8.0 Hz, 1H), 7.19 (d, *J* = 8.0 Hz, 1H), 7.84 (d, *J* = 8.8 Hz, 1H), 9.467 (s, 2OH).^{13}C NMR (100 MHz, Acetone-d_6) δ 15.83, 24.27, 34.33, 61.88, 103.58, 104.83, 109.46, 120.54, 125.25, 128.23, 131.89, 132.94, 149.08, 149.91, 165.04, 165.72, 166.93, 170.25.HRMS (ESI-TOF) *m/z*: $[M+Na]^+$ calcd for $C_{19}H_{20}NaO_6^+$ requires: 367.1152; found 367.1164.

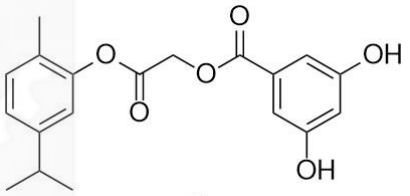

5

2-[(5-isopropyl-2-methyl)phenoxy]-2-oxoethyl 3,5-dihydroxybenzoate (5) white solid (0.437 g, 1.94 mmol, 81%), ^{1}H NMR (400 MHz, Acetone-d_6) δ 1.19 (d, *J* = 7.2 Hz, 6H), 2.14 (s, 3H), 2.87 (sept, *J* = 7.2 Hz, 1H), 5.15 (s, 2H), 6.70 (t, *J* = 2.4 Hz), 6.96 (d, *J* = 1.6 Hz, 1H), 7.03 (dd, *J* =1.6, 9.6 Hz, 1H), 7.16 (d, *J* = 9.6 Hz, 1H), 7.17 (d, *J* =2.0, 2.4 Hz, 2H), 8.68 (s, 2OH).^{13}C NMR (100 MHz, Acetone-d_6) δ 15.78, 24.17, 34.14, 61.82, 108.66, 109.01, 120.36, 125.07, 128.02, 131.73, 131.99, 148.87, 149.71, 159.45, 166.49, 167.09. HRMS (ESI-TOF) *m/z*: $[M+Na]^+$ calcd for $C_{19}H_{20}NaO_6^+$ requires: 367.1152; found 367.1128.

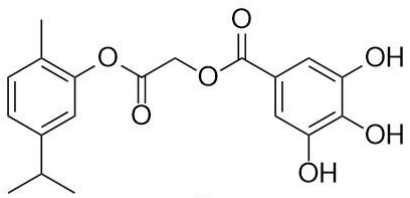

6

2-[(5-isopropyl-2-methyl)phenoxy]-2-oxoethyl3,4,5-trihydroxybenzoate (6) yellowish white solid (0.679 g, 1.21 mmol, 60%), ^{1}H NMR (400 MHz, Acetone-d_6) δ 1.21 (d, *J* =6.8 Hz, 6H), 2.16 (s, 3H),), 2.89 (sept, *J* =6.8 Hz, 1H), 5.16 (s, 2H), 6.98 (d, *J* =1.6 Hz, 1H), 7.06 (dd, *J* = 1.6, 8.0 Hz, 1H), 7.18 (d, *J* =8.0 Hz, 1H),

7.29 (s, 2H), 8.35 (s, 3OH). ^{13}C NMR (100 MHz, Acetone-d_6) δ 15.80, 24.20, 34.18, 61.63, 110.28, 120.43, 120.67, 125.04, 128.10, 131.75, 139.40, 146.12, 148.89, 149.79, 166.53, 167.34. HRMS (ESI-TOF) *m/z*: $[M+Na]^+$ calcd for $C_{19}H_{20}NaO_7^+$ requires: 383.1101; found 383.1099.

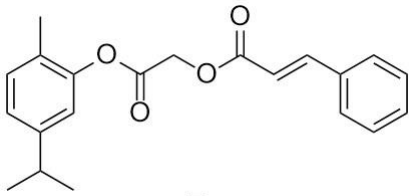

7

2-[(5-isopropyl-2-methyl)phenoxy]-2-oxoethyl (2E)-3-phenylprop-2-enoate (7) white solid (0.59 g, 1.7 mmol, 87%), ^{1}H NMR (400 MHz, Acetone-d_6) δ 1.22 (d, *J* = 6.8 Hz, 6H), 2.37 (s, 3H), 2.89 (sept, *J* =6.8 Hz, 1H), 5.14 (s, 2H), 6.70 (d, *J* =16.0 Hz, 1H), 7.03 (s, 1H), 7.07 (d, *J* = 8.0 Hz, 1H), 7.20 (d, *J* = 8.0 Hz, 1H), 7.40 (t, *J* =1.2 Hz, 3H), 7.63 (d, *J* =1.2 Hz, 2H), 7.87 (d, *J* =16.0 Hz, 1H). ^{13}C NMR (100 MHz, Acetone-d_6) δ 15.92, 24.32, 34.11, 61.43, 117.56, 120.40, 124.99, 128.05, 129.08, 129.71, 131.40, 131.73, 134.89, 146.81, 148.76, 149.74, 166.64, 167.06. HRMS (ESI-TOF) m/z: $[M+Na]^+$ calcd for $C_{21}H_{22}NaO_4^+$ requires: 361.1410; found 361.1420.

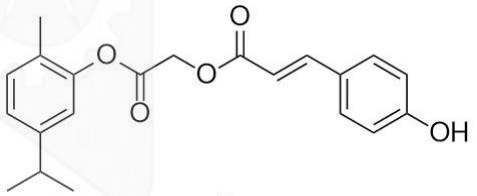

8

2-[(5-isopropyl-2-methyl)phenoxy]-2-oxoethyl (2E)-3-(4-hydroxyphenyl)prop-2-enoate (8) white solid (0.65 g, 1.8 mmol, 87%), ^{1}H NMR (400 MHz, Acetone-d_6) 1.20 (d, *J* = 6.8 Hz, 6H), 2.14 (s, 3H), 2.90 (sept, *J* = 6.8 Hz, 1H), 5.03 (s, 2H), 6.48 (d, *J* = 16.0 Hz, 1H), 6.92 (ddd, *J* =2.0, 2.8,9.6 Hz, 2H), 6.95 (d, *J* = 1.6 Hz, 1H), 7.06 (dd, *J* =1.6, 8.0 Hz, 1H), 7.18 (d, *J* = 8.0 Hz, 1H), 7.59 (ddd, *J* =2.0, 2.8, 9.6 Hz, 2H), 7.74 (d, *J* = 16.0 Hz, 1H), 9.08 (s, OH). ^{13}C NMR (100 MHz, Acetone-d_6) δ 15.84, 24.25, 34.29, 61.38, 114.19, 116.83, 120.55, 125.12, 126.75, 128.26, 131.29, 131.82, 147.02, 148.98, 149.95, 161.05, 167.17, 167.38. HRMS (ESI-TOF) m/z: $[M+Na]^+$ calcd for $C_{21}H_{22}NaO_5^+$ requires: 377.1359; found 377.1342.

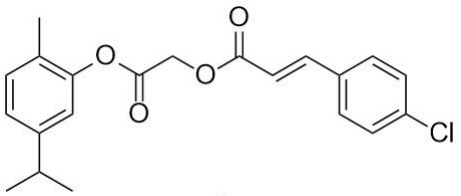

9

2-[(5-isopropyl-2-methyl)phenoxy]-2-oxoethyl (2E)-3-(4-chlorophenyl)prop-2-enoate (9) white solid (0.64 g, 1.7 mmol,

84%), ^{1}H NMR (400 MHz, Acetone-d_6), 1.20 (d, J = 6.8 Hz, 6H), 2.16 (s, 3H), 3.03 (sept, J = 6.8 Hz, 1H), 5.09 (s, 2H), 6.68 (d, J = 16.0 Hz, 1H), 6.97 (d, J = 1.6 Hz), 7.05 (dd, J = 8.0, 1.6 Hz, 1H), 7.18 (d, J = 8.0 Hz, 1H), 7.44 (ddd, J =1.6, 2.4, 6.86 Hz, 2H), 7.69 (ddd, J =1.6, 2.4, 6.8 Hz, 2H), 7.78 (d, J = 16.0 Hz, 1H).^{13}C NMR (100 MHz, Acetone-d_6) δ 15.88, 24.25, 34.25, 61.58, 118.54, 120.49, 125.12, 128.18, 129.97, 130.78, 131.83, 133.93, 136.82, 145.31, 148.92, 149.87, 166.55, 167.12. HRMS (ESI-TOF) m/z: $[M+Na]^+$ calcd for $C_{21}H_{21}ClNaO_4^+$ requires: 395.1021; found 395.1002.

2-[(5-isopropyl-2-methyl)phenoxy]-2-oxoethyl (2E)-3-(2,4-dihydroxyphenyl)prop-2-enoate (10) white solid (0.57 g, 1.5 mmol, 76%), ^{1}H NMR (400 MHz, Acetone-d_6), 1.19 (d, J = 7.2 Hz, 6H), 2.14 (s, 3H), 2.88 (sept, J = 7.2 Hz, 1H), 5.03 (s, 2H), 6.46 (dd, J =2.4, 8.8 Hz, 1H), 6.51 (d, J = 2.4 Hz, 1H), 6.60 (d, J = 16.0 Hz, 1H), 6.94 (d, J = 1.6 Hz, 1H), 7.03 (dd, J = 1.6, 8.0 Hz, 1H), 7.16 (d, J = 8.0 Hz, 1H), 7.48 (d, J = 8.8, Hz, 1H), 8.09 (d, J = 16.0 Hz, 1H), 9.07 (s, 2OH). ^{13}C NMR (100 MHz, Acetone-d_6) δ 15.81, 24.21, 34.19, 61.19, 103.64, 109.12, 113.52, 114.42, 120.47, 125.02, 128.16, 131.65, 131.74, 142.82, 148.88, 149.85, 159.44, 162.01, 167.47, 167.80. HRMS (ESI-TOF) m/z: $[M+Na]^+$ calcd for $C_{21}H_{22}NaO_6^+$ requires: 393.1309; found 393.1301.

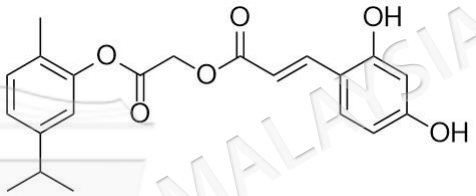

10

3.4 GENERAL PROCEDURE TO SYNTHESIZE COMPOUND 11

The synthesis of compound **11** involves several steps, as described below.

3.4.1 5-Isopropyl-2-methylphenyl 3-chloropropanoate (23a)

CA (0.154 mL, 1.00 mmol) was dissolved in DCM (2.0 mL) and cooled to 0°C. Py (0.121 mL, 1.50 mmol) was then slowly added drop by drop, followed by chloropropionyl chloride (0.119 mL, 1.25 mmol). The reaction mixture was stirred continuously at 0°C for 2 hours. After the reaction, the mixture was quenched with

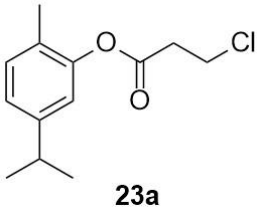

23a

saturated NH_4Cl (2 mL) and extracted with EtOAc (3 x 10 mL). The organic layer was washed with brine and dried with Na_2SO_4, and the solvent was evaporated under a vacuum. The crude product was further purified by column chromatography on silica gel (Hexane/EtOAc = 100:0 → 90:10, v/v) to afford compound **23a** (0.16 g, 0.68 mmol, 68%) as a colorless oil. ^{1}H NMR (400 MHz, $CDCl_3$) δ 1.25 (d, *J* = 6.9 Hz, 6H), 2.17 (s, 3H), 2.89 (spt, *J* = 6.9 Hz, 1H), 3.08 (t, *J* = 6.4 Hz, 2H), 3.90 (t, *J* = 6.4 Hz, 2H), 6.89 (d, *J* = 1.4 Hz, 1H), 7.04 (dd, *J* = 1.4, 7.8 Hz, 1H), 7.17 (d, *J* = 7.8 Hz, 1H). ^{13}C NMR (100 MHz, $CDCl_3$) δ 15.82, 23.84, 33.50, 37.54, 38.94, 119.58, 124.32, 127.06, 130.93, 148.11, 148.95, 168.56. HRMS (ESI-TOF) *m/z*: $[M + H]^+$ calcd for $C_{13}H_{18}ClO_2^+$ requires: 241.0990, found: 241.0986.

3.4.2 5-Isopropyl-2-methylphenyl acrylate (24)

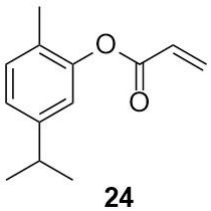

24

CA (0.154 mL, 1.00 mmol) and TEA (0.139 mL, 1.00 mmol) were mixed in DCM (2.5 mL) at 0°C. 3-chloropropionyl chloride (0.095 mL, 1.0 mmol) was added dropwise to the reaction mixture under constant stirring for 1 hour. The reaction mixture was stirred at room temperature for 3 hours. The reaction mixture was washed with water, extracted with ethyl acetate (10 mL x 3), and dried over anhydrous Na_2SO_4. The crude product was further purified by column chromatography on silica gel (Hexane/EtOAc = 100:0 → 90:10, v/v) to afford compound **24** (0.11 g, 0.54 mmol, 54%) as a colorless oil. ^{1}H NMR (400 MHz, $CDCl_3$) δ 1.29 (d, *J* = 6.9 Hz, 6H), 2.20 (s, 3H), 2.93 (spt, *J* = 6.9 Hz, 1H), 6.04 (dd, *J* = 10.3, 1.1 Hz, 1H), 6.39 (m, 1H), 6.66 (dd, *J* = 17.4, 1.1 Hz, 1H), 6.97 (d, *J* = 1.4 Hz,1H), 7.08 (dd, *J* = 7.8, 1.4 Hz, 1H), 7.21 (d, *J* = 7.8 Hz, 1H). ^{13}C NMR (100 MHz, $CDCl_3$) δ 15.64, 23.80, 33.47, 119.61, 124.08, 127.11, 127.76, 130.80, 132.23, 147.96, 149.02, 164.20. HRMS (ESI-TOF) *m/z*: $[M + H]^+$ calcd for $C_{13}H_{17}O_2^+$ requires: 205.1223; found 205.1219.

3.4.3 5-Isopropyl-2-methylphenyl 3-(benzyloxy)propanoate (25)

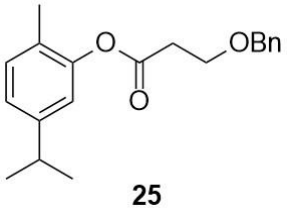

25

To a solution of CA (0.069 mL, 0.45 mmol) in DMF (1.0 mL) was added 3-(benzyloxy)propanoic acid (0.090 g, 0.50 mmol), succeeded by EDC.HCl (0.13 g, 0.68 mmol) and

DMAP (0.028 g, 0.23 mmol). The resulting mixture underwent overnight stirring at room temperature. Post-reaction, it was diluted with 10 mL of ethyl acetate, then subjected to sequential washing with 1 mL of 1 N HCl and 10 mL of water. Subsequent drying with Na_2SO_4, filtration, and concentration ensued. The crude product was purified by column chromatography on silica gel (Hexane/DCM/EtOAc = 175:25:10, v/v) to afford compound **25** (0.13 g, 0.41 mmol, 91%) as a colorless oil. ^{1}H NMR (400 MHz, $CDCl_3$) δ 1.23 (d, *J* = 6.9 Hz, 6H), 2.13 (s, 3H), 2.88 (m, 3H), 3.90 (t, *J* = 6.2 Hz, 2H), 4.60 (s, 2H), 6.87 (s, 1H), 7.02 (d, *J* = 7.8 Hz, 1H), 7.15 (d, *J* = 7.8 Hz, 1H), 7.30 – 7.37 (5H, m). ^{13}C NMR (100 MHz, $CDCl_3$) δ 15.76, 23.87, 33.51, 35.21, 65.70, 73.21, 119.74, 124.13, 127.19, 127.68, 128.38, 130.83, 137.96, 148.00, 149.17, 169.92. HRMS (ESI-TOF) *m/z*: $[M + Na]^+$ calcd for $C_{20}H_{24}NaO_3^+$ requires: 335.1618; found 335.1637.

3.4.4 5-Isopropyl-2-methylphenyl 3-hydroxypropanoate (26)

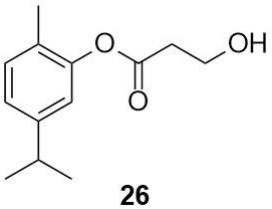

26

In a reaction setup, compound **25** (0.094 g, 0.30 mmol) was dissolved in 1.5 mL of ethanol. Subsequently, 0.03 mmol of 10% palladium on charcoal was added, and the solution was stirred under a hydrogen atmosphere at room temperature overnight. The resulting suspension was then filtered through celite©, washed with diethyl ether, and concentrated under vacuum. The crude product obtained underwent further purification via column chromatography on silica gel (Hexane/EtOAc = 100: 0 → 70:30, v/v) to afford compound **26** (0.060 g, 0.27 mmol, 90%) as a colorless oil. ^{1}H NMR (400 MHz, $CDCl_3$) δ 1.25 (d, *J* = 6.9 Hz, 6H), 2.15 (s, 3H), 2.65 (t, *J* = 5.7 Hz, OH), 2.89 (m, 3H), 3.99 (q, *J* = 5.7 Hz, 2H), 6.89 (s, 1H), 7.04 (d, *J* = 7.8 Hz, 1H), 7.16 (d, *J* = 7.8 Hz, 1H). ^{13}C NMR (100 MHz, $CDCl_3$) δ 15.38, 23.49, 33.14, 36.47, 57.77, 119.28, 123.91, 126.66, 130.54, 147.74, 148.59, 170.76. HRMS (ESI-TOF) *m/z*: $[M + Na]^+$ calcd for $C_{13}H_{18}NaO_3^+$ requires: 245.1148; found 245.1159.

3.4.5 3-((*tert*-Butyldimethylsilyl)oxy)benzoic acid (27)

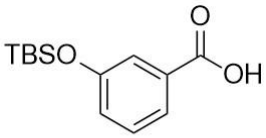

27

Compound**27** (white solid, 0.44 g, 1.7 mmol, 96%) was synthesized using the reported method, and its ^{1}H NMR spectrum was identical to that reported in the literature (Philippe et al. 2023). TEA (0.75 mL, 5.42 mmol) was added to 3HA (0.25 g, 1.81 mmol) in DCM (2.5 mL). Subsequently, a solution of TBSCl (0.55 g, 3.63 mmol) in DCM (1.25 mL) was added to the mixture and stirred for 2 hours at 25^{o}C. The mixture was concentrated under reduced pressure, yielding a residue. NaOH solution (2M, 1.0 mL) was added to the residue dissolved in THF (2.5 mL). The mixture was stirred for 0.5 hours at 25^{o}C. Water (10 mL) was added to the solution and its pH was adjusted to 6 with HCl solution (1 M). The mixture was extracted with EtOAC (10 mL x 3). The combined organic layer was washed with brine (10 mL), dried, filtered, and concentrated under reduced pressure. The residue was purified by silica gel column chromatography (Hexane/EtOAc = 100: 0 → 0:100, v/v) to give compound **27** (white solid, 0.44 g, 1.7 mmol, 96%).^{1}H NMR (400 MHz, $CDCl_3$) δ 0.23 (s, 6H), 1.00 (s, 9H), 7.10 (m, 1H), 7.36 (t, *J* = 8.0 Hz, 1H), 7.57 (s, 1H), 7.73 (d, *J* = 8.0 Hz, 1H).

3.4.6 3-(5-Isopropyl-2-methylphenoxy)-3-oxopropyl 3-((*tert*-butyldimethylsilyl)oxy)benzoate (28)

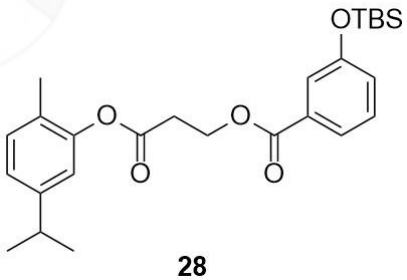

28

Compound **27** (0.095 g, 0.38 mmol) was dissolved in 2.5 mL of DCM. 1-(3-Dimethylaminopropyl)-3-ethylcarbodiimide hydrochloride (EDC.HCl) (0.10 g, 0.52 mmol) was added to the solution, followed by 4-dimethylaminopyridine (DMAP) (0.061 g, 0.50 mmol). The reaction mixture was stirred at room temperature for 1 hour. Then, compound **26** (0.056 g, 0.25 mmol) was added to the reaction mixture and stirred at room temperature overnight. The mixture was diluted with AcOEt (5 mL), washed with HCl (1N, 1 mL) and water (5 mL), then dried, filtered, and concentrated. The crude product was purified using column chromatography on silica gel (Hexane/DCM/EtOAc = 175:25:10, v/v) to afford compound **28** (0.073 g, 0.16 mmol, 64%) as a colorless gel. ^{1}H NMR (400 MHz,

$CDCl_3$) δ 0.22 (s, 6H), 1.00 (s, 9H), 1.22 (d, *J* = 6.9 Hz, 6H), 2.13 (s, 3H), 2.87 (spt, *J* = 6.9 Hz, 1H),3.07 (t, *J* = 6.2 Hz, 2H), 4.73 (t, *J* = 6.2 Hz, 2H), 6.87 (s, 1H), 7.05 (m, 2H), 7.14 (d, *J* = 7.8 Hz, 1H), 7.30 (t, *J* = 7.8 Hz, 1H), 7.53 (s, 1H), 7.67 (d, *J* = 7.8 Hz, 1H). ^{13}C NMR (100 MHz, $CDCl_3$) δ −4.49, 15.76, 18.13, 23.83, 25.59, 33.48, 34.06, 60.40, 119.59, 121.04, 122.59, 124.25, 124.97, 127.00, 129.38, 130.87, 131.11, 148.08, 149.01, 155.72, 166.06, 168.90. HRMS (ESI-TOF) *m/z*: $[M + Na]^+$ calcd for $C_{26}H_{36}NaO_5Si^+$ requires: 479.2224; found 479.2248.

3.4.7 3-(5-Isopropyl-2-methylphenoxy)-3-oxopropyl 3-hydroxybenzoate (11)

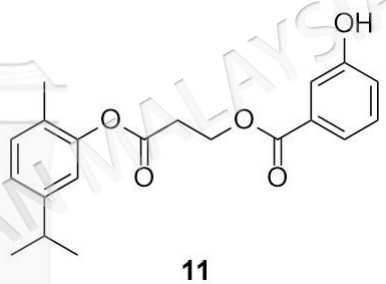

11

The first trial to remove the TBS group in compound **28** was done using tetrabutylammonium fluoride (TBAF). TBAF (1 M in THF, 0.130 mL, 0.130 mmol) was added to a solution of compound **28** (0.046 g, 0.10 mmol) in THF (3.0 mL). The reaction mixture was stirred at room temperature for 4 hours. Subsequently, the reaction was subjected to washing with brine, drying over Na_2SO_4, and concentration in vacuo. The residue was purified by column chromatography on silica gel (Hexane/AcOEt = 100:0 → 90:10, v/v). Unfortunately, the obtained product was not the desired product, but compound **24** in quantitatively amount (0.020 g, 0.10 mmol). An alternative method was explored using HF-Py; however, compound **28** needed to be resynthesized first. After obtaining a sufficient quantity of compound **28**, the compound (0.046 g, 0.10 mmol) was dissolved in 1.0 mL of THF, followed by the addition of 0.400 mL of pyridine at 0 °C. The solution was treated with 0.100 mL of HF-pyridine and warmed to 25 °C before shaking for 1 hour. TLC (EtOAc/hexanes, 20:80) was used to monitor the progress. Once completed, a 1:1 solution of AcOEt and saturated aqueous $NaHCO_3$ (3 mL) was added. AcOEt was used to dilute the reaction mixture. The organic phases were washed with aqueous NaCl and dried with Na_2SO_4. The crude product was purified using column chromatography on silica gel (Hexane/EtOAc = 100:0 → 80:20, v/v) to afford compound **11**(0.034 g, 0.10 mmol, quant.) as a white solid. ^1H NMR (400 MHz, $CDCl_3$) δ 1.20 (d, *J* = 6.9 Hz, 6H), 2.12 (s, 3H), 2.85 (spt, *J* = 6.9 Hz, 1H),3.06 (t, *J* = 6.0 Hz, 2H), 4.73 (t, *J* = 6.0 Hz, 2H), 6.29 (br.s., OH), 6.86 (s, 1H), 7.02 (m, 2H), 7.13 (d, *J* = 7.8 Hz, 1H), 7.28 (t, *J* = 7.8

Hz, 1H), 7.54 (s, 1H), 7.60 (d, *J* = 7.8 Hz, 1H). ^{13}C NMR (100 MHz, $CDCl_3$) δ 15.41, 23.48, 33.16, 33.77, 60.24, 115.98, 119.23, 120.20, 121.44, 124.05, 126.67, 129.35, 130.61, 147.86, 148.63, 155.74, 165.99, 168.96. HRMS (ESI-TOF) *m/z*: $[M + Na]^+$ calcd for $C_{20}H_{22}NaO_5^+$ requires: 365.1359; found 365.1354.

3.5 GENERAL PROCEDURE TO SYNTHESIZE COMPOUND 12

The synthesis of compound **12** involves two-step reactions, as described below.

3.5.1 5-Isopropyl-2-methylphenyl 4-chlorobutanoate (23b)

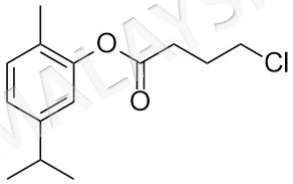

23b

According to the procedure for the synthesis of compound **22**, compound **23b** (0.13 g, 0.50 mmol, quant.) was obtained as a colorless oil from CA (0.078 mL, 0.50 mmol) and 4-chlorobutyryl chloride (0.056 mL, 0.50 mmol). ^{1}H NMR (400 MHz, $CDCl_3$) δ 1.26 (d, *J* = 6.9 Hz, 6H), 2.16 (s, 3H), 2.25 (quin, *J* = 6.8 Hz, 2H), 2.81 (t, *J* = 6.8 Hz, 2H), 2.90 (spt, *J* = 6.9 Hz, 1H), 3.70 (t, *J* = 6.8 Hz, 2H), 6.89 (d, *J* = 1.4 Hz, 1H), 7.05 (dd, *J* = 7.8,1.4 Hz, 1H), 7.17 (d, *J* = 7.8 Hz, 1H). ^{13}C NMR (100 MHz, $CDCl_3$) δ 15.40, 23.50, 27.21, 30.66, 33.15, 43.55, 119.29, 123.79, 126.64, 130.52, 147.70, 148.72, 170.55. HRMS (ESI-TOF) *m/z*: $[M + Na]^+$ calcd for $C_{14}H_{19}ClNaO_2^+$ requires: 277.0966; found 277.0943.

3.5.2 4-(5-Isopropyl-2-methylphenoxy)-4-oxobutyl 3-hydroxybenzoate (12)

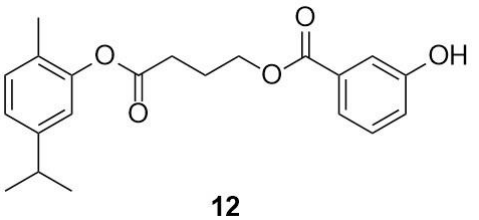

12

3-hydroxybenzoic acid (3HA) (0.069 g, 0.50 mmol) was dissolved in 0.5 mL of DMF. Subsequently, $NaHCO_3$ (0.13 g, 1.5 mmol) and KI (0.017 g, 0.10 mmol) were added to the solution of 3HA while stirring continuously for 1 hour at room temperature. Following this, a solution containing compound **23b** (0.13 g, 0.51 mmol) in 0.5 mL of DMF was added to the mixture, and the reaction was allowed to proceed with stirring at 70 °C overnight. Upon completion of the reaction, the resulting mixture was cautiously poured into 2 mL of water and then subjected to extraction with EtOAc (3 x 10 mL). The organic layer was washed

with water and subsequently dried over anhydrous Na_2SO_4. The solvent was then removed under a vacuum, and the crude product was purified by column chromatography on silica gel (Hexane/EtOAc = 100:0 → 80:20, v/v) to afford compound **12**(0.15 g, 0.41 mmol, 82%) as a white solid. ^{1}H NMR (400 MHz, $CDCl_3$) δ 1.20 (d, *J* = 6.9 Hz, 6H), 2.12 (s, 3H), 2.26 (quin, *J* = 6.6 Hz, 2H), 2.82 (m, 3H), 4.44 (t, *J* = 6.6 Hz, 2H), 6.07 (br. s., OH), 6.84 (s, 1H), 7.03 (d, m, 2H), 7.14 (d, *J* = 7.8 Hz, 1H), 7.30 (t, *J* = 7.8 Hz, 1H), 7.49 (s, 1H), 7.62 (d, *J* = 7.8 Hz, 1H). ^{13}C NMR (100 MHz, $CDCl_3$) δ 15.44, 23.50, 23.80, 30.75, 33.16, 63.90, 115.88, 119.41, 120.06, 121.48, 123.88, 126.70, 129.38, 130.61, 130.93, 147.87, 148.71, 155.64, 166.19, 171.24. HRMS (ESI-TOF) *m/z*: $[M + Na]^+$ calcd for $C_{21}H_{24}NaO_5^+$ requires: 379.1516; found 379.1504.

3.6 GENERAL PROCEDURE TO SYNTHESIZE COMPOUND 13

The synthesis of compound **13** consists of a two-step reaction process, detailed below.

3.6.1 2-(2-Bromoethoxy)-4-isopropyl-1-methylbenzene (29a)

CA (0.102 mL, 0.658 mmol) was heated at 70°C and stirred with 1,2-dibromoethane (0.75 mL). Subsequently, the reaction mixture was treated with KOH (0.055 g, 1.0 mmol), which was continuously stirred for 6 hours. Upon completion of the reaction, the mixture was cooled to room temperature and filtered to eliminate the colorless solid precipitate. The crude product was purified by column chromatography on silica gel (Hexane/EtOAc = 100:0 → 95:5, v/v) to afford compound **29a** (0.12 g, 0.47 mmol, 72%) as a colorless oil. ^{1}H NMR (400 MHz, $CDCl_3$) δ 1.28 (d, *J* = 6.9 Hz, 6H), 2.26 (s, 3H), 2.90 (spt, *J* = 6.9 Hz, 1H), 3.69 (t, *J* = 6.4 Hz, 2H), 4.33 (t, *J* = 6.4 Hz, 2H), 6.71 (s, 1H), 6.81 (dd, *J* = 7.6, 1.1 Hz,1H), 7.11 (d, *J* = 7.6 Hz, 1H). ^{13}C NMR (100 MHz, $CDCl_3$) δ 15.74, 24.08, 29.54, 34.05, 67.98, 109.97, 118.87, 124.49, 130.66, 147.93, 156.12. HRMS (ESI-TOF) *m/z*: $[M + H]^+$ calcd for $C_{12}H_{18}BrO^+$ requires: 257.0536; found: 257.0551.

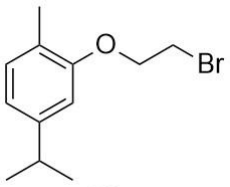

29a

3.6.2 2-(5-Isopropyl-2-methylphenoxy)ethyl 3-hydroxybenzoate (13)

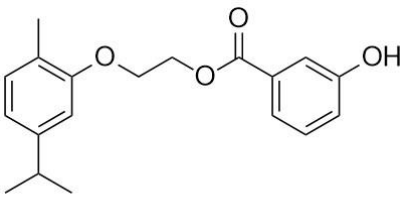

13

According to the procedure for the synthesis of compound **12**, compound **13** (0.15 g, 0.48 mmol, 96%) was obtained as a white solid from compound **29a** (0.13 g, 0.51 mmol) and 3HA (0.069 g, 0.50 mmol). ^{1}H NMR (400 MHz, $CDCl_3$) δ 1.24 (d, *J* = 6.9 Hz, 6H), 2.19 (s, 3H), 2.85 (m, 1H), 4.32 (m, 2H), 4.68 (m, 2H), 5.25 (s, OH), 6.73 (s, 1H), 6.77 (d, *J* = 7.8 Hz,1H), 7.06 (m, 2H), 7.31 (t, *J* = 8.0 Hz, 1H), 7.50 (d, *J* = 1.4 Hz, 1H), 7.63 (d, *J* = 7.8 Hz, 1H). ^{13}C NMR (100 MHz, $CDCl_3$) δ 15.47, 23.78, 33.78, 63.41, 65.85, 109.66, 115.99, 118.36, 119.97, 121.84, 124.21, 129.41, 130.30, 131.01, 147.69, 155.31, 156.30, 166.07. HRMS (ESI-TOF) *m/z*: $[M + Na]^+$ calcd for $C_{19}H_{22}NaO_4^+$ requires: 337.1410; found 337.1432.

3.7 GENERAL PROCEDURE TO SYNTHESIZE COMPOUND 14

The synthesis of compound **14** consists of a two-step reaction process, detailed below.

3.7.1 2-(3-Bromopropoxy)-4-isopropyl-1-methylbenzene (29b)

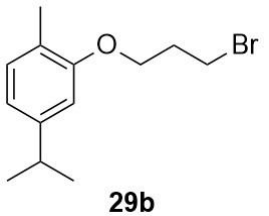

29b

According to the procedure for the synthesis of compound **29a**, compound **29b** (0.17 g, 0.63 mmol, 96%) was obtained as a colorless oil from CA (0.102 mL, 0.658 mmol) and 1,3-dibromopropane (0.75 mL). ^{1}H NMR (400 MHz, $CDCl_3$) δ 1.27 (d, *J* = 6.9 Hz, 6H), 2.20 (s, 3H), 2.36 (quin, *J* = 6.4 Hz, 2H), 2.89 (spt, *J* = 6.9 Hz, 1H), 3.66 (t, *J* = 6.4 Hz, 2H), 4.13 (t, *J* = 6.4 Hz, 2H), 6.73 (s, 1H), 6.77 (d, *J* = 7.8 Hz, 1H), 7.08 (d, *J* = 7.8 Hz, 1H).^{13}C NMR (100 MHz, $CDCl_3$) δ 15.77, 24.11, 30.20, 32.64, 34.11, 65.13, 109.49, 118.27, 124.05, 130.45, 147.95, 156.61. HRMS (ESI-TOF) *m/z*: $[M + H]^+$ calcd for$C_{13}H_{20}BrO^+$ requires: 271.0692; found 271.0704.

3.7.2 3-(5-Isopropyl-2-methylphenoxy)propyl 3-hydroxybenzoate (14)

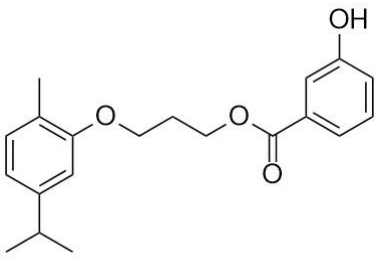

14

According to the procedure for the synthesis of compound **12**, compound **14** (0.14 g, 0.43 mmol, 86%) was obtained as a white solid from compound **29b** (0.14 g, 0.52 mmol) and 3HA (0.069 g, 0.50 mmol). ^{1}H NMR (400 MHz, $CDCl_3$) δ 1.23 (d, *J* = 6.9 Hz, 6H), 2.19 (s, 3H), 2.27 (quin, *J* = 6.4 Hz, 2H), 2.85 (spt, *J* = 6.9 Hz, 1H), 4.14 (t, *J* = 6.4 Hz, 2H), 4.54 (t, *J* = 6.4 Hz, 2H), 6.22 (s, OH), 6.71 (s, 1H), 6.74 (d, *J* = 7.8 Hz,1H), 7.05 (m, 2H), 7.29 (m, 1H), 7.51 (m, 1H), 7.59 (d, *J* = 7.8 Hz, 1H). ^{13}C NMR (100 MHz, $CDCl_3$) δ 15.80, 24.11, 28.93, 34.11, 62.07, 64.20, 109.45, 116.30, 118.16, 120.21, 121.66, 124.18, 129.60, 130.47, 131.59, 147.93, 156.07, 156.81, 166.46. HRMS (ESI-TOF) *m/z*: $[M + Na]^+$ calcd for $C_{20}H_{24}NaO_4^+$ requires: 351.1567; found 351.1560.

3.8 GENERAL PROCEDURE TO SYNTHESIZE COMPOUND 15

The synthesis of compound **15** consists of a two-step reaction process, detailed below.

3.8.1 2-(4-Bromobutoxy)-4-isopropyl-1-methylbenzene (29c)

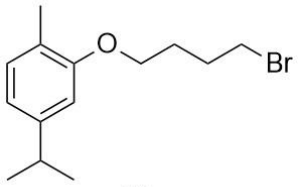

29c

According to the procedure for the synthesis of compound **29a**, compound **29c** (0.18 g, 0.63 mmol, 96%) was obtained as a colorless oil from CA (0.102 mL, 0.658 mmol) and 1,4-dibromobutane (0.75 mL). ^{1}H NMR (400 MHz, $CDCl_3$) δ 1.26 (d, *J* = 6.9 Hz, 6H), 1.98 (m, 2H) 2.12 (m, 2H), 2.20 (s, 3H), 2.88 (spt, *J* = 6.9 Hz, 1H), 3.53 (t, *J* = 6.6 Hz, 2H), 4.03 (t, *J* = 6.6 Hz, 2H), 6.70 (s, 1H), 6.75 (d, *J* = 7.3 Hz,1H), 7.07 (d, *J* = 7.3 Hz, 1H).^{13}C NMR (100 MHz, $CDCl_3$) δ 15.83, 24.12, 27.99, 29.64, 33.62, 34.13, 66.64, 109.24, 118.03, 124.01, 130.40, 147.88, 156.84. HRMS (ESI-TOF) *m/z*: $[M + H]^+$ calcd for $C_{14}H_{22}BrO^+$ requires: 285.0849; found 285.0846.

3.8.2 4-(5-Isopropyl-2-methylphenoxy)butyl 3-hydroxybenzoate (15)

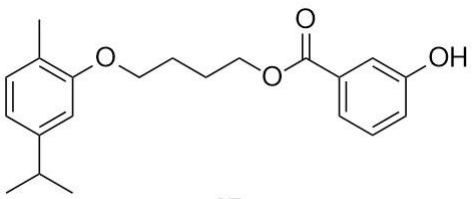

15

According to the procedure for the synthesis of compound **12**, compound **15** (0.14 g, 0.40 mmol, 81%) was obtained as a white solid from compound **29c** (0.14 g, 0.49 mmol) and 3HA (0.069 g, 0.50 mmol). ^{1}H NMR (400 MHz, $CDCl_3$) δ 1.24 (d, *J* = 6.4 Hz, 6H), 2.04 (m, 4H), 2.21 (s, 3H), 2.87 (spt, *J* = 6.4 Hz, 1H), 4.07 (t, *J* = 4.8 Hz, 2H), 4.43 (t, *J* = 4.8 Hz, 2H), 5.24 (s, OH), 6.71 (s, 1H), 6.76 (d, *J* = 7.8 Hz,1H), 7.06 (m, 2H), 7.31 (t, *J* = 7.8 Hz, 1H), 7.45 (s, 1H), 7.62 (d, *J* = 7.8 Hz, 1H). ^{13}C NMR (100 MHz, $CDCl_3$) δ 15.53, 23.78, 25.12, 26.04, 33.81, 64.80, 66.65, 109.03, 115.81, 117.63, 119.80, 121.61, 123.82, 129.37, 130.09, 131.33, 147.64, 155.37, 156.63, 166.21. HRMS (ESI-TOF) *m/z*: $[M + Na]^+$ calcd for $C_{21}H_{26}NaO_4^+$ requires: 365.1723; found 365.1709.

3.9 GENERAL PROCEDURE TO SYNTHESIZE COMPOUND 16

The synthesis of compound **16** consists of a three-step reaction process, detailed below.

3.9.1 4-(((*tert*-Butyldimethylsilyl)oxy)methyl)-5-isopropyl-2-methylphenyl 2-chloroacetate (31a)

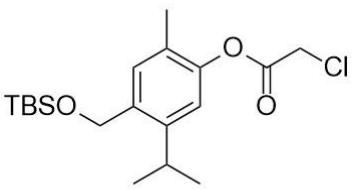

31a

According to the procedure for the synthesis of compound **22**, compound **31a** (0.15 g, 0.40 mmol, 80%) was obtained as a colorless oil from compound **30** (0.15 g, 0.51 mmol) and chloroacetyl chloride (0.040 mL, 0.50 mmol). ^{1}H NMR (400 MHz, $CDCl_3$) δ 0.12 (s, 6H), 0.95 (s, 9H), 1.21 (d, *J* = 6.9 Hz, 6H), 2.16 (s, 3H), 3.10 (spt, *J* = 6.9 Hz, 1H), 4.32 (s, 2H), 4.73 (s, 2H), 6.93 (s, 1H), 7.27 (s, 1H). ^{13}C NMR (100 MHz, $CDCl_3$) δ −5.62, 15.39, 18.04, 23.31, 25.61, 27.86, 40.42, 62.14, 117.67, 126.19, 129.91, 135.55, 145.15, 147.93, 165.34. HRMS (ESI-TOF) *m/z*: $[M + Na]^+$ calcd for $C_{19}H_{31}ClNaO_3Si^+$ requires: 393.1623; found 393.1622.

3.9.2 2-(4-(((*tert*-Butyldimethylsilyl)oxy)methyl)-5-isopropyl-2-methylphenoxy)-2-oxoethyl 3-hydroxybenzoate (32a)

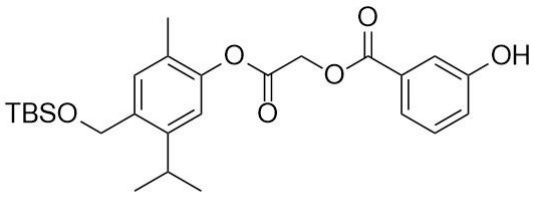

32a

3HA (0.028 g, 0.20 mmol), KI (0.003 g, 0.2 mmol), TEA (0.028 mL, 0.20 mmol), and compound **31a** (0.059 g, 0.20 mmol) in DMF (0.5 mL) were mixed and stirred at room temperature for 12 hours. After the completion of the reaction, the mixture was poured into ice (2 mL) and continuously stirred. The product was extracted with ethyl acetate (3x10 mL). The crude product was obtained after the solvent was removed under reduced pressure. Subsequently, the product was purified by silica gel column chromatography on silica gel (Hexane/EtOAc = 100:0 → 60:40, v/v) to afford compound **32a** (0.085 g, 0.18 mmol, 90%) as a colorless gel.^{1}H NMR (400 MHz, $CDCl_3$) δ 0.10 (s, 6H), 0.94 (s, 9H), 1.19 (d, *J* = 6.9 Hz, 6H), 2.17 (s, 3H), 3.09 (spt, *J* = 6.9 Hz, 1H), 4.71 (s, 2H), 5.11 (s, 2H), 5.39 (s, OH), 6.95 (s, 1H), 7.04 (d, *J* = 8.0 Hz, 1H), 7.25 (br.s., 1H), 7.31 (t, *J* = 8.0 Hz, 1H), 7.56 (s, 1H), 7.69 (d, *J* = 8.0 Hz, 1H).^{13}C NMR (100 MHz, $CDCl_3$) δ −5.61, 15.49, 18.05, 23.32, 25.62, 27.88, 60.78, 62.19, 116.24, 117.86, 120.45, 122.03, 126.39, 129.47, 129.95, 130.02, 135.40, 145.13, 147.71, 155.42, 165.45, 166.03. HRMS (ESI-TOF) *m/z*: $[M + Na]^+$ calcd for $C_{26}H_{36}NaO_6Si^+$ requires: 495.2173; found 495.2163.

3.9.3 2-(4-(Hydroxymethyl)-5-isopropyl-2-methylphenoxy)-2-oxoethyl 3-hydroxybenzoate (16)

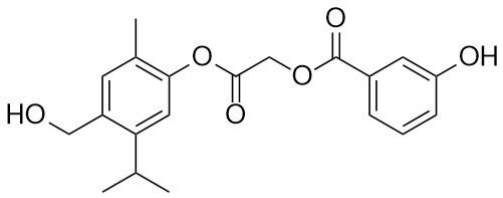

16

According to the procedure for the synthesis of compound **11**, compound **16** (0.029 g, 0.080 mmol, 80%) was obtained as a white solid from compound **32a** (0.047 g, 0.10 mmol) and HF-pyridine (0.100 mL). ^{1}H NMR (400 MHz, Methanol-d_4) δ 1.17 (d, *J* = 6.4 Hz, 6H), 2.11 (s, 3H), 3.19 (m, 1H), 4.59 (s, 2H), 5.09 (s, 2H), 6.96 (s, 1H), 7.01 (m, 1H), 7.19 (s, 1H), 7.27 (t, *J* = 8.0 Hz, 1H), 7.47 (s, 1H), 7.53 (d, *J* = 8.0 Hz, 1H).^{13}C NMR (100 MHz, Methanol-

d4) δ15.71, 24.11, 29.46, 62.17, 62.33, 117.18, 119.55, 121.72, 121.84, 128.18, 130.67, 131.56, 132.29, 137.01, 147.49, 149.84, 158.83, 167.47, 168.14. HRMS (ESI-TOF) *m/z*: $[M + Na]^+$ calcd for $C_{20}H_{22}NaO_6^+$ requires: 381.1309; found 381.1298.

3.10 GENERAL PROCEDURE TO SYNTHESIZE COMPOUND 17

The synthesis of compound **17** consists of a four-step reaction process, detailed below.

3.10.1 4-(((*tert*-Butyldimethylsilyl)oxy)methyl)-5-isopropyl-2-methylphenyl 3-(benzyloxy)propanoate (33)

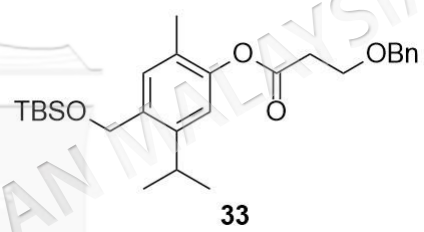

33

According to the procedure for the synthesis of compound **25**, compound **33** (0.43 g, 0.94 mmol, 94%) was obtained as a colorless oil from compound **30** (0.29 g, 0.10 mmol) and 3-(benzyloxy)propanoic acid (0.22 g, 1.2 mmol).[1]H NMR (400 MHz, $CDCl_3$) δ 0.13 (s, 6H), 0.96 (s, 9H), 1.22 (d, *J* = 6.9 Hz, 6H), 2.13 (s, 3H), 2.90 (t, *J* = 6.2 Hz, 2H), 3.12 (m, 1H), 3.91 (t, *J* = 6.2 Hz, 2H), 4.61 (s, 2H), 4.74 (s, 2H), 6.91 (s, 1H), 7.26 (s, 1H), 7.31–7.39 (m, 5H). ^{13}C NMR (100 MHz, $CDCl_3$) δ −5.62, 15.51, 18.03, 23.34, 25.61, 27.84, 34.87, 62.25, 65.39, 72.88, 118.08, 126.49, 127.33, 128.05, 129.81, 134.94, 137.64, 144.92, 148.33, 169.57. HRMS (ESI-TOF) *m/z*: $[M + Na]^+$ calcd for $C_{27}H_{40}NaO_4Si^+$ requires: 479.2588; found 479.2597.

3.10.2 4-(((*tert*-Butyldimethylsilyl)oxy)methyl)-5-isopropyl-2-methylphenyl 3-hydroxypropanoate (34)

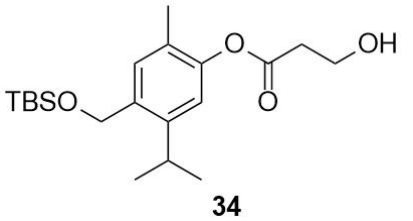

34

According to the procedure for the synthesis of compound **26**, compound **34** (0.22 g, 0.60 mmol, 80%) was obtained as a colorless oil from compound **33** (0.34 g, 0.75 mmol). ^{1}H NMR (400 MHz, $CDCl_3$) δ 0.11 (s, 6H), 0.95 (s, 9H), 1.21 (d, *J* = 6.9 Hz, 6H), 2.15 (s, 3H), 2.40 (m, OH), 2.86 (t, *J* = 5.5 Hz, 2H), 3.10 (spt, *J* = 6.9 Hz, 1H), 4.00 (q, *J* = 5.5 Hz, 2H), 4.72 (s, 2H), 6.90 (s, 1H), 7.26 (s, 1H). ^{13}C NMR (400 MHz, $CDCl_3$) δ −5.61, 15.54, 18.05, 23.35, 25.61, 27.85, 36.43, 57.88, 62.21,

117.99, 126.33, 129.86, 135.18, 145.05, 148.08, 170.89. HRMS (ESI-TOF) *m/z*: $[M + Na]^+$ calcd for $C_{20}H_{34}NaO_4Si^+$ requires: 389.2119; found 389.2133.

3.10.3 3-(4-(((*tert*-Butyldimethylsilyl)oxy)methyl)-5-isopropyl-2-methylphenoxy)-3-oxopropyl 3-((*tert*-butyldimethylsilyl)oxy)benzoate (35)

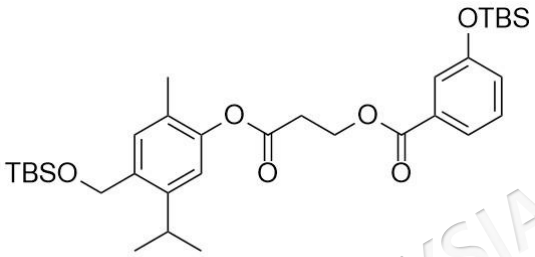

35

According to the procedure for the synthesis of compound **28**, compound **35** (0.096 g, 0.16 mmol, 64%) was obtained as a colorless gel from compound **34** (0.092 g, 0.25 mmol) and compound **27** (0.10 g, 0.38 mmol). ^{1}H NMR (400 MHz, $CDCl_3$) δ 0.10 (s, 6H), 0.21 (s, 6H), 0.94 (s, 9H), 0.99 (s, 9H), 1.18 (d, *J* = 6.9 Hz, 6H), 2.13 (s, 3H), 3.09 (m, 3H), 4.72 (m, 4H), 6.88 (s, 1H), 7.05 (m, 1H), 7.24 (s, 1H), 7.29 (t, *J* = 8.0 Hz, 1H), 7.52 (m, 1H), 7.66 (d, *J* = 8.0 Hz, 1H). ^{13}C NMR (100 MHz, $CDCl_3$) δ −5.61, −4.78, 15.57, 17.85, 18.05, 23.33, 25.30, 25.62, 27.83, 33.79, 60.12, 62.19, 117.95, 120.77, 122.28, 124.67, 126.34, 129.08, 129.81, 130.82, 135.15, 145.01, 148.17, 155.43, 165.78, 168.64. HRMS (ESI-TOF) *m/z*: $[M + Na]^+$ calcd for $C_{33}H_{52}NaO_6Si_2^+$ requires: 623.3195; found 623.3186.

3.10.4 3-(4-(Hydroxymethyl)-5-isopropyl-2-methylphenoxy)-3-oxopropyl 3-hydroxybenzoate (17)

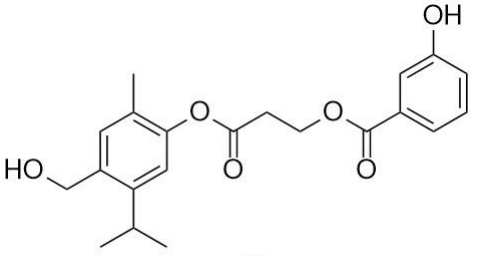

17

According to the procedure for the synthesis of compound **11**, compound **17** (0.056 g, 0.15 mmol, quant.) was obtained as a white solid from **35** (0.090 g, 0.15 mmol) and HF-pyridine (0.200 mL). ^{1}H NMR (400 MHz, Methanol-d_4) δ 1.12 (d, *J* = 6.9 Hz, 6H), 2.05 (s, 3H), 3.04 (t, *J* = 6.0 Hz, 2H), 3.16 (spt, *J* = 6.9 Hz, 1H),4.57 (s, 2H), 4.62 (t, *J* = 6.0 Hz, 2H), 6.86 (s, 1H), 6.99 (dd, *J* = 1.8, 8.0 Hz, 1H), 7.16 (s, 1H), 7.24 (t, *J* = 8.0 Hz, 1H), 7.41 (d, *J* = 2.3 Hz, 1H), 7.47 (m, 1H).^{13}C NMR (100 MHz, Methanol-d4) δ 15.82, 24.10, 29.42, 34.83, 61.17, 62.36, 117.03, 119.65, 121.36, 121.54, 128.11,

130.59, 132.22, 132.27, 136.76, 147.46, 150.31, 158.84, 167.65, 170.99. HRMS (ESI-TOF) *m/z*: $[M + Na]^+$ calcd for $C_{21}H_{24}NaO_6^+$ requires: 395.1465; found 395.1463.

3.11 GENERAL PROCEDURE TO SYNTHESIZE COMPOUND 18

The synthesis of compound **18** involves three-step reactions, as described below.

3.11.1 4-(((*tert*-Butyldimethylsilyl)oxy)methyl)-5-isopropyl-2-methylphenyl 4-chlorobutanoate (31b)

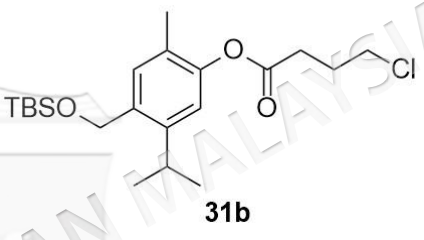

31b

According to the procedure for the synthesis of compound **23b**, compound **31b** (0.20 g, 0.50 mmol, 98%) was obtained as a colorless oil from compound **30** (0.15 g, 0.51 mmol) and 4-chlorobutyryl chloride (0.056 mL, 0.50 mmol). ^{1}H NMR (400 MHz, $CDCl_3$) δ 0.12 (s, 6H), 0.95 (s, 9H), 1.22 (d, *J* = 6.9 Hz, 6H), 2.15 (s, 3H), 2.24 (quin, *J* = 6.6 Hz, 2H), 2.80 (t, *J* = 6.6 Hz, 2H), 3.12 (m, 1H), 3.70 (t, *J* = 6.6 Hz, 2H), 4.73 (s, 2H), 6.90 (s, 1H), 7.26 (s, 1H). ^{13}C NMR (100 MHz, $CDCl_3$) δ −5.32, 15.82, 18.32, 23.64, 25.90, 27.56, 28.14, 31.03, 43.92, 62.53, 118.30, 126.60, 130.15, 135.32, 145.31, 148.54, 170.92. HRMS (ESI-TOF) *m/z*: $[M + Na]^+$ calcd for $C_{21}H_{35}ClNaO_3Si^+$ requires: 421.1936; found 421.1952.

3.11.2 4-(4-(((*tert*-Butyldimethylsilyl)oxy)methyl)-5-isopropyl-2-methylphenoxy)-4-oxobutyl 3-hydroxybenzoate) (32b)

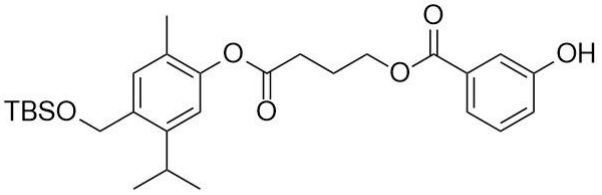

32b

According to the procedure for the synthesis of compound **12**, compound **32b** (0.20 g, 0.40 mmol, 80%) was obtained as a white solid from compound **31b** (0.20 g, 0.50 mmol) and 3HA (0.069 g, 0.50 mmol). ^{1}H NMR (400 MHz, $CDCl_3$) δ 0.12 (s, 6H), 0.95 (s, 9H), 1.19 (d, *J* = 6.9 Hz, 6H), 2.13 (s, 3H), 2.26 (quin, *J* = 6.8 Hz, 2H), 2.79 (t, *J* = 6.8 Hz, 2H), 3.10 (m, 1H), 4.45 (t, *J* = 6.8 Hz, 2H), 4.72 (s, 2H), 6.82 (br. s., OH), 6.89 (s, 1H), 7.01 (dd, *J* = 2.1,8.0 Hz, 1H), 7.25 (s, 1H), 7.28 (m, 1H), 7.53 (s,

1H), 7.60 (d, *J* = 8.0 Hz, 1H). ^{13}C NMR (100 MHz, $CDCl_3$) δ −5.30, 15.87, 18.36, 23.62, 24.17, 25.93, 28.17, 30.92, 62.54, 64.06, 116.26, 118.33, 120.32, 121.78, 126.65, 129.66, 130.19, 131.32, 135.38, 145.36, 148.55, 155.94, 166.44, 171.34. HRMS (ESI-TOF) *m/z*: $[M + Na]^+$ calcd for $C_{28}H_{40}NaO_6Si^+$ requires: 523.2486; found 523.2477.

3.11.3 4-(4-(Hydroxymethyl)-5-isopropyl-2-methylphenoxy)-4-oxobutyl 3-hydroxybenzoate (18)

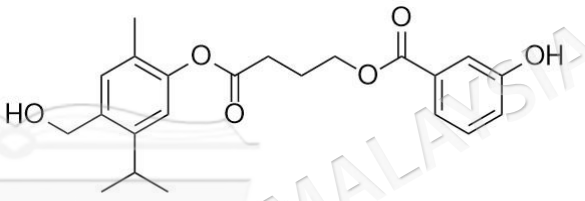

18

TBAF (1 M in THF, 0.192 mL, 0.192 mmol) was added to a solution of compound **32b** (0.080 g, 0.16 mmol) in THF (3.0 mL). The reaction mixture was stirred at room temperature for 4 hours. Subsequently, the reaction was subjected to washing with brine, drying over Na_2SO_4, and concentration in vacuo. The resulting residue was purified by column chromatography on silica gel (Hexane/EtOAc = 100:0 → 60:40, v/v) to afford compound **18** (0.032 g, 0.11 mmol, 70%) as white solid. ^{1}HNMR (400 MHz, Methanol-d_4) δ 1.15 (d, *J* = 6.9 Hz, 6H), 2.06 (s, 3H), 2.15 (quin, *J* = 6.8 Hz, 2H), 2.75 (t, *J* = 6.8 Hz, 2H), 3.18 (spt, *J* = 6.9 Hz, 1H), 4.37 (t, *J* = 6.8 Hz, 2H), 4.58 (s, 2H), 6.88 (s, 1H), 6.98 (dd, *J* = 2.1, 7.6 Hz, 1H), 7.17 (s, 1H), 7.23 (m, 1H), 7.41 (d, *J* = 2.3 Hz, 1H), 7.46 (d, *J* = 7.6 Hz, 1H). ^{13}C NMR (100 MHz, Methanol-d4) δ 16.24, 24.55, 25.56, 29.89, 31.80, 62.81, 65.38, 117.37, 120.18, 121.67, 121.99, 128.50, 131.01, 132.64, 132.94, 137.05, 147.83, 150.83, 159.20, 168.39, 173.41. HRMS (ESI-TOF) *m/z*: $[M + Na]^+$ calcd for $C_{22}H_{26}NaO_6^+$ requires: 409.1622; found 409.1605.

3.12 GENERAL PROCEDURE TO SYNTHESIZE COMPOUND 19

The synthesis of compound **19** involves three-step reactions, as described below.

3.12.1 ((4-(2-Bromoethoxy)-2-isopropyl-5-methylbenzyl)oxy)(*tert*-butyl)dimethylsilane (36a)

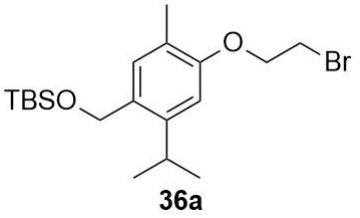

36a

According to the procedure for the synthesis of compound **29a**, compound **36a** (0.18 g, 0.46 mmol, 70%) was obtained as a colorless oil from compound **30**(0.19 g, 0.66 mmol) and 1,3-dibromoethane (0.75 mL). ^{1}H NMR (400 MHz, $CDCl_3$) δ 0.14 (s, 6H), 0.97 (s, 9H), 1.27 (d, *J* = 6.9 Hz, 6H), 2.26 (s, 3H), 3.22 (spt, *J* = 6.9 Hz, 1H), 3.69 (t, *J* = 6.4 Hz, 2H), 4.33 (t, *J* = 6.4 Hz, 2H), 4.72 (s, 2H), 6.76 (s, 1H), 7.16 (s, 1H). ^{13}C NMR (100 MHz, $CDCl_3$) δ −5.24, 15.71, 18.35, 23.92, 25.95, 28.46, 29.54, 62.86, 68.20, 108.75, 124.07, 130.26, 130.78, 145.48, 155.77. HRMS (ESI-TOF) *m/z*: $[M + H]^+$ calcd for $C_{19}H_{34}BrO_2Si^+$ requires: 401.1506; found 401.1523.

3.12.2 2-(4-(((*tert*-Butyldimethylsilyl)oxy)methyl)-5-isopropyl-2-methylphenoxy)ethyl 3-hydroxybenzoate (37a)

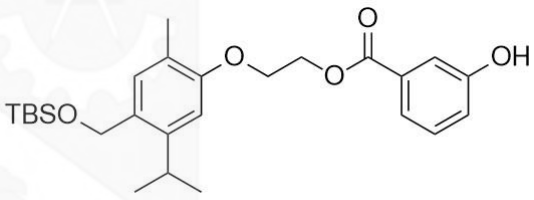

37a

According to the procedure for the synthesis of compound **12**, compound **37a** (0.22 g, 0.48 mmol, 96%) was obtained as a white solid from compound **36a** (0.20 g, 0.50 mmol) and 3HA (0.069 g, 0.50 mmol). ^{1}H NMR (400 MHz, $CDCl_3$) δ 0.12 (s, 6H), 0.95 (s, 9H), 1.22 (d, *J* = 6.9 Hz, 6H), 2.19 (s, 3H), 3.19 (spt, *J* = 6.9 Hz, 1H), 4.33 (m, 2H), 4.68 (m, 4H), 6.27 (br. s., OH), 6.79 (s, 1H), 7.03 (dd, *J* = 8.0, 2.1 Hz, 1H), 7.12 (s, 1H), 7.28 (m, 1H), 7.42 (s, 1H), 7.61 (d, *J* = 8.0 Hz, 1H). ^{13}C NMR (100 MHz, $CDCl_3$) δ −4.24, 15.73, 18.41, 23.90, 25.98, 28.51, 62.96, 63.96, 66.51, 109.04, 116.33, 120.56, 121.86, 124.23, 129.61, 129.92, 130.93, 131.03, 145.63, 155.97, 156.42, 166.69. HRMS (ESI-TOF) *m/z*: $[M + Na]^+$ calcd for $C_{26}H_{38}NaO_5Si^+$ requires: 481.2381; found 481.2397.

3.12.3 2-(4-(Hydroxymethyl)-5-isopropyl-2-methylphenoxy)ethyl 3-hydroxybenzoate (19)

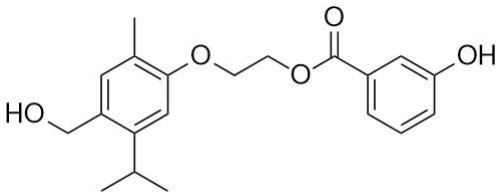

19

According to the procedure for the synthesis of compound **18**, compound **19** (0.069 g, 0.20 mmol, quant.) was obtained as a white solid from compound **37a** (0.092 g, 0.20 mmol) and TBAF (1 M in THF, 0.336 mL, 0.336 mmol). ^{1}H NMR (400 MHz, Methanol-d$_4$) δ 1.19 (d, J = 6.9 Hz, 6H), 2.10 (s, 3H), 3.21 (m, 1H), 4.29 (m, 2H), 4.52 (s, 2H), 4.59 (m, 2H), 6.83 (s, 1H), 6.97 (m, 1H), 7.02 (s, 1H), 7.23 (t, J = 7.8 Hz, 1H), 7.38 (m, 1H), 7.44 (d, J = 7.8 Hz, 1H). ^{13}C NMR (100 MHz, Methanol-d4) δ 15.97, 24.58, 30.04, 62.84, 64.93, 67.91, 110.24, 117.23, 121.47, 121.82, 125.25, 130.74, 131.35, 132.66, 132.92, 147.63, 158.23, 158.97, 168.15. HRMS (ESI-TOF) *m/z*: [M + Na]$^+$ calcd for $C_{20}H_{24}NaO_5^+$ requires: 367.1516; found 367.1525.

3.13 GENERAL PROCEDURE TO SYNTHESIZE COMPOUND 20

The synthesis of compound **20** involves three-step reactions, as described below.

3.13.1 (4-(3-Bromopropoxy)-2-isopropyl-5-methylbenzyl)oxy)(*tert*-butyl)dimethylsilane (36b)

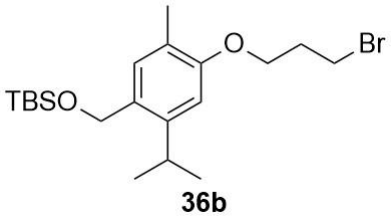

36b

According to the procedure for the synthesis of compound **29a**, compound **36b** (0.26 g, 0.62 mmol, 94%) was obtained as a colorless oil from compound **30**(0.19 g, 0.66 mmol) and 1,3-dibromopropane (0.75 mL).^{1}H NMR (400 MHz, $CDCl_3$) δ 0.17 (s, 6H), 1.00 (s, 9H), 1.31 (d, J = 6.9 Hz, 6H), 2.26 (s, 3H), 2.39 (quint, J = 6.4 Hz, 2H), 3.26 (m, 1H), 3.69 (t, J = 6.4 Hz, 2H), 4.17 (t, J = 6.4 Hz, 2H), 4.74 (s, 2H), 6.82 (s, 1H), 7.17 (s, 1H). ^{13}C NMR (100 MHz, $CDCl_3$) δ −5.24, 15.72, 18.33, 23.94, 25.95, 28.50, 30.13, 32.64, 62.90, 65.25, 108.12, 123.56, 129.59, 130.65, 145.48, 156.24. HRMS (ESI-TOF) *m/z*: [M + H]$^+$ calcd for $C_{20}H_{36}BrO_2Si^+$ requires: 415.1662; found 415.1674.

3.13.2 3-(4-(((*tert*-Butyldimethylsilyl)oxy)methyl)-5-isopropyl-2-methylphenoxy)propyl 3-hydroxybenzoate (37b)

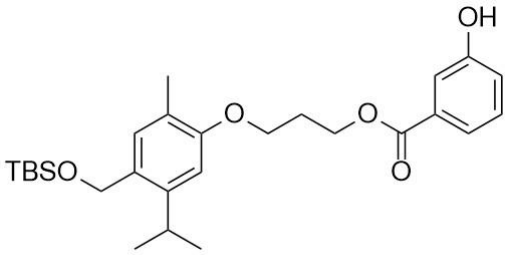

37b

According to the procedure for the synthesis of compound **12**, compound **37b** (0.21 g, 0.44 mmol, 88%) was obtained as a white solid from compound **36b** (0.21 g, 0.50 mmol) and 3HA (0.069 g, 0.50 mmol). ^{1}H NMR (400 MHz, $CDCl_3$) δ 0.11 (s, 6H), 0.94 (s, 9H), 1.22 (d, *J* = 6.9 Hz, 6H), 2.19 (s, 3H), 2.27 (quin, *J* = 6.0 Hz, 2H), 3.19 (spt, *J* = 6.9 Hz, 1H), 4.15 (t, *J* = 6.0 Hz, 2H), 4.55 (t, *J* = 6.0 Hz, 2H), 4.68 (s, 2H), 5.99 (br. s., OH), 6.75 (s, 1H), 7.04 (dd, *J* = 8.0, 2.3 Hz, 1H), 7.10 (s, 1H), 7.29 (t, *J* = 8.0 Hz, 1H), 7.52 (s, 1H), 7.60 (d, *J* = 8.0 Hz, 1H). ^{13}C NMR (100 MHz, $CDCl_3$) δ −5.24, 15.72, 18.38, 23.93, 25.97, 28.52, 28.85, 62.26, 62.96, 64.40, 108.14, 116.30, 120.32, 121.77, 123.77, 129.45, 129.62, 130.79, 131.42, 145.51, 155.91, 156.40, 166.70. HRMS (ESI-TOF) *m/z*: $[M + Na]^+$ calcd for $C_{27}H_{40}NaO_5Si^+$ requires: 495.2537; found 495.2548.

3.13.3 3-(4-(Hydroxymethyl)-5-isopropyl-2-methylphenoxy)propyl 3-hydroxybenzoate (20)

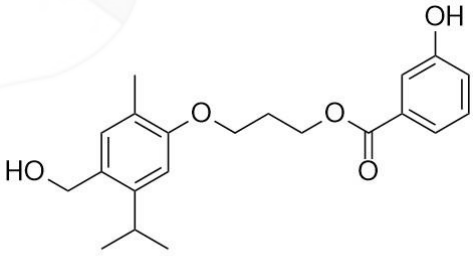

20

According to the procedure for the synthesis of compound **18**, compound **20** (0.036 g, 0.10 mmol, quant.) was obtained as a white solid from compound **37b** (0.047 g, 0.10 mmol) and TBAF (1 M in THF, 0.120 mL, 0.120 mmol). ^{1}H NMR (400 MHz, Methanol-d_4) δ 1.22 (d, *J* = 6.4 Hz, 6H), 2.15 (s, 3H), 2.25 (quin, *J* = 6.0 Hz, 2H), 3.24 (m, 1H), 4.16 (t, *J* = 6.0 Hz, 2H), 4.51 (t, *J* = 6.0 Hz, 2H), 4.55 (s, 2H), 6.82 (s, 1H), 7.00 (dd, *J* = 8.0, 2.3 Hz, 1H), 7.05 (s, 1H), 7.27 (t, *J* = 8.0 Hz, 1H), 7.42 (s, 1H), 7.48 (d, *J* = 8.0 Hz, 1H).^{13}C NMR (100 MHz, Methanol-d_4) δ 15.99, 24.58, 30.04, 30.17, 62.87, 63.29, 65.88, 109.60, 117.15, 121.39, 121.72, 124.90, 130.74, 130.88, 132.84, 132.89, 147.58,

158.32, 159.00, 168.24. HRMS (ESI-TOF) *m/z*: $[M + Na]^+$ calcd for $C_{21}H_{26}NaO_5^+$ requires: 381.1672; found 381.1682.

3.14 GENERAL PROCEDURE TO SYNTHESIZE COMPOUND 21

The synthesis of compound **21** involves three-step reactions, as described below.

3.14.1 (4-(4-Bromobutoxy)-2-isopropyl-5-methylbenzyl)oxy)(*tert*-butyl)dimethylsilane (36c)

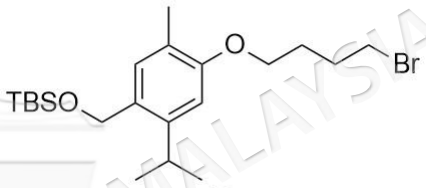

36c

According to the procedure for the synthesis of compound **29a**, compound **36c** (0.27 g, 0.63 mmol, 96%) was obtained as a colorless oil from compound **30** (0.19 g, 0.66 mmol) and 1,3-dibromobutane (0.75 mL). ^{1}H NMR (400 MHz, $CDCl_3$) δ 0.19 (s, 6H), 1.03 (s, 9H), 1.33 (d, *J* = 6.9 Hz, 6H), 2.04 (m, 2H), 2.18 (m, 2H), 2.28 (s, 3H), 3.28 (m, 1H), 3.58 (t, *J* = 6.6 Hz, 2H), 4.10 (t, *J* = 6.6 Hz, 2H), 4.77 (s, 2H), 6.82 (s, 1H), 7.19 (s, 1H). ^{13}C NMR (100 MHz, $CDCl_3$) δ −5.26, 15.75, 18.29, 23.94, 25.93, 27.96, 28.47, 29.60, 33.45, 62.92, 66.73, 107.81, 123.43, 129.31, 130.62, 145.39, 156.44. HRMS (ESI-TOF) *m/z*: $[M + H]^+$ calcd for $C_{21}H_{38}BrO_2Si^+$ requires: 429.1819; found 429.1806.

3.14.2 4-(4-(((*tert*-Butyldimethylsilyl)oxy)methyl)-5-isopropyl-2-methylphenoxy)butyl 3-hydroxybenzoate (37c)

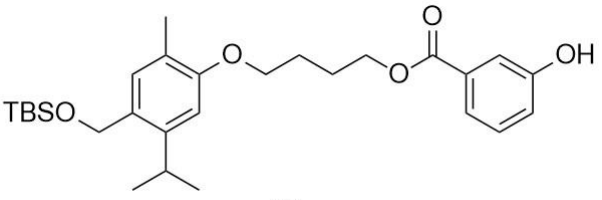

37c

According to the procedure for the synthesis of compound **12**, compound **37c** (0.20 g, 0.42 mmol, 84%) was obtained as a white solid from compound **36c** (0.22 g, 0.50 mmol) and 3HA (0.069 g, 0.50 mmol). ^{1}H NMR (400 MHz, $CDCl_3$) δ 0.16 (s, 6H), 0.99 (s, 9H), 1.27 (d, *J* = 6.9 Hz, 6H), 2.03 (m, 4H), 2.24 (s, 3H), 3.24 (spt, *J* = 6.9 Hz, 1H), 4.08 (t, *J* = 5.5 Hz, 2H), 4.46 (t, *J* = 5.5 Hz, 2H), 4.74 (s, 2H), 6.78 (s, 1H), 6.93 (br. s., OH), 7.06 (dd, *J* = 8.0, 2.1 Hz, 1H), 7.15 (s, 1H), 7.30 (t, *J* = 8.0 Hz, 1H), 7.62 (m, 2H). ^{13}C NMR (100 MHz, $CDCl_3$) δ −5.25, 15.74, 18.35, 23.90, 25.46,

25.95, 26.17, 28.50, 62.99, 65.18, 67.20, 107.99, 116.35, 120.42, 121.49, 123.61, 129.08, 129.54, 130.79, 131.23, 145.49, 156.16, 156.54, 167.10. HRMS (ESI-TOF) *m/z*: $[M + Na]^+$ calcd for $C_{28}H_{42}NaO_5Si^+$ requires: 509.2694, found 509.2685.

3.14.3 4-(4-(Hydroxymethyl)-5-isopropyl-2-methylphenoxy)butyl 3-hydroxybenzoate (21)

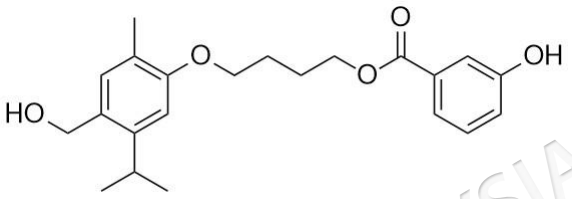

21

According to the procedure for the synthesis of compound **18**, compound **21** (0.12 g, 0.32 mmol, quant.) was obtained as a white solid from compound **37c** (0.16 g, 0.32 mmol) and TBAF (1 M in THF, 0.384 mL, 0.384 mmol). ^{1}H NMR (400 MHz, Methanol-d_4) δ 1.18 (d, *J* = 6.9 Hz, 6H), 1.93 (m, 4H), 2.11 (s, 3H), 3.21 (m, 1H), 4.01 (t, *J* = 6.0 Hz, 2H), 4.34 (t, *J* = 6.0 Hz, 2H), 4.51 (s, 2H), 6.75 (s, 1H), 6.96 (dd, *J* = 8.0, 1.6 Hz, 1H), 7.00 (s, 1H), 7.21 (t, *J* = 8.0 Hz, 1H), 7.38 (m, 1H), 7.42 (d, *J* = 8.0 Hz, 1H).^{13}C NMR (100 MHz, Methanol-d_4) δ 16.27, 24.82, 27.17, 27.71, 30.25, 63.10, 66.37, 68.89, 109.52, 117.34, 121.55, 121.90, 124.94, 130.80, 130.95, 133.06, 133.12, 147.71, 158.63, 159.19, 168.52. HRMS (ESI-TOF) *m/z*: $[M + Na]^+$ calcd for $C_{22}H_{28}NaO_5^+$ requires: 395.1829; found 395.1827.

3.15 *IN VITRO* EVALUATION METHOD

3.15.1 *In vitro* Cardioprotective Evaluation of CA and CPAHs 1–10 (Department of Physiology, Faculty of Medicine, UKM)

The H9c2 cardiomyocyte cell line, procured from Thermo Fisher Scientific, was cultured in DMEM supplemented with 10% FBS and 1% penicillin. Cells were maintained in monolayer culture conditions at 37°C and 5% CO_2, with media refreshed every two days. Subculturing was performed when cells reached 80% confluence.

The viability of H9c2 cardiomyocytes was measured using 3-(4,5-dimethylthiazol-2-yl)-2,5-diphenyltetrazolium bromide (MTT) assay. H9c2 cells were

seeded in 96-well plates at a density of 5000 cells/well and allowed to attach for 48 h. To assess the cytotoxicity of the parent compounds (CA and 3,4-dihydroxybenzoic acid) and CPAHs **1–10**, cardiomyocytes were treated with compounds at concentrations ranging from 0.01 to 100 μg/mL for 48 h. Following the treatment, MTT reagent (5 mg/mL) was added to the culture medium for 4 h at 37°C. Formazan formed in each well was dissolved in 100 μL of dimethyl sulfoxide (DMSO), and absorbance at 570 nm was measured using a microplate reader. Subsequently, to determine the protective effects of the parent compounds and CPAHs **1–10** on the viability of DOX-induced cardiomyocytes, H9c2 cells were pre-treated with or without non-toxicparent compounds and CPAHs **1–10** concentrations for 24 h prior to induction with 10 μM DOX for another 24 h.

3.15.2 *In vitro* Cardioprotective Evaluation of CPAHs 11–21 (Department of Chemistry and Biomolecular Sciences, Faculty of Engineering, Gifu University)

The H9c2 cardiomyocyte cell line from the American Type Culture Collection was cultured in DMEM supplemented with 5% heat-inactivated fetal bovine serum, 100 units/mL penicillin, and 100 μg/mL streptomycin. Cultures were maintained in a monolayer format at 37°C and 5% CO_2. When the confluence reached 80%, subculturing took place.

The cell viability of H9c2 cardiomyocytes was determined using the Cell Counting Kit 8 (WST-8) from Dojindo, Kumamoto, Japan. H9c2 cells were seeded into 96-well plates at a density of 5000 cells per well and left to adhere for about 24 h. Cardiomyocytes were exposed to 10 μM concentrations of compounds **11–21**, CA, 3HA, or vehicle (dimethyl sulfoxide) for 48 h to assess the cytotoxicity of both parent compounds and conjugates. During the final two hours of treatment, WST-8 solution was added to the culture medium and incubated at 37°C per the manufacturer's instructions. The difference in absorbance at 450 and 620 nm was used to determine cell viability, with the absorbance of untreated cells set to 1.0. Subsequently, to test the compounds' protective effects against DOX-induced cardiomyocyte damage, H9c2 cells were pre-treated with or without compounds **11–21**, CA, or 3HA at a concentration of 10 μM, or vehicle for 24 h before being exposed to 3 μM DOX

(Cosmo Bio Co. Ltd., Tokyo, Japan) for an additional 24 h. The cell viability was then measured as described above.

3.16 STATISTICAL ANALYSIS OF DATA

GraphPad Prism 8.0 software was used to analyze data, with results presented as mean ± standard deviation (SEM). One-way ANOVA with post hoc Tukey was used to analyze normally distributed data. p-values less than 0.05 were considered significant.

3.17 SAR ANALYSIS

With the successful synthesis of compounds **1–21** and the subsequent evaluation of their cardioprotective activity *in vitro*, a SAR analysis becomes feasible. This analysis starts by identifying critical structural features—such as functional groups, ring systems, and chain lengths—that significantly influence the compounds' biological activity. By systematically assessing how modifications to these structural components affect biological efficacy, a qualitative SAR framework can be developed. This approach builds upon the research framework presented in the study by Kollárová-Brázdová et al. (2020); Cuadrado et al. (2022); Sarian et al. (2017).

CHAPTER IV

RESULTS AND DISCUSSION

4.1 INTRODUCTION

This chapter presents the research findings from the study on the design and synthesis of CPAHs. The results of the *in vitro* cardioprotector evaluation of CPAHs against DOX-induced cardiomyocyte cell death and the establishment of SAR among the CPAHs, respectively are discussed in this chapter.

4.2 SYNTHESIS OF CPAH

Due to previous findings suggesting the cardioprotective nature of CA and PA (Imran et al. 2022; Liu et al. 2022), this study focused on investigating the cardioprotective potential of CPAH. The combination or hybridization of two molecules with distinct pharmacophores yet similar pharmacological properties is known to yield a synergistic effect or enhance the targeted delivery of the parent drug to a specific site. This strategy is commonly employed in treating various diseases, including cardiovascular, neurodegenerative, cancerous, inflammatory, and infectious disorders, as extensively documented (Aljuffali et al. 2016). Additionally, this approach could enhance physicochemical characteristics, drug delivery mechanisms, and biopharmaceutical properties, as highlighted in previous research (Das et al. 2010).

Previous studies have identified the active sites at C-4, C-6, and the hydroxy group (-OH) of CA as promising targets for developing potent pharmaceutical candidates (Retnosari et al. 2024). To optimize the integration of PA into the CA structure, the phenolic group of CA was selected as a critical site for modification. Furthermore, compounds (**1–10**) were synthesized, consisting of hybrid CA

derivatives with various hydroxybenzoic or cinnamic acids connected via a diester linker (Ashraf et al. 2017). In the first series, six CPAHs (**1–6**) were initially developed based on HBA and a diester linker, as shown in Figure 4.1. This investigation explored benzoic acids featuring varying numbers and positions of -OH groups, aiming to establish a comprehensive SAR.

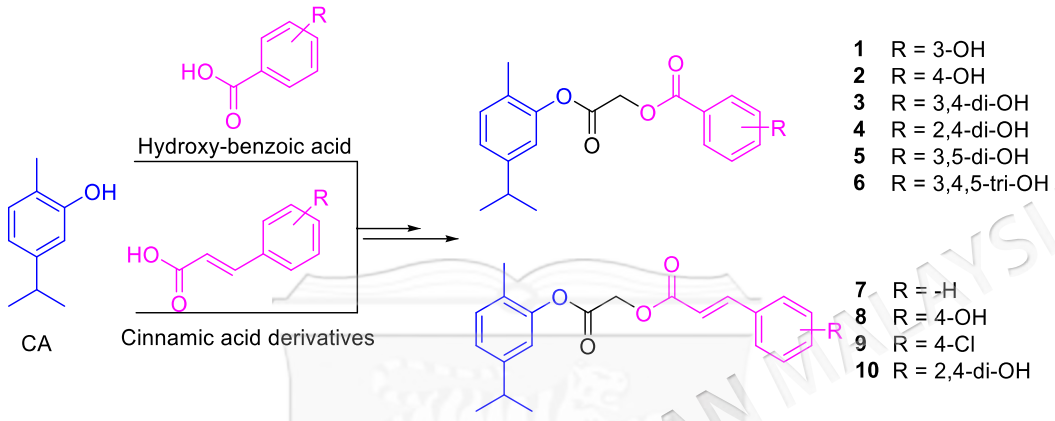

Figure 4.1 Structures of the synthesized CA conjugated hydroxy-benzoic/cinnamic acid (**1–10**)

In the second series, compounds **7–10** were specifically designed by replacing the benzoic acid with cinnamic acid derivatives, as shown in Figure 4.1. This innovative approach aimed to explore the role of the cinnamic acid scaffold in modulating the activity of CPAH. Both benzoic acid and cinnamic acid derivatives demonstrated potential as cardioprotective agents. Various parameters were systematically examined to understand the SAR further, including the substitution of -OH groups with -Cl groups, the reduction in the number of -OH groups, and the manipulation of both the number and position of -OH groups.

A further exploration involved the manipulation of the linker structure, focusing on the modification of 3HA and CA. Consequently, in this investigation, 3HA was linked with CA via alkyl or acyl linkers comprising two, three, or four carbons at the hydroxyphenol position, yielding two series of conjugates, as shown in Figure 4.2. In Series 1, the 3HA moiety was incorporated into the phenolic hydroxy group of CA through acyl (**11–12**) or alkyl (**13–15**) linkers of varying lengths.

To confirm the key role of the CA scaffold and further enhance modification, CA was also transformed into 4-hydroxymethylcarvacrol. Mastelić et al. (2008) reported that 4-hydroxymethylcarvacrol exhibits superior antioxidant activity compared to CA. Introducing the 3HA moiety into 4-hydroxymethylcarvacrol could potentially augment the cardioprotective properties of CA. Consequently, two additional series (**16–18** and **19–21**) were devised and synthesized (Figure 4.2). These series mirrored the previous ones (**11–12** and **13–15**), but CA was substituted with 4-hydroxymethylcarvacrol. As a result, a total of 21 conjugates were synthesized.

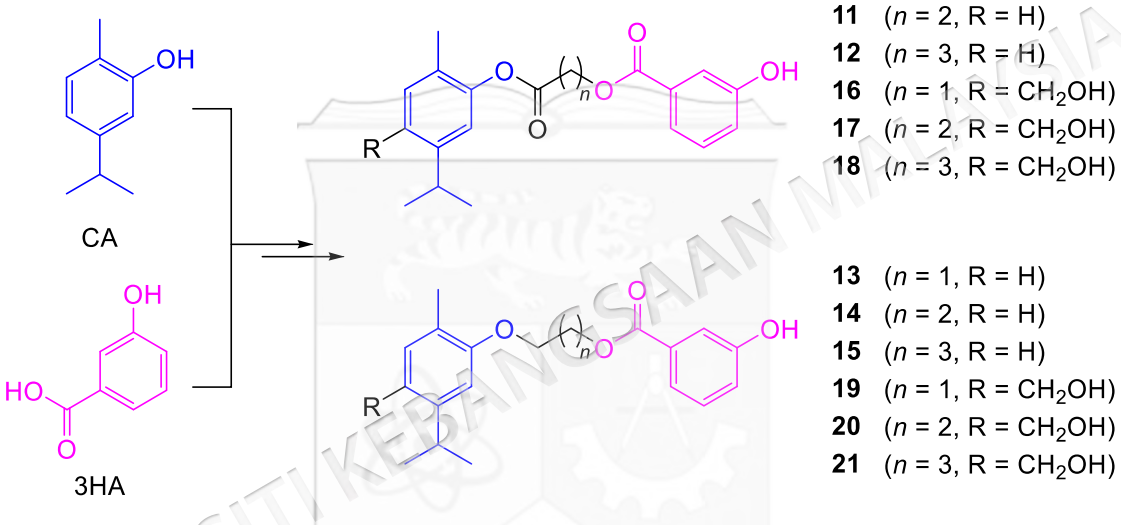

Figure 4.2 Structures of the synthesized CA conjugated 3HA (**11–21**)

As previously described, the synthesis of **1–10** has been reported in the literature (Ashraf et al. 2017). However, these compounds were re-synthesized and their protective effects against DIC were evaluated in this study to further explore the SAR within this series. There are two-step reactions to synthesize compounds **1–10**, as shown in Scheme 4.1. In the first step, an intermediate (**22**) was formed via an esterification reaction by mixing CA and chloroacetyl chloride in the presence of TEA as a base and DCM as a solvent. The mixture was then stirred for 4 hours at room temperature. The plausible mechanism for the formation of compound **22** involves the deprotonation of the phenolic hydroxy group of CA by TEA, yielding deprotonated CA as a nucleophile. The deprotonated CA then attacks the carbonyl group of chloroacetyl chloride, forming compound **22** and releasing Cl^-, which is subsequently neutralized by the protonated TEA. The structure of compound **22** was further

confirmed by ^{1}H-NMR data, i.e., singlet peak at δ 4.55 ppm representing methylene protons of chloroacetyl moiety, as shown in Appendix A. Furthermore, the typical singlet at δ 7.98 ppm representing phenolic hydroxy of CA was absent. The EI-MS further confirmed these predictions with a peak at *m/z* = 226.1 [M^{+}], representing the molecular mass of compound **22**.

Moreover, the reaction proceeded to the second step, where appropriate benzoic acid or cinnamic acid derivatives were incorporated via nucleophilic substitution reaction to obtain compounds **1–10**. The terminal methylene carbon-containing chloro group was attacked by the deprotonated carboxyl group of benzoic acid derivatives (nucleophile). The presence of TEA assists the appropriate benzoic/cinnamic acid derivatives to undergo a deprotonation reaction. The reaction was executed by stirring the mixture of benzoic/cinnamic acid derivatives, TEA, KI, compound **22**, and dimethyl formamide for 24 h at room temperature. The reaction scheme for synthesizing compounds **1–10** can be seen in Scheme 4.1.

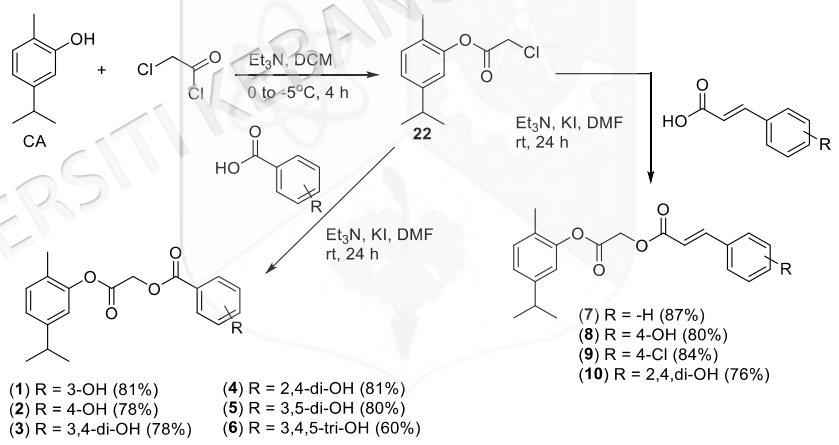

Scheme 4.1 The synthetic pathway of compounds **1**–**10**

The structures of compounds **1–10** were confirmed by ^{1}H-NMR, ^{13}C-NMR, and mass spectroscopic data. Compound **1** was obtained as a yellowish-white solid. The ^{13}C-NMR spectrum of compound **1** showed 18 signals corresponding to 19 carbons, consisting of 14 sp^2 and 5 sp^3 carbons, as shown in Appendix B. Two signals at a chemical shift of 167.05 and 166.48 ppm represent two ester carbonyl bonds. The ^{1}H-NMR spectrum of compound **1** showed a series of aromatic signals corresponding to one unit of 1-substituted-3-hydroxyphenyl [δ 7.68 (dd, 1H), 7.66 (dd, 1H), 7.38 (dd, 1H), 7.19 (ddd, 1H)] from the benzoic acid skeleton, and one unit of 1,2,5-

trisubstituted-phenyl [δ 7.17 (d, 1H), 7.05 (dd, 1H) and 7.00 (d, 1H) from the CA skeleton. The signal at δ 8.84 (s, 1H) indicated the presence of a substituted -OH group on the 1-substituted-3-hydroxyphenyl skeleton. Furthermore, the ^{1}H-NMR spectrum revealed aliphatic proton signals [δ 2.88 (sept, 1H), 2.17 (s, 3H), and 1.19 (d, 6H)] representing the sp^3 carbon on the CA skeleton. Furthermore, the signal at δ 5.199 (s, 2H) is the methylene signal that connects the CA skeleton and benzoic acid. The HRMS further confirmed the structure of compound **1** identified by a peak at *m/z* = 351.1202 ([M + Na]$^{+}$), representing the molecular mass of compound **1**. A comparison of ^{1}H and ^{13}C-NMR data from compound **1** reported in the literature provides additional evidence for its structure (Ashraf et al. 2017). Compounds **2-10**'s structure was confirmed using the same method.

Furthermore, compounds **11–12** were synthesized using a two-step reaction process, adopting the method used for synthesizing compound **1**, as shown in Scheme 4.2. Initially, the phenol of CA was functionalized to form an appropriate chloroacyl intermediate (**23a–b**) *via* the esterification reaction with a proper acid chloride in the presence of TEA and DCM. Surprisingly, only compound **23b** was successfully synthesized under these conditions. The formation of compound **23a** was conspicuously absent, with the reaction predominantly yielding an α,β-unsaturated carbonyl compound (**24**) through an elimination process. To address this unexpected challenge, the strength of the base was strategically modulated using pyridine (Py), which effectively reduced the formation of compound **24**. This modification facilitated the desired esterification reaction, allowing for the synthesis of compound **23b**.

Subsequently, 3HA was introduced via nucleophilic substitution. Only compound **12** was successfully obtained in high yields using KI as a nucleophile and TEA or $NaHCO_3$ as a base. On the other hand, compound **11** was not obtained during an attempt to react compound **23a** with 3HA in the presence of various bases such as TEA, potassium carbonate (K_2CO_3), and $NaHCO_3$. Instead, the most common byproduct observed was compound **24**. Using Py as a base reduced the formation of compound **24** but did not promote the formation of compound**11** (data not shown).

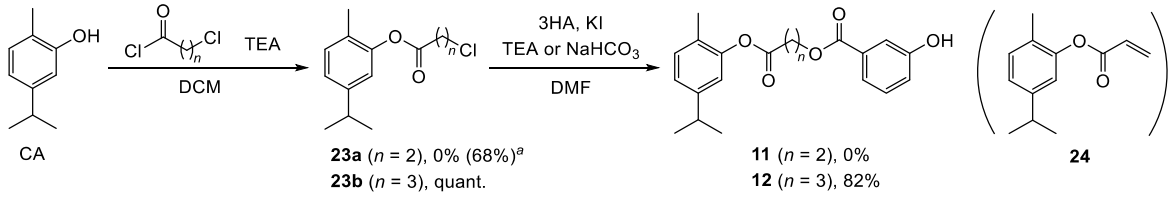

[a] Pyridine was used in place of TEA.

Scheme 4.2 The synthetic pathway of compounds **11**–**12**

The predominance of compound **24** emphasizes the importance of thoroughly investigating alternative synthetic routes to produce compound **11** effectively. As a result, compound **26** was used as an intermediate instead of **23a**, serving as a nucleophilic source to prevent the possibility of an elimination reaction. This change facilitated the condensation reaction with 3HA, which resulted in the successful synthesis of compound **11**, as illustrated in Scheme 4.3.

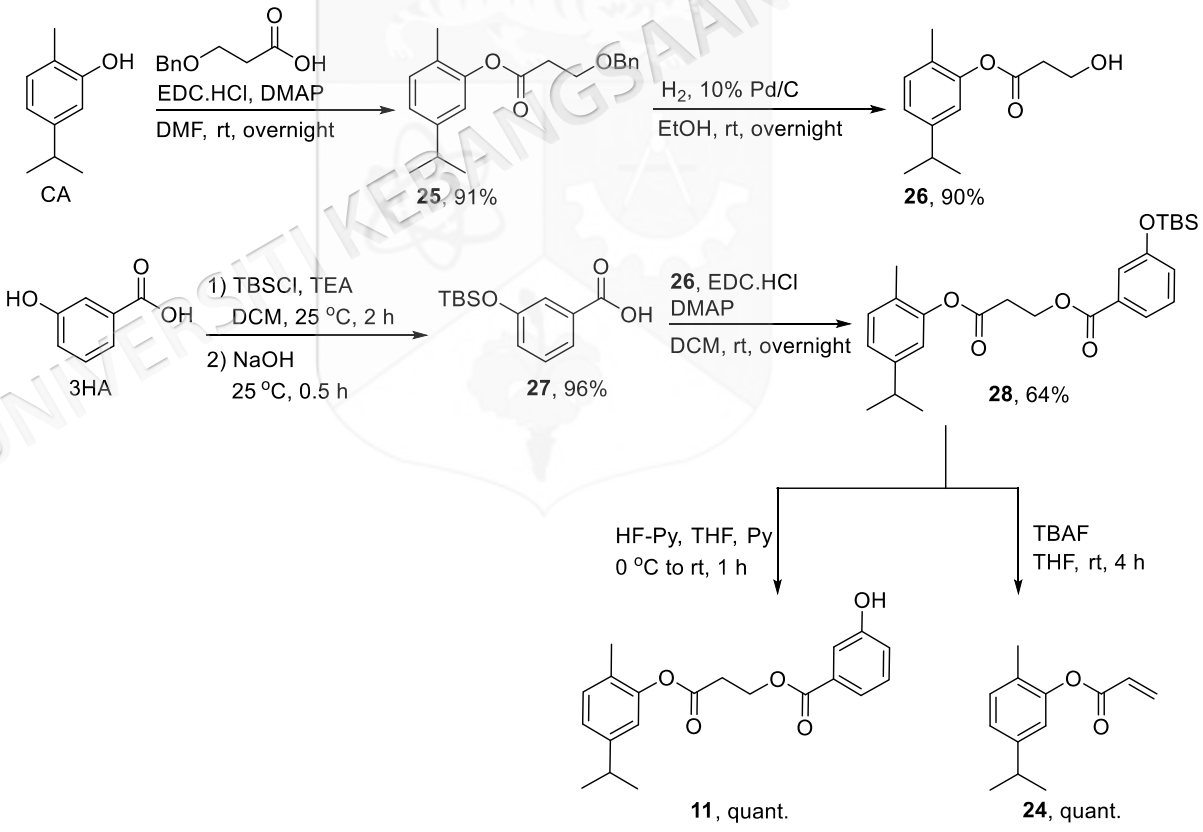

Scheme 4.3 The synthetic pathway of compound **11**

The synthesis of compound **11** was initiated with a condensation reaction between 3-(benzyloxy)propanoic acid and CA, involving an esterification reaction

between the aliphatic carboxylic acid group of 3-(benzyloxy)propanoic acid and the hydroxyphenolic group of CA. The Steglich esterification method was selected for this study due to its widespread application in similar reactions. This method utilized 1-ethyl-3-(3-dimethylaminopropyl)carbodiimide hydrochloride (EDC·HCl) as a coupling agent and 4-dimethylaminopyridine (DMAP) as a catalyst (Tomoda et al. 2010), resulting in the formation of compound **25**. The proposed reaction mechanism is illustrated in Figure 4.3. In this reaction, EDC·HCl activates the carboxylic acid by forming an *O*-acylisourea intermediate, which exhibits reactivity akin to a carboxylic acid anhydride. DMAP, acting as a nucleophilic catalyst, enhances the reaction rate by initially reacting with the *O*-acylisourea to generate a more reactive amide intermediate. This intermediate then rapidly reacts with CA to form compound **25**. By functioning as an acyl transfer reagent, DMAP facilitates the overall esterification process.

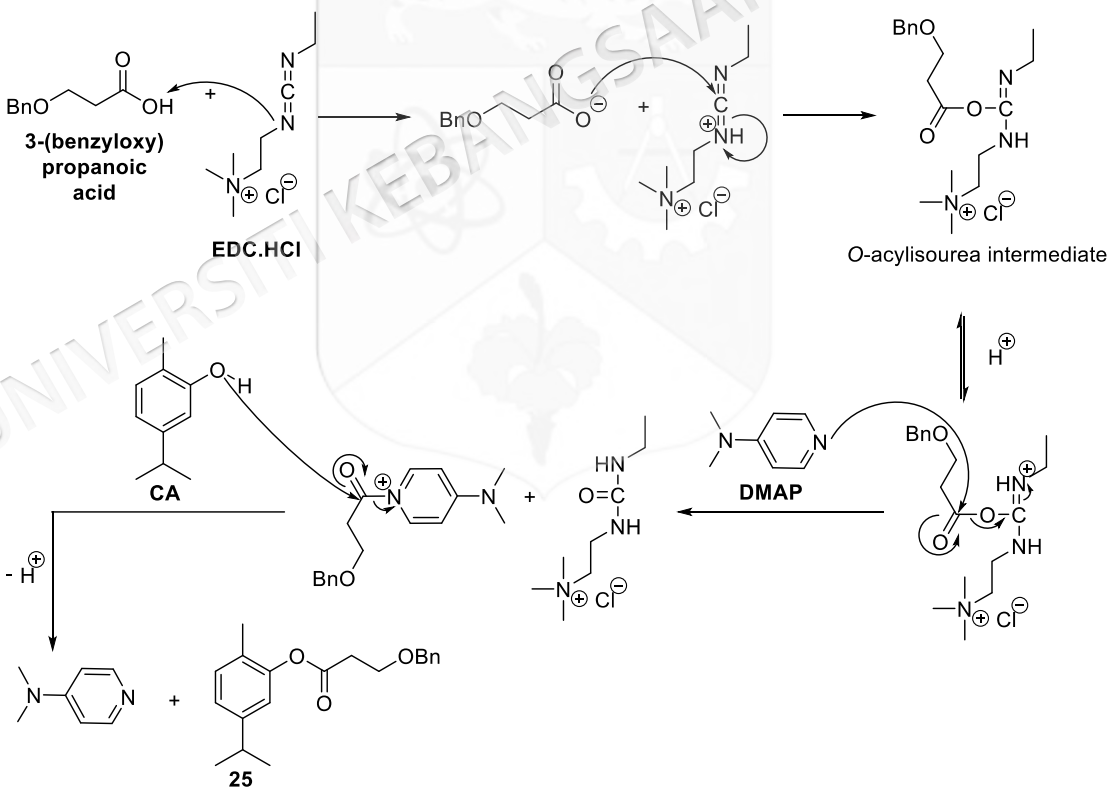

Figure 4.3 Proposed mechanism for the formation of compound **25**

The benzyl group in compound **25** was successfully removed through palladium-catalyzed hydrogenation, affording compound **26** in a satisfactory overall yield (Kinarivala et al. 2016). The proposed mechanism for this deprotection reaction

is illustrated in Figure 4.4. The deprotection reaction follows a catalytic cycle that begins with the coordination of the benzyl-protected compound (**25**) to a Pd(0) catalyst, which undergoes oxidative addition to form a palladium(II) complex. Subsequently, excess molecular hydrogen (H_2) binds to the Pd(II) center, facilitating the heterolytic cleavage of H_2 and the formation of two Pd–H bonds. One hydrogen atom is transferred to the benzyl group, resulting in the cleavage of the benzyl moiety and the formation of compound **26**. Reductive elimination then occurs, releasing toluene as a by-product and regenerating the Pd(0) catalyst. This regeneration completes the catalytic cycle, enabling the Pd(0) species to participate in further hydrogenation steps.

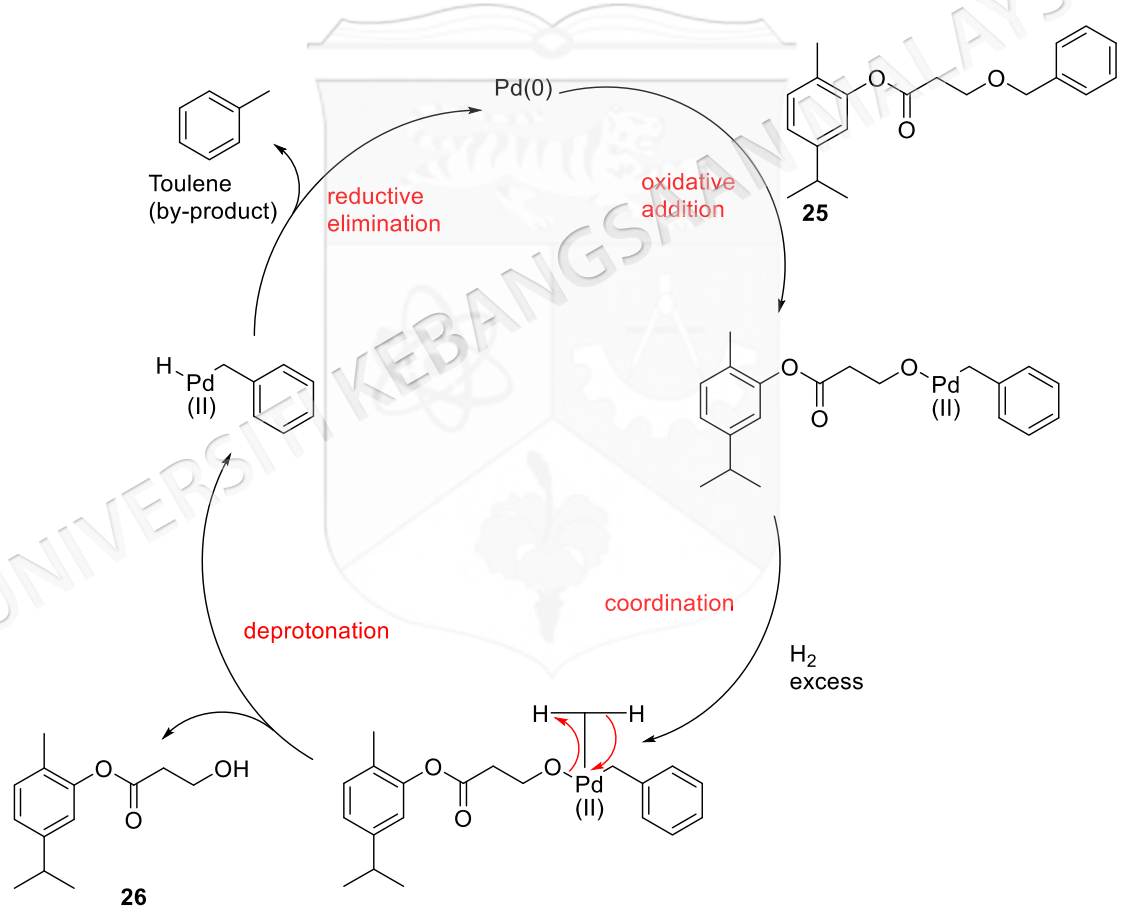

Figure 4.4 Proposed mechanism for the formation of compound **26**

Before the condensation reaction between compound **26** and 3HA was performed, protecting the phenolic hydroxy group in 3HA was imperative to avoid undesired products. This protective modification was accomplished by treatment with tert-butyldimethylsilyl chloride (TBSCl), as reported by Philippe et al. (2023),

resulting in the formation of compound **27** with a high yield. Subsequent condensation of compound **26** with **27**, employing EDC.HCl and DMAP yielded compound **28** in a moderate yield. However, removing the TBS group from compound **28** posed a slight challenge. Using tetrabutylammonium fluoride (TBAF) as a deprotection reagent (James et al. 2007) resulted in the elimination reaction, yielding compound **24** quantitatively. In contrast, when HF-pyridine (HF-Py) was employed as the deprotection reagent (Boger 2010), the reaction proceeded smoothly, yielding the desired product (compound **11**) in quantitative yield. The deprotection mechanism involves the nucleophilic attack of the fluoride ion (F^-) on the silicon atom of the TBS group. HF-Py serves as the source of fluoride ion in solution, where the fluoride ion coordinates to the silicon atom, promoting the cleavage of the Si–O bond. This results in the liberation of the phenolic hydroxy group (–OH), restoring the original hydroxyl functionality in the molecule, yielding compound **11**. This optimized synthetic route highlights the importance of selecting appropriate protective group reagents and reaction conditions, ensuring the efficient synthesis of compound **11**.

Additionally, the investigation extended to synthesizing compounds**13–15**, as delineated in Scheme 4.4. The initial step necessitated the attachment of the alkyl linker to CA via an O-alkylation reaction. The appropriate alkyl linkers were introduced to CA with potassium hydroxide (KOH) as a base (Attanasi et al. 2004). The reaction mixture was maintained at 70°C for 6 hours, forming appropriate intermediates (**29a–c**). Subsequently, the nucleophilic reaction was conducted between the corresponding intermediates in the presence of $NaHCO_3$ and KI in the second step. This led to the successful synthesis of compounds **13–15** in high yield.

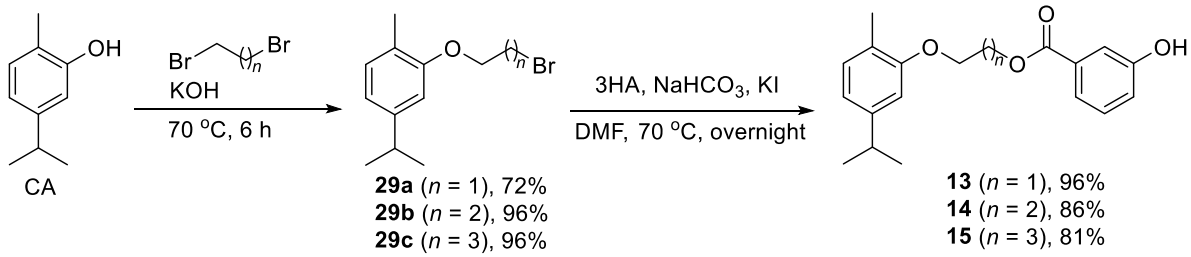

Scheme 4.4 The synthetic pathway of compounds **13–15**

To synthesize compounds **16–21**, it is imperative to initially modify the structure of CA by incorporating the -CH_2OH group at the *para* position. This structural alteration was achieved by employing the previously reported methodology for the hydroxymethylation of CA (Mastelić, et al. 2008). Compounds **16** and **18** were obtained by a process similar to that used for compounds **1** and **12**, with CA being substituted by 4-(((tert-butyldimethylsilyl)oxy)methyl)-5-isopropyl-2-methylphenol (**30**), as shown in Scheme 4.5. However, removing the TBS protecting group from compound **32a** was challenging. Initial experiments with TBAF were complicated, involving an additional step of breaking the ester bond in the linker (data not shown). Remarkably, the pursuit of an optimized deprotection strategy led to the adoption of HF-Py (Boger 2010), as a more efficient reagent. This alternative approach facilitated the selective removal of the TBS group and effectively mitigated the unintended cleavage of the ester bond, resulting in compound **16** with an exceptionally high yield. Surprisingly, a different result was observed in the attempt to remove the TBS group in compound **32b.** By using TBAF (James et al. 2007), the TBS group was removed successfully, yielding moderate results of compound **18**. In addition to successfully synthesizing compounds **16** and **18**, compound **17** was also synthesized using a method similar to that employed for compound **11** to prevent the formation of unwanted elimination products. However, CA was substituted with the structurally distinct precursor compound **30**, as depicted in Scheme 4.6.

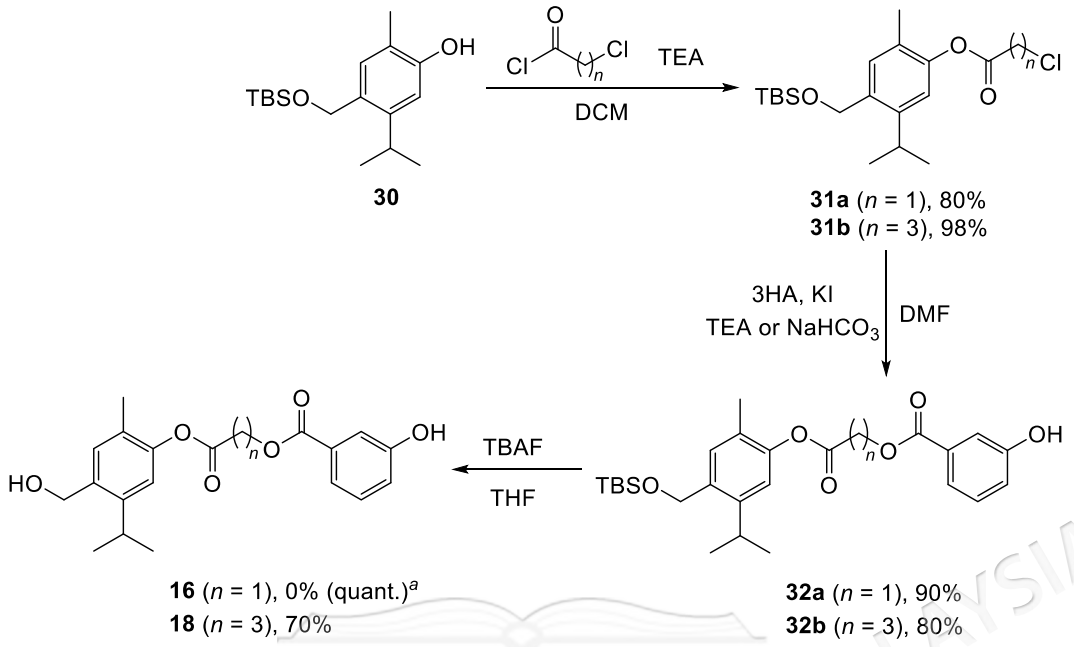

[a] HF-Py and Py was used in place of TBAF.

Scheme 4.5 The synthetic pathway of compounds **16** and **18**

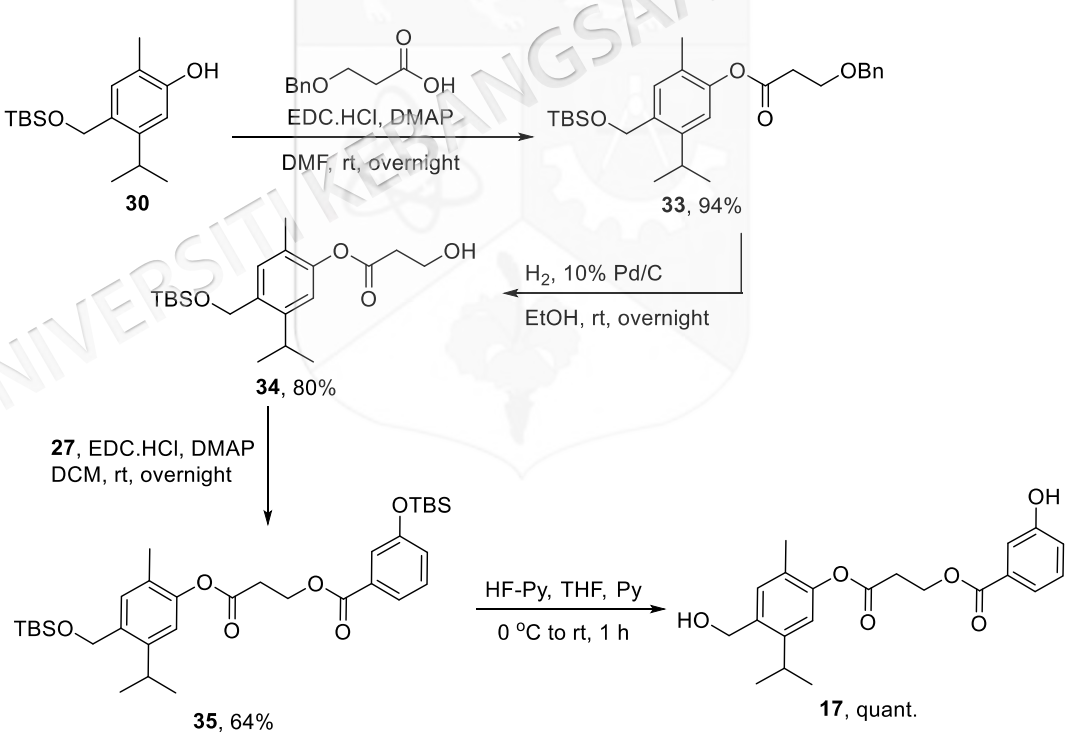

Scheme 4.6 The synthetic pathway of compound **17**

Furthermore, to expand the synthetic scope of compound **30**, a series of transformations were carried out to introduce an alkyl linker moiety through an *O*-alkylation reaction, followed by a strategically designed nucleophilic reaction with 3HA. This approach resulted in the successful synthesis of a diverse range of

compounds, specifically compounds **19–21**, as illustrated in Scheme 4.7. Notably, the TBS group in compounds **37a–c** was easily removed without producing any degradation products in the presence of TBAF. This result contrasts sharply with that observed in hybrids with a diester linker, indicating a significant difference in stability favoring the ether linkage over the ester linker.

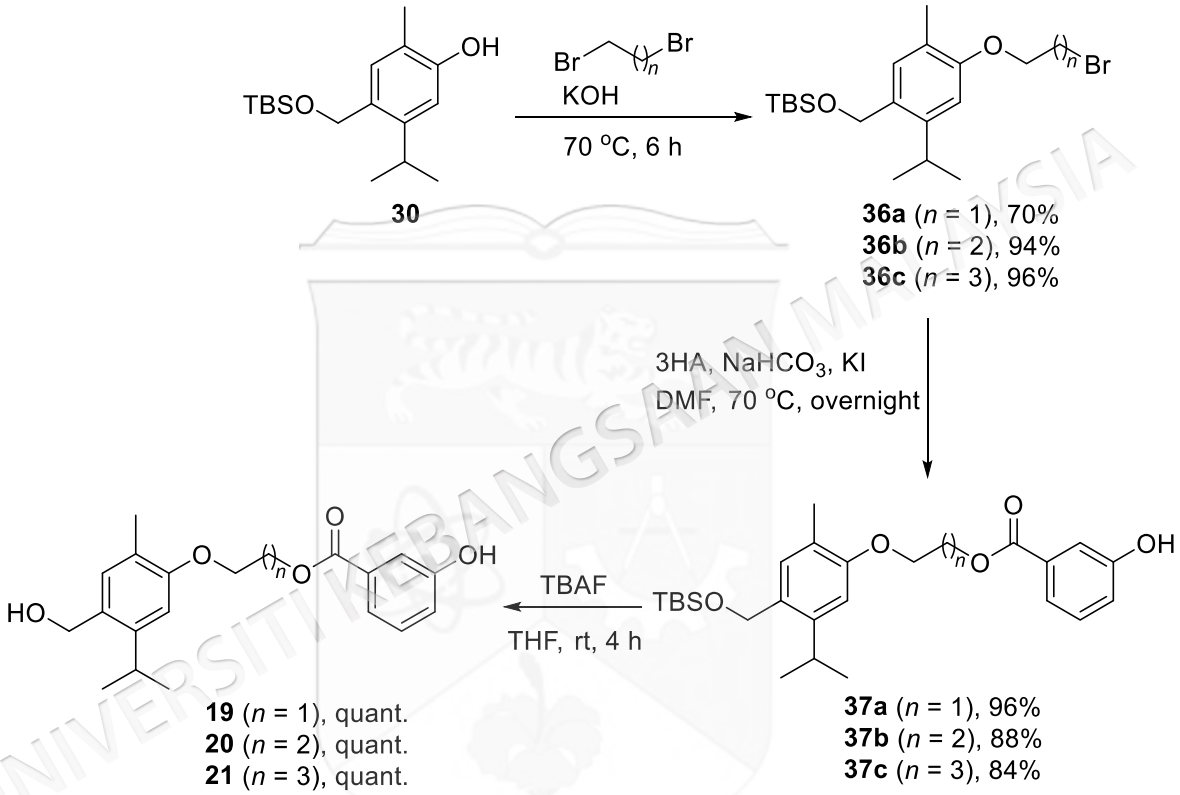

Scheme 4.7 The synthetic pathway of compounds **19–21**

4.3 CARDIOPROTECTOR EVALUATION OF CPAH AGAINST DIC

4.3.1 Cardioprotective Evaluation of CA

The protective effects of CA, as a parent compound, against DIC were evaluated *in vitro*. After 48 hours of exposure to CA concentrations ranging from 0.067 to 670 µM (0.01–100 µg/mL), cardiomyocyte viability was assessed using the MTT assay. CA exhibited a non-toxic profile to cardiomyocytes within the concentration range of 0.067 to 0.670 µM. However, at higher concentrations (6.70 to 670 µM), a significant reduction in cardiomyocyte viability was observed (Figure 4.5a) ($p<0.05$). These

findings are consistent with the results of Jamhiri et al. (2019), who reported that CA concentrations between 0.01 and 1 µM did not induce toxicity in H9c2 cells. Consequently, CA concentrations between 0.067 and 0.670 µM were considered non-toxic and used in the subsequent phase of the MTT assay.

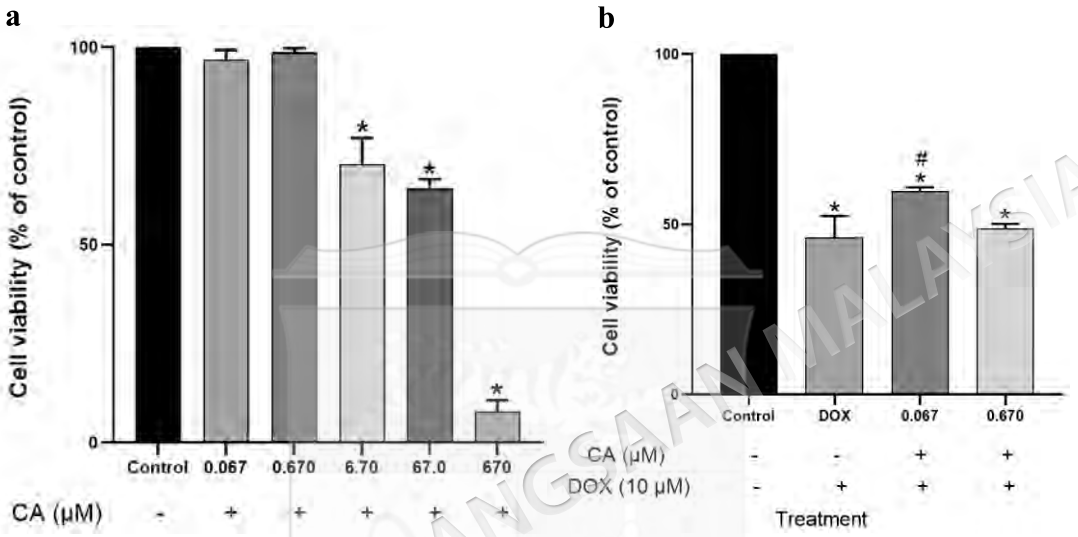

Figure 4.5 Protective effect of CA against DIC in H9c2 cardiomyocytes. (a) Toxicity of CA in H9c2 cardiomyocytes was determined by MTT assay following treatment with CA (0.067–670 µM) for 48 h. (b) H9c2 was pretreated with non-toxic CAconcentrations (0.067–0.670 µM) followed by induction with 10 µM DOX for an additional 24 h. Data are shown as mean ± SEM, n = 6. *p<0.05 vs. control, #p<0.05 vs. DOX-induced group.

In the second phase, H9c2 cells were pre-treated with non-toxic CA concentrations prior to DOX induction to assess CA's cardioprotective effect. The results demonstrated that 10 µM DOX significantly reduced cardiomyocyte viability to 46.61 ± 0.55% compared to the control ($p<0.05$), confirming DOX's potent cardiotoxicity (Figure 4.5b). Notably, pre-treatment with 0.067 µM CA significantly improved cardiomyocyte viability compared to the DOX-only group ($p<0.05$). However, higher CA concentrations (0.67 µM) did not yield a further increase in viability relative to the DOX-treated group, indicating that higher concentrations of CA did not offer enhanced protection against DIC. This observation aligns with Jamhiri et al. (2019), who also reported the absence of a dose-dependent protective response in the context of cardiac hypertrophy.

The lack of a dose-dependent protective response may be influenced by several factors, including CA's mechanism of action, pharmacodynamics, and biological modulation pathways. These factors can affect CA's efficacy at different concentrations, leading to the observed non-linear response. For instance, certain drugs, such as SGLT-2 inhibitors, known for their cardioprotective properties, exhibit variable efficacy depending on factors like heart health, the type of cardiac damage, and dosing. In some cases, lower doses provide protection, while higher doses do not confer additional benefits (Lahnwong et al. 2018). Similarly, volatile anesthetics used for cardioprotection in ischemia-reperfusion injuries activate protective pathways, such as K-ATP channels, but their effectiveness does not always correlate with higher doses (Van Allen et al. 2012). A comparable non-linear dose-response has also been observed with folic acid in cardioprotection, where efficacy depends on factors like dose, ischemia duration, and anesthetic regimen (Zuurbier et al. 2014).

4.3.2 Cardioprotective evaluation of CPAHs 1–10 and 3,4-dihydroxybenzoic acid

The method used to evaluate the cardioprotective effect of CA was applied to assess the cardioprotective potential of CPAHs (**1–10**). Additionally, 3,4-dihydroxybenzoic acid (3,4-HB), representing the phenolic acid scaffold, was investigated to determine the contribution of this scaffold to the activity of the hybrids. Prior to this, the toxicity of the CPAHs and 3,4-HB was evaluated. Cardiomyocyte viability was measured using the MTT assay after 48 hours of exposure to concentrations ranging from 0.01 to 100 μg/mL. The cytotoxicity results are presented in Figure 4.6.

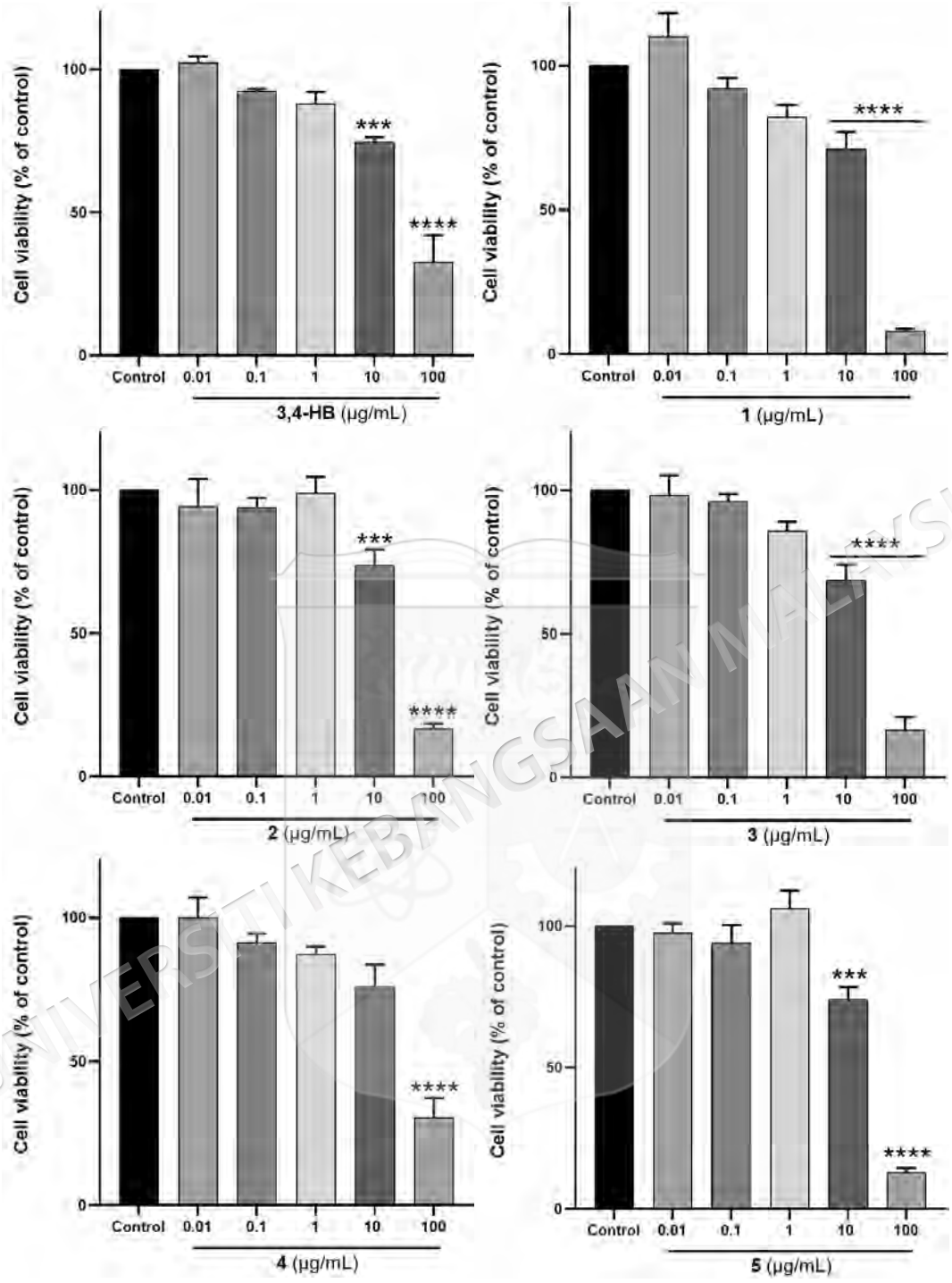

To be continued…

… continuation

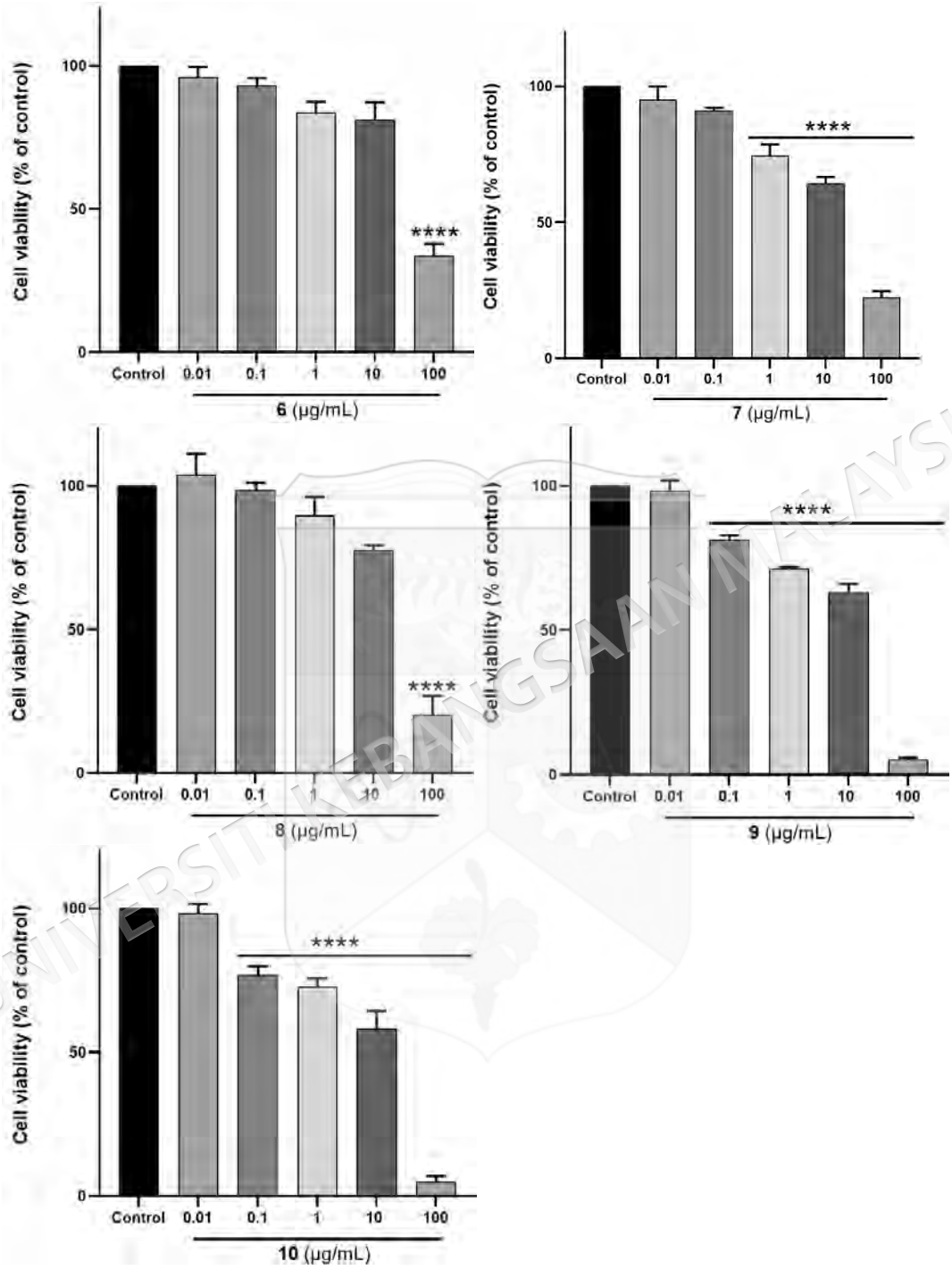

Figure 4.6 The effect of 3,4-HB and CPAHs (**1**–**10**) on H9c2 cells. Data are shown as mean ± SEM, n = 6. ***p<0.001 vs. control, ****p<0.0001

Exposure to varying concentrations of the 3,4-HB and CPAHs (**1**–**10**), up to 100 µg/mL, revealed a wide range of toxicity in H9c2 cells. 3,4-HB exhibited a non-toxic profile at concentrations of 0.01–1 µg/mL. However, at 10 µg/mL (64.88 µM),

3,4-HB demonstrated significant toxicity, reducing H9c2 cell viability to below 80% ($p < 0.001$). This finding contradicts the results of Shafiee et al. (2023), who reported that 3,4-HB did not show toxicity in H9c2 cells at concentrations ranging from 1 to 100 µM. The discrepancy might arise from differences in experimental protocols. In the current study, H9c2 cells were exposed to 3,4-HB for 48 hours, whereas Shafiee et al.'s experiments involved a shorter incubation period of 24 hours. Prolonged exposure could potentially increase the likelihood of observing toxic effects, as it allows more time for compound interaction with cellular targets, accumulation, or metabolic activation.

The CPAHs containing CA and HBAs (**1–6**) did not exhibit any cytotoxicity at concentrations ranging from 0.01 to 1 µg/mL (0.03–30 µM), maintaining cell viability at 80% or above. In contrast, among the CA-HCA hybrids (**7–10**), only compound **8** displayed a remarkably non-toxic profile against cardiomyocytes within the 0.01 to 10 µg/mL concentration range. Meanwhile, compounds **7**, **9**, and **10** demonstrated non-toxicity only at a concentration of 0.01 µg/mL. Based on these findings, concentrations ranging from 0.01 to 1 µg/mL, categorized as non-toxic, were chosen for subsequent experiments to assess the cardioprotective activity of CPAHs against DIC-induced damage in the H9c2 cell model.

Furthermore, a DIC model in H9c2 cardiomyocytes was used to explore the synthesized compounds' cardioprotective activity. The potential of CPAHs as cardioprotective agents was evaluated in cells treated with DOX in the presence of tested compounds. The cell viability of H9c2 cells after being treated with DOX (10 µM) or co-treated with test compound at 0.01, 0.1, and 1 µg/mL was determined. As shown in Figure 4.7, 10 µM DOX significantly reduced cardiomyocyte viability compared to the control, indicating the potent cardiotoxic effect of DOX.

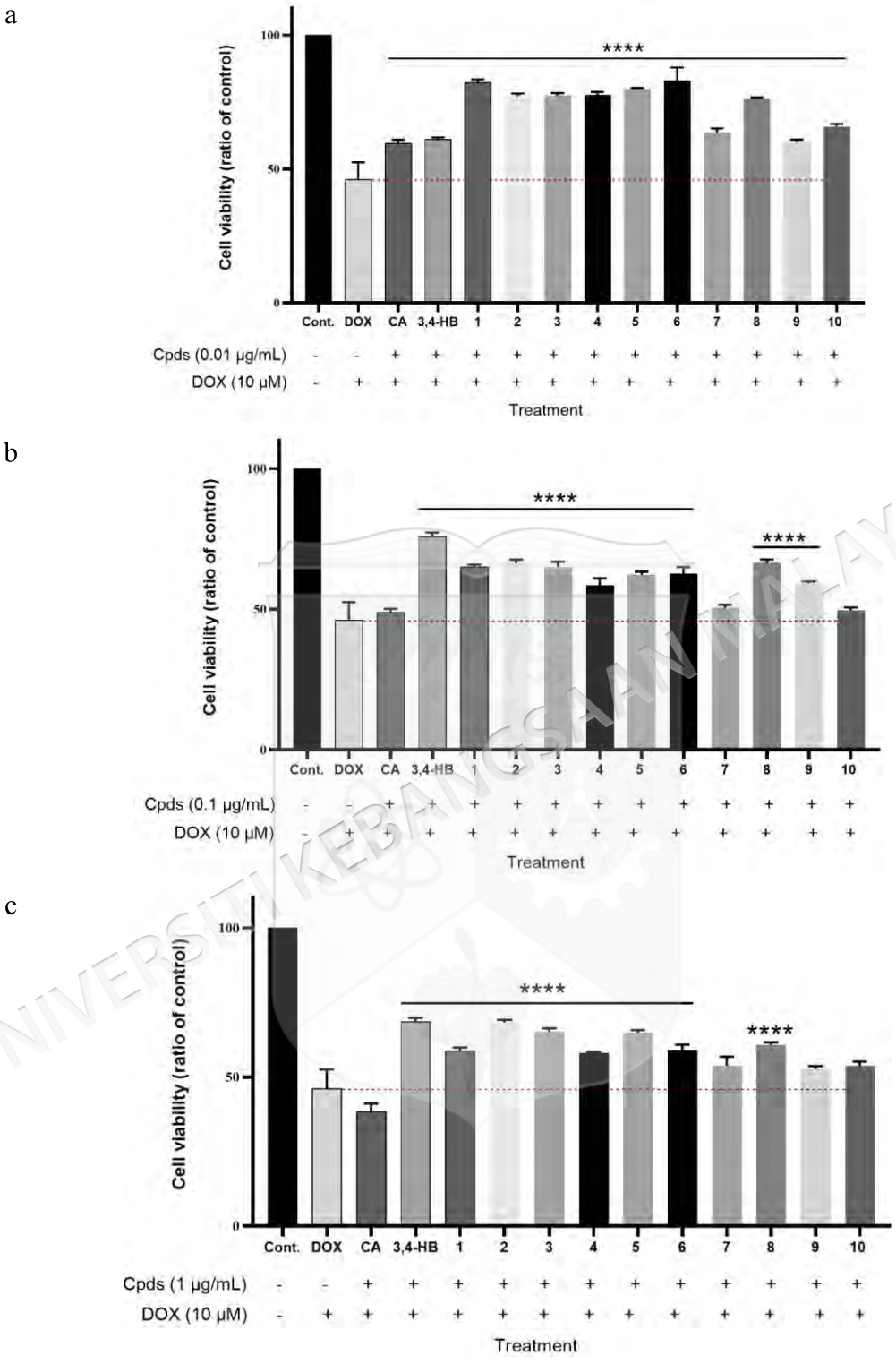

Figure 4.7 Protective effect of the parent compounds and **1**–**10** against DIC in H9c2 cardiomyocytes at concentration (a) 0.01 µg/mL, (b) 0.1 µg/mL, (c) 1 µg/mL. Data are shown as mean ± SEM, n = 6. ****p < 0.0001 vs. DOX-induced group

Forming cardioprotective agent hybrids (CPAHs) by combining CA with HBA and HCA resulted in compounds **1**–**10**. These compounds demonstrated increased cell

viability in H9c2 cells treated with DOX. These results indicated that such modification promotes protective activity. Specifically, linking 3-hydroxybenzoic acid, 4-hydroxybenzoic acid, 3,4-dihydroxybenzoic acid, 2,4-dihydroxybenzoic acid, 3,5-dihydroxybenzoic acid, or gallic acid to CA through a diester linker produced compounds **1–6**, all of which exhibited strong protective activity. These compounds significantly increased cell viability in DOX-treated H9c2 cells at concentrations of 0.01–1 μg/mL (0.03–30μM, $p<0.0001$), surpassing the protective effects of CA, the parent compound. The introduction of HBA into CA was crucial for their enhanced activity. Data confirmed that the protective effect of 3,4-HB, as a representative HBA scaffold, against DIC in the H9c2 cell model was higher than that of CA. Additionally, linking cinnamic acid, 4-hydroxycinnamic acid, 4-chlorocinnamic acid, or 2,4-dihydroxycinnamic acid yielded compounds **7–10**. These compounds significantly increased the survival rate of H9c2 cells treated with DOX at a concentration of 0.01 μg/mL (0.03 μM) ($p<0.0001$). Notably, compound **8** exhibited a protective effect comparable to CPAHs containing the HBA scaffold, enhancing the viability of H9c2 cells across the same concentration range ($p<0.0001$). However, higher concentrations of compounds **7**, **9**, and **10** did not correlate with increased cardioprotective effects and instead tended to exhibit toxic effects, indicating a narrow therapeutic window. In conclusion, at a low concentration of 0.01 μg/mL (0.03 μM), the hybrids (**1–10**) demonstrated a protective effect against DIC in H9c2 cells, exhibiting greater efficacy than CA alone.

4.3.3 Cardioprotective evaluation of CPAHs 11 – 21

To deepen the understanding of the structure-activity relationship (SAR) related to the cardioprotective activity of CPAHs, compounds **11–15** were synthesized to evaluate the impact of the linker on their efficacy. Similarly, compounds **16–21** were prepared to investigate the role of the CA scaffold. This section presents the *in vitro* cardioprotective evaluation of the parent compounds (CA and 3HA) alongside compounds **11–21**. Compound **1** was included as a comparator, given its incorporation of hydroxybenzoic acid (3HA), which was utilized in the transformations essential for synthesizing compounds **11–21**.

Initially, to elucidate the cytotoxic effects of DOX and to ensure the selected dosage of the synthetic compounds would not induce toxicity in the H9c2 cardiomyoblasts, H9c2 cells were exposed to DOX, the parent compounds, and the synthetic compounds. Cell viability was determined 48 h post-treatment using the Cell Counting Kit, employing a WST-8 reagent. As Figure 4.8demonstrates, the exposure of H9c2 cells to DOX (3 μM) for 48 h induced significant cytotoxicity ($p<0.05$), resulting in a decrease in cell viability, in line with the previous study (Sangweni et al. 2020; Zhou et al. 2022). However, treating the parent compounds and their hybrids (**1**, **11–21**) for 48 h showed no significant toxic effect on H9c2 cells.

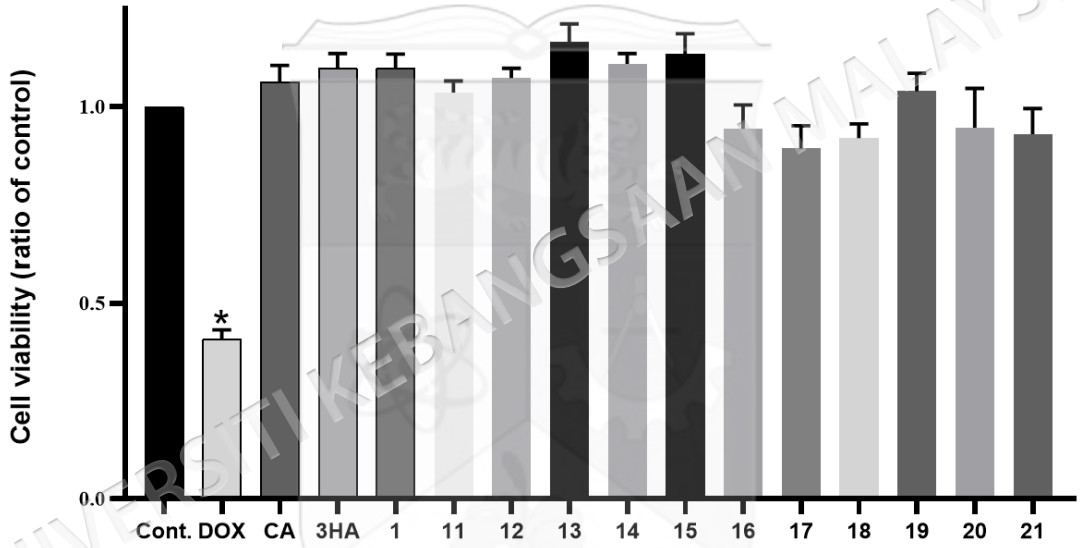

Figure 4.8 Effect of DOX (3 μM), **1**, **11–21** (10 μM), and the parent compounds (10 μM) on H9c2 cell viability after 48 h treatment. Values represent the mean ± SEM from three individual experiments. *P<0.05 vs. control.

The potential of the hybrids as cardioprotective agents was evaluated in cells treated with DOX in the presence of non-toxic compounds. Cell viability decreased to 64% in the DOX group compared to the untreated control group. Following a 24 h pre-incubation period with the parent compounds and their hybrids, it became evident that **15** exhibited significant cardioprotective efficacy, as evidenced by a notable increase in the percentage of viable cells compared to the DOX group ($p<0.05$, Figure 4.9). Furthermore, it can be observed that CA and 3HA, as the parent compounds, did not demonstrate cardioprotective activity against DOX-induced H9c2 cell death. The result was contrasted with CA's *in vivo* results (El-Sayed et al. 2016; Jafarinezhad et

al. 2019). This suggests that the presence of both the CA unit and the 3HA moiety is essential for cardioprotective effects, as the highest protection is achieved with **15**.

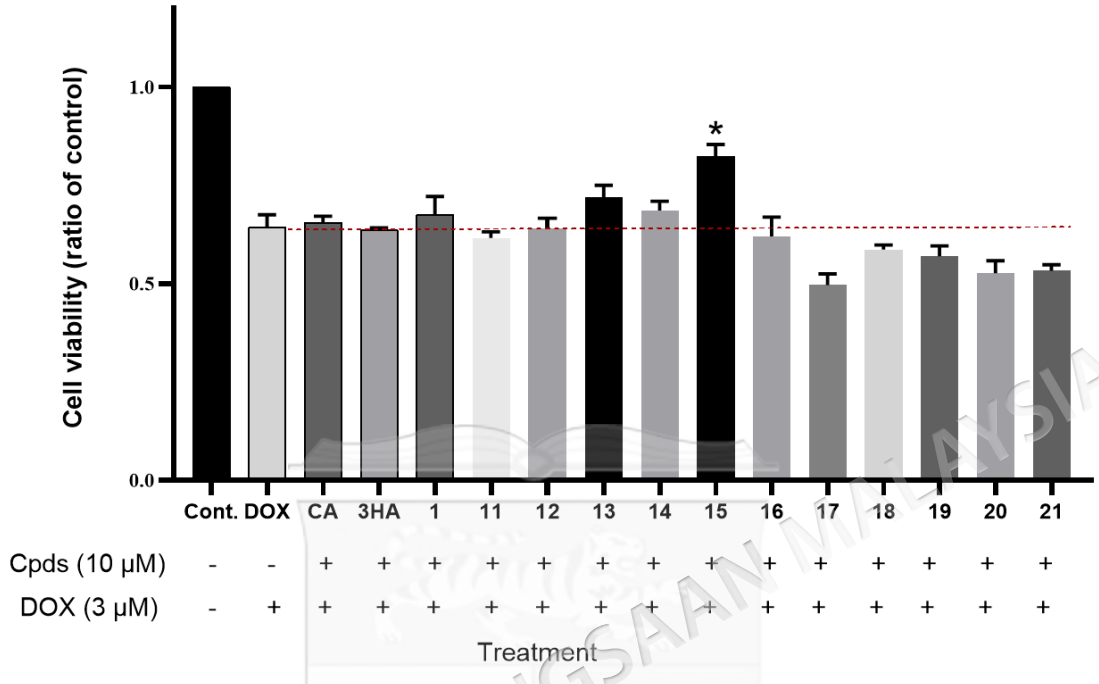

Figure 4.9 Protective effect of the parent compounds and **1**, **11**–**21** against DIC in H9c2 cardiomyocytes. H9c2 was pretreated with non-toxic compounds (10 μM) for 24 h followed by induction with 3 μM DOX for an additional 24 h. Data are shown as mean ± SEM, n = 3. *p<0.05 vs. DOX-induced group.

4.4 SAR OF CPAH AS POTENT CARDIOPROTECTOR AGAINST DIC

The SAR analysis, as summarized in Figure 4.10, offers critical insights into the cardioprotective potential of the hybrids. Compounds containing both CA and HBA scaffolds (**1**–**6**) demonstrated cardioprotective activity at concentrations ranging from 0.01 to 1 μg/mL (0.03–30 μM), exhibiting greater efficacy than CA alone. These results indicate that the integration of HBA into the CA framework plays a pivotal role in enhancing cardioprotective activity. The findings further suggest that HBA represents the scaffold with the most favorable SAR for cardioprotective efficacy, aligning with and reinforcing conclusions from prior research.

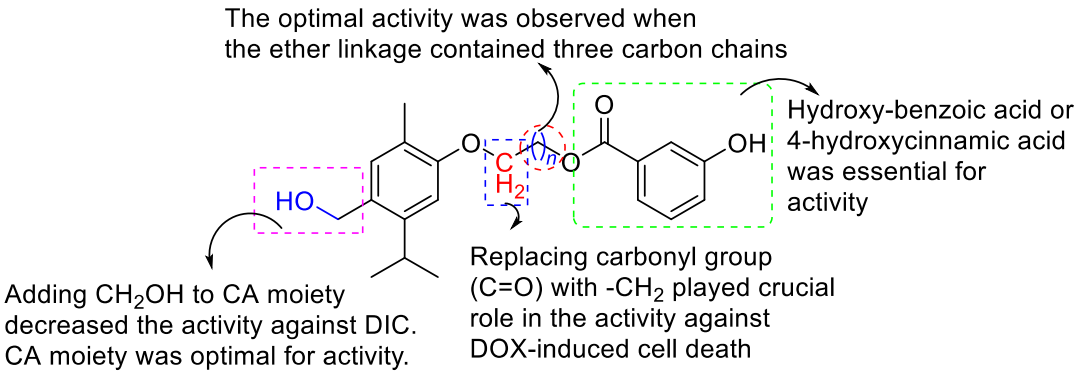

Figure 4.10 SAR analysis of CPAHs

HBAs have been widely recognized for their potential to mitigate DIC through antioxidant and anti-inflammatory mechanisms. Shafiee et al. (2023) reported that 3,4-HB protects cardiomyocytes from DIC-related damage by reducing total oxidant capacity and suppressing inflammatory processes via inhibition of Toll-like receptor 4 (TLR4) signaling. Furthermore, 3,4-HB exhibits a range of pharmacological activities, including anti-inflammatory, antioxidant, anti-cell death, anti-apoptotic, and chemoprotective effects, which collectively contribute to its cardioprotective efficacy (Okpara et al. 2022). Similarly, gallic acid has demonstrated significant cardioprotective effects against DIC. It alleviates electrocardiographic (ECG) abnormalities, reduces oxidative stress, and mitigates pathological tissue damage. These effects are accompanied by decreased levels of creatinine kinase-muscle brain (CK-MB), lactate dehydrogenase (LDH), and expression of pro-inflammatory markers such as TNF-α and Cox-2 (Ekinci et al. 2021; Omóbòwálé et al. 2018). Additionally, methyl gallate, a derivative of gallic acid, has been shown to confer cardioprotection against DIC in female rats by suppressing oxidative stress (Ahmed et al., 2021). The esterification of gallic acid appears to preserve its cardioprotective properties, highlighting the importance of the HBA scaffold in its activity. Collectively, these findings suggest that the antioxidant properties of the HBA scaffold in hybrids of CA and benzoic acid play a pivotal role in mitigating DIC.

Variations in the number and position of hydroxy groups within the benzoic acid scaffold did not significantly affect the cardioprotective activity of CPAHs (**1**–**6**). This observation indicates that the configuration of hydroxy groups is not a primary factor influencing their cardioprotective effects. Similar trends have been observed for

HBA, where HBAs with differing numbers of hydroxy groups consistently exhibited cardioprotective efficacy. This pattern aligns with findings from studies on flavonoids and their cardioprotective effects against DIC. For example, quercetin (Dong et al. 2014) and kaempferol (Xiao et al. 2014), both members of the flavonol group, differ only in the number of hydroxyl groups on their B rings but exhibit similar cardioprotective activities. Likewise, flavones such as baicalein (Sahu et al. 2016), 7,8-dihydroxyflavone (Zhao et al. 2019), and 7,8,3′-trihydroxyflavone (Zhao et al. 2023), which vary in the number and position of hydroxyl groups across two rings, as illustrated in Figure 4.11, have also demonstrated cardioprotective efficacy against DIC. These findings collectively emphasize that the antioxidant properties of these compounds, rather than the exact number or position of hydroxygroups, play a pivotal role in their cardioprotective activities.

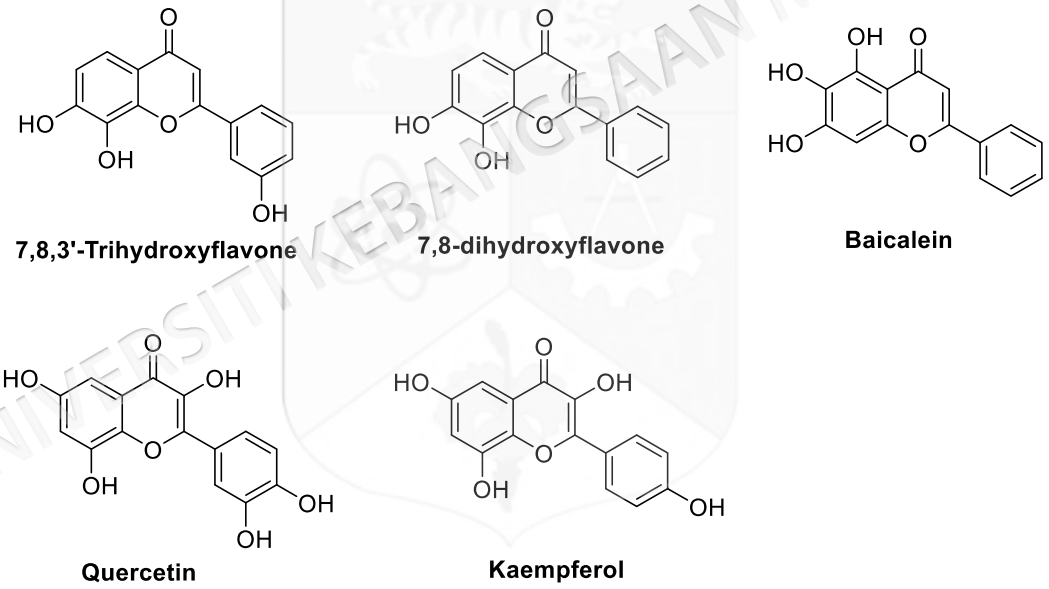

Figure 4.11 Examples of flavonoids demonstrating cardioprotective activities against DIC

Among the CPAHs derived from cinnamic acid and its derivatives (**7**–**10**), only compound **8**, containing a 4-hydroxycinnamic acid scaffold, demonstrated notable cardioprotective activity against DIC across a range of concentrations (0.03–30 μM). At higher concentrations (3–30 μM), compounds **7**, **9**, and **10** failed to significantly protect H9c2 cells from DIC. This pattern suggests that the absence of a hydroxygroup, as in compound **7**, or the substitution of the *para*-position hydroxy group with a chloro group, as in compound **9**, reduces activity. Furthermore,

introducing an additional hydroxy group on the cinnamic ring, as in compound **10**, also diminishes activity. These findings highlight the critical role of the 4-hydroxycinnamic acid moiety as an essential scaffold for the cardioprotective activity of CPAHs. This conclusion is supported by previous findings that 4-hydroxycoumaric acid exhibits antioxidant potential (Foti et al. 1996). Additionally, studies have shown that 4-hydroxycinnamic acid provides significant protection against DIC by reducing oxidative stress (Abdel-Wahab et al. 2003; Shiromwar and Chidrawar 2011). Further research indicates 4-hydroxycinnamic acid modulates autophagy and apoptosis induced by DOX, as evidenced by increased expression of protective markers such as Bcl-2, mTOR, Nrf-2, and Akt, and decreased levels of apoptotic markers including Bad, caspase-3, Bax, Atg-6, and Atg-8 (Sunitha et al. 2018). These findings strongly suggest that the cardioprotective activity of CPAHs is closely linked to their antioxidant properties.

To identify the physicochemical properties critical for optimal cardioprotective activity, the influence of linker structure on the efficacy of the hybrids was systematically investigated. This analysis aimed to elucidate the relationship between linker variation and biological activity, thereby providing insights into optimizing the pharmacological potential of these hybrids. Replacing the ester bond attached to the CA skeleton with an ether linkage significantly enhanced activity, as demonstrated in compounds **13–15**. The increased flexibility of alkyl linkers likely facilitates better interaction of the hybrids with their biological targets (Dong et al. 2022). Furthermore, the number of carbons in the ether linkage emerged as a crucial determinant, with maximum activity observed when the linker contained four carbons, as exemplified by compound **15**. In contrast, for hybrids with an ester linkage, optimal activity was achieved with a two-carbon linker, as observed in compound **1**. This finding aligns with research by Wang et al. (2023), which reported that the length of the alkyl linker between artemisinin and isatin significantly influenced activity, with two-carbon linkers outperforming three-carbon linkers. These results underscore the importance of linker flexibility and length in determining the physicochemical properties of the hybrids. Variations in linker structure affect lipophilicity and solubility, which, in turn, influence the bioavailability of the compounds, further highlighting their role in optimizing cardioprotective efficacy.

Extensive research has established that oxidative stress is a major contributor to DIC (Jamhiri et al. 2019). To enhance antioxidant properties, a CH_2OH moiety was incorporated into the CA scaffold, an approach previously reported to improve antioxidant activity of CA (Mastelić et al. 2008). However, efforts to improve the antioxidant capacity by modifying the CA structure, as seen in compounds **16–21**, were unsuccessful in mitigating DOX-induced cellular damage. Instead of providing cardioprotective benefits, these compounds demonstrated significant toxicity, evidenced by a decrease in cell viability compared to the DOX-treated control group. These findings suggest that the unmodified CA scaffold retains the most favorable SAR for cardioprotective activity. This conclusion is further supported by previous *in vitro* and *in vivo* studies that consistently validate the efficacy of the original CA scaffold in providing cardioprotection. Yu et al. (2013) found that CA had cardioprotective properties against myocardial ischemic damage in a rat model of acute myocardial infarction. Similarly, Chen et al. (2017) discovered that CA had a cardioprotective effect in a rat model of myocardial ischemia-reperfusion injury, which was linked to the activation of the MAPK/ERK and Akt/eNOS intracellular signaling pathways.

On the other hand, Jamhiri et al. (2019) observed the protective effect of CA against cardiac hypertrophy both *in vitro* and *in vivo*. CA reduced the size of rat cardiomyocyte H9c2 cells and inhibited the transcriptional expression of atrial natriuretic peptide (ANP) mRNA, a prominent indicator of cardiac hypertrophy. Furthermore, CA treatment induces hypotension and bradycardia in hypertensive rats by inhibiting extracellular Ca^{2+} influx, which modulates the cardiovascular system (Dias et al. 2022). CA also prevents endothelial dysfunction in hypertensive animals by increasing endothelial progenitor cell mobilization and lowering oxidative stress and senescence (Gonçalves et al. 2023). CA can potentially treat sepsis-induced cardiomyopathy by inhibiting lipopolysaccharide-induced changes through NLRP3 inflammasome inhibition and autophagy activation, thereby mitigating oxidative damage, histopathological changes, inflammation, and cardiac dysfunction (Joshi et al. 2023). However, the current research only covers validating the potential cardioprotective activity of the hybrids through *in vitro* assessment. Further

investigations are warranted to elucidate the mechanisms of action at the molecular level governing this observed potency in strategizing future therapy to mitigate DIC.

CHAPTER V

CONCLUSION AND FUTURE WORKS

5.1 SUMMARY

In summary, this research successfully met all its objectives, culminating in synthesizing and characterizing 21 CPAHs with moderate to high yield. These included ten previously known hybrids (**1–10**) and eleven novel hybrid compounds (**11–21**). CPAHs (**1–10**) were synthesized by attaching a linker through the reaction of CA with chloroacetyl chloride in the presence of TEA and DCM to form an intermediate (**22**). This intermediate was then hybridized with the appropriate HBA or HCA to produce the final compounds (**1–10**). For compound **12**, the synthesis method was modified by replacing TEA with sodium bicarbonate as a base in the final step. Additionally, a different approach was used to synthesize compound **11**. The reaction between CA and 3-choropropionyl chloride in the presence of a strong base typically results in an unwanted product (**24**) due to esterification followed by an elimination reaction. By using the intermediate as a nucleophilic source, this adjustment facilitated a successful condensation reaction with 3HA, resulting in the synthesis of compound **11**. Furthermore, the synthesis of compounds **13–15** involved a nucleophilic substitution reaction in the presence of potassium hydroxide to attach a linker (appropriate alkyl dihalide) via the O-alkyl chain to CA. This was followed by hybridization with 3HA through another nucleophilic substitution, facilitated by sodium bicarbonate. For the synthesis of compounds **16–21**, a similar method was employed as for compounds **1** and **11–15**, with the key difference being the use of 4-hydroxycarvacrol as the starting material instead of CA. Additionally, there was a final step involving the removal of the TBS group using tetrabutylammonium fluoride

(TBAF) or HF-pyridine. All the synthesized product was characterized by using NMR spectroscopy and HRMS.

Moreover, the cytotoxic evaluation against cardiomyocytes (H9c2 cells) revealed that compounds **1–6** and **8** exhibited no toxicity at concentrations ranging from 0.01 to 1 μg/mL (0.03 – 30 μM). In contrast, compounds **7**, **9**, and **10** were non-toxic only at the lowest concentration of 0.01 μg/mL (0.03 μM). Additionally, compounds **11–21** showed no significant toxic effect on cell viability at a concentration of 10 μM. The examinations on the cardioprotector efficacy of all the synthesized hybrid compounds against DIC in the H9c2 cell model showed that the hybrid making from CA and HBA (**1–6**) has strong protective activity at varied concentrations (0.03 – 30 μM), surpassing the protective effects of CA, the parent compound. Moreover, among the hybrids derived from CA and cinnamic acid derivatives, only compound **8** exhibited a protective effect similar to CPAHs with a HBA scaffold at comparable concentrations. However, compounds **7**, **9**, and **10** did not demonstrate enhanced cardioprotective effects at higher concentrations and instead showed toxic effects. Interestingly, for the cardioprotective evaluation of compounds **11–21**, only compound **15** has protector activity against DOX-induced cell death in the H9c2 cell model.

The SAR analysis based on our outcomes uncovered that conjugating HBA with CA is crucial for enhancing the cardioprotective activity of the parent compound. Additionally, while the number and position of hydroxygroups did not significantly impact efficacy, the presence of at least one hydroxy group attached to the benzoic acid moiety was essential for activity. Moreover, the 4-hydroxycinnamic acid moiety emerged as a vital scaffold for the cardioprotective activity of CPAH. It became evident that the type and number of carbons in the linker were crucial, with optimal activity achieved when the linker contained an ether linkage with four carbon atoms. Additionally, the current CA scaffold possesses the most favorable SAR for cardioprotection activity.

The results of this study indicate that hybrid compounds **1–6**, **8**, and **15** demonstrated good cardioprotective activity against DIC in the H9c2 cell model.

These findings highlight the promising therapeutic potential of these hybrid compounds as cardioprotective agents, warranting further experimental validation and development.

5.2 FUTURE STUDIES

The CA and PA moieties demonstrate significant potential across various applications, and CPAHs present an exciting opportunity for exploration in other biological applications and detection methods. Future work should focus on hybridizing CA with other natural phenolic acids known for their cardioprotective activity, such as salicylic acid, vanillic acid, syringic acid, caffeic acid, sinapic acid, and ferulic acid. Additionally, further investigation into the role of linkers on activity is recommended, particularly by lengthening the chain. However, hybrids with linkers longer than four carbons tend to have limited water solubility, so synthesizing CPAHs containing a sugar moiety should be explored to address this limitation. Overall, the CPAHs reported (**1–21**) exhibited a broad range of cardioprotective activity against DIC in the H9c2 cell model. This provides new insights into studying their *in vivo* effects and elucidating the molecular mechanisms underlying their ability to suppress DIC. Furthermore, developing novel CPAHs could lead to additional biological applications, including enhanced cardioprotective activity.

REFERENCES

Abdelgawad, I.Y., Sadak, K.T., Lone, D.W., Dabour, M.S., Niedernhofer, L.J. & Zordoky, B.N. 2021. Molecular mechanisms and cardiovascular implications of cancer therapy-induced senescence. *Pharmacol Ther.* 221: 107751.

Abdel-Wahab, M.H., El-Mahdy, M.A., Abd-Ellah, M.F., Helal, G.K., Khalifa, F. & Hamada, F.M. 2003. Influence of p-coumaric acid on doxorubicin-induced oxidative stress in rat's heart. *Pharmacol Res.* 48(5): 461–465.

Abdul Ghani, M.A., Ugusman, A., Latip, J. & Zainalabidin, S. 2023. Role of terpenophenolics in modulating inflammation and apoptosis in cardiovascular diseases: a review. *Int J Mol Sci.* 24(6): 5339.

Abushouk, A.I., Ismail, A., Salem, A.M.A., Afifi, A.M. & Abdel-Daim, M.M. 2017. Cardioprotective mechanisms of phytochemicals against doxorubicin-induced cardiotoxicity. *Biomed Pharmacother.* 90: 935–946.

Abu-Risha, S.E., Sokar, S.S., Elbohoty, H.R. & Elsisi, A.E. 2023. Combined carvacrol and cilostazol ameliorate ethanol-induced liver fibrosis in rats: possible role of SIRT1/Nrf2/HO-1 pathway. *Int Immunopharmacol.* 116: 109750.

Adhikari, A., Asdaq, S., Al Hawaj, M.A., Chakraborty, M., Thapa, G., Bhuyan, N.R., Imran, M., Alshammari, M.K., Alshehri, M.M., Harshan, A.A., Alanazi, A., Alhazmi, B.D. & Sreeharsha, N. 2021. Anticancer drug-induced cardiotoxicity: insights and pharmacogenetics. *Pharmaceuticals* 14(10): 970.

Ahmed, A.Z., Satyam, S.M., Shetty, P. & D'Souza, M.R. 2021. Methyl gallate attenuates doxorubicin-induced cardiotoxicity in rats by suppressing oxidative stress. *Scientifica (Cairo)* 2021: 6694340.

Ali, T., Tahir, S., Majeed, S.T., Majeed, R., Bashir, R., Mir, S.A., Jan, I., Bader, G.N. & Andrabi, K.I. 2024. Recent advances in the pharmacological properties and molecular mechanisms of carvacrol. *Rev Bras Farmacogn.* 34: 35–47.

Aljuffali, I.A., Lin, C.F., Chen, C.H. & Fang, J.Y. 2016. The codrug approach for facilitating drug delivery and bioactivity. *Expert Opin Drug Deliv.* 13(9): 1311–1325.

Alkreathy, H.M., Damanhouri, Z.A., Ahmed, N., Slevin, M. & Osman, A.-M. M. 2012. Mechanisms of cardioprotective effect of aged garlic extract against doxorubicin-induced cardiotoxicity. *Integr Cancer Ther.* 11(4): 364–370.

Anand, U., Dey, A., Chandel, A.K.S., Sanyal, R., Mishra, A., Pandey, D.K., De Falco, V., Upadhyay, A., Kandimalla, R., Chaudhary, A., Dhanjal, J.K., Dewanjee, S., Vallamkondu, J. & Pérez de la Lastra, J.M. 2023. Cancer chemotherapy and beyond: current status, drug candidates, associated risks and progress in targeted therapeutics. *Genes Dis.* 10(4): 1367–1401.

Andre, W.P., Ribeiro, W.L., Cavalcante, G.S., dos Santos, J.M., Macedo, I.T., de Paula, H.C., de Freitas, R.M., de Morais, S.M., de Melo, J.V. & Bevilaqua, C.M. 2016. Comparative efficacy and toxic effects of carvacryl acetate and carvacrol on sheep gastrointestinal nematodes and mice. *Vet Parasitol.* 218: 52–58.

Andricopulo, A.D. & Montanari, C.A. 2005. Structure-activity relationships for the design of small-molecule inhibitors. *Mini Rev Med Chem.* 5(6): 585–593.

Aneja, B., Azam, M., Alam, S., Perwez, A., Maguire, R., Yadava, U., Kavanagh, K., Daniliuc, C.G., Rizvi, M.M.A., Haq, Q.M.R. & Abid, M. 2018. Natural product-based 1,2,3-triazole/sulfonate analogues as potential chemotherapeutic agents for bacterial infections. *ACS Omega* 3(6): 6912–6930.

Angsutararux, P., Luanpitpong, S. & Issaragrisil, S. 2015. Chemotherapy-induced cardiotoxicity: overview of the roles of oxidative stress. *Oxid Med Cell Longev.* 2015: 795602.

Alokam, R., Jeankumar, V.U., Sridevi, J.P., Matikonda, S.S., Peddi, S., Alvala, M., Yogeeswari, P. & Sriram, D. 2014. Identification and structure-activity relationship study of carvacrol derivatives as *Mycobacterium tuberculosis* chorismate mutase inhibitors. *J Enzyme Inhib Med Chem.* 29(4): 547–554.

Ashraf, Z., Rafiq, M., Nadeem, H., Hassan, M., Afzal, S., Waseem, M., Afzal, K. & Latip, J. 2017. Carvacrol derivatives as mushroom tyrosinase inhibitors; synthesis, kinetics mechanism and molecular docking studies. *PLoS One* 12(5): e0178069.

Aswar, U., Mahajan, U., Kandhare, A. & Aswar, M. 2019. Ferulic acid ameliorates doxorubicin-induced cardiac toxicity in rats. *Naunyn Schmiedebergs Arch Pharmacol.* 392(6): 659–668.

Attanasi, O.A., Sole, R.D., Filippone, P., Ianne, R., Mazzetto, S.E., Mele, G. & Vasapollo, G. 2004. Synthesis of fullerene-cardanol derivatives. *Synlett.* 0799–0802.

Azizah, Ab.M., Nor Saleha, I.T., Noor H.A., Asmah, Z.A. & Mastulu, W. 2015. *Malaysian National Cancer Registry Report 2007-2011.*Putrajaya: Penerbit The National Cancer Institute, Ministry of Health: Putrajaya.

Bagchi, A.K., Malik, A., Akolkar, G., Jassal, D.S. & Singal, P.K. 2021. Endoplasmic reticulum stress promotes iNOS/NO and influences inflammation in the development of doxorubicin-induced cardiomyopathy. *Antioxidants* 10(12): 1897.

Bansal, N., Adams, M.J., Ganatra, S., Colan, S.D., Aggarwal, S., Steiner, R., Amdani, S., Lipshultz, E.R. & Lipshultz, S.E. 2019. Strategies to prevent anthracycline-induced cardiotoxicity in cancer survivors. *Cardiooncology* 5: 18.

Bansal, A., Saleh-E-In, M.M., Kar, P., Roy, A. & Sharma, N.R. 2022. Synthesis of carvacrol derivatives as potential new anticancer agent against lung cancer. *Molecules* 27(14): 4597.

Bassanetti, I., Mauro, C., Buschini, A., Montalbano, S., Leonardi, G., Pelagatti, P., Tosi, G., Massi, P., Fiorentini, L. & Rogolino, D. 2016. Investigation of antibacterial activity of new classes of essential oils derivatives. *Food Control* 73: 606–612.

Behranvand, N., Nasri, F., Zolfaghari Emameh, R., Khani, P., Hosseini, A., Garssen, J. & Falak, R. 2022. Chemotherapy: a double-edged sword in cancer treatment. *Cancer Immunol Immunother.*71(3): 527.

Ben Arfa, A., Combes, S., Preziosi-Belloy, L., Gontard, N. & Chalier, P. 2006. Antimicrobial activity of carvacrol related to its chemical structure. *Lett Appl Microbiol.* 43(2): 149–154.

Berridge, M.V., Herst, P.M. & Tan, A.S. 2005. Tetrazolium dyes as tools in cell biology: new insights into their cellular reduction. *Biotechnol Annu Rev.* 11: 127–152.

Białecka-Florjańczyk, E., Fabiszewska, A. & Zieniuk, B. 2018. Phenolic acids derivatives - biotechnological methods of synthesis and bioactivity. *Curr Pharm Biotechnol.* 19(14): 1098–1113.

Bin Jardan, Y.A., Ansari, M.A., Raish, M., Alkharfy, K.M., Ahad, A., Al-Jenoobi, F.I., Haq, N., Khan, M.R. & Ahmad, A. 2020. Sinapic acid ameliorates oxidative stress, inflammation, and apoptosis in acute doxorubicin-induced cardiotoxicity via the Nf-κB-mediated pathway. *Biomed Res Int.*2020: 3921796.

Bkhaitan, M.M., Alarjah, M., Mirza, A.Z., Abdalla, A.N., El-Said, H.M. & Faidah, H.S. 2018. Preparation and biological evaluation of metronidazole derivatives with monoterpenes and eugenol. *Chem Biol Drug Des.* 92(6): 1954–1962.

Boger, L.D. (2010). Alpha-keto heterocycles as faah inhibitors. *U.S. Patent No. WO 2010/*005572 A2. Washington, DC: U.S. Patent and Trademark Office.

Bonfim, R.R., Paiva-Souza, I.O., Moraes, J.P., Pereira, D.S., Santos, C.A., Santana, D.G., Thomazzi, S.M., Ferro, J.N., Barreto, E.O., Sousa, D.P. & Camargo, E.A. 2014. Isopropoxy-carvacrol, a derivative obtained from carvacrol, reduces acute inflammation and nociception in rodents. *Basic Clin Pharmacol Toxicol.* 115(3): 237–243.

Branco, A.F., Sampaio, S.F., Moreira, A.C., Holy, J., Wallace, K.B., Baldeiras, I., Oliveira, P.J. & Sardão, V.A. 2012. Differentiation-dependent doxorubicin toxicity on H9c2 cardiomyoblasts. *Cardiovasc Toxicol.* 12(4): 326–340.

Bray, F., Laversanne, M., Weiderpass, E. & Soerjomataram, I. 2021. The ever-increasing importance of cancer as a leading cause of premature death worldwide. *Cancer* 127(16): 3029–3030.

Bray, F., Laversanne, M., Sung, H., Ferlay, J., Siegel, R.L., Soerjomataram, I. & Jemal, A. 2024. Global cancer statistics 2022: GLOBOCAN estimates of incidence and mortality worldwide for 36 cancers in 185 countries. *CA Cancer J Clin.* 74(3): 229–263.

Brotzman, N., Xu, Y., Graybill, A., Cocolas, A., Ressler, A., Seeram, N.P., Ma, H. & Henry, G.E. 2019. Synthesis and tyrosinase inhibitory activities of 4-oxobutanoate derivatives of carvacrol and thymol.*Bioorg. Med. Chem. Lett.* 29: 56–58.

Butler, M.S., Robertson, A.A. & Cooper, M.A. 2014. Natural product and natural product derived drugs in clinical trials. *Nat Prod Rep.* 31(11): 1612–1661.

Chacko, S.M., Nevin, K.G., Dhanyakrishnan, R. & Kumar, B.P. 2015. Protective effect of p-coumaric acid against doxorubicin induced toxicity in H9c2 cardiomyoblast cell lines. *Toxicol Rep.* 2: 1213–1221.

Chang, W.T., Li, J., Haung, H.H., Liu, H., Han, M., Ramachandran, S., Li, C.Q., Sharp, W.W., Hamann, K.J., Yuan, C.S., Hoek, T.L. & Shao, Z.H. 2011. Baicalein protects against doxorubicin-induced cardiotoxicity by attenuation of mitochondrial oxidant injury and JNK activation. *J Cell Biochem.* 112(10): 2873–2881.

Chatterjee, K., Zhang, J., Honbo, N. & Karliner, J.S. 2010. Doxorubicin cardiomyopathy. *Cardiology.* 115(2): 155–162.

Chen, B., Peng, X., Pentassuglia, L., Lim, C.C. Sawyer, D.B. 2007. Molcular and cellular mechanisms of anthracycline cardiotoxicity. *Cardiovasc Toxicol.* 7(2): 114–121.

Chen, Y., Ba, L., Huang, W., Liu, Y., Pan, H., Mingyao, E., Shi, P., Wang, Y., Li, S., Qi, H., Sun, H. & Cao, Y. 2017. Role of carvacrol in cardioprotection against myocardial ischemia/reperfusion injury in rats through activation of MAPK/ERK and Akt/eNOS signaling pathways. *Eur J Pharmacol.* 796: 90–100.

Choi, H.J., Seon, M.R., Lim, S.S., Kim, J.S., Chun, H.S. & Park, J.H. 2008. Hexane/ethanol extract of *Glycyrrhiza uralensislicorice* suppresses doxorubicin-induced apoptosis in H9c2 rat cardiac myoblasts. *Exp Biol Med (Maywood).* 233(12): 1554–1560.

Chung, W.B. & Youn, H.J. 2016. Pathophysiology and preventive strategies of anthracycline-induced cardiotoxicity. *Korean J Intern Med.* 31(4): 625–633.

Cicalău, G.I.P., Babes, P.A., Calniceanu, H., Popa, A., Ciavoi, G., Iova, G.M., Ganea, M. & Scrobotă, I. 2021. Anti-inflammatory and antioxidant properties of carvacrol and magnolol, in periodontal disease and diabetes mellitus. *Molecules* 26(22): 6899.

Concepción, R.L., Froylán, I.V., Herminia, I.P.M., Norberto, M.A., Héctor, J.S.Z. & Yeniel, G.C. 2013. In vitro assessment of the acaricidal activity of computer-

selected analogues of carvacrol and salicylic acid on *Rhipicephalus* (Boophilus) *microplus*. *Exp Appl Acarol.* 61(2): 251–257.

Cuadrado, I., Oramas-Royo, S., González-Cofrade, L., Amesty, Á., Hortelano, S., Estévez-Braun, A. & de Las Heras, B. 2023. Labdane conjugates protect cardiomyocytes from doxorubicin-induced cardiotoxicity. *Drug Dev Res.* 84(1): 84–95.

Dallons, M., Schepkens, C., Dupuis, A., Tagliatti, V. & Colet, J.M. 2020. New insights about doxorubicin-induced toxicity to cardiomyoblast-derived h9c2 cells and dexrazoxane cytoprotective effect: contribution of in vitro 1h-nmr metabonomics. *Front Pharmacol.* 11: 79.

Damasceno, S.R., Oliveira, F.R., Carvalho, N.S., Brito, C.F., Silva, I.S., Sousa, F.B., Silva, R.O., Sousa, D.P., Barbosa, A.L., Freitas, R.M. & Medeiros, J.V. 2014. Carvacryl acetate, a derivative of carvacrol, reduces nociceptive and inflammatory response in mice. *Life Sci.* 94(1): 58–66.

Das, N., Dhanawat, M., Dash, B., Nagarwal, R.C. & Shrivastava, S.K. 2010. Codrug: an efficient approach for drug optimization. *Eur J Pharm Sci.* 41(5): 571–588.

Department of Statistic Malaysia. 2023. Statistics on Causes of Death, Malaysia, 2023. https://www.dosm.gov.my/portal-main/release-content/statistics-on-causes-of-death-malaysia-2023 [24 July 2024].

De Castro, M.R.C., Naves, R.F., Bernardes, A., da Silva, C.C., Perez, C.N., Moura, A.F., de Moraes, M.O. & Martins, F.T. 2020. Tandem chalcone-sulfonamide hybridization, cyclization and further Claisen–Schmidt condensation: tuning molecular diversity through reaction time and order and catalyst. *Arab J Chem.* 13(1): 1345–1354.

De Mesquita, B.M., do Nascimento, P.G.G., Souza, L.G.S., de Farias, I.F., da Silva, R.A.C., de Lemos, T.L.G., Monte, F.J.Q., Oliveira, I.R., Trevisan, M.T.S, da Silva, H.C. & Santiago, G.M.P. 2018. Synthesis, larvicidal and acetylcholinesterase inhibitory activities of carvacrol/thymol and derivatives. *Quím Nova.* 41(4): 412–416.

De Moraes, J., Carvalho, A.A., Nakano, E., de Almeida, A.A., Marques, T.H., Andrade, L.N., de Freitas, R.M. & de Sousa, D.P. 2013. Anthelmintic activity of carvacryl acetate against *Schistosoma mansoni*. *Parasitol Res.* 112(2): 603–610.

De Oliveira, A.S., Llanes, L.C., Brighente, I.M.C., Nunes, R.J., Yunes, R.A., Junior, N.M., Baumgart, A.M.K., Aust, A.N. & Cruz, A.B. 2016. New sulfonamides derived from carvacrol: compounds with high antibacterial activity against resistant *Staphylococcus aureus* strains. *J Biosci Med. 4:* 105–114.

De Santana, M.T., Silva, V.B., de Brito, R.G., dos Santos, P.L., de Holanda Cavalcanti, S.C., Barreto, E.O., de Souza Ferro, J.N., dos Santos, M.R., de Sousa Araújo, A.A. & Quintans-Júnior, L.J. 2014. Synthesis and

pharmacological evaluation of carvacrol propionate. *Inflammation.* 37(5): 1575–1587.

De Souza, G.H.A., Dos Santos Radai, J.A., Mattos Vaz, M.S., Esther da Silva, K., Fraga, T.L., Barbosa, L.S. & Simionatto S. 2021. In vitro and in vivo antibacterial activity assays of carvacrol: A candidate for development of innovative treatments against KPC-producing *Klebsiella pneumoniae*. *PLoS One* 16(2): e0246003.

Dias, C.J., Costa, H.A., Alves Dias-Filho, C.A., Ferreira, A.C., Rodrigues, B., Irigoyen, M.C., Romão Borges, A.C., de Andadre Martins, V., Branco Vidal, F.C., Ribeiro, R.M., Filho, N.S. & Mostarda, C.T. 2022. Carvacrol reduces blood pressure, arterial responsiveness and increases expression of MAS receptors in spontaneously hypertensive rats. *Eur J Pharmacol.* 917: 174717.

Dong, M., Zheng, G., Gao, F., Li, M. & Zhong, C. 2022. Three-carbon linked dihydroartemisinin-isatin hybrids: design, synthesis and their antiproliferative anticancer activity. *Front Pharmacol.* 13: 834317.

Dong, Q., Chen, L., Lu, Q., Sharma, S., Li, L., Morimoto, S. & Wang, G. 2014. Quercetin attenuates doxorubicin cardiotoxicity by modulating Bmi-1 expression. *Br J Pharmacol.* 171(19): 4440–4454.

Dong-Hyuk, C., I-Rang, L., Jong-Ho, K., Mi-Na, K., Yong-Hyun, K., Kyong, H.P., Seong-Mi, P. & Wan, J.S. 2020. Protective effects of statin and angiotensin receptor blocker in a rat model of doxorubicin- and trastuzumab-induced cardiomyopathy. *JAm Soc Echocardiogr.* 33(10): 1253–1263.

Dulf, P.L., Mocan, M., Coadă, C.A., Dulf, D.V., Moldovan, R., Baldea, I., Farcas, A.D., Blendea, D. & Filip, A.G. 2023. Doxorubicin-induced acute cardiotoxicity is associated with increased oxidative stress, autophagy, and inflammation in a murine model. *Naunyn Schmiedebergs Arch Pharmacol.* 396(6): 1105–1115.

Ekinci Akdemir, F.N., Yildirim, S., Kandemir, F.M., Tanyeli, A., Küçükler, S. & Bahaeddin Dortbudak, M. 2021. Protective effects of gallic acid on doxorubicin-induced cardiotoxicity, an experimantal study. *Arch Physiol Biochem.* 127(3): 258–265.

El-Sayed el-SM, Mansour, A.M. & Abdul-Hameed, M.S. 2016. Thymol and carvacrol prevent doxorubicin-induced cardiotoxicity by abrogation of oxidative stress, inflammation, and apoptosis in rats. *J Biochem Mol Toxicol.* 30(1): 37–44.

Fabbri, J., Maggiore, M.A., Pensel, P.E., Denegri, G.M., Gende, L.B. & Elissondo, M.C. 2016. In vitro and in vivo efficacy of carvacrol against *Echinococcus granulosus*. *Acta Trop.* 164: 272–279.

Fachini-Queiroz, F.C., Kummer, R., Estevão-Silva, C.F., Carvalho, M.D., Cunha, J.M., Grespan, R., Bersani-Amado, C.A. & Cuman, R.K. 2012. Effects of thymol and carvacrol, constituents of *Thymus vulgaris L*. essential oil, on the inflammatory response. *Evid Based Complement Alternat Med.* 2012: 657026.

Ferlay, J., Ervik, M., Lam, F., et al. 2024. Global cancer observatory: cancer today (version 1.0). International agency for research on cancer. https://gco.iarc.who.int/en [24 July 2024].

Foti, M., Piattelli, M., Baratta, M.T. & Ruberto, G. 1996. Flavonoids, coumarins, and cinnamic acids as antioxidants in a micellar system. structure−activity relationship. *J Agric Food Chem.* 44(2): 497–501.

Friedman, D.L., Whitton, J., Leisenring, W., Mertens, A.C., Hammond, S., Stovall, M., Donaldson, S.S., Meadows, A.T., Robison, L.L. & Neglia, J.P. 2010. Subsequent neoplasms in 5-year survivors of childhood cancer: the childhood cancer survivor study. *J Natl Cancer Inst.* 102(14): 1083–1095.

Ghasemi, M., Turnbull, T., Sebastian, S. & Kempson, I. 2021. The MTT assay: utility, limitations, pitfalls, and interpretation in bulk and single-cell analysis. *Int J Mol Sci.* 22(23): 12827.

Gonçalves, T.A.F., Lima, V.S., de Almeida, A.J.P.O., de Arruda, A.V., Veras, A.C.M.F., Lima, T.T., Soares, E.M.C., Santos, A.C.D., Vasconcelos, M.E.C., de Almeida Feitosa, M.S., Veras, R.C. & de Medeiros, I.A. 2023. Carvacrol improves vascular function in hypertensive animals by modulating endothelial progenitor cells. *Nutrients* 15(13): 3032.

Guimarães, A.G., Oliveira, G.F., Melo, M.S., Cavalcanti, S.C., Antoniolli, A.R., Bonjardim, L.R., Silva, F.A., Santos, J.P., Rocha, R.F., Moreira, J.C., Araújo, A.A., Gelain, D.P. & Quintans-Júnior, L.J. 2010. Bioassay-guided evaluation of antioxidant and antinociceptive activities of carvacrol. *Basic Clin Pharmacol Toxicol.* 107(6): 949–957.

Günes-Bayir, A., Kiziltan, H.S., Kocyigit, A., Güler, E.M., Karataş, E. & Toprak, A. 2017. Effects of natural phenolic compound carvacrol on the human gastric adenocarcinoma (AGS) cells in vitro. *Anticancer Drugs* 28(5): 522–530.

Hanušová, V., Boušová, I. & Skálová, L. 2011. Possibilities to increase the effectiveness of doxorubicin in cancer cells killing. *Drug Metab Rev.* 43(4): 540–557.

Hao, Y., Li, J. & Shi, L. 2021. A carvacrol-rich essential oil extracted from Oregano (*Origanum vulgare* “Hot & Spicy”) exerts potent antibacterial effects against *Staphylococcus aureus*. *Front Microbiol.*12: 741861.

Hasinoff, B.B., Patel, D. & Wu, X. 2020. A QSAR study that compares the ability of bisdioxopiperazine analogs of the doxorubicin cardioprotective agent dexrazoxane (ICRF-187) to protect myocytes with DNA topoisomerase II inhibition. *Toxicol Appl Pharmacol.* 399: 115038.

Heidarian, E. & Keloushadi, M. 2019. Antiproliferative and anti-invasion effects of carvacrol on PC3 human prostate cancer cells through reducing pSTAT3, pAKT, and pERK1/2 signaling proteins. *Int J Prev Med.* 10: 156.

Howerton, S.B., Nagpal, A. & Williams, L.D. 2003. Surprising roles of electrostatic interactions in DNA-ligand complexes. *Biopolymers.* 69(1): 87–99.

Huang, W., Xu, R., Zhou, B., Lin, C., Guo, Y., Xu, H. & Guo, X. 2022. Clinical manifestations, monitoring, and prognosis: a review of cardiotoxicity after antitumor strategy. *Front Cardiovasc Med.* 9: 912329.

Imran, M., Aslam, M., Alsagaby, S.A., Saeed, F., Ahmad, I., Afzaal, M., Arshad, M.U., Abdelgawad, M.A., El-Ghorab, A.H., Khames, A., Shariati, M.A., Ahmad, A., Hussain, M., Imran, A. & Islam, S. 2022. Therapeutic application of carvacrol: a comprehensive review. *Food Sci Nutr.*10(11): 3544–3561.

Jafarinezhad, Z., Rafati, A., Ketabchi, F., Noorafshan, A. & Karbalay-Doust, S. 2019. Cardioprotective effects of curcumin and carvacrol in doxorubicin-treated rats: Stereological study. *Food Sci Nutr.* 7(11): 3581–3588.

James, A., Stefan, B., Gianni, C., Miles, C., Phil, E., Joerg, H., Annika, K., Karin, K., Christopher, M., Sahil, P., Laszlo, R., Didier, R., Mark, S. & Liselotte, O. 2007. Substituted isoindoles as bace inhibitors and their use. European Patent No. EP 2035378 A1. Paris: European Patent Office.

Jamhiri, M., Safi Dahaj, F., Astani, A., Hejazian, S.H., Hafizibarjin, Z., Ghobadi, M., Moradi, A., Khoradmehr, A. & Safari, F. 2019. Carvacrol ameliorates pathological cardiac hypertrophy in both In-vivo and In-vitro models. *Iran J Pharm Res.* 18(3): 1380–1394.

Jones, R.L., Swanton, C. & Ewer, M.S. 2006. Anthracycline cardiotoxicity. *Expert Opin Drug Saf.* 5(6): 791–809.

Joshi, S., Kundu, S., Priya, V.V., Kulhari, U., Mugale, M.N. & Sahu, B.D. 2023. Anti-inflammatory activity of carvacrol protects the heart from lipopolysaccharide-induced cardiac dysfunction by inhibiting pyroptosis via NLRP3/Caspase1/Gasdermin D signaling axis. *Life Sci.* 324: 121743.

Jukic, M., Politeo, O., Maksimovic, M., Milos, M. & Milos, M. 2007. In vitro acetylcholinesterase inhibitory properties of thymol, carvacrol and their derivatives thymoquinone and thymohydroquinone. *Phytother Res.* 21(3): 259–261.

Kabir, S., Lingappa, N. & Mayrovitz, H. 2022. Potential therapeutic treatments for doxorubicin-induced cardiomyopathy. *Cureus*4(1): e21154.

Kalyanaraman, B. 2017. Teaching the basics of cancer metabolism: developing antitumor strategies by exploiting the differences between normal and cancer cell metabolism. *Redox Biol.* 12: 833–842.

Khajavi Rad, A. & Mohebbati, R. 2019. *Zataria multiflora* extract and carvacrol affect cardiotoxicity induced by adriamycin in rat. *J Basic Clin Physiol Pharmacol*.30(1): 73–79.

Khazdair, M.R., Moshtagh, M., Anaeigoudari, A., Jafari, S. & Kazemi, T. 2024. Protective effects of carvacrol on lipid profiles, oxidative stress, hypertension, and cardiac dysfunction – a comprehensive review.*Food Sci. Nutr.* 12: 3137–3149.

Kinarivala, N., Suh, J.H., Botros, M., Webb, P. & Trippier, P.C. 2016. Pharmacophore elucidation of phosphoiodyn A - Potent and selective peroxisome proliferator-activated receptor β/δ agonists with neuroprotective activity. *Bioorg Med Chem Lett.* 26(8): 1889–1893.

Koczurkiewicz-Adamczyk, P., Klaś, K., Gunia-Krzyżak, A., Piska, K., Andrysiak, K., Stępniewski, J., Lasota, S., Wójcik-Pszczoła, K., Dulak, J., Madeja, Z. & Pękala, E. 2021. Cinnamic acid derivatives as cardioprotective agents against oxidative and structural damage induced by doxorubicin. *Int J Mol Sci.* 22*:* 6217.

Koh, J.S., Yi, C.O., Heo, R.W., Ahn, J.W., Park, J.R., Lee, J.E., Kim, J.H., Hwang, J.Y. & Roh, G.S. 2015. Protective effect of cilostazol against doxorubicin-induced cardiomyopathy in mice. *Free Radic Biol Med*. 89: 54–61.

Kollárová-Brázdová, P., Jirkovská, A., Karabanovich, G., Pokorná, Z., Bavlovič Piskáčková, H., Jirkovský, E., Kubeš, J., Lenčová-Popelová, O., Mazurová, Y., Adamcová, M., Skalická, V., Štěrbová-Kovaříková, P., Roh, J., Šimůnek, T. & Štěrba, M. 2020. Investigation of structure-activity relationships of dexrazoxane analogs reveals topoisomerase II*β* interaction as a prerequisite for effective protection against anthracycline cardiotoxicity. *J Pharmacol Exp Ther.* 373(3): 402–415.

Kondo, N., Takahashi, A., Ono, K. & Ohnishi, T. 2010. DNA damage induced by alkylating agents and repair pathways. *J Nucleic Acids.* 2010: 543531.

Kong, C.Y., Guo, Z., Song, P., Zhang, X., Yuan, Y.P., Teng, T., Yan, L. & Tang, Q. Z. 2022. Underlying the mechanisms of doxorubicin-induced acute cardiotoxicity: oxidative stress and cell death. *Int J Biol Sci.* 18(2): 760–770.

Konig, I.F.M., Gonçalves, R.R.P., Oliveira, M.V.S., Silva, C.M., Thomasi, S.S., Peconick, A.P. & Remedio, R.N. 2019. Sublethal concentrations of acetylcarvacrol strongly impact oocyte development of engorged female cattle ticks *Rhipicephalus microplus* (Canestrini, 1888) (Acari: Ixodidae). *Ticks Tick Borne Dis.* 10(4): 766–774.

Kumar, N. & Goel, N. 2019. Phenolic acids: natural versatile molecules with promising therapeutic applications. *Biotechnol Rep (Amst).* 24: e00370.

Lahnwong, C., Chattipakorn, S.C. & Chattipakorn, N. 2018. Potential mechanisms responsible for cardioprotective effects of sodium–glucose co-transporter 2 inhibitors. *Cardiovasc Diabetol*. 17: 101.

Leger, K., Slone, T., Lemler, M., Leonard, D., Cochran, C., Bowman, W.P., Bashore, L. & Winick, N. 2015. Subclinical cardiotoxicity in childhood cancer survivors

exposed to very low dose anthracycline therapy. *Pediatr Blood Cancer* 62(1): 123–127.

Li, T.K. & Liu, L.F. 2001. Tumor cell death induced by topoisomerase-targeting drugs. *Annu Rev Pharmacol Toxicol.* 41: 53– 77.

Li, Z., Hua, C., Pan, X., Fu, X. & Wu, W. 2016. Carvacrol exerts neuroprotective effects via suppression of the inflammatory response in middle cerebral artery occlusion rats. *Inflammation* 39(4): 1566–1572.

Li, X. 2023. Doxorubicin-mediated cardiac dysfunction: Revisiting molecular interactions, pharmacological compounds and (nano)theranostic platforms. *Environ Res.* 234: 116504.

Lipshultz, S.E., Scully, R.E., Lipsitz, S.R., Sallan, S.E., Silverman, L.B., Miller, T.L., Barry, E.V., Asselin, B.L., Athale, U., Clavell, L.A., Larsen, E., Moghrabi, A., Samson, Y., Michon, B., Schorin, M.A., Cohen, H.J., Neuberg, D.S., Orav, E.J. & Colan, S.D. 2010. Assessment of dexrazoxane as a cardioprotectant in doxorubicin-treated children with high-risk acute lymphoblastic leukaemia: long-term follow-up of a prospective, randomised, multicentre trial. *Lancet Oncol.* 11(10): 950–961.

Lipshultz, S.E., Lipsitz, S.R., Kutok, J.L., Miller, T.L., Colan, S.D., Neuberg, D.S., Stevenson, K.E., Fleming, M.D., Sallan, S.E., Franco, V.I., Henkel, J.M., Asselin, B.L., Athale, U.H., Clavell, L.A., Michon, B., Laverdiere, C., Larsen, E., Kelly, K.M. & Silverman, L.B. 2013. Impact of hemochromatosis gene mutations on cardiac status in doxorubicin-treated survivors of childhood high-risk leukemia. *Cancer* 119(19):3555–62.

Liu, X., Tian, R., Tao, H., Wu, J., Yang, L., Zhang, Y. & Meng, X. 2022. The cardioprotective potentials and the involved mechanisms of phenolic acids in drug-induced cardiotoxicity. *Eur J Pharmacol.* 936: 175362.

Llana-Ruiz-Cabello, M., Gutiérrez-Praena, D., Puerto, M., Pichardo, S., Jos, A. & Cameán, A.M. 2015. In vitro pro-oxidant/antioxidant role of carvacrol, thymol and their mixture in the intestinal Caco-2 cell line. *Toxicol In Vitro*. 29(4): 647–656.

Lupo Jr, A. T., Nakatsu, T., Caldwell, J., Kang, R. K., Cilia, A. T., Van Loveren, A. G. & Villamaria, L.2000. Substituted phenols as fragrance, flavor and antimicrobial compounds. U.S. Patent No. 6,110,888. Washington, DC: U.S. Patent and Trademark Office.

Malik, D., Mahendiratta, S., Kaur, H. & Medhi, B. 2021. Futuristic approach to cancer treatment. *Gene* 805:145906.

Marinelli, L., Fornasari, E., Eusepi, P., Ciulla, M., Genovese, S., Epifano, F., Fiorito, S., Turkez, H., Örtücü, S., Mingoia, M., Simoni, S., Pugnaloni, A., Di Stefano, A. & Cacciatore, I. 2019. Carvacrol prodrugs as novel antimicrobial agents. *Eur J Med Chem.* 178: 515–529.

Marinello, J., Delcuratolo, M. & Capranico, G. 2018. Anthracyclines as topoisomerase II poisons: from early studies to new perspectives. *Int J Mol Sci.* 19(11): 3480.

Martins-Teixeira M.B. & Carvalho, I. 2020. Antitumour anthracyclines: progress and perspectives. *ChemMedChem.* 15(11): 933–948.

Marty, M., Espié, M., Llombart, A., Monnier, A., Rapoport, B.L. & Stahalova, V. 2006. Multicenter randomized phase III study of the cardioprotective effect of dexrazoxane (cardioxane) in advanced/metastatic breast cancer patients treated with anthracycline-based chemotherapy. *Ann Oncol.* 17(4): 614–622.

Mastelić, J., Jerković, I., Blazević, I., Poljak-Blazi, M., Borović, S., Ivancić-Baće, I., Smrecki, V., Zarković, N., Brcić-Kostic, K., Vikić-Topić, D. & Müller, N. 2008. Comparative study on the antioxidant and biological activities of carvacrol, thymol, and eugenol derivatives. *J Agric Food Chem.* 56(11): 3989–3996.

Mathela, C.S., Singh, K.K. & Gupta, V.K. 2010. Synthesis and in vitro antibacterial activity of thymol and carvacrol derivatives. *Acta Pol Pharm.* 67(4): 375–380.

Mbese, Z., Nell, M., Fonkui, Y.T., Ndinteh, D.T., Steenkamp, V. & Aderibigbe, B.A. 2022. Hybrid compounds containing carvacrol scaffold: in vitro antibacterial and cytotoxicity evaluation. *Recent Adv Antiinfect Drug Discov.* 17(1): 54–68.

Melo, F.H., Venâncio, E.T., de Sousa, D.P., de França Fonteles, M.M., de Vasconcelos, S.M., Viana, G.S. & de Sousa, F.C. 2010. Anxiolytic-like effect of carvacrol (5-isopropyl-2-methylphenol) in mice: involvement with GABAergic transmission. *Fundam Clin Pharmacol.* 24(4): 437–443.

Melo, F.H., Moura, B.A., de Sousa, D.P., de Vasconcelos, S.M., Macedo, D.S., Fonteles, M.M., Viana, G.S. & de Sousa, F.C. 2011. Antidepressant-like effect of carvacrol (5-Isopropyl-2-methylphenol) in mice: involvement of dopaminergic system. *Fundam Clin Pharmacol.* 25(3): 362–367.

Meng, C., Wang, X., Fan, L., Fan, Y., Yan, Z., Wang, Y., Li, Y., Zhang, J. & Lv, S. 2024. A new perspective in the prevention and treatment of antitumor therapy-related cardiotoxicity: Intestinal microecology. *Biomed Pharmacother.* 170: 115588.

Minotti, G., Menna, P., Salvatorelli, E., Cairo, G. & Gianni, L. 2004. Anthracyclines: molecular advances and pharmacologic developments in antitumor activity and cardiotoxicity. *Pharmacol Rev.* 56(2): 185–229.

Mobaraki, M., Faraji, A., Zare, M., Dolati, P., Ataei M. & Manshadi, H.R.D. 2017. Molecular mechanisms of cardiotoxicity: a review on major side-effects of doxorubicin. *Indian J Pharm Sci.* 79: 335–344.

Monahan, D.S., Flaherty, E., Hameed, A. & Duffy, G.P. 2021. Resveratrol significantly improves cell survival in comparison to dexrazoxane and

carvedilol in a h9c2 model of doxorubicin induced cardiotoxicity. *Biomed Pharmacother.* 140: 111702.

More, U.B., Narkhede, H.P., Dalal, D.S. & Mahulikar, P.P. 2007. Synthesis of biologically active carvacrol compounds using different solvents and supports. *Synth Commun.*37: 1957–1964.

Narkhede, H., More, U., Dalal, D. & Mahulikar, P. 2008. Solid-supported synthesis of bioactive carvacrol compounds using microwaves. *Synth Commun.*38: 2413–2418.

Natal, C.M., Pereira, D.M., Pereira, R.B., Fernandes, M.J.G., Fortes, A.G., Castanheira, E.M.S. & Gonçalves, M.S.T. 2021. Carvacrol Derivatives with Potential Insecticidal Activity. *Chem Proc.* 3(1): 37.

Nepali. K., Sharma, S., Sharma, M., Bedi, P.M. & Dhar, K.L. 2014. Rational approaches, design strategies, structure activity relationship and mechanistic insights for anticancer hybrids. *Eur J Med Chem.* 77: 422–487.

Nesterkina, M., Bilokon, S., Alieksieieva, T., Chebotar, S. & Kravchenko, I. 2020. Toxic effect and genotoxicity of carvacrol ethers in *Drosophila melanogaster*. *Mutat Res.* 821: 111713.

Nikumbh, V.P., Tare, V.S. & Mahulikar, P.P. 2003. Eco-friendly pest management using monoterpenoids-III: antibacterial efficacy of carvacrol derivatives. *JSciInd Res.* 62: 1086–1089.

Nitiss, J.L. 2009. Targeting DNA topoisomerase II in cancer chemotherapy. *Nat Rev Cancer.* 9(5): 338–350.

Novato, T., Gomes, G.A., Zeringóta, V., Franco, C.T., de Oliveira, D.R., Melo, D., de Carvalho, M.G., Daemon, E. & de Oliveira Monteiro, C.M. 2018. In vitro assessment of the acaricidal activity of carvacrol, thymol, eugenol and their acetylated derivatives on *Rhipicephalus microplus* (Acari: Ixodidae). *Vet Parasitol.* 260: 1–4.

Okpara, E.S., Adedara, I.A., Guo, X., Klos, M.L., Farombi, E.O. Han, S. 2022. Molecular mechanisms associated with the chemoprotective role of protocatechuic acid and its potential benefits in the amelioration of doxorubicin-induced cardiotoxicity: A review. *Toxicol Rep.* 9: 1713–1724.

Oliveira, G.H., Dupont, M., Naftel, D., Myers, S.L., Yuan, Y., Wilson Tang, W.H., Gonzalez-Stawinski, G., Young, J.B., Taylor, D.O. & Starling, R.C. 2014. Increased need for right ventricular support in patients with chemotherapy-induced cardiomyopathy undergoing mechanical circulatory support: outcomes from the intermacs registry (interagency registry for mechanically assisted circulatory support). *JAm Coll Cardiol.*63(3): 240–248.

Omóbòwálé, T.O., Oyagbemi, A.A., Folasire, A.M., Ajibade, T.O., Asenuga, E.R., Adejumobi, O.A., Ola-Davies, O.E., Oyetola, O., James, G., Adedapo, A.A. &

Yakubu, M.A. 2018. Ameliorative effect of gallic acid on doxorubicin-induced cardiac dysfunction in rats. *J Basic Clin Physiol Pharmacol.* 29(1): 19–27.

Patil, J.U., Suryawanshi, K.C., Patil, P.B., Chaudhary, S.R. & Pawar, N.S. 2010. Synthesis and antibacterial activity of carvacryl ethers. *J Asian Nat Prod Res.* 12(2): 129–33.

Pecoraro, M., Del Pizzo, M., Marzocco, S., Sorrentino, R., Ciccarelli, M., Iaccarino, G., Pinto, A. & Popolo, A. 2016. Inflammatory mediators in a short-time mouse model of doxorubicin-induced cardiotoxicity. *Toxicol Appl Pharmacol.* 293: 44–52.

Pete, U.D., Zade, C.M., Bhosale, J.D., Tupe, S.G., Chaudhary, P.M., Dikundwar, A.G. & Bendre, R.S. 2012. Hybrid molecules of carvacrol and benzoyl urea/thiourea with potential applications in agriculture and medicine. *Bioorg Med Chem Lett.* 22(17): 5550–5554.

Philippe, N., Omri, E., Simone, B., Andreas, G. & Marc, L. 2023. ACSS2 inhibitors and methods of use thereof. *Australian Patent No. AU 2018370096 B2*. Melbourne: Australian Patent Office.

Pilau, M.R., Alves, S.H., Weiblen, R., Arenhart, S., Cueto, A.P. & Lovato, L.T. 2011. Antiviral activity of the *Lippia graveolens* (Mexican oregano) essential oil and its main compound carvacrol against human and animal viruses. *Braz J Microbiol.* 42(4): 1616–1624.

Pinheiro, P.F., Menini, L.A.P., Bernardes, P.C., Saraiva, S.H., Carneiro, J.W.M., Costa, A.V., Arruda, T.R., Lage, M.R., Gonçalves, P.M., Bernardes, C.O., Alvarenga, E.S. & Menini, L. 2018. Semisynthetic phenol derivatives obtained from natural phenols: antimicrobial activity and molecular properties. *J Agric Food Chem.* 66(1): 323–330.

Pires, L.F., Costa, L.M., Silva, O.A., de Almeida, A.A., Cerqueira, G.S., de Sousa, D.P. & de Freitas, R.M. 2013. Anxiolytic-like effects of carvacryl acetate, a derivative of carvacrol, in mice. *Pharmacol Biochem Behav.* 112: 42–58.

Pires, L.F., Costa, L.M., de Almeida, A.A., Silva, O.A., Cerqueira, G.S., de Sousa, D.P. & de Freitas, R.M. 2014. Is there a correlation between in vitro antioxidant potential and in vivo effect of carvacryl acetate against oxidative stress in mice hippocampus?. *Neurochem Res.* 39(4): 758–769.

Präbst, K., Engelhardt, H., Ringgeler, S. & Hübner, H. 2017. Basic colorimetric proliferation assays: MTT, WST, and resazurin. In: Gilbert, D., Friedrich, O. (eds) cell viability assays. *Methods in molecular biology*, vol 1601. Humana Press: New York.

Priscilla, D.H. & Prince, P.S. 2009. Cardioprotective effect of gallic acid on cardiac troponin-T, cardiac marker enzymes, lipid peroxidation products and antioxidants in experimentally induced myocardial infarction in Wistar rats. *Chem Biol Interact.* 179(2-3): 118–124.

Psotová, J., Chlopcíková, S., Miketová, P. & Simánek, V. 2005. Cytoprotectivity of *Prunella vulgaris* on doxorubicin-treated rat cardiomyocytes. *Fitoterapia* 76(6): 556–561.

Qin, H. & Wang, Y. 2009. Exploring DNA-binding proteins with in vivo chemical cross-linking and mass spectrometry. *J Proteome Res.* 8(4): 1983–1991.

Rai, G., Mishra, S., Suman, S. & Shukla, Y. 2016. Resveratrol improves the anticancer effects of doxorubicin in vitro and in vivo models: a mechanistic insight. *Phytomedicine* 23(3): 233–242.

Rajappa, S., Singh, M., Uehara, R., Schachterle, S.E. & Setia, S. 2023. Cancer incidence and mortality trends in Asia based on regions and human development index levels: an analyses from GLOBOCAN 2020. *Curr Med Res Opin.* 39(8): 1127–1137.

Rajput, J.D., Bagul, S.D., Hosamani, A.A. Patil, M.M. & Bendre, R.S. 2017. Synthesis, characterizations, biological activities and docking studies of novel dihydroxy derivatives of natural phenolic monoterpenoids containing azomethine linkage. *Res Chem Intermed.* 43: 5377–5393.

Rankovic, M., Draginic, N., Jeremic, J., Samanovic, A.M., Stojkov, S., Mitrovic, S., Jeremic, N., Radonjic, T., Srejovic, I., Bolevich, S., Svistunov, A., Jakovljevic, V. & Turnic, T.N. 2021. Protective role of vitamin B1 in doxorubicin-induced cardiotoxicity in rats: focus on hemodynamic, redox, and apoptotic markers in heart. *Front Physiol.* 12: 690619.

Rashmi, H.B. & Negi, P.S. 2020. Phenolic acids from vegetables: a review on processing stability and health benefits. *Food Res Int.* 136: 109298.

Retnosari, R., Ali, A.H., Zainalabidin, S., Ugusman, A., Oka, N. & Latip, J. 2024. The recent discovery of a promising pharmacological scaffold derived from carvacrol: a review. *BioorMed Chem Lett.* 109: 129826.

Sadeghzadeh, S., Hejazian, S.H., Jamhiri, M., Hafizibarjin, Z. & Safari, F. 2018. The effect of carvacrol on transcription levels of Bcl-2 family proteins in hypertrophied heart of rats. *Physiol Pharmacol. (Iran)* 22: 54–62.

Sahu, B.D., Kumar, J.M., Kuncha, M., Borkar, R.M., Srinivas, R. & Sistla, R. 2016. Baicalein alleviates doxorubicin-induced cardiotoxicity via suppression of myocardial oxidative stress and apoptosis in mice. *Life Sci.* 144: 8–18.

Sangweni, N.F., Moremane, M., Riedel, S., van Vuuren, D., Huisamen, B., Mabasa, L., Barry, R. & Johnson, R. 2020. The prophylactic effect of pinocembrin against doxorubicin-induced cardiotoxicity in an in vitro h9c2 cell model. *Front Pharmacol.* 11: 1172.

Sangweni, N.F., van Vuuren, D., Mabasa, L., Gabuza, K., Huisamen, B., Naidoo, S., Barry, R. & Johnson, R. 2022. Prevention of anthracycline-induced cardiotoxicity: the good and bad of current and alternative therapies. *Front Cardiovasc Med.* 9: 907266.

Sarian, M.N., Ahmed, Q.U., Mat So'ad, S.Z., Alhassan, A.M., Murugesu, S., Perumal, V., Syed Mohamad, S.N.A., Khatib, A. & Latip, J. 2017. Antioxidant and antidiabetic effects of flavonoids: a structure-activity relationship based study. *Biomed Res Int.* 2017: 8386065.

Sawicki, K.T., Sala, V., Prever, L., Hirsch, E., Ardehali, H. & Ghigo, A. 2021. Preventing and treating anthracycline cardiotoxicity: new insights. *Annu Rev Pharmacol Toxicol.* 61: 309–332.

Saxena, M., Saxena, J. & Pradhan, A. 2012. Flavonoids and phenolic acids as antioxidants in plants and human health. *Int J Pharm Sci Rev Res.* 16: 130–134.

Schliemann, D., Ismail, R., Donnelly, M., Cardwell, C.R. & Su, T.T. 2020. Cancer symptom and risk factor awareness in Malaysia: findings from a nationwide cross-sectional study. *BMC Public Health* 20(1): 464.

Semaming, Y., Kumfu, S., Pannangpetch, P., Chattipakorn, S.C. & Chattipakorn, N. 2014. Protocatechuic acid exerts a cardioprotective effect in type 1 diabetic rats. *J Endocrinol*. 223(1): 13–23.

Shafiee, F., Safaeian, L. & Gorbani, F. 2023. Protective effects of protocatechuic acid against doxorubicin- and arsenic trioxide-induced toxicity in cardiomyocytes. *Res Pharm Sci.* 18(2): 149–158.

Shaikh, F., Dupuis, L.L., Alexander, S., Gupta, A., Mertens, L. & Nathan, P.C. Cardioprotection and second malignant neoplasms associated with dexrazoxane in children receiving anthracycline chemotherapy: a systematic review and meta-analysis. *J Natl Cancer Inst.* 108(4): djv357.

Sheibani, M., Azizi, Y., Shayan, M., Nezamoleslami, S., Eslami, F., Farjoo, M.H. & Dehpour, A.R. 2022. Doxorubicin-induced cardiotoxicity: an overview on pre-clinical therapeutic approaches. *Cardiovasc Toxicol.* 22(4): 292–310.

Shiromwar, S.S. & Chidrawar, V.R. 2011. Combined effects of p-coumaric acid and naringenin against doxorubicin-induced cardiotoxicity in rats. *Pharmacognosy Res.* 3(3): 214–219.

Silva, V.B., Travassos, D.L., Nepel, A., Barison, A., Costa, E.V., Scotti, L., Scotti, M.T., Mendonça-Junior, F.J.B., La Corte Dos Santos, R. & de Holanda Cavalcanti, S.C. 2017. Synthesis and chemometrics of thymol and carvacrol derivatives as larvicides against Aedes aegypti. *J Arthropod Borne Dis*. 11(2): 315–330.

Sirangelo, I., Sapio, L., Ragone, A., Naviglio, S., Iannuzzi, C., Barone, D., Giordano, A. & Borriello, M. 2020. Vanillin prevents doxorubicin-induced apoptosis and oxidative stress in rat h9c2 cardiomyocytes. *Nutrients* 12(8): 2317.

Sisto, F., Carradori, S., Guglielmi, P., Traversi, C.B., Spano, M., Sobolev, A.P., Secci, D., Di Marcantonio, M.C., Haloci, E., Grande, R. & Mincione, G. 2020. Synthesis and biological evaluation of carvacrol-based derivatives as dual

inhibitors of *H. pylori* strains and AGS cell proliferation. *Pharmaceuticals (Basel)*13(11): 405.

Songbo, M., Lang, H., Xinyong, C., Bin, X., Ping, Z. & Liang, S. 2019. Oxidative stress injury in doxorubicin-induced cardiotoxicity. *Toxicol Lett.* 307: 41–48.

Sonowal, H., Pal, P.B., Srivastava, S.K. & Ramana, K.V. 2017. Aldose reductase inhibitor increases doxorubicin-sensitivity of colon cancer cells and decreases cardiomyopathy [abstract]. In: Proceedings of the American Association for Cancer Research Annual Meeting 2017; 2017 Apr 1-5; Washington, DC. Philadelphia (PA): AACR; *Cancer Res* 77(13 Suppl).

Stěrba, M., Popelová, O., Vávrová, A., Jirkovský, E., Kovaříková, P., Geršl, V. & Simůnek, T. 2013. Oxidative stress, redox signaling, and metal chelation in anthracycline cardiotoxicity and pharmacological cardioprotection. *Antioxid Redox Signal.* 18(8): 899–929.

Stockert, J.C., Horobin, R.W., Colombo, L.L. & Blázquez-Castro, A. Tetrazolium salts and formazan products in cell biology: Viability assessment, fluorescence imaging, and labeling perspectives. *Acta Histochem.* 120(3):159–167.

Stuper-Szablewska, K. & Perkowski, J. 2019. Phenolic acids in cereal grain: occurrence, biosynthesis, metabolism and role in living organisms. *Crit Rev Food Sci Nutr.* 59(4): 664–675.

Sung, H., Ferlay, J., Siegel, R.L., Laversanne, M., Soerjomataram, I., Jemal, A. & Bray, F. 2021. Global cancer statistics 2020: globocan estimates of incidence and mortality worldwide for 36 cancers in 185 countries. *CA Cancer J Clin.* 71(3): 209–249.

Sunitha, M.C., Dhanyakrishnan, R., PrakashKumar, B. & Nevin, K.G. 2018. p-Coumaric acid mediated protection of H9c2 cells from doxorubicin-induced cardiotoxicity: involvement of augmented Nrf2 and autophagy. *Biomed Pharmacother.* 102: 823–832.

Swain, S.M., Whaley, F.S. & Ewer, M.S. 2003. Congestive heart failure in patients treated with doxorubicin. *Cancer* 97(11): 2869–2879.

Tan, S.C., Poh, W.T., Yong, A.C.H., Chua, E.W., Ooi, J., Mahmud, R., Thiagarajan, M. & Stanslas, J. 2023. Challenges and strategies for improving access to cancer drugs in malaysia: summary of opinions expressed at the 2nd MACR international scientific conference 2022. *Cancer Manag Res.* 15: 851–862.

Tan, X., Wang, D.B., Lu, X., Wei, H., Zhu, R., Zhu, S.S., Jiang, H. & Yang, Z.J. 2010. Doxorubicin induces apoptosis in H9c2 cardiomyocytes: role of overexpressed eukaryotic translation initiation factor 5A. *Biol Pharm Bull.* 33(10): 1666–1672.

Tang, X.L., Liu, J.X., Dong, W., Li, P., Li, L., Lin, C.R., Zheng, Y.Q., Cong, W.H. & Hou, J.C. 2014. Cardioprotective effect of protocatechuic acid on myocardial ischemia/reperfusion injury. *J Pharmacol Sci.* 125(2): 176–183.

Tiwari, K., Wavdhane, M., Haque, S., Govender, T., Kruger, H.G., Mishra, M.K., Chandra, R. & Tiwari, D. 2015. A sensitive WST-8-based bioassay for PEGylated granulocyte colony stimulating factor using the NFS-60 cell line. *Pharm Biol.* 53(6): 849–854.

Tomoda, H., Nagamitsu, T. &Omura, S. 2010. Pyripyropene derivative having acat2-inhibiting activity. *European PatentNo. EP 2228376 A1*. Paris: European Patent Office.

Uddin, A., Singh, V., Irfan, I., Mohammad, T., Singh Hada, R., Imtaiyaz Hassan, M., Abid, M. & Singh, S. 2020. Identification and structure-activity relationship (SAR) studies of carvacrol derivatives as potential anti-malarial against Plasmodium falciparum falcipain-2 protease. *Bioorg Chem.* 103:104142.

Van Allen, N.R., Krafft, P.R., Leitzke, A.S., Applegate, R.L., Tang, J. & Zhang, J.H. 2012. The role of volatile anesthetics in cardioprotection: a systematic review. *Med Gas Res.* 2(1): 22.

van Dalen, E.C., Caron, H.N., Dickinson, H.O., Kremer, L.C. 2011. Cardioprotective interventions for cancer patients receiving anthracyclines. *Cochrane Database Syst Rev.* 2011(6): CD003917.

van der Zanden, S.Y., Qiao, X. & Neefjes, J. 2021. New insights into the activities and toxicities of the old anticancer drug doxorubicin. *FEBS J.* 288(21): 6095–6111.

Vejpongsa, P. & Yeh, E.T. 2014. Prevention of anthracycline-induced cardiotoxicity: challenges and opportunities. *J Am Coll Cardiol.* 64(9): 938–945.

Vijaya Padma, V., Poornima, P., Prakash, C. & Bhavani, R. 2013. Oral treatment with gallic acid and quercetin alleviates lindane-induced cardiotoxicity in rats. *Can J Physiol Pharmacol.* 91(2): 134–140.

Wang, K., Jiang, S., Pu, T., Fan, L., Su, F. & Ye, M. 2018. Antifungal activity of phenolic monoterpenes and structure-related compounds against plant pathogenic fungi. *Nat Prod Res.* 33: 1–8.

Wang, K., Jiang, S., Yang, Y., Fan, L., Su, F. & Ye, M. 2019. Synthesis and antifungal activity of carvacrol and thymol esters with heteroaromatic carboxylic acids. *Nat Prod Res.* 33(13):1924–1930.

Wang, R., Huang, R., Yuan, Y., Wang, Z. & Shen, K. 2023. Two-carbon tethered artemisinin-isatin hybrids: design, synthesis, anti-breast cancer potential, and in silico study. *Front Mol Biosci.* 10: 1293763.

Wenningmann, N., Knapp, M., Ande, A., Vaidya, T.R. & Ait-Oudhia, S. 2019. Insights into doxorubicin-induced cardiotoxicity: molecular mechanisms, preventive strategies, and early monitoring. *Mol Pharmacol.* 96(2): 219–232.

WHO. 2022. Cancer today: Malaysia sheet. https://gco.iarc.fr/today/en/fact-sheets-populations#countries [24 July 2024].

Witek, P., Korga, A., Burdan, F., Ostrowska, M., Nosowska, B., Iwan, M. & Dudka, J. 2016. The effect of a number of H9c2 rat cardiomyocytes passage on repeatability of cytotoxicity study results. *Cytotechnology* 68(6): 2407–2415.

Xiao, J., Sun, G.B., Sun, B., Wu, Y., He, L., Wang, X., Chen, R.C., Cao, L., Ren, X.Y. & Sun, X.B. 2012. Kaempferol protects against doxorubicin-induced cardiotoxicity in vivo and in vitro. *Toxicology.* 292(1): 53–62.

Xiao, Y., Li, B., Liu, J. & Ma, X. 2018. Carvacrol ameliorates inflammatory response in interleukin 1β-stimulated human chondrocytes. *Mol Med Rep.* 17(3): 3987–3992.

Yadav, G.D. & Kamble, S.B. 2009. Synthesis of carvacrol by Friedel–Crafts alkylation of o-cresol with isopropanol using superacidic catalyst UDCaT-5. *J ChemTechnolBiotechnol.* 84: 1499–1508.

Yan, X., Zhang, Y.L., Zhang, L., Zou, L.X., Chen, C., Liu, Y., Xia, Y.L. & Li, H.H. 2019. Gallic acid suppresses cardiac hypertrophic remodeling and heart failure. *Mol Nutr Food Res.* 63(5): e1800807.

Yu, W., Liu, Q. & Zhu, S. 2013. Carvacrol protects against acute myocardial infarction of rats via anti-oxidative and anti-apoptotic pathways. *Biol Pharm Bull.* 36(4): 579–584.

Zhao, L., Qi, Y., Xu, L., Tao, X., Han, X., Yin, L. & Peng, J. 2018. MicroRNA-140-5p aggravates doxorubicin-induced cardiotoxicity by promoting myocardial oxidative stress via targeting Nrf2 and Sirt2. *Redox Biol.* 15: 284–296.

Zhao, J., Du, J., Pan, Y., Chen, T., Zhao, L., Zhu, Y., Chen, Y., Zheng, Y., Liu, Y., Sun, L., Hang, P. & Du, Z. 2019. Activation of cardiac TrkB receptor by its small molecular agonist 7,8-dihydroxyflavone inhibits doxorubicin-induced cardiotoxicity via enhancing mitochondrial oxidative phosphorylation. *Free Radic Biol Med.* 130: 557–567.

Zhao, J., Yu, H.Q., Ge, F.Q., Zhang, M.R., Song, Y.C., Guo, D.D., Li, Q.H., Zhu, H. & Hang, P.Z. 2023. 7,8,3'-Trihydroxyflavone prevents doxorubicin-induced cardiotoxicity and mitochondrial dysfunction via activating Akt signaling pathway in H9c2 cells. *Cell Signal.* 112: 110924.

Zhou, L., Han, Y., Yang, Q., Xin, B., Chi, M., Huo, Y., Guo, C. & Sun, X. 2022. Scutellarin attenuates doxorubicin-induced oxidative stress, DNA damage, mitochondrial dysfunction, apoptosis and autophagy in H9c2 cells, cardiac fibroblasts and HUVECs. *Toxicol In Vitro.* 82: 105366.

Zuurbier, C.J., Heinen, A., Koeman, A., Stuifbergen, R., Hakvoort, T.B., Weber, N.C. & Hollmann, M.W. 2014. Cardioprotective efficacy depends critically on pharmacological dose, duration of ischaemia, health status of animals and choice of anaesthetic regimen: a case study with folic acid. *J Transl Med.* 12: 325.

APPENDIX A
^{1}H NMR SPECTRUM OF 5-ISOPROPYL-2-METHYLPHENYL 2-CHLOROACETATE (22)

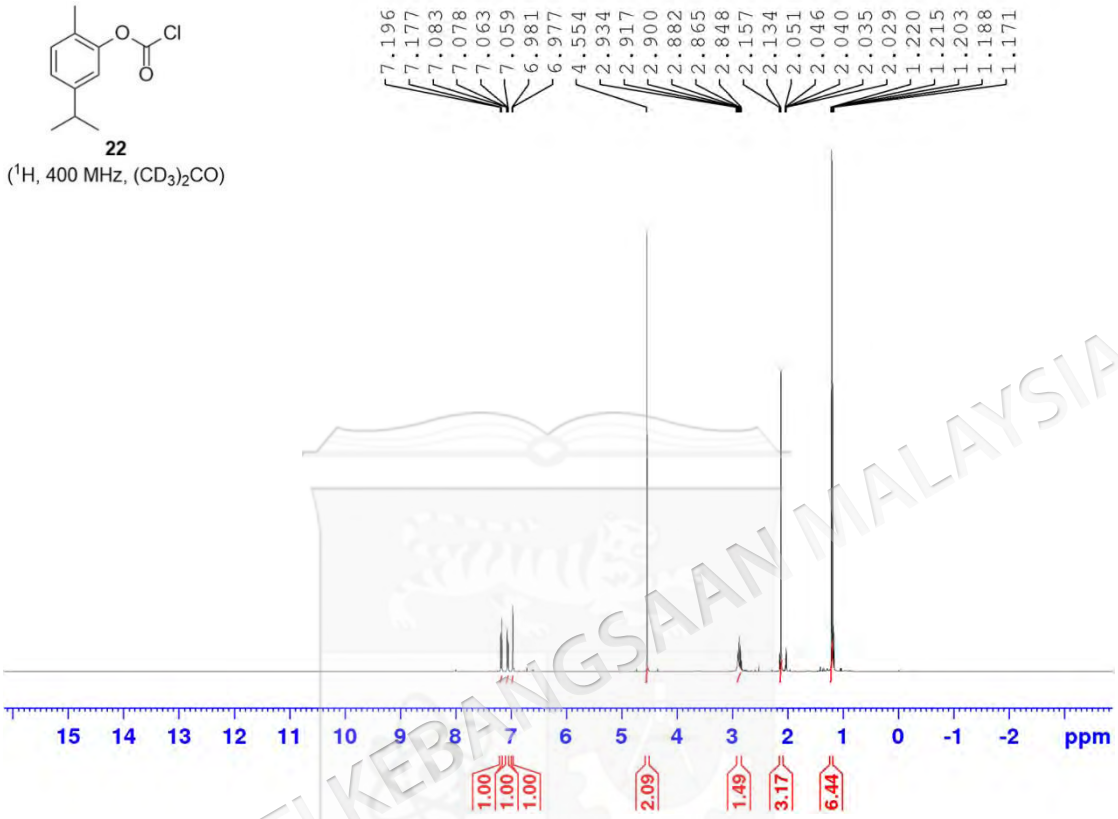

APPENDIX B
^{1}H AND ^{13}C NMR SPECTRA OF 2-[2-METHYL-5-(PROPAN-2-YL)PHENOXY]-2-OXOETHYL 3-HYDROXYBENZOATE (1)

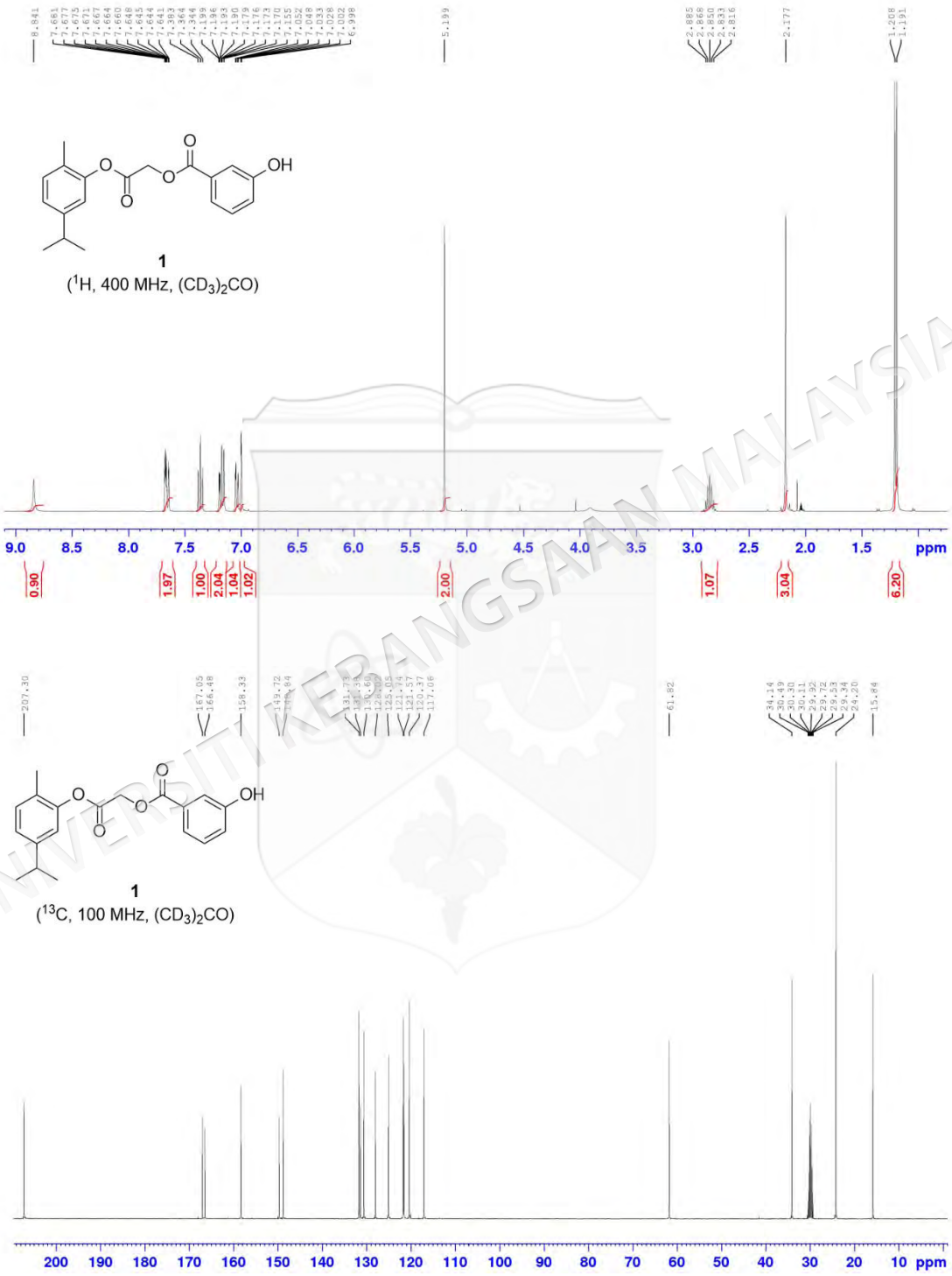

APPENDIX C
^{1}H AND ^{13}C NMR SPECTRA OF 2-[2-METHYL-5-(PROPAN-2-YL)PHENOXY]-2-OXOETHYL 4-HYDROXYBENZOATE (2)

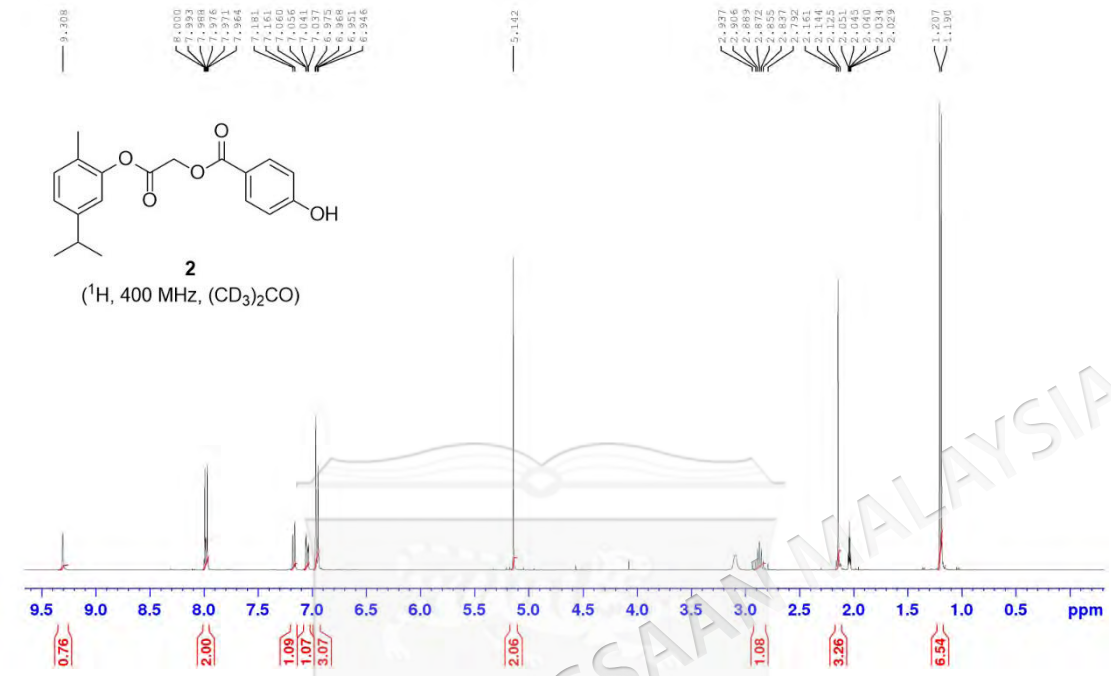

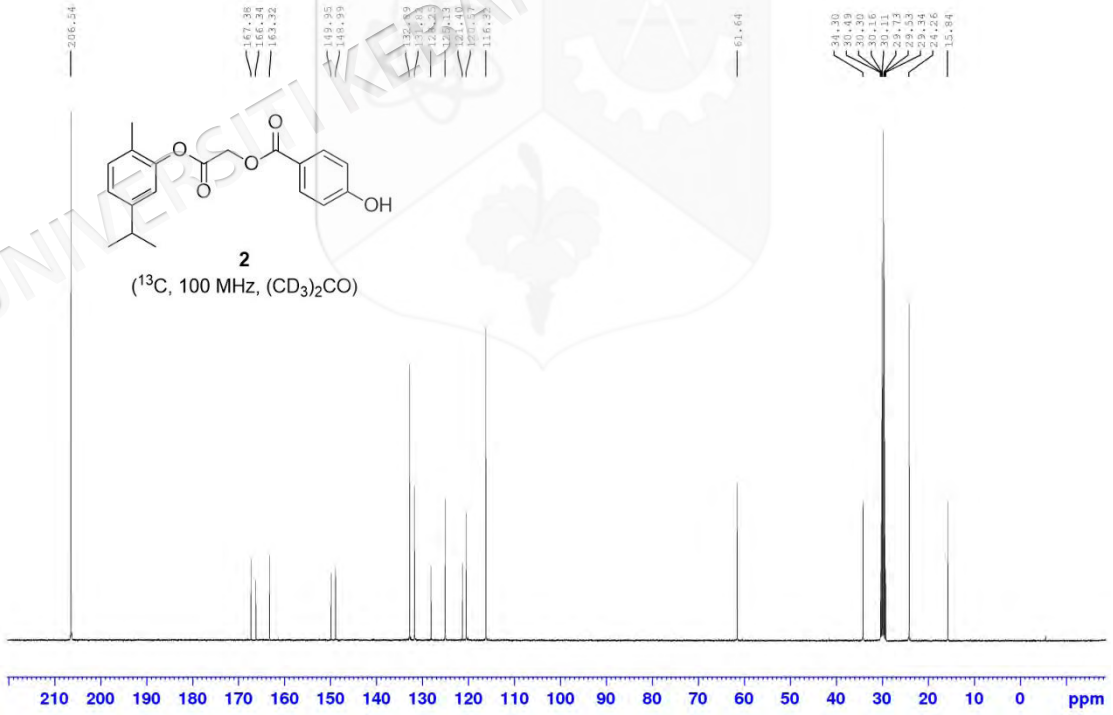

APPENDIX D

^{1}H AND ^{13}C NMR SPECTRAOF 2-[2-METHYL-5-(PROPAN-2-YL)PHENOXY]-2-OXOETHYL 3,4-DIHYDROXYBENZOATE (3)

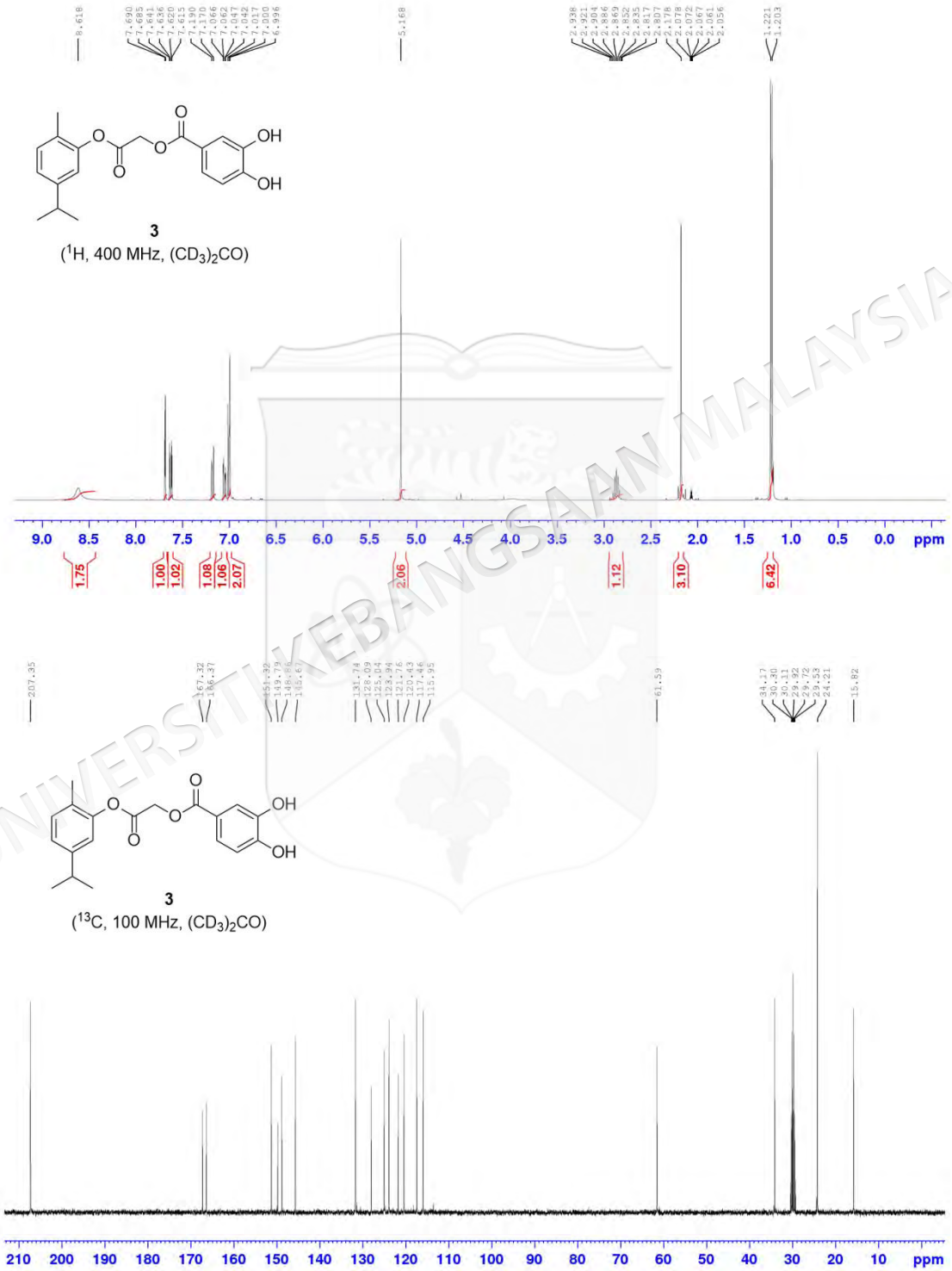

APPENDIX E

^{1}H-AND ^{13}C NMR SPECTRA OF 2-[2-METHYL-5-(PROPAN-2-YL)PHENOXY]-2-OXOETHYL 2,4-DIHYDROXYBENZOATE (4)

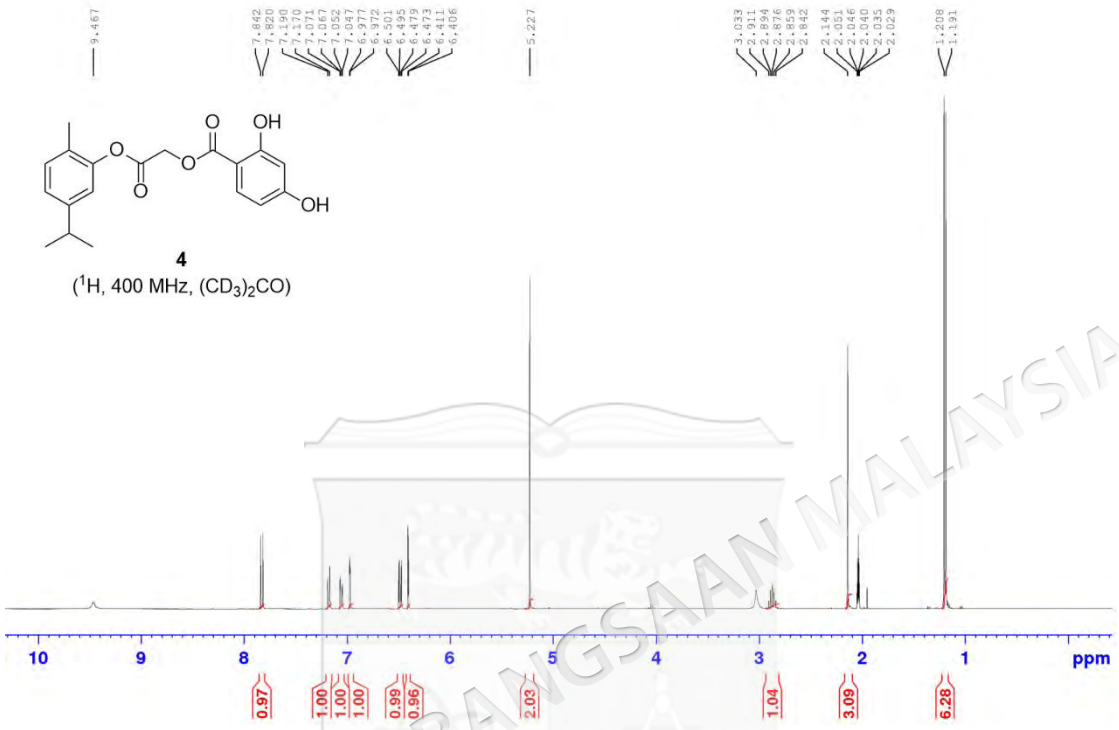

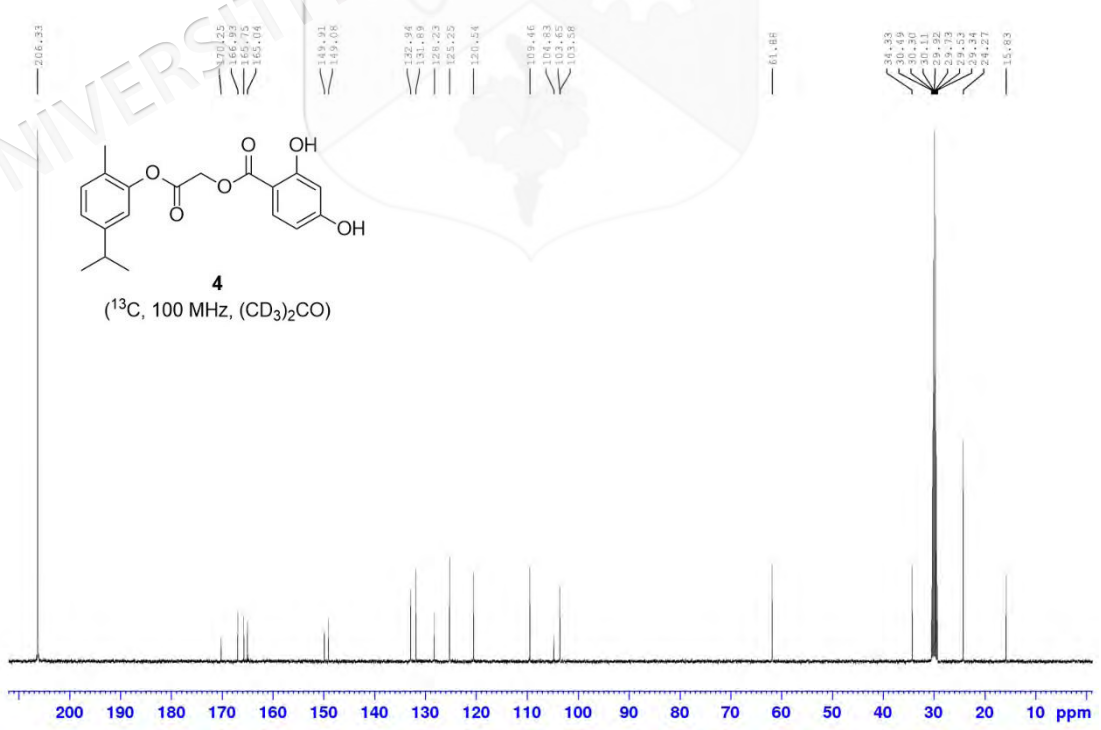

APPENDIX F

^{1}H AND ^{13}C NMR SPECTRA OF 2-[2-METHYL-5-(PROPAN-2-YL)PHENOXY]-2-OXOETHYL 3,5-DIHYDROXYBENZOATE (5)

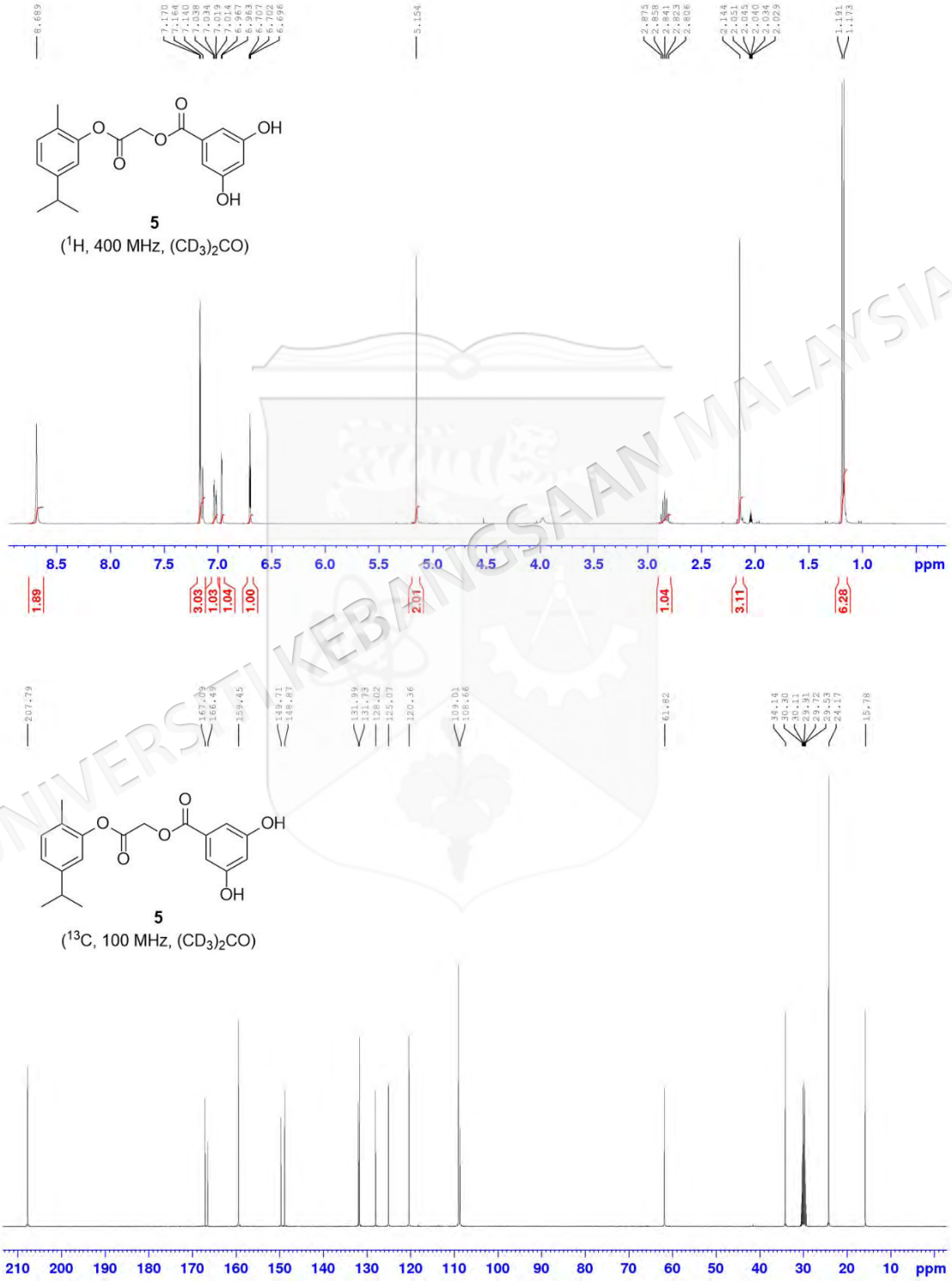

APPENDIX G

^{1}H AND ^{13}C NMR SPECTRA OF 2-[2-METHYL-5-(PROPAN-2-YL)PHENOXY]-2-OXOETHYL 3,4,5-TRIHYDROXYBENZOATE (6)

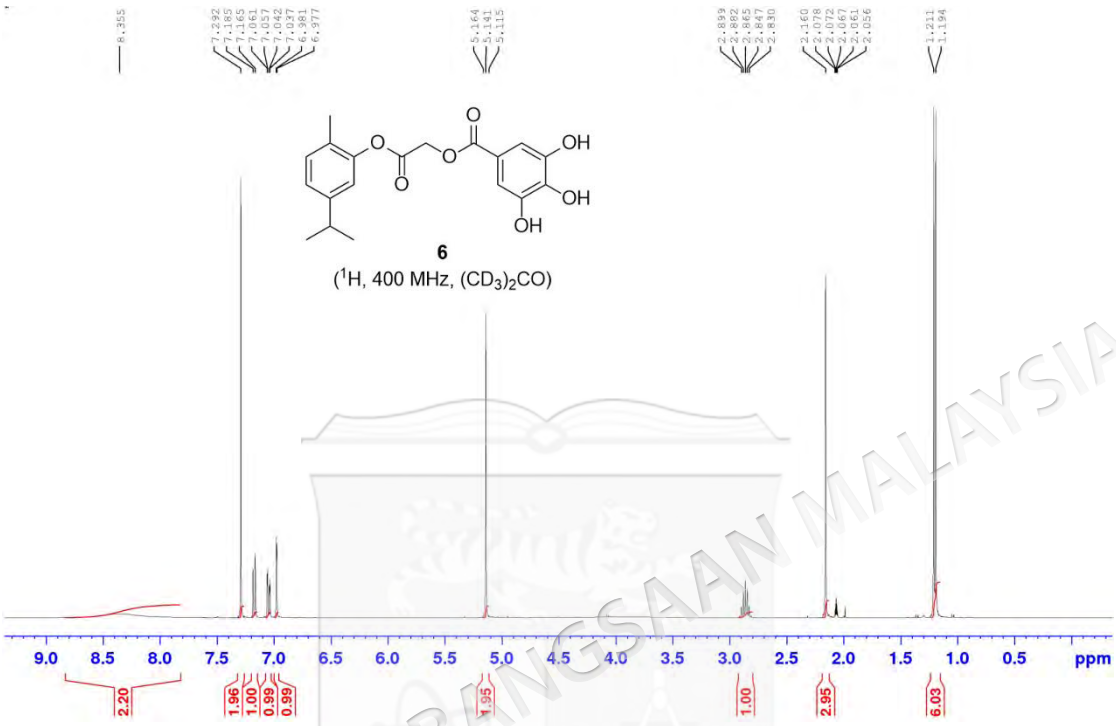

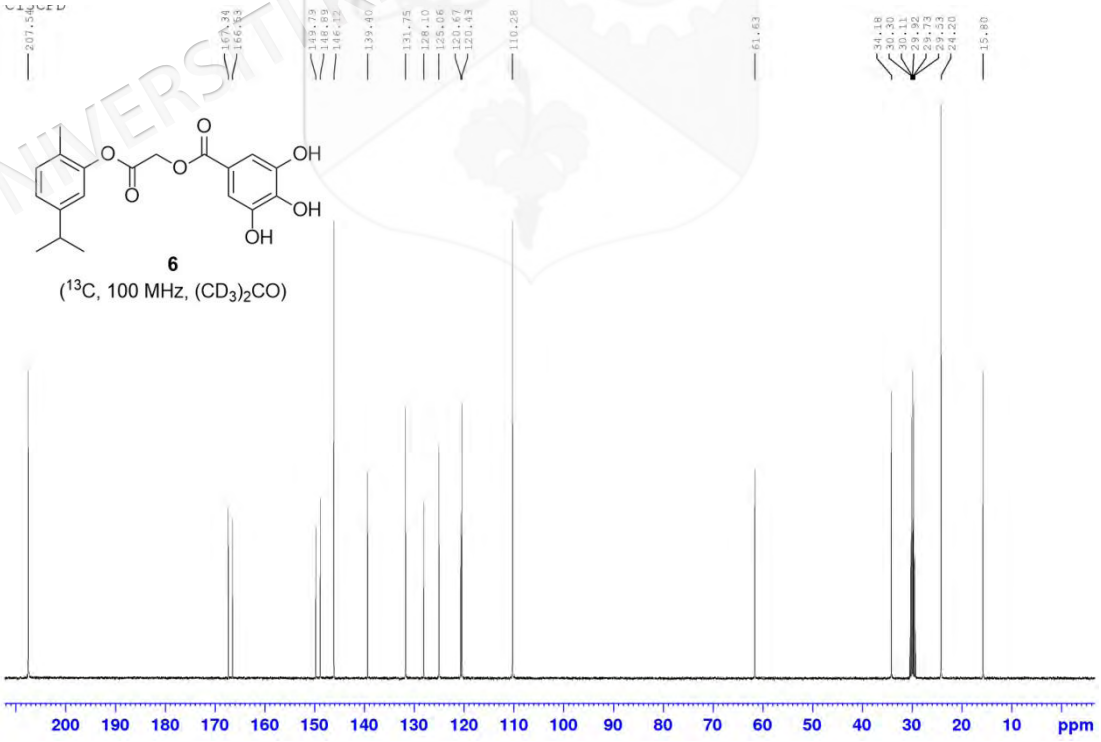

APPENDIX H

^{1}H AND ^{13}C NMR SPECTRA OF 2-[2-METHYL-5-(PROPAN-2-YL)PHENOXY]-2-OXOETHYL (2E)-3-PHENYLPROP-2-ENOATE (7)

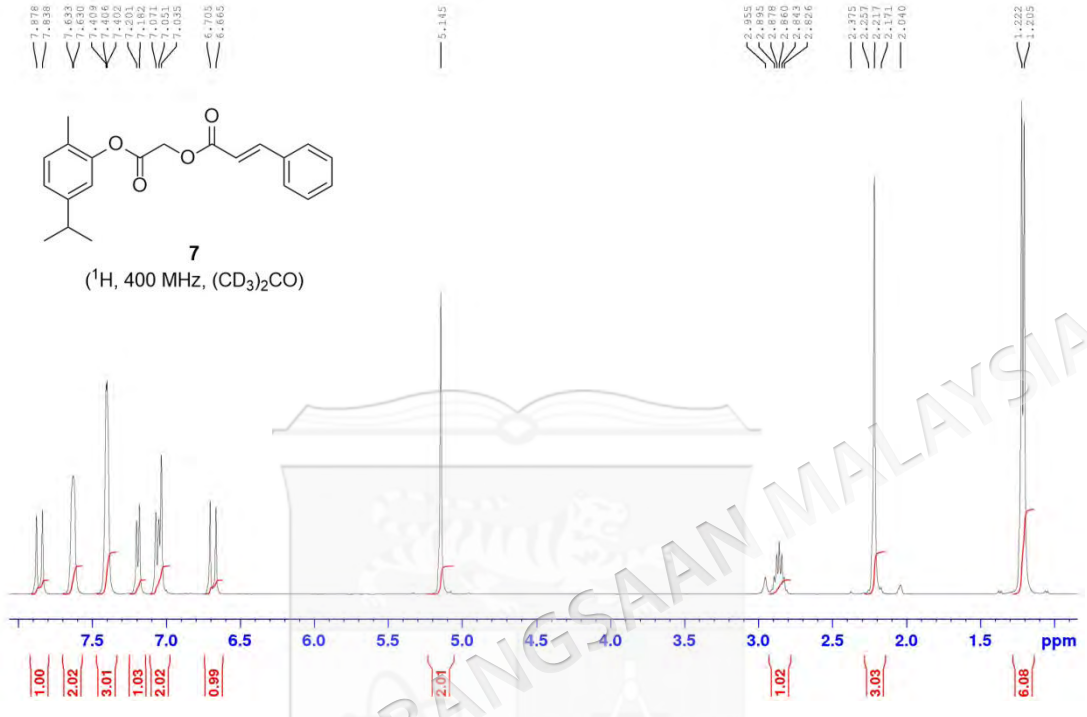

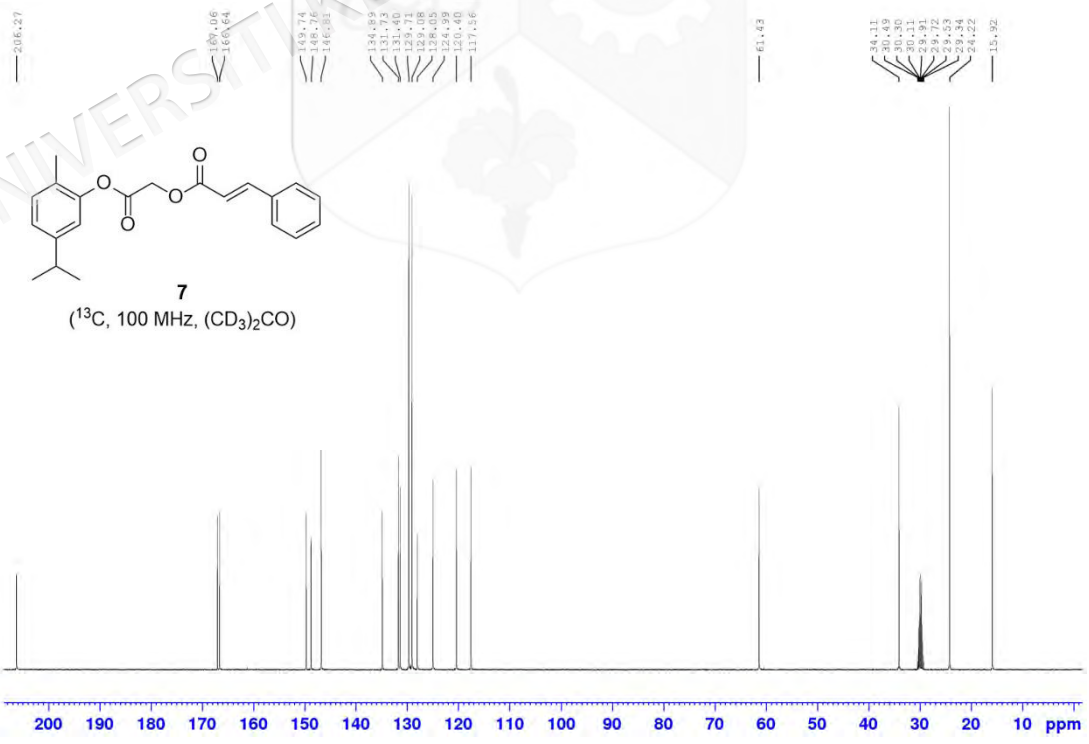

APPENDIX I

^{1}H AND ^{13}C NMR SPECTRA OF 2-[2-METHYL-5-(PROPAN-2-YL)PHENOXY]-2-OXOETHYL (2E)-3-(4-HYDROXYPHENYL)PROP-2-ENOATE (8)

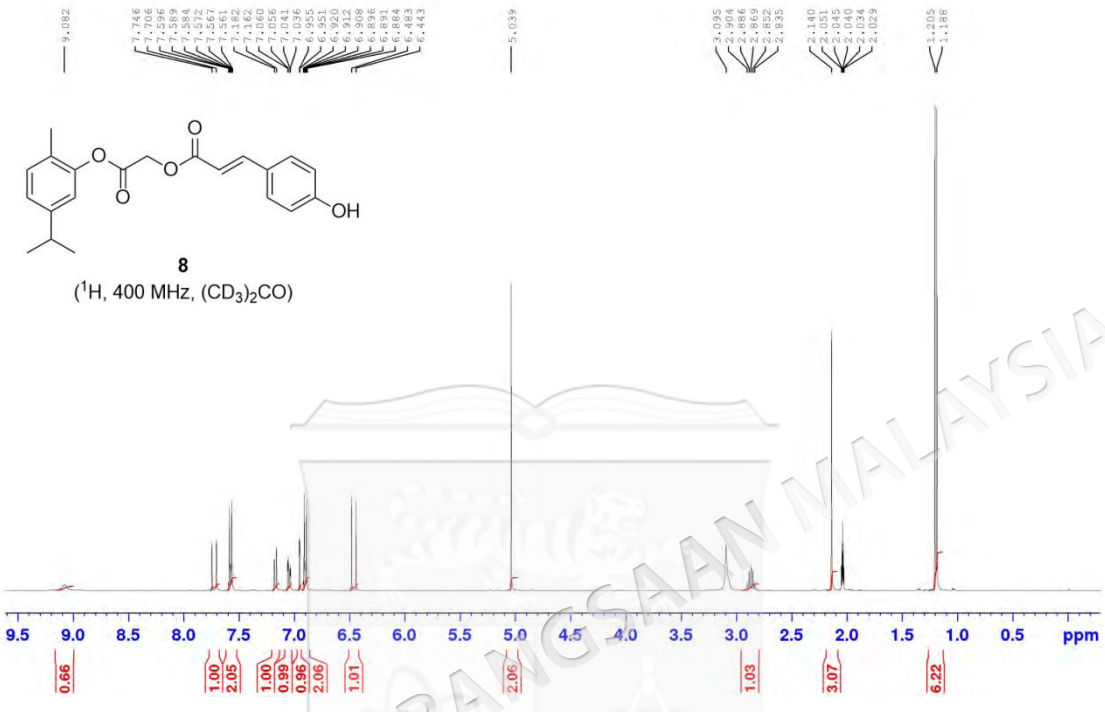

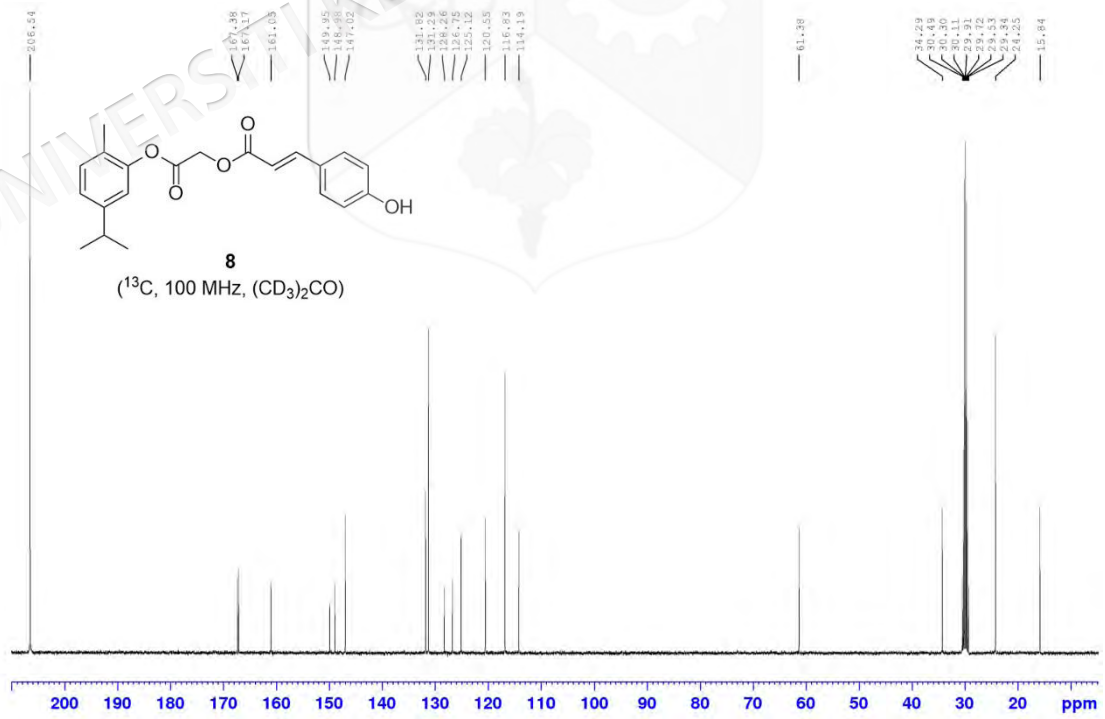

APPENDIX J

^{1}H AND ^{13}C NMR SPECTRA OF 2-[2-METHYL-5-(PROPAN-2-YL)PHENOXY]-2-OXOETHYL (2E)-3-(4-CHLOROPHENYL)PROP-2-ENOATE (9)

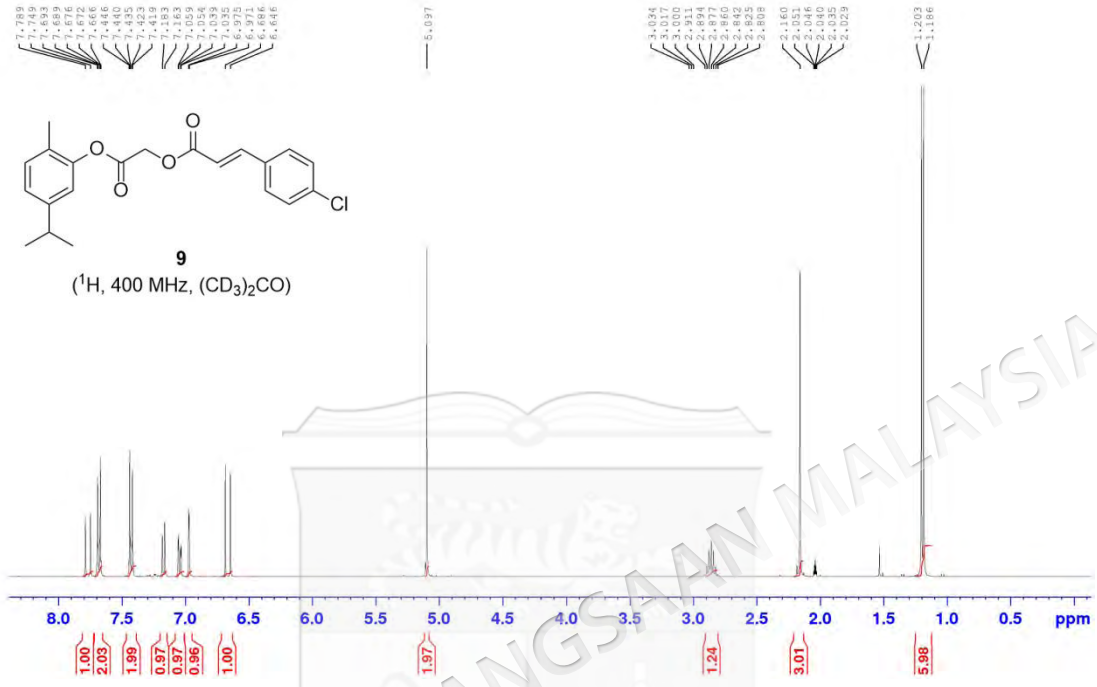

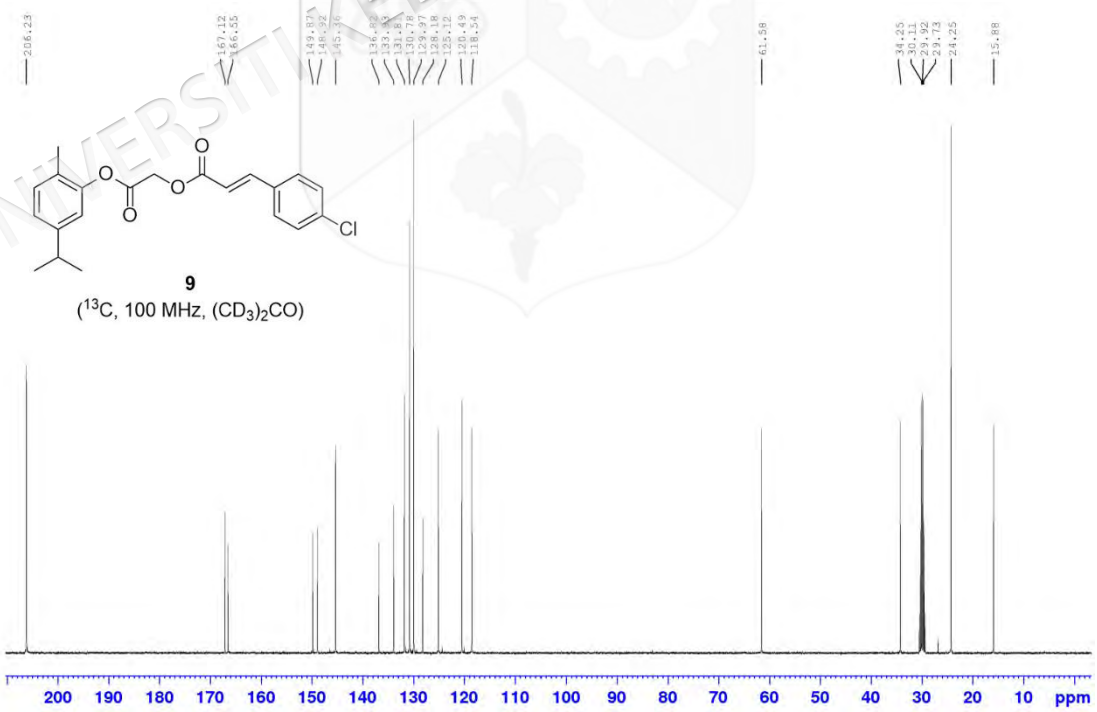

APPENDIX K

^{1}H AND ^{13}C NMR SPECTRA OF 2-[2-METHYL-5-(PROPAN-2-YL)PHENOXY]-2-OXOETHYL (2E)-3-(2,4-DIHYDROXYPHENYL)PROP-2-ENOATE (10)

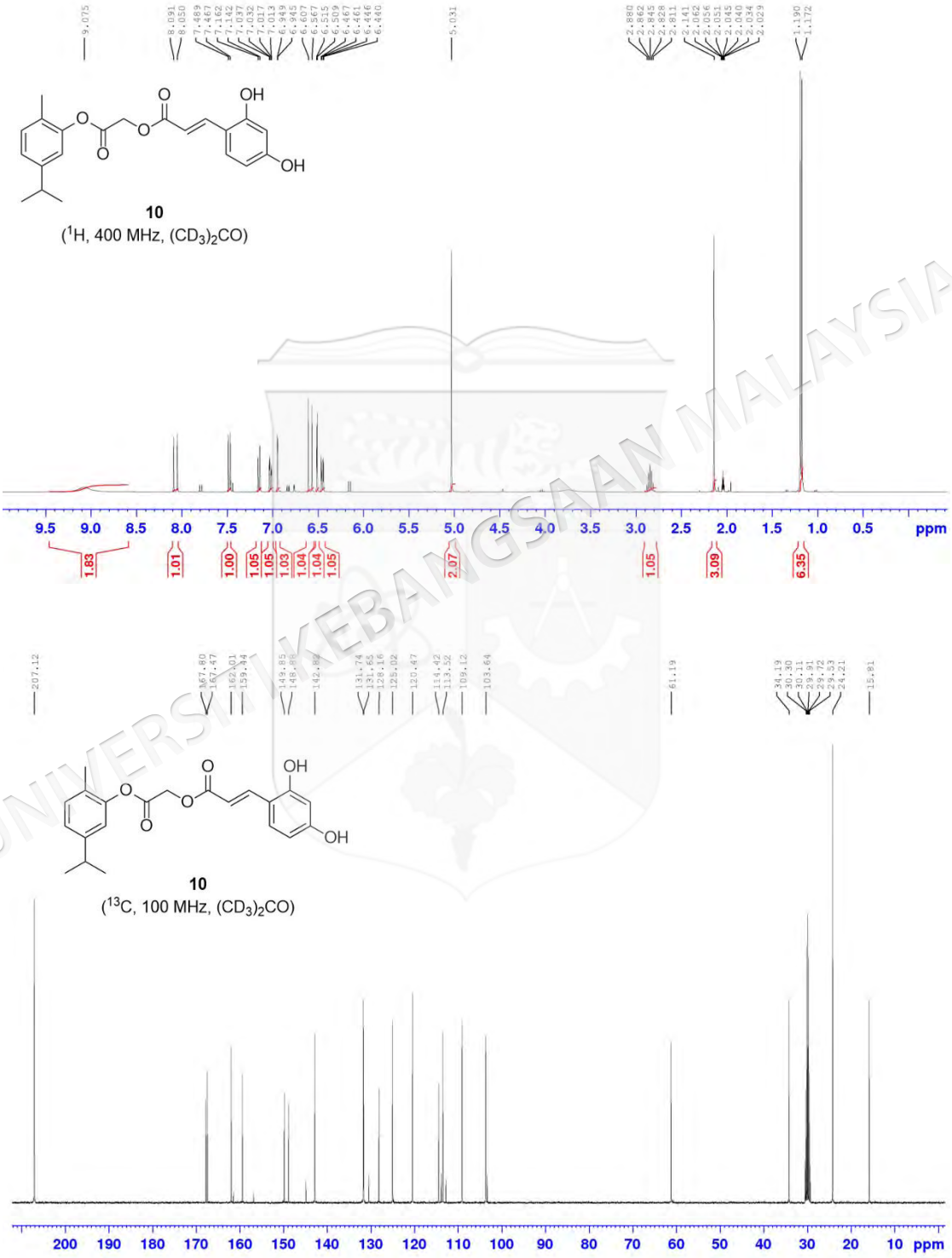

APPENDIX L

^{1}H AND ^{13}C NMR SPECTRA OF 5-ISOPROPYL-2-METHYLPHENYL 3-CHLOROPROPANOATE (23a)

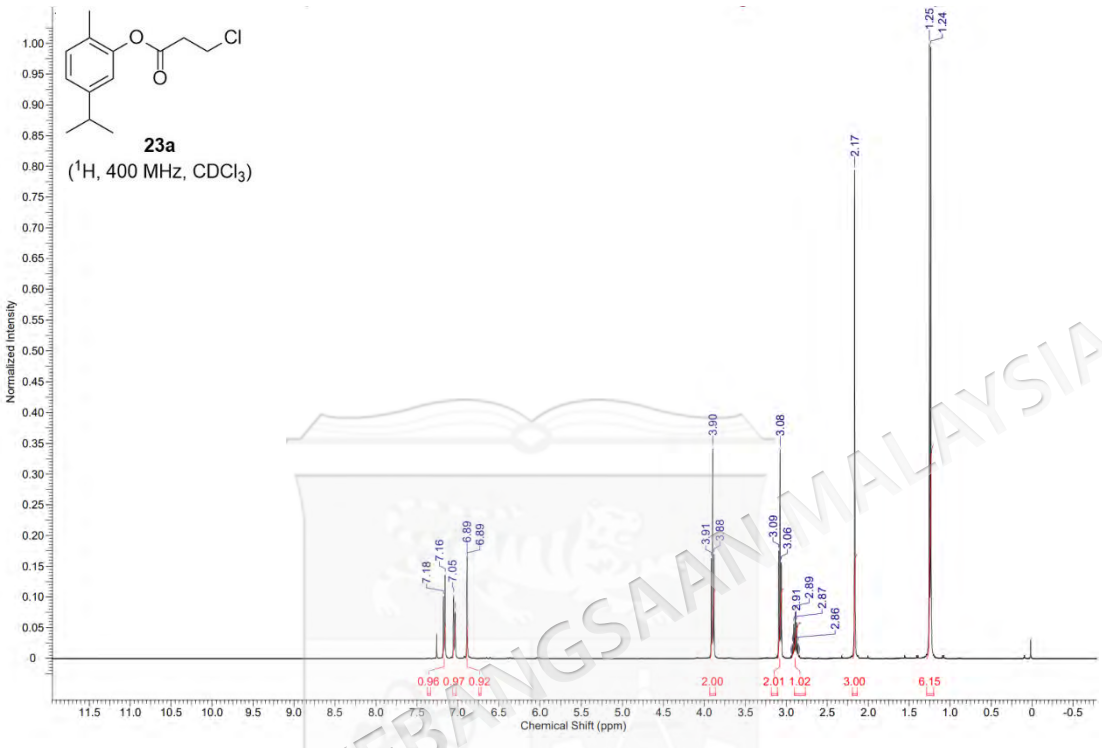

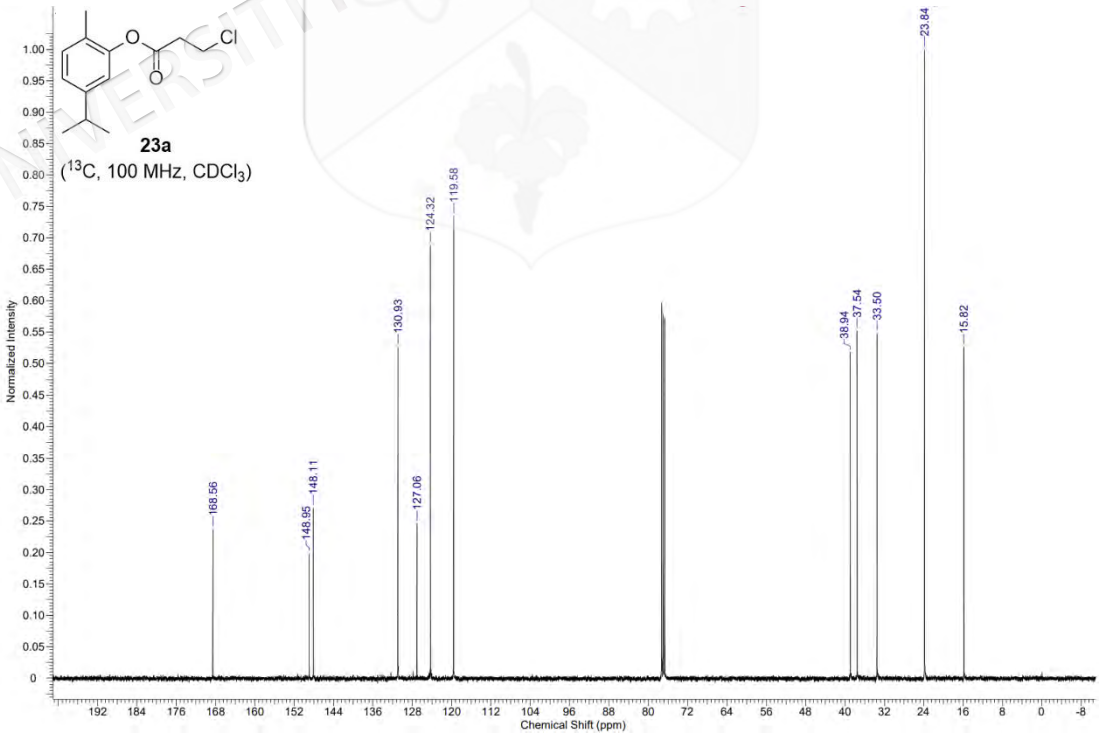

APPENDIX M

^{1}H AND ^{13}C NMR SPECTRA OF 5-ISOPROPYL-2-METHYLPHENYL ACRYLATE (24)

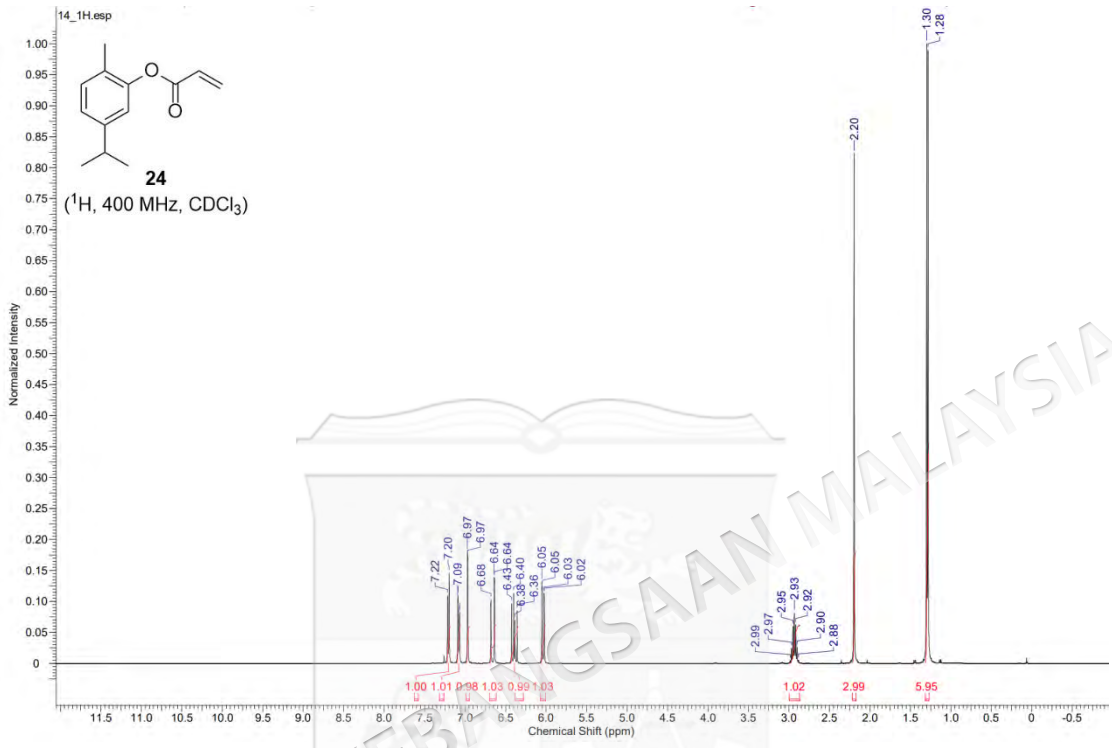

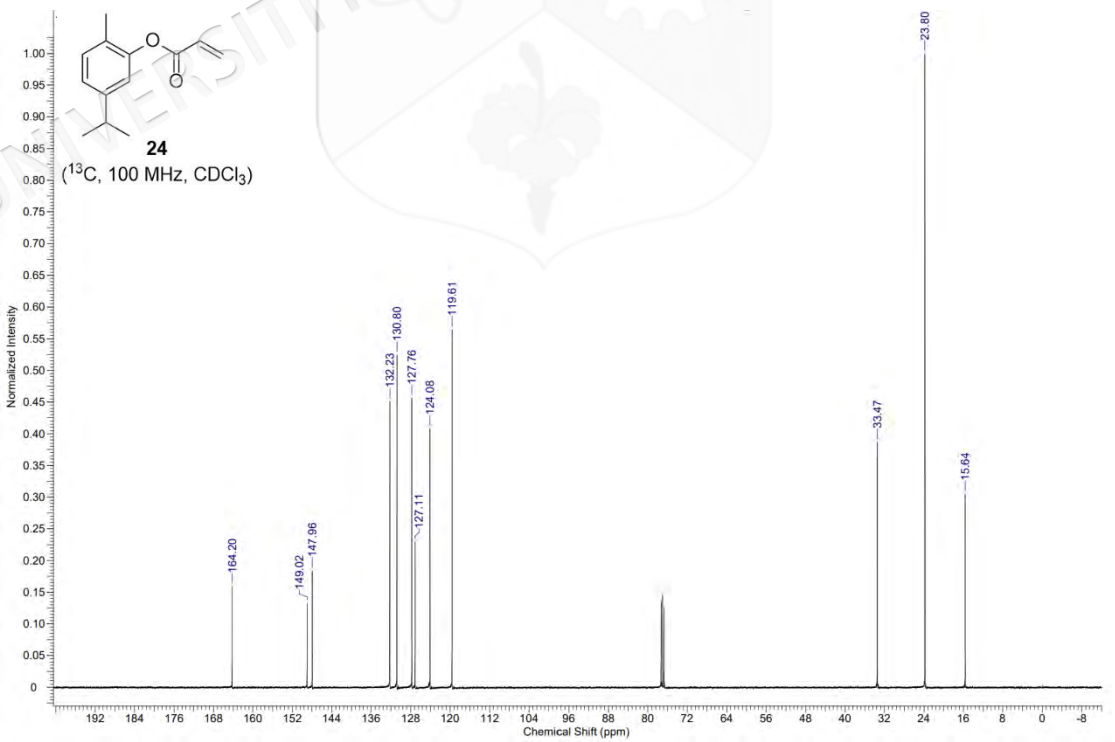

APPENDIX N

^{1}H AND ^{13}C NMR SPECTRA OF 5-ISOPROPYL-2-METHYLPHENYL 3-(BENZYLOXY)PROPANOATE (25)

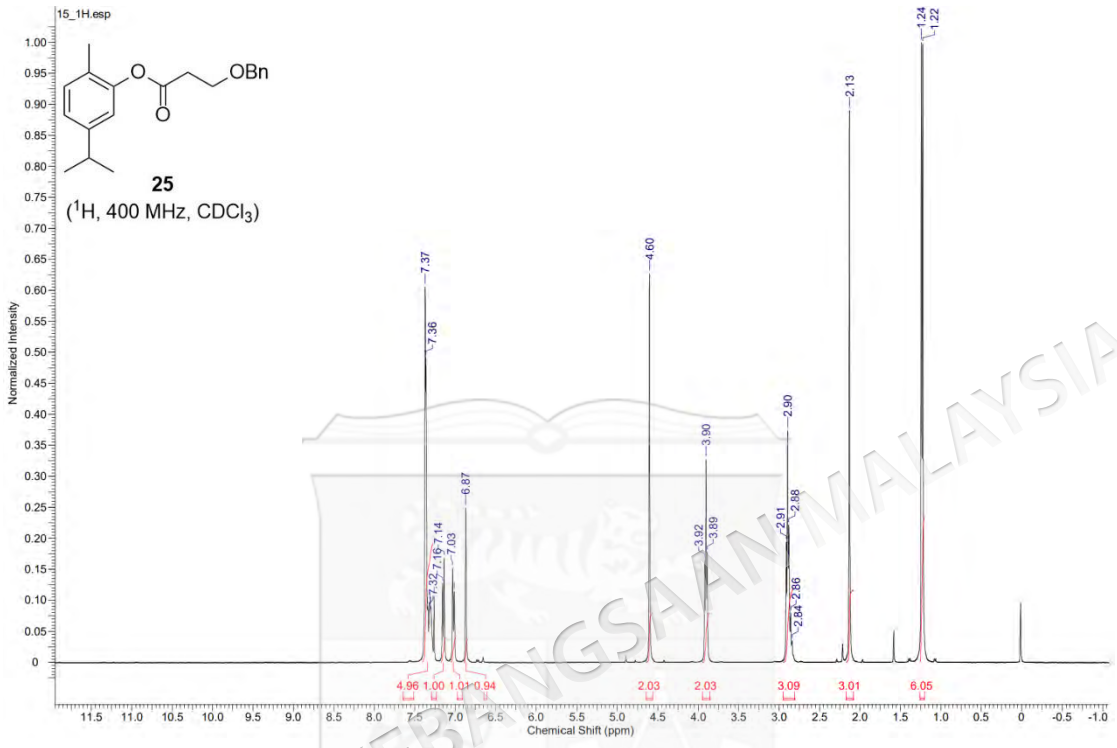

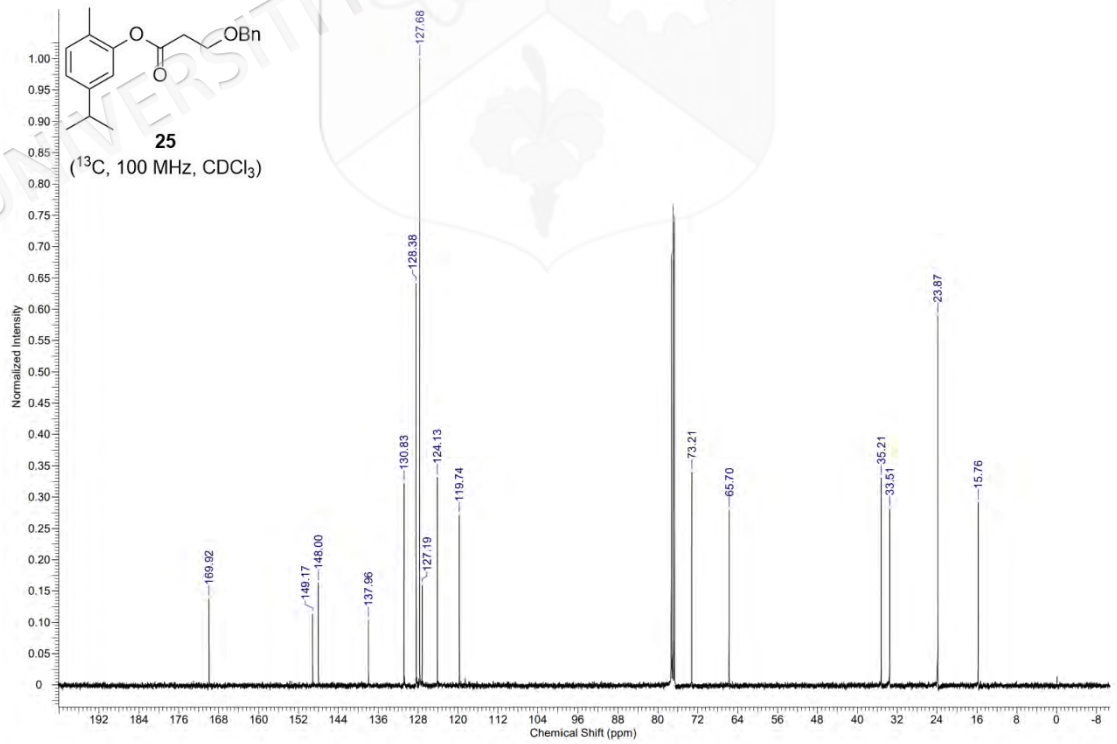

APPENDIX O

^{1}H AND ^{13}C NMR SPECTRA OF 5-ISOPROPYL-2-METHYLPHENYL 3-HYDROXYPROPANOATE (26)

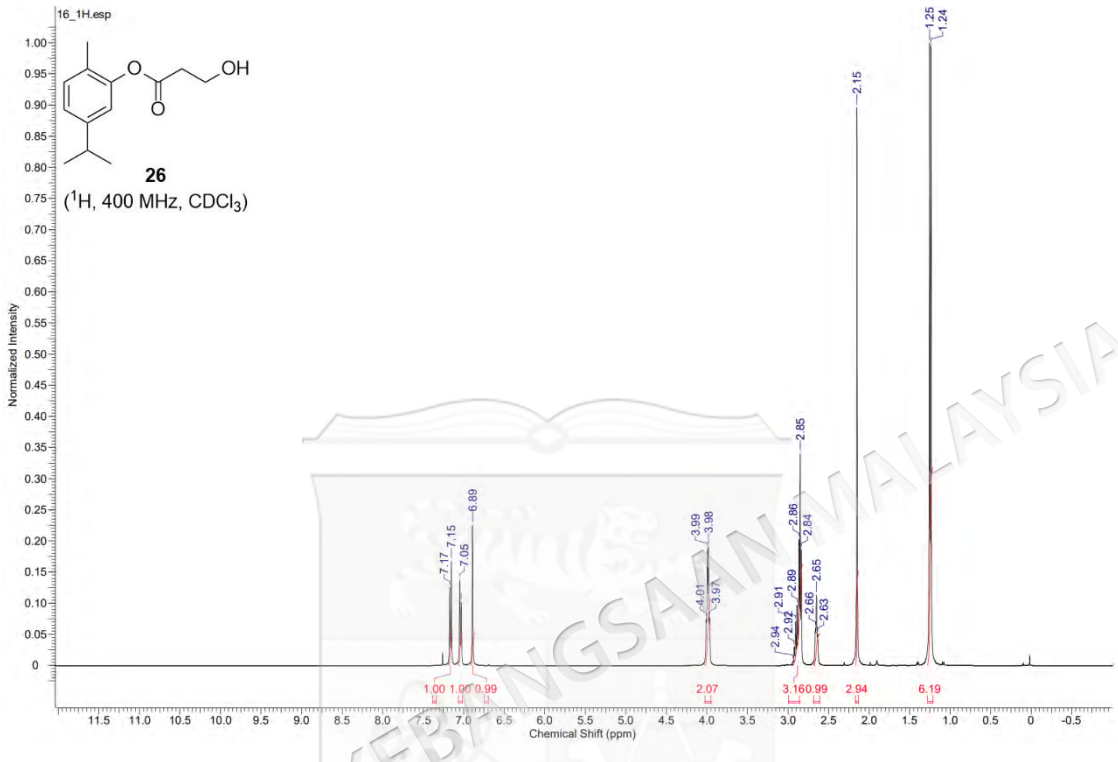

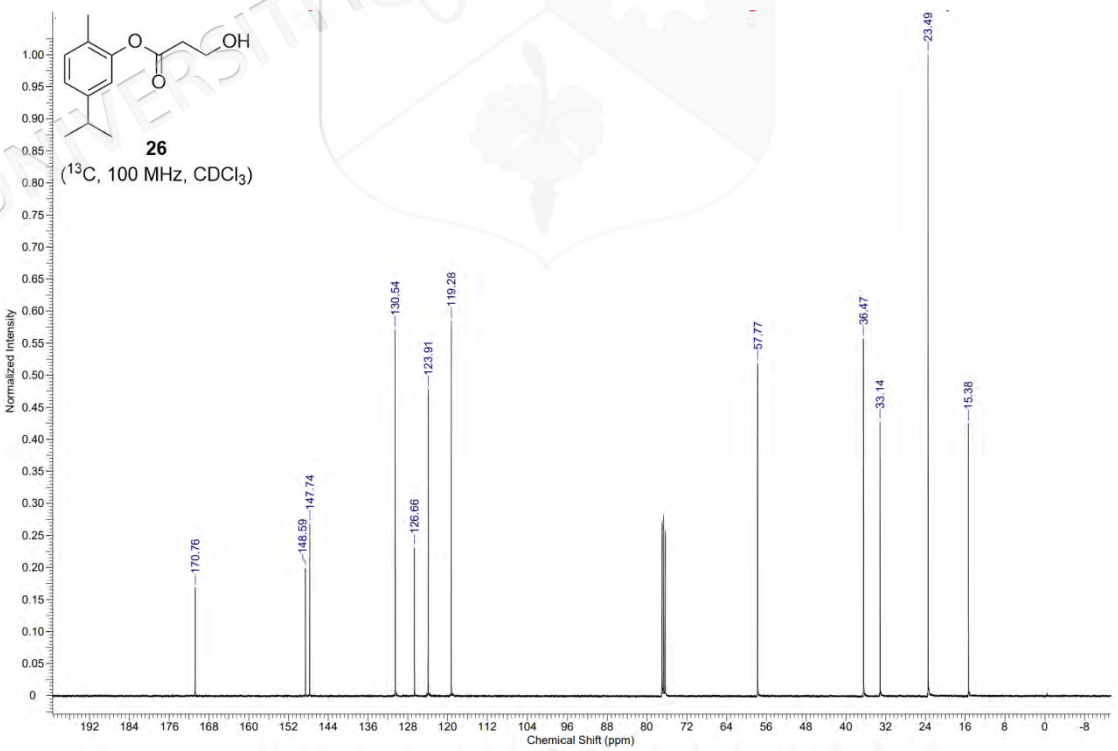

APPENDIX P

^{1}H-NMR SPECTRUM OF 3-((TERT-BUTYLDIMETHYLSILYL)OXY)BENZOIC ACID (27)

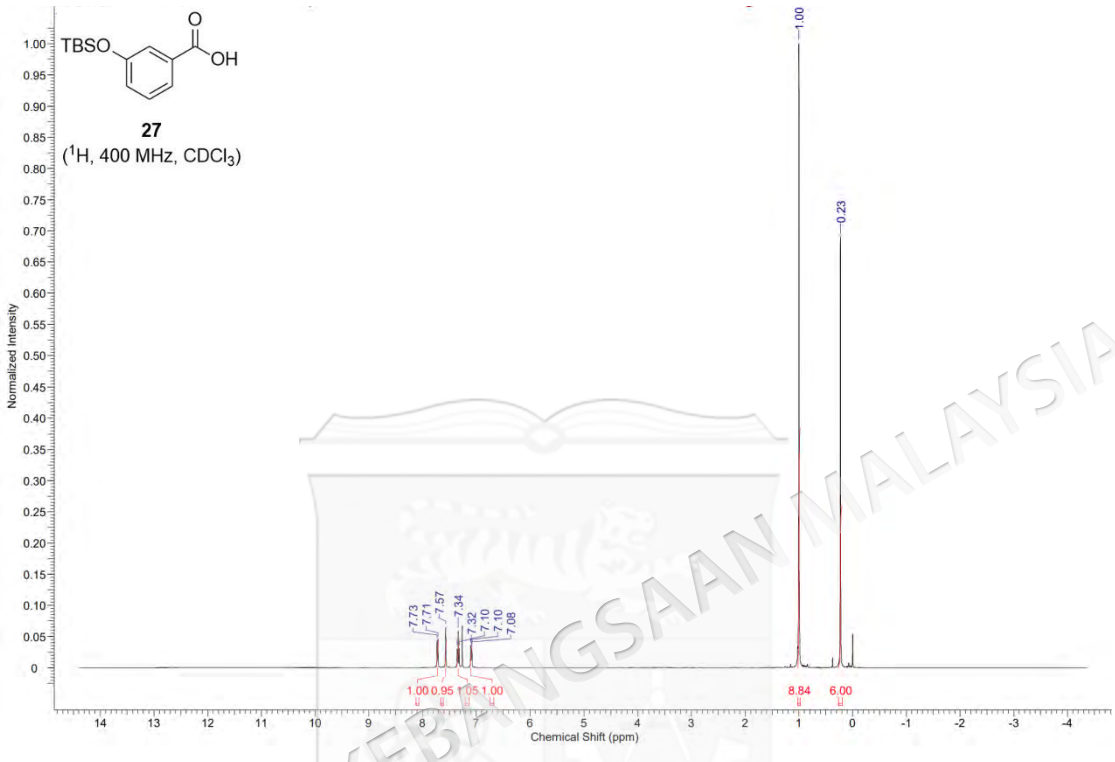

APPENDIX Q

^{1}H AND ^{13}C NMR SPECTRA OF 3-(5-ISOPROPYL-2-METHYLPHENOXY)-3-OXOPROPYL 3-((TERT-BUTYLDIMETHYLSILYL)OXY)BENZOATE (28)

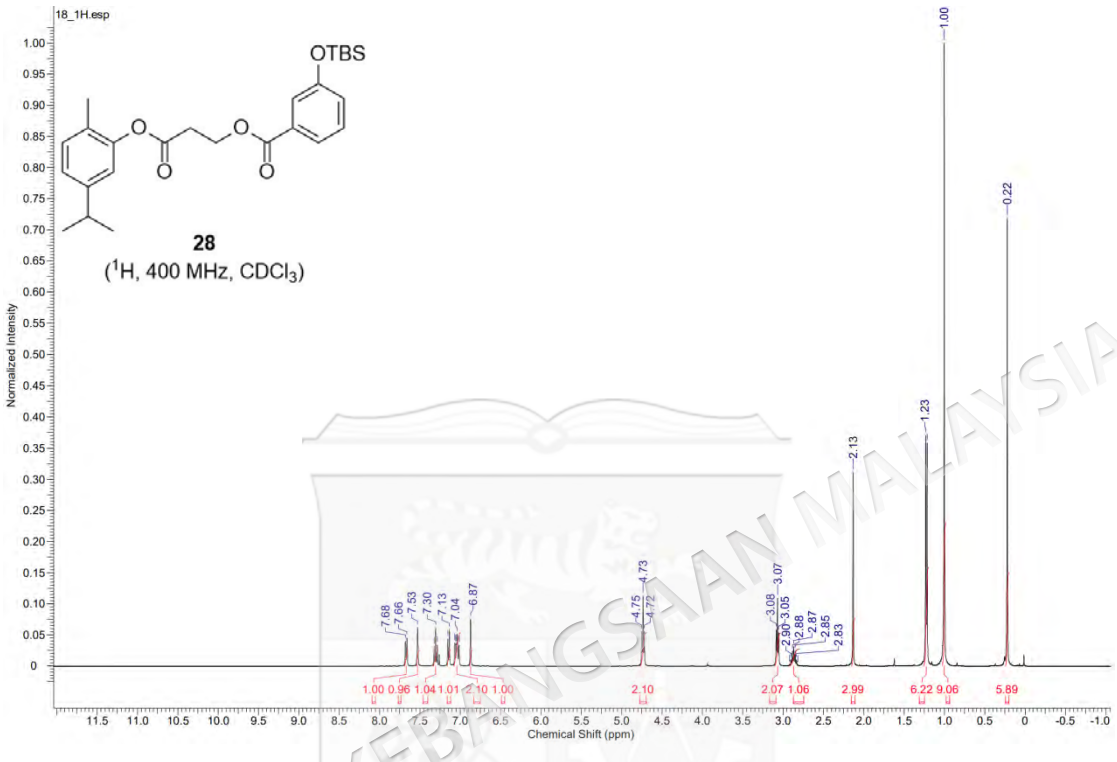

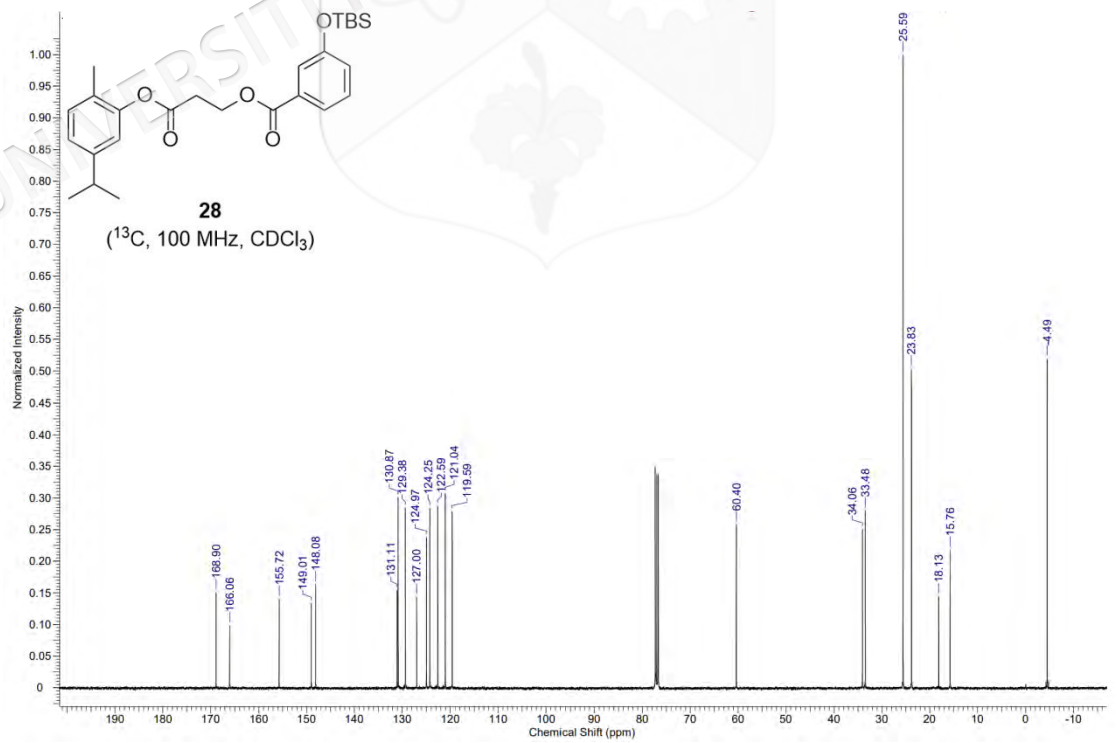

APPENDIX R

^{1}H AND ^{13}C NMR SPECTRA OF 3-(5-ISOPROPYL-2-METHYLPHENOXY)-3-OXOPROPYL 3-HYDROXYBENZOATE (11)

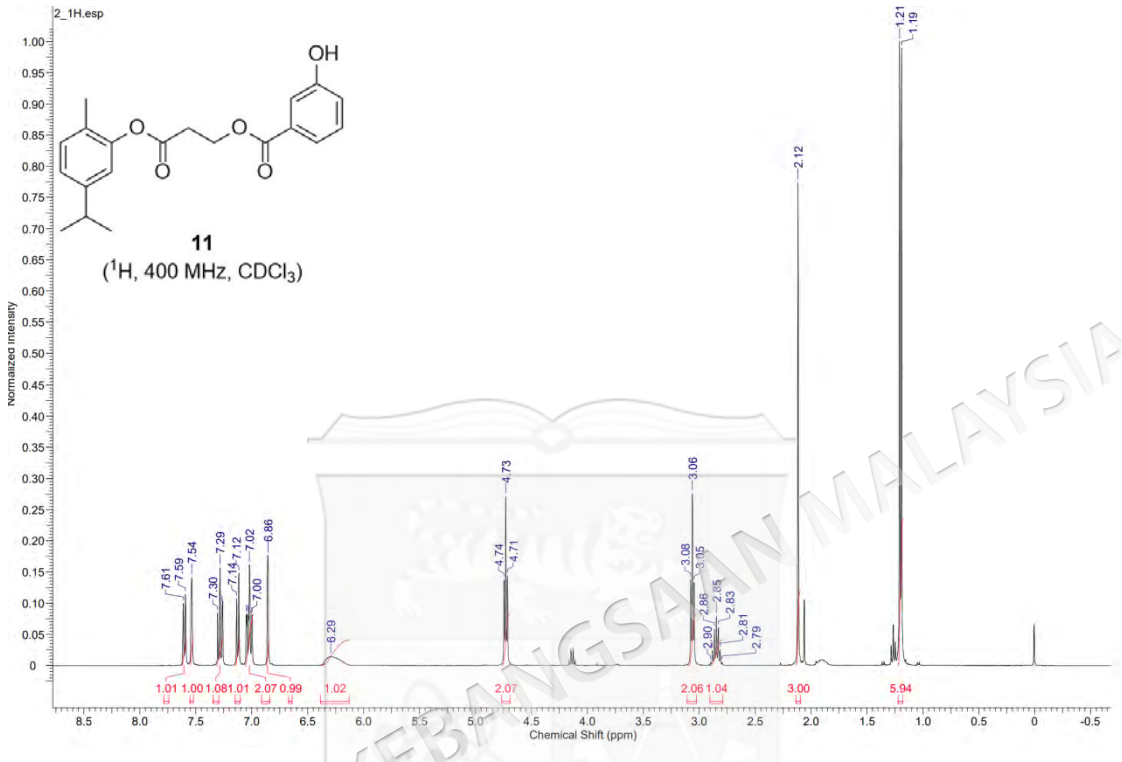

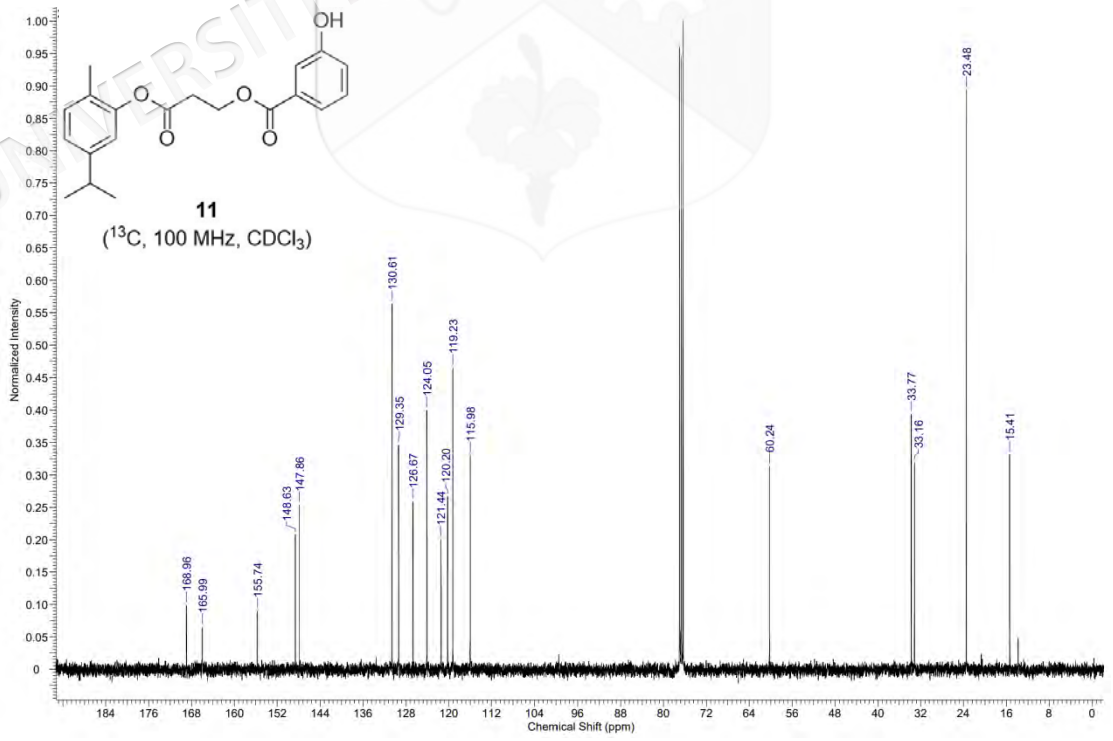

APPENDIX S

^{1}H AND ^{13}C NMR SPECTRA OF 5-ISOPROPYL-2-METHYLPHENYL 4-CHLOROBUTANOATE (23b)

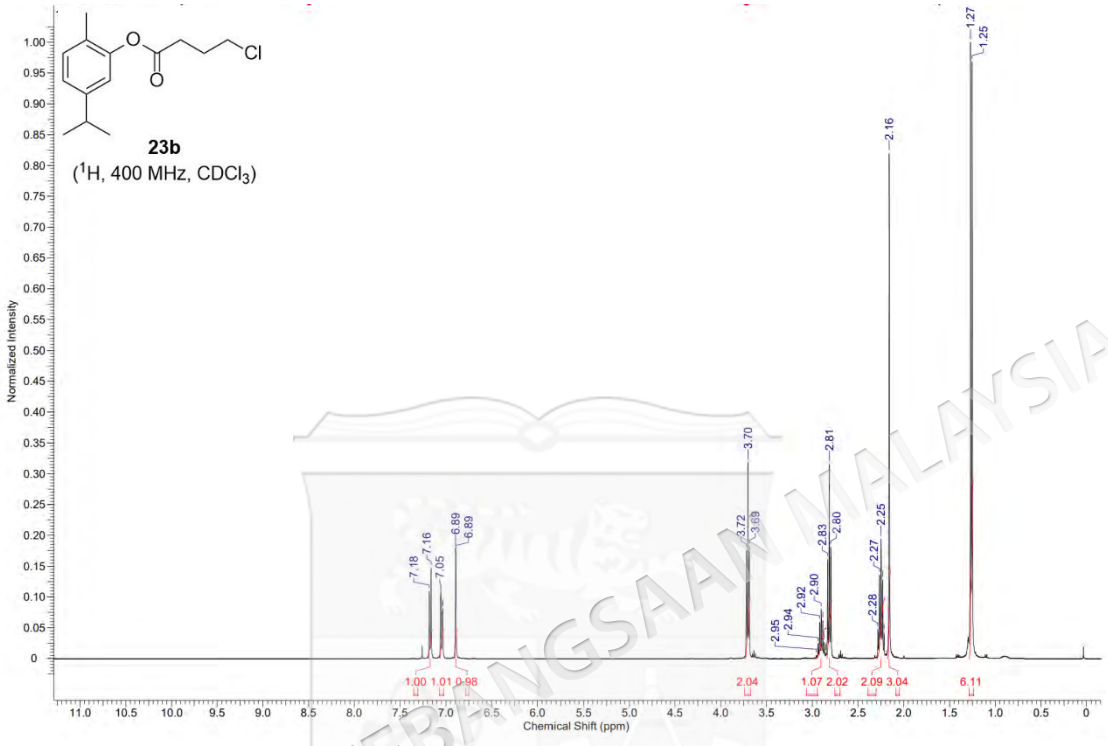

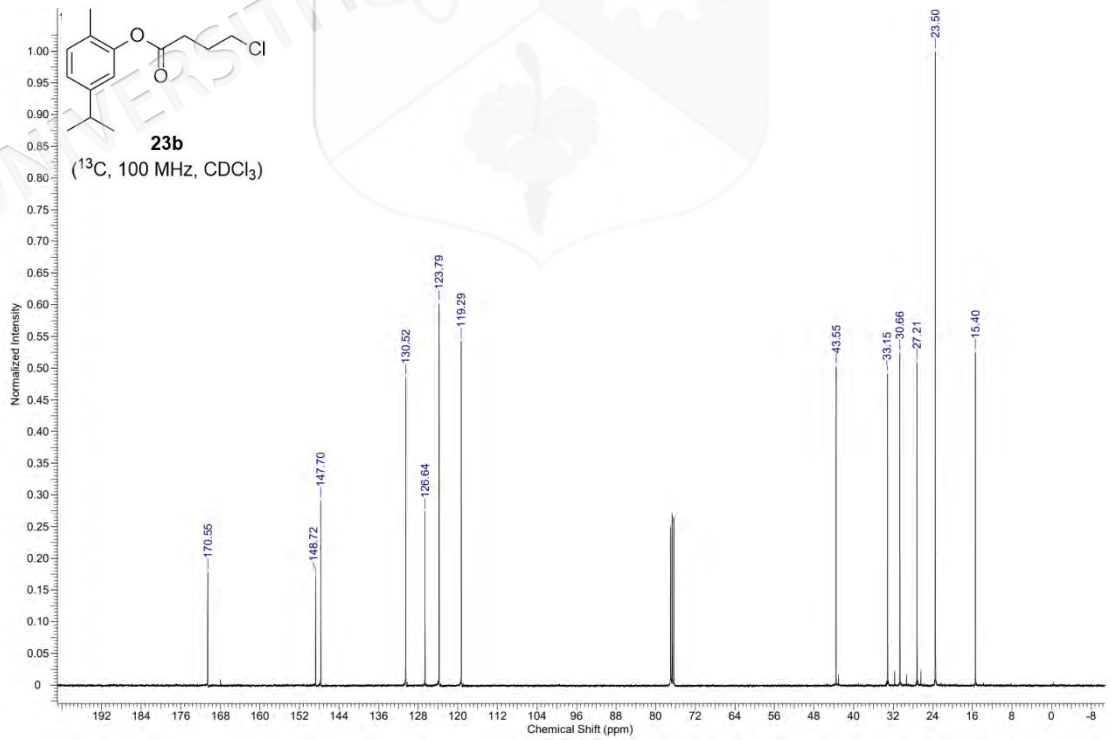

APPENDIX T

^{1}H AND ^{13}C NMR SPECTRA OF 4-(5-ISOPROPYL-2-METHYLPHENOXY)-4-OXOBUTYL 3-HYDROXYBENZOATE (12)

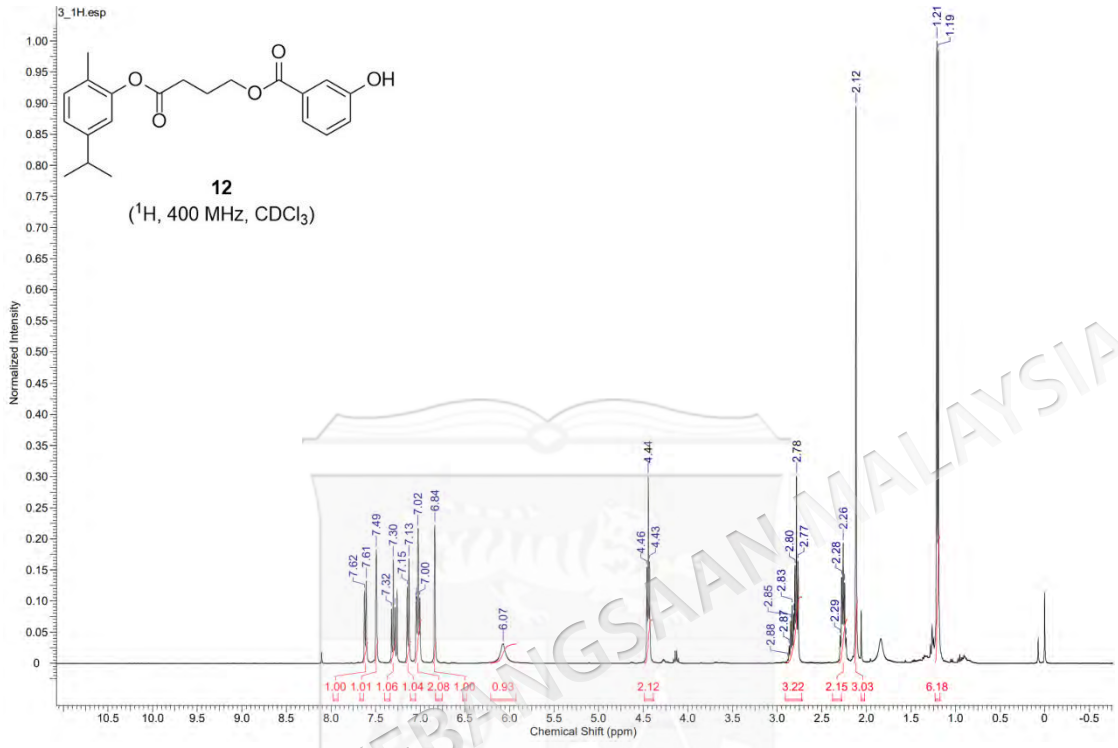

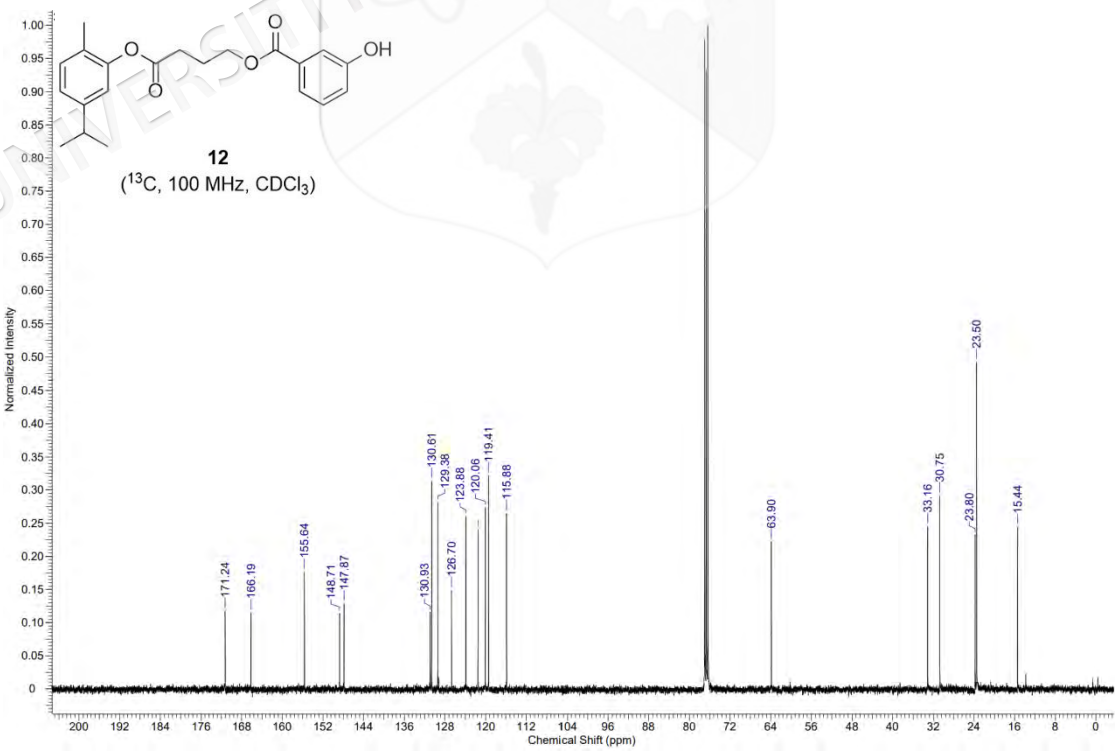

APPENDIX U

^{1}H AND ^{13}C NMR SPECTRA OF 2-(2-BROMOETHOXY)-4-ISOPROPYL-1-METHYLBENZENE (29a)

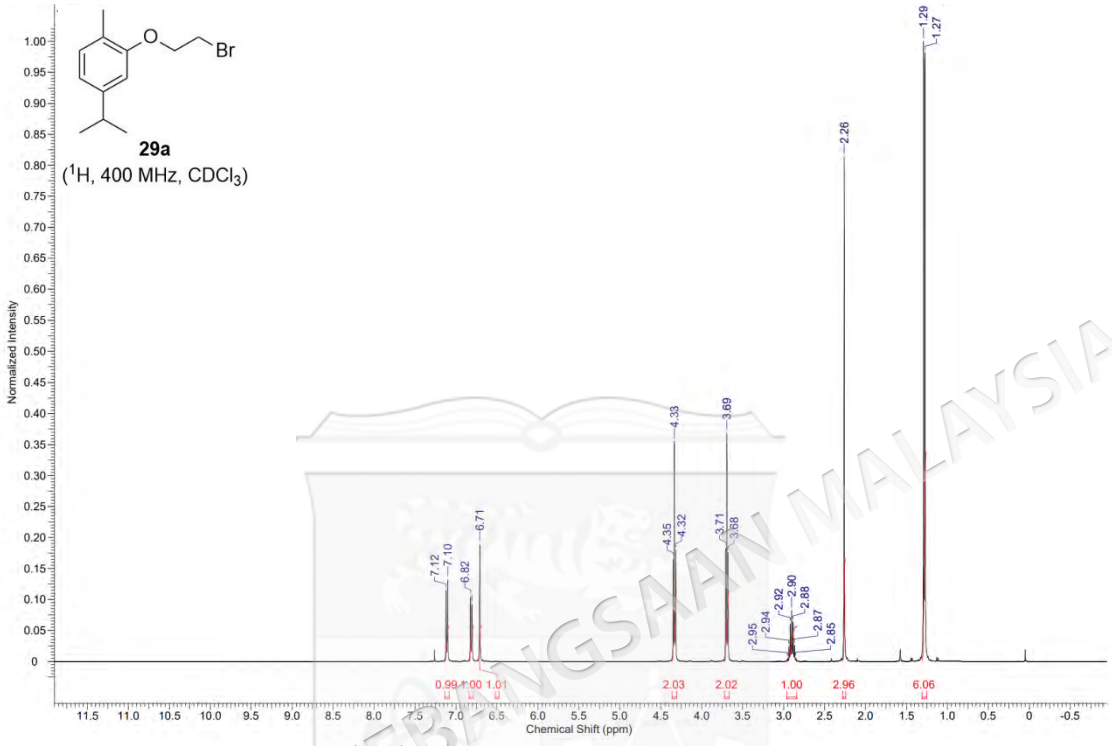

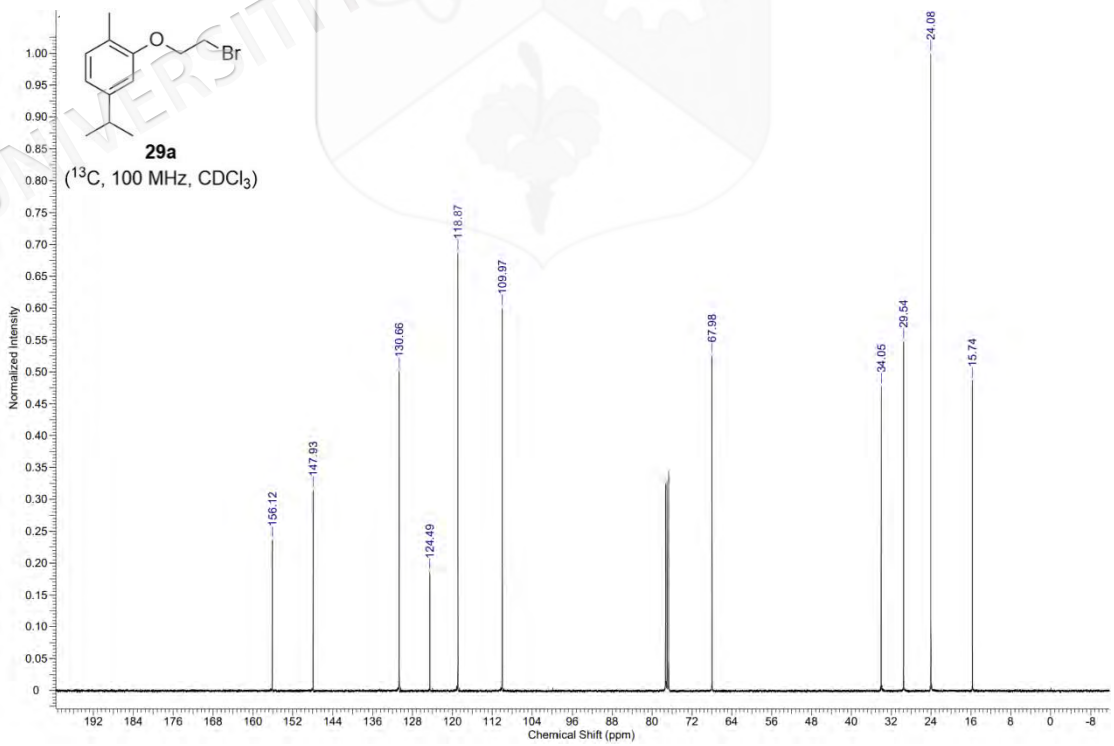

APPENDIX V

^{1}H AND ^{13}C NMR SPECTRA OF 2-(5-ISOPROPYL-2-METHYLPHENOXY)ETHYL 3-HYDROXYBENZOATE (13)

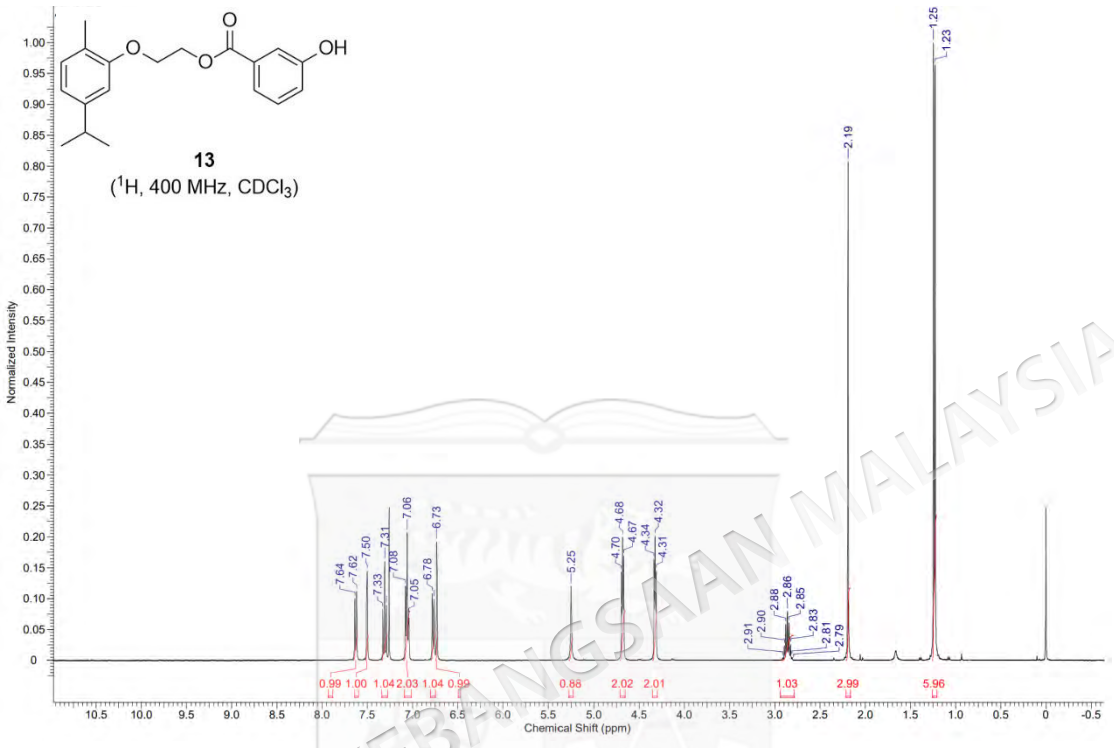

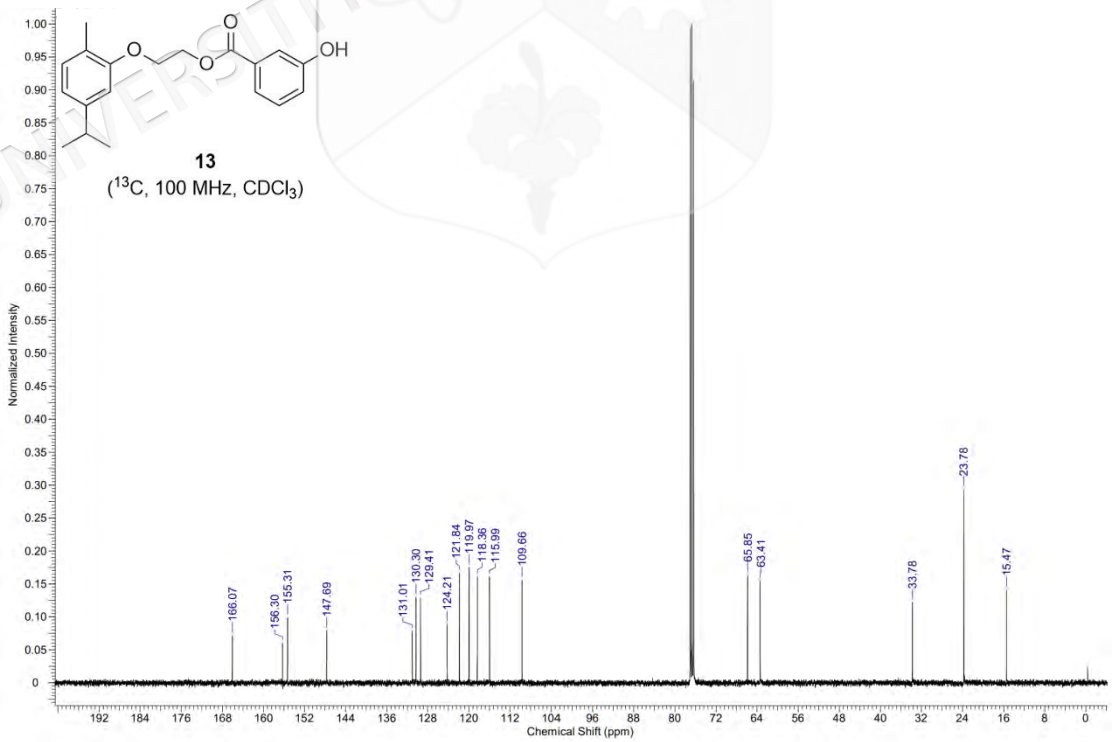

APPENDIX W

^{1}H AND ^{13}C NMR SPECTRA OF 2-(3-BROMOPROPOXY)-4-ISOPROPYL-1-METHYLBENZENE (29b)

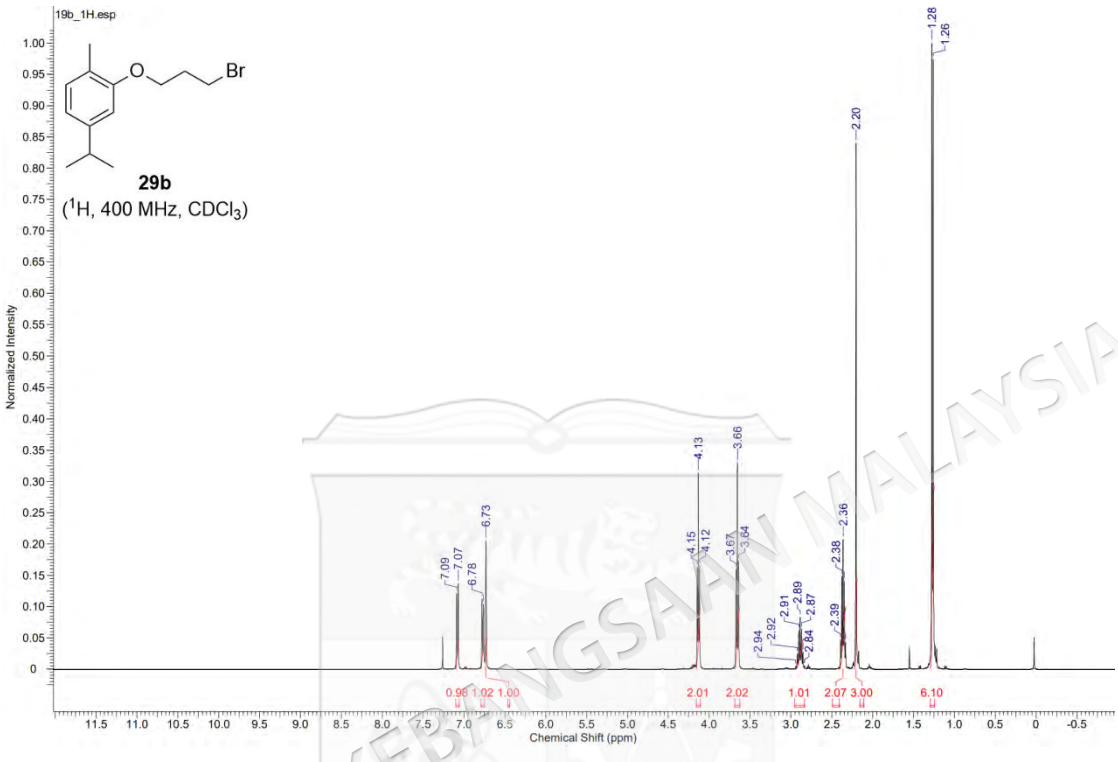

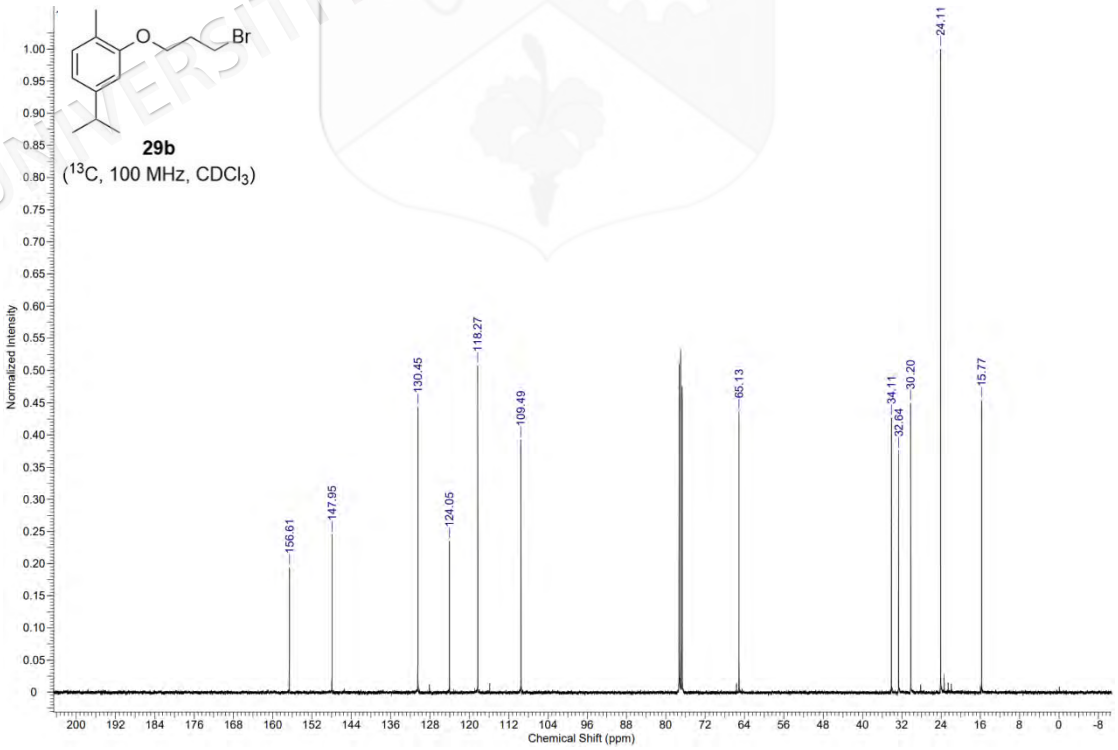

APPENDIX X

^{1}H AND ^{13}C NMR SPECTRA OF 3-(5-ISOPROPYL-2-METHYLPHENOXY)PROPYL 3-HYDROXYBENZOATE (14)

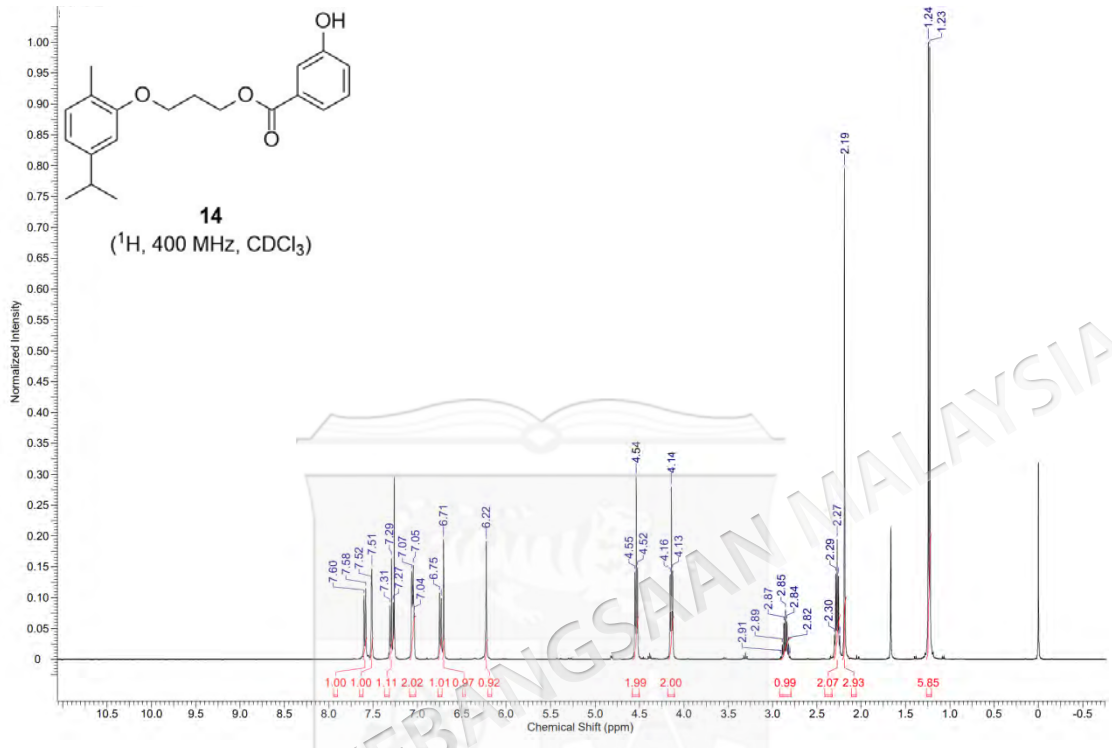

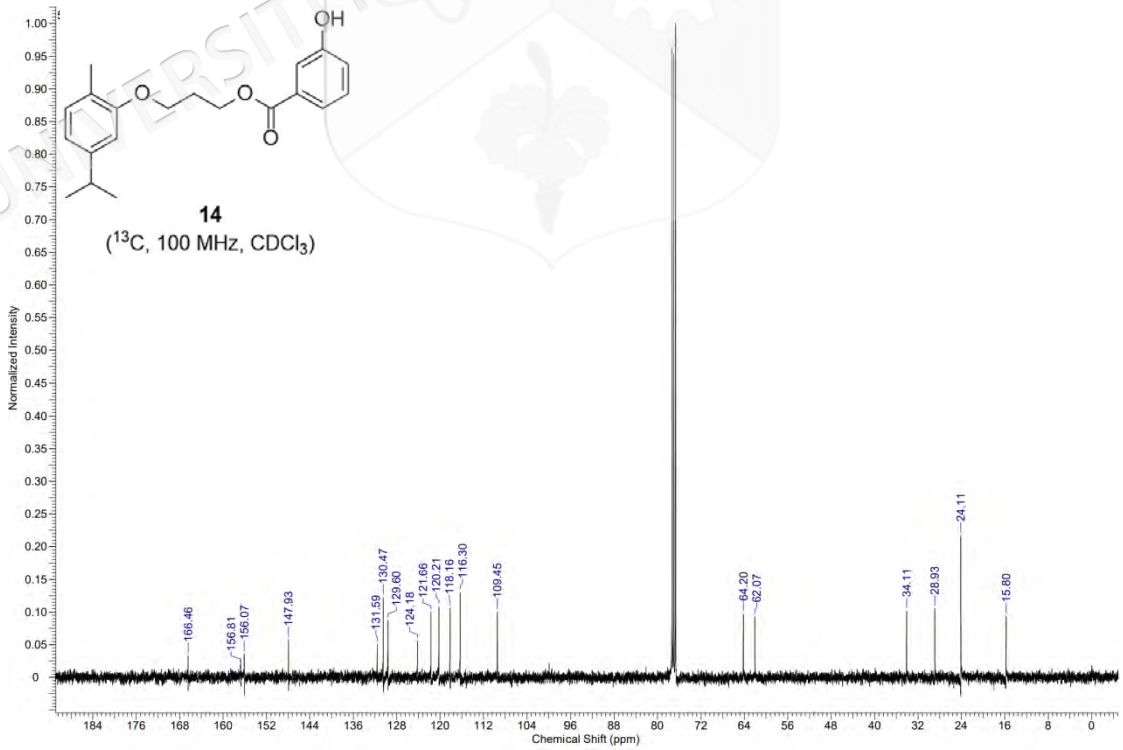

APPENDIX Y

^{1} AND ^{13}C NMR SPECTRA OF 2-(4-BROMOBUTOXY)-4-ISOPROPYL-1-METHYLBENZENE (29c)

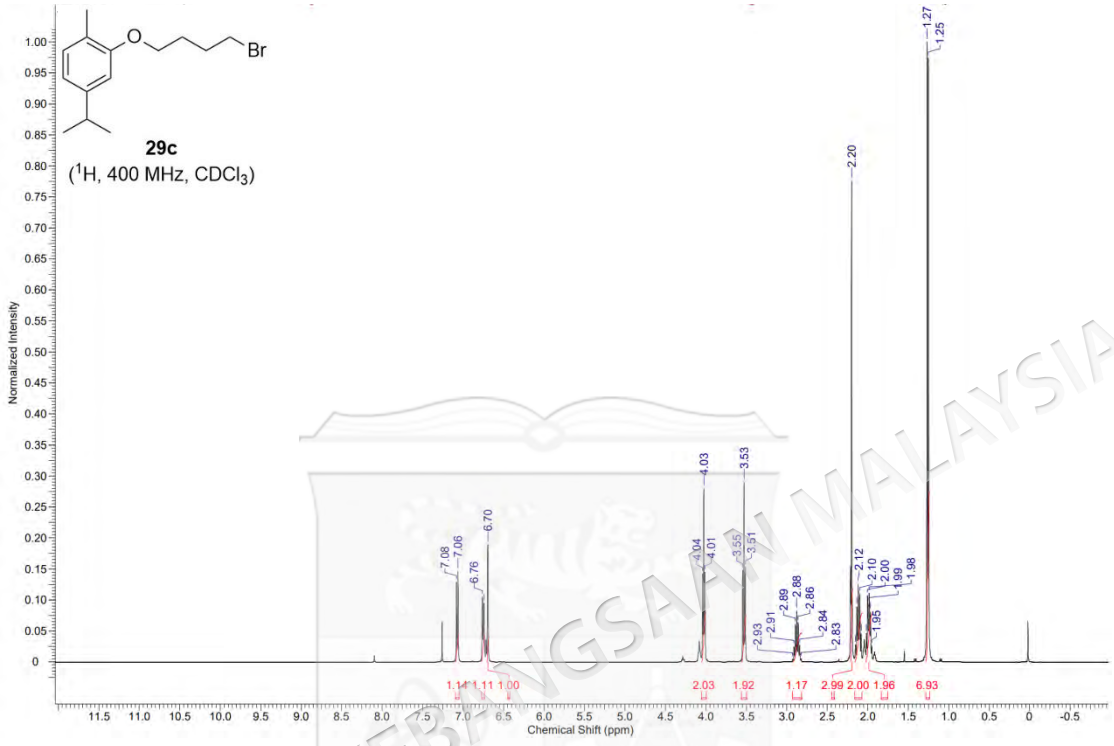

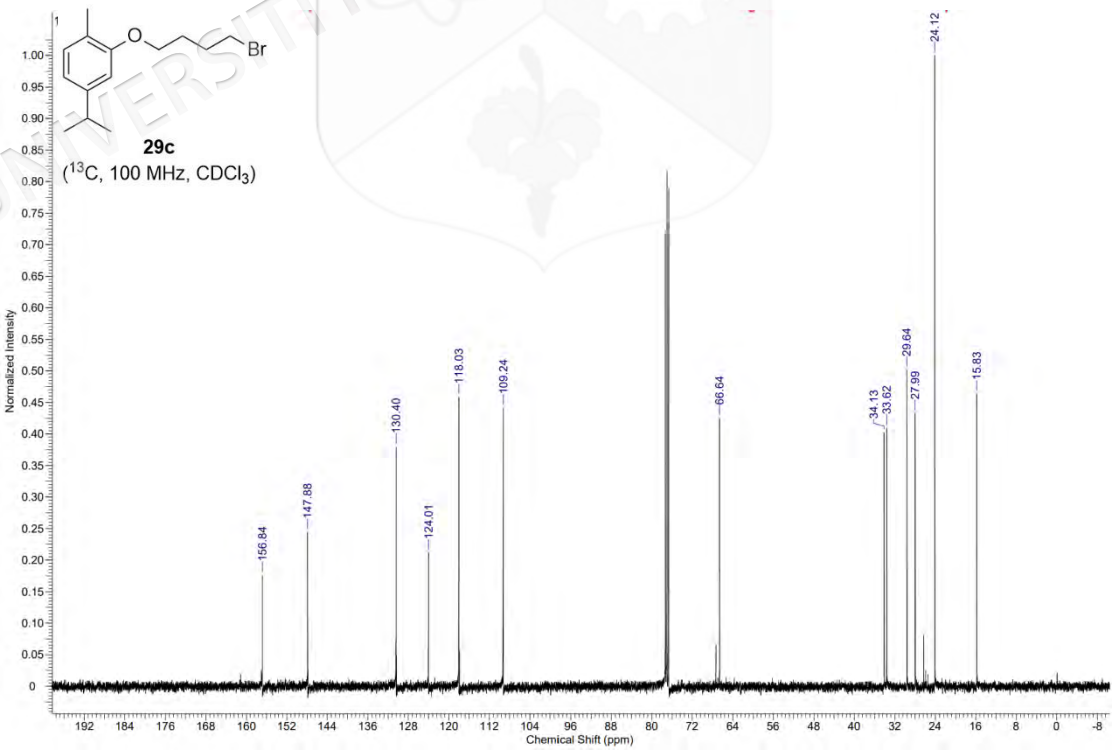

APPENDIX Z

^{1}H AND ^{13}C NMR SPECTRA OF 4-(5-ISOPROPYL-2-METHYLPHENOXY)BUTYL 3-HYDROXYBENZOATE (15)

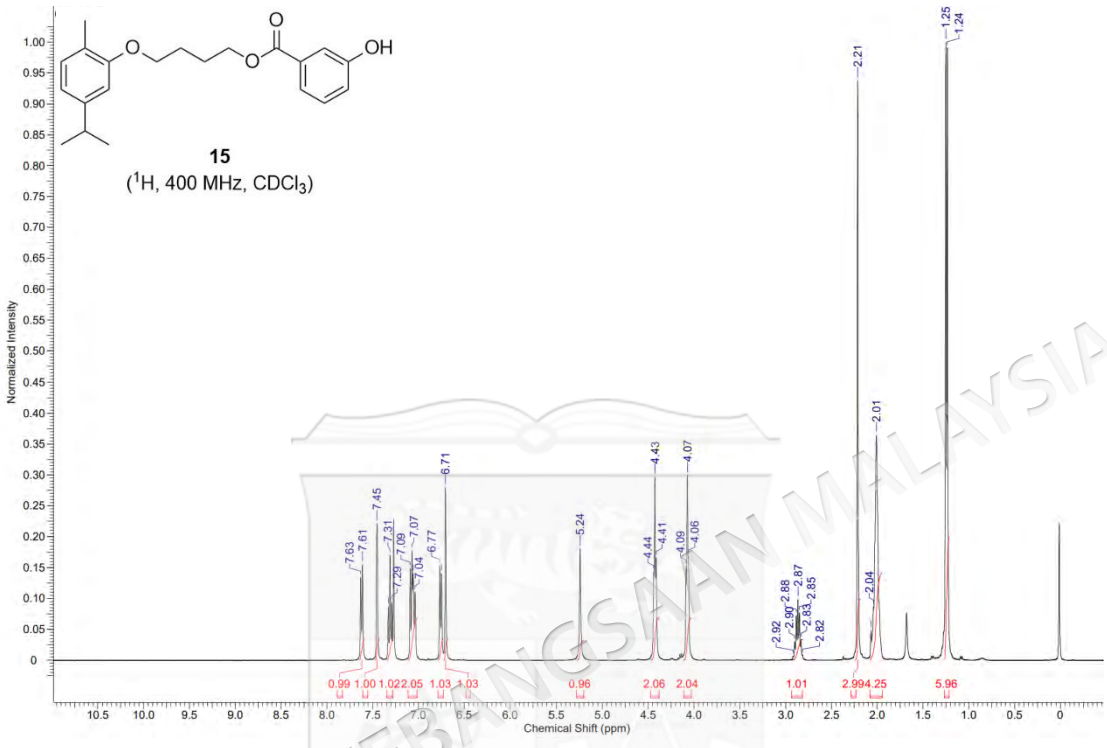

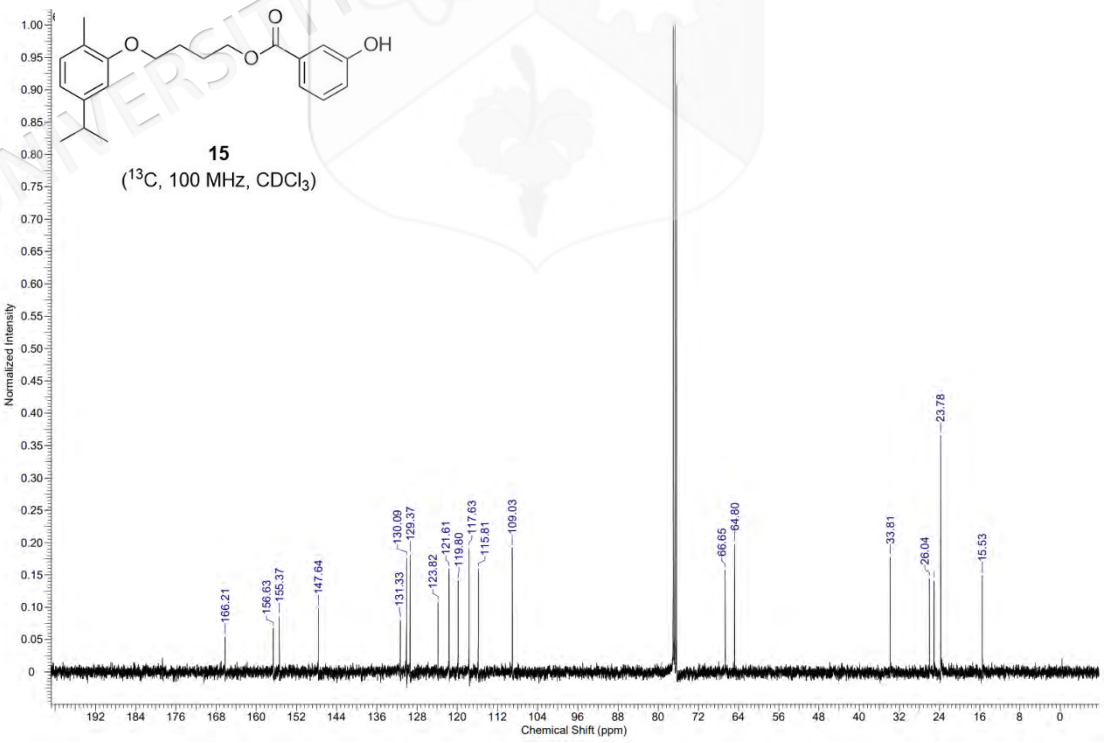

APPENDIX AA

^{1}H AND ^{13}C NMR SPECTRA OF 4-(((TERT-BUTYLDIMETHYLSILYL)OXY)METHYL)-5-ISOPROPYL-2-METHYLPHENYL 2-CHLOROACETATE (31a)

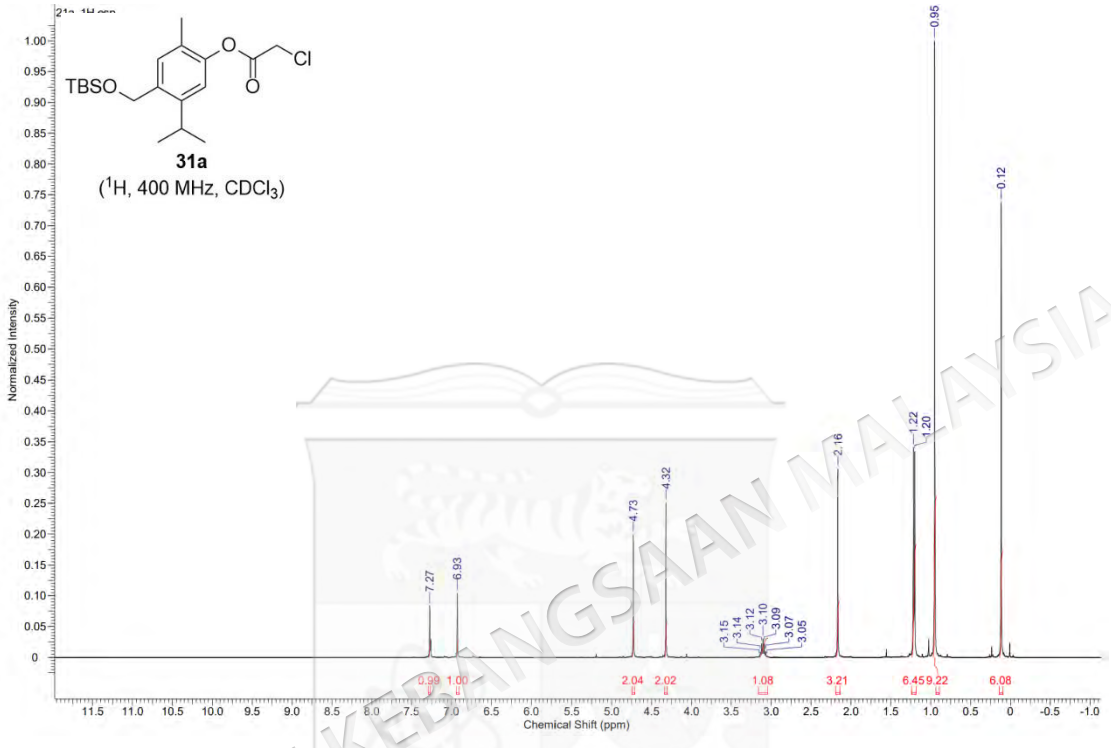

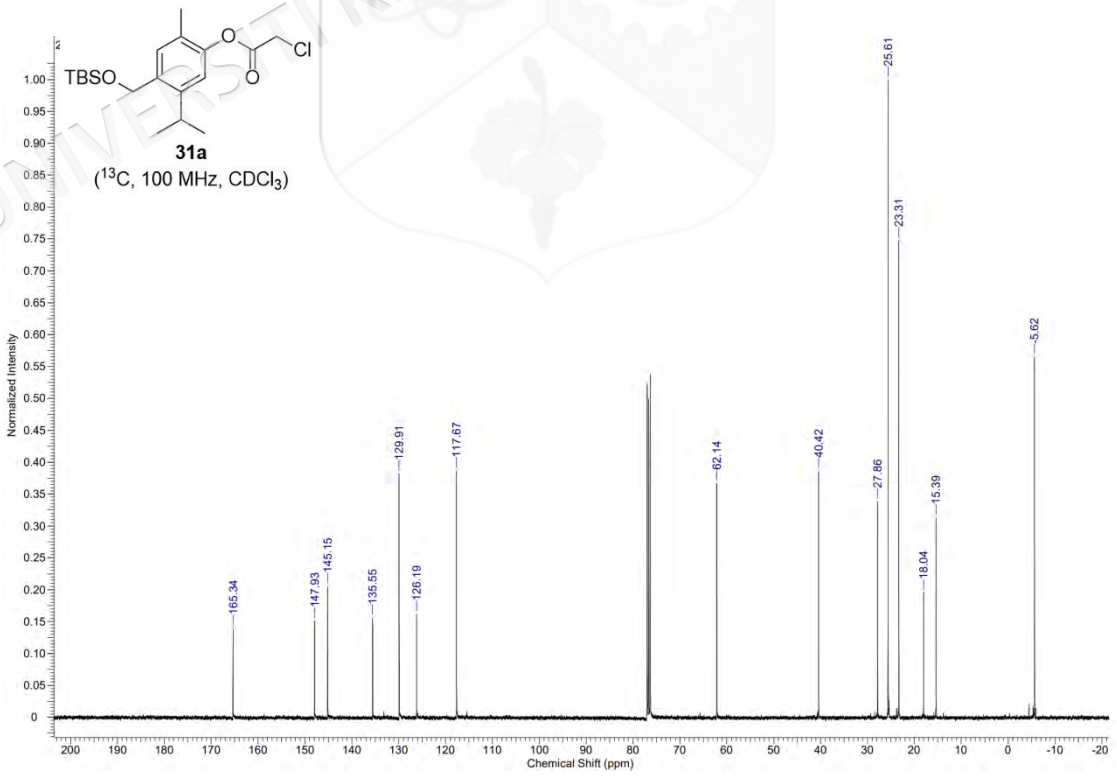

APPENDIX BB

^{1}H AND ^{13}C NMR SPECTRA OF 2-(4-(((TERT-BUTYLDIMETHYLSILYL)OXY)METHYL)-5-ISOPROPYL-2-METHYLPHENOXY)-2-OXOETHYL 3-HYDROXYBENZOATE (32a)

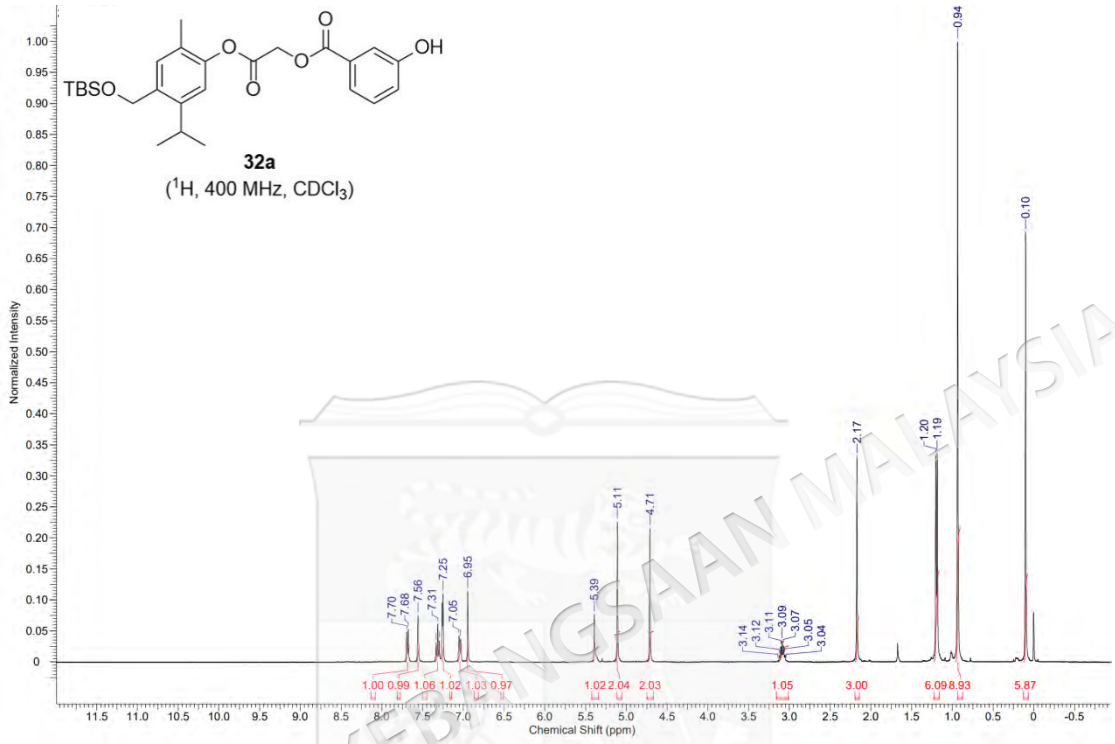

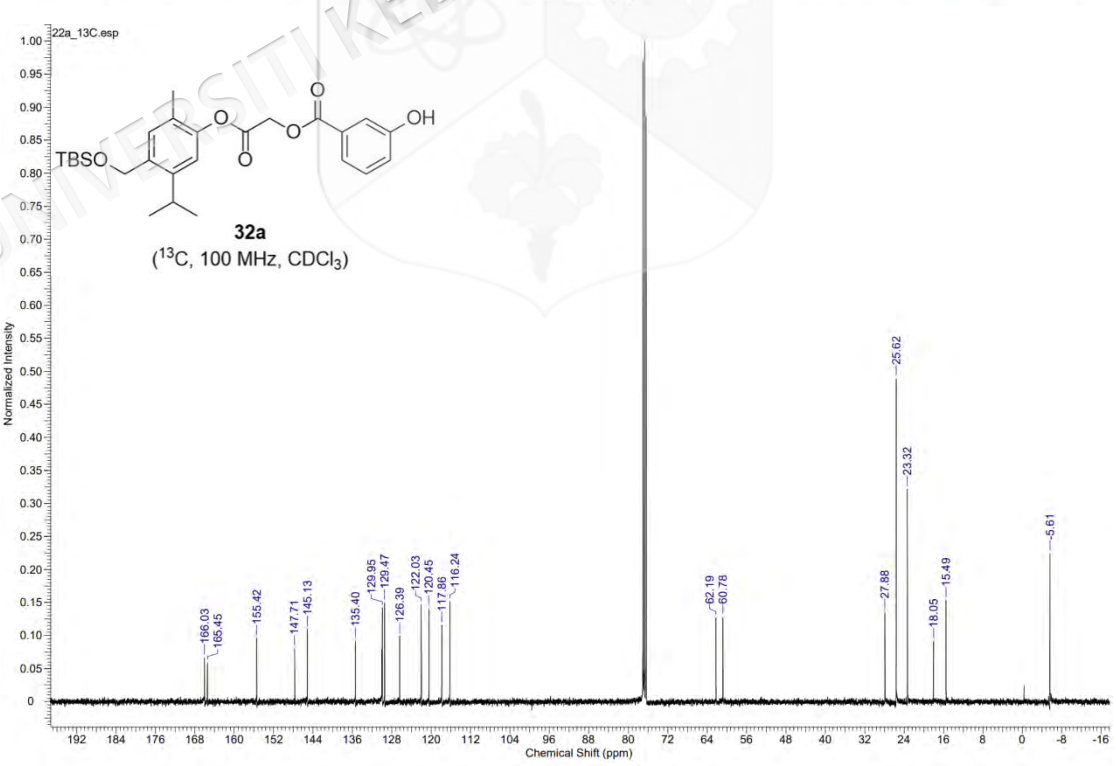

APPENDIX CC

^{1}H AND ^{13}C NMR SPECTRA OF 2-(4-(HYDROXYMETHYL)-5-ISOPROPYL-2-METHYLPHENOXY)-2-OXOETHYL 3-HYDROXYBENZOATE (16)

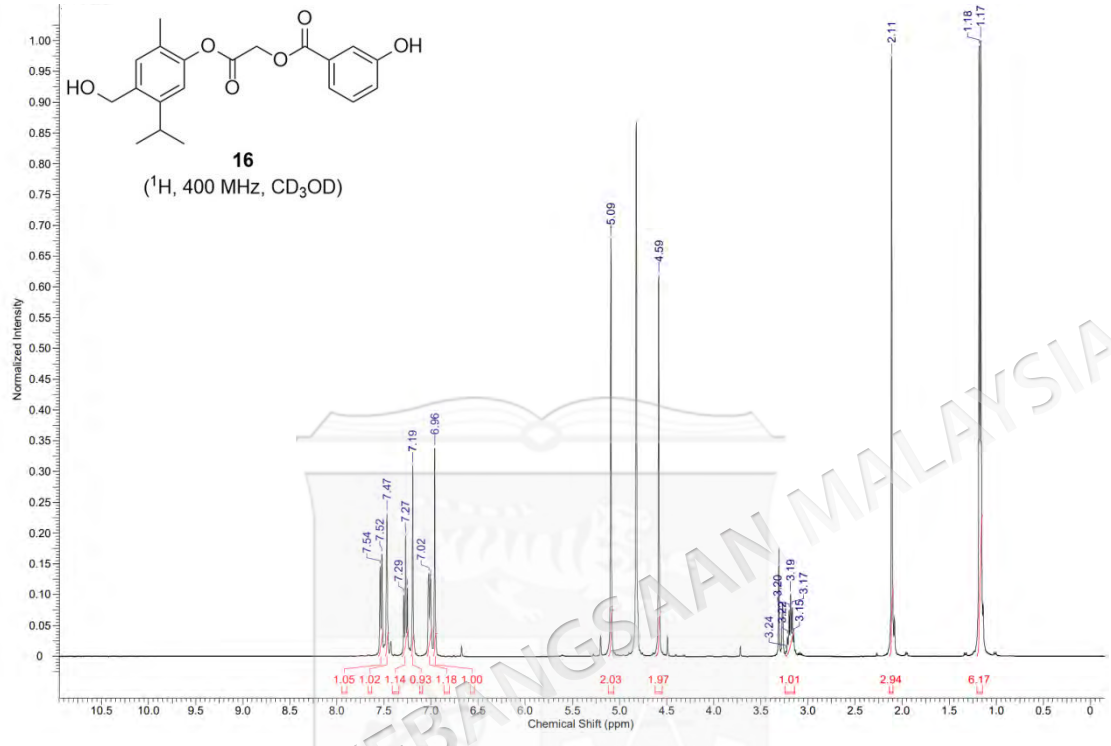

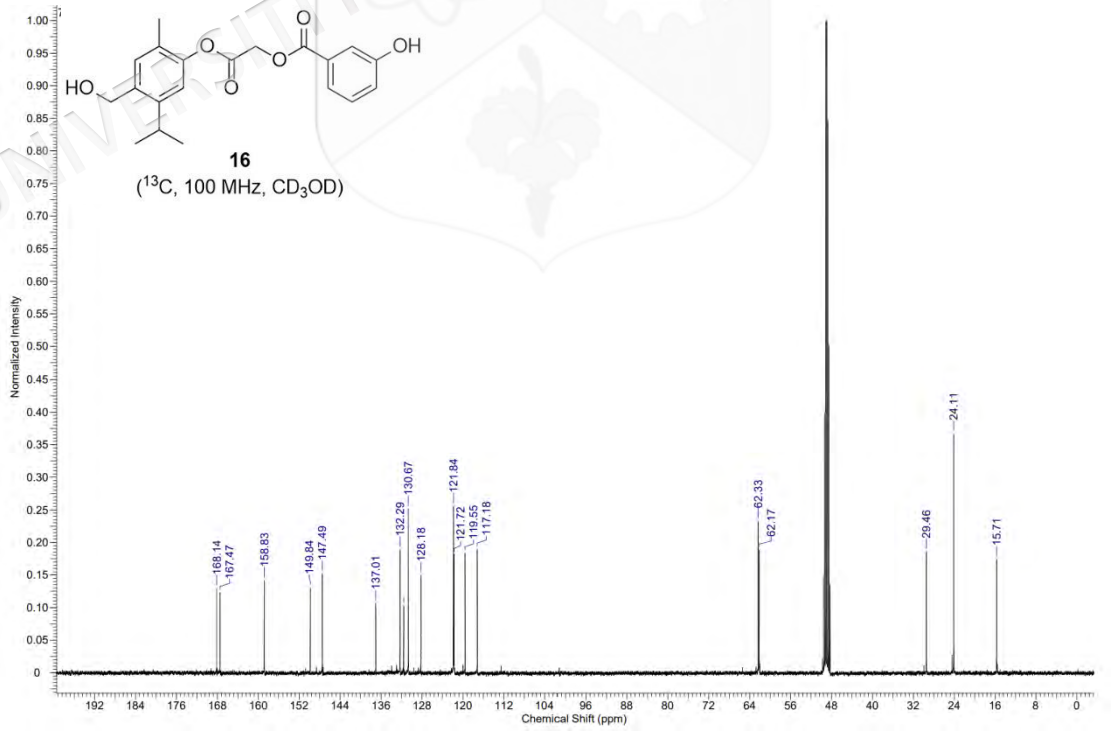

APPENDIX DD

^{1}H AND ^{13}C NMR SPECTRA OF 4-(((TERT-BUTYLDIMETHYLSILYL)OXY)METHYL)-5-ISOPROPYL-2-METHYLPHENYL 3-(BENZYLOXY)PROPANOATE (33)

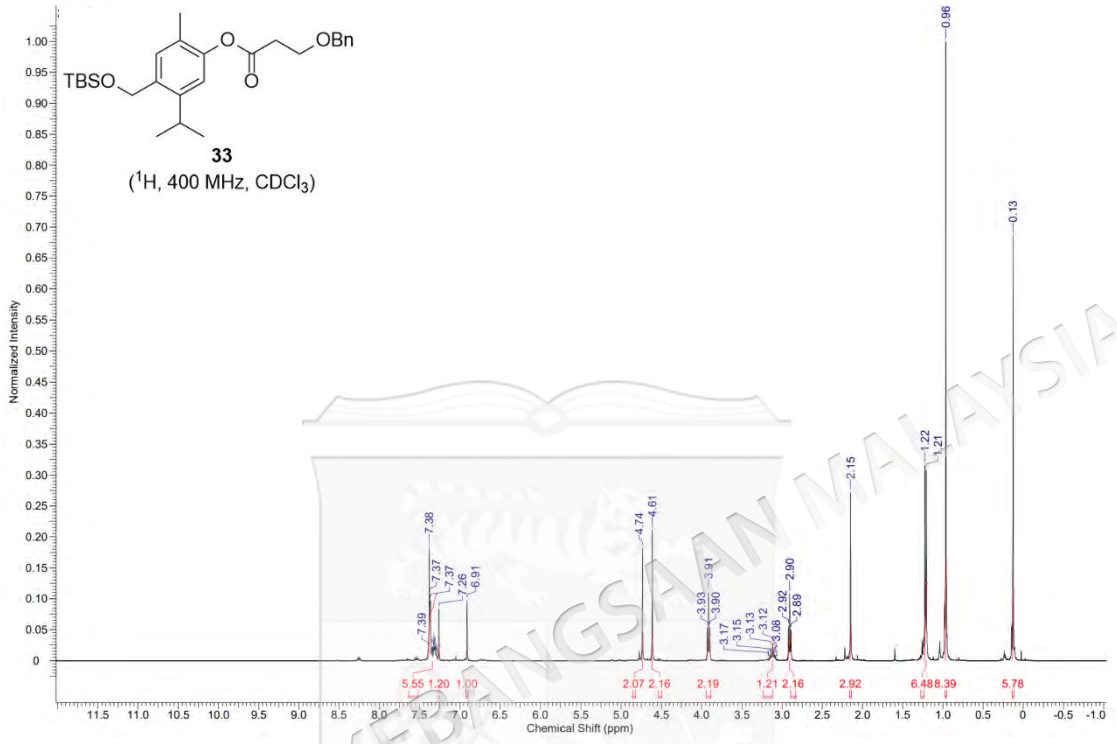

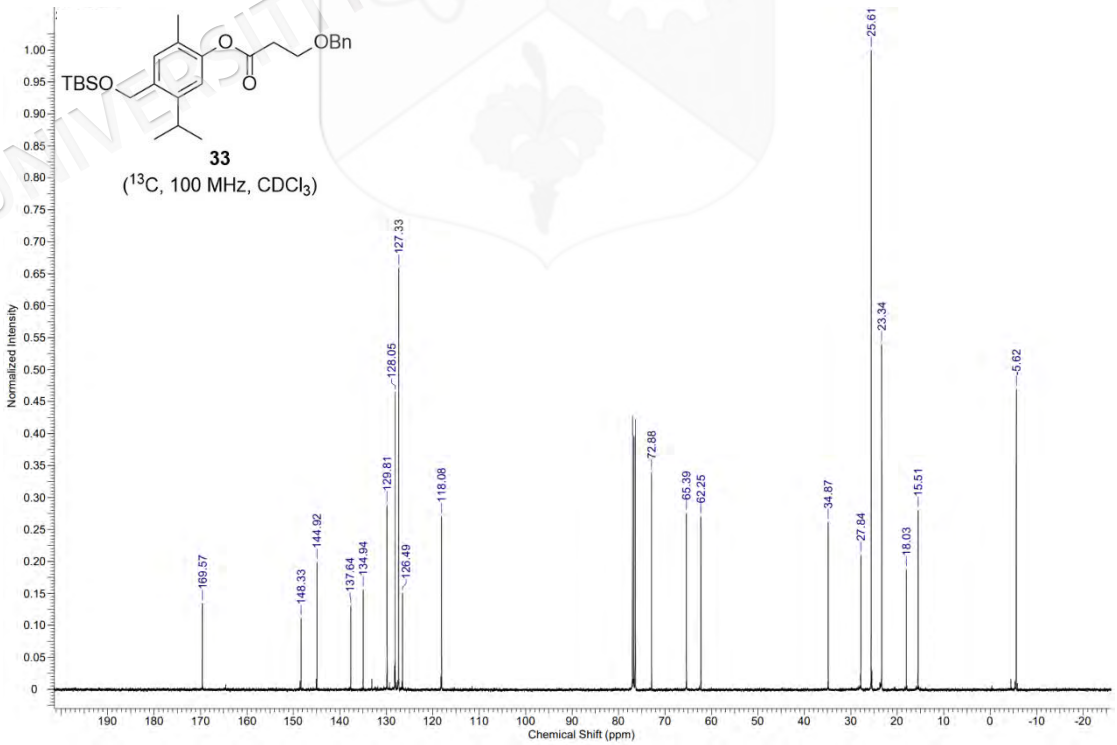

APPENDIX EE

^{1}H AND ^{13}C NMR SPECTRA OF 4-(((TERT-BUTYLDIMETHYLSILYL)OXY)METHYL)-5-ISOPROPYL-2-METHYLPHENYL 3-HYDROXYPROPANOATE (34)

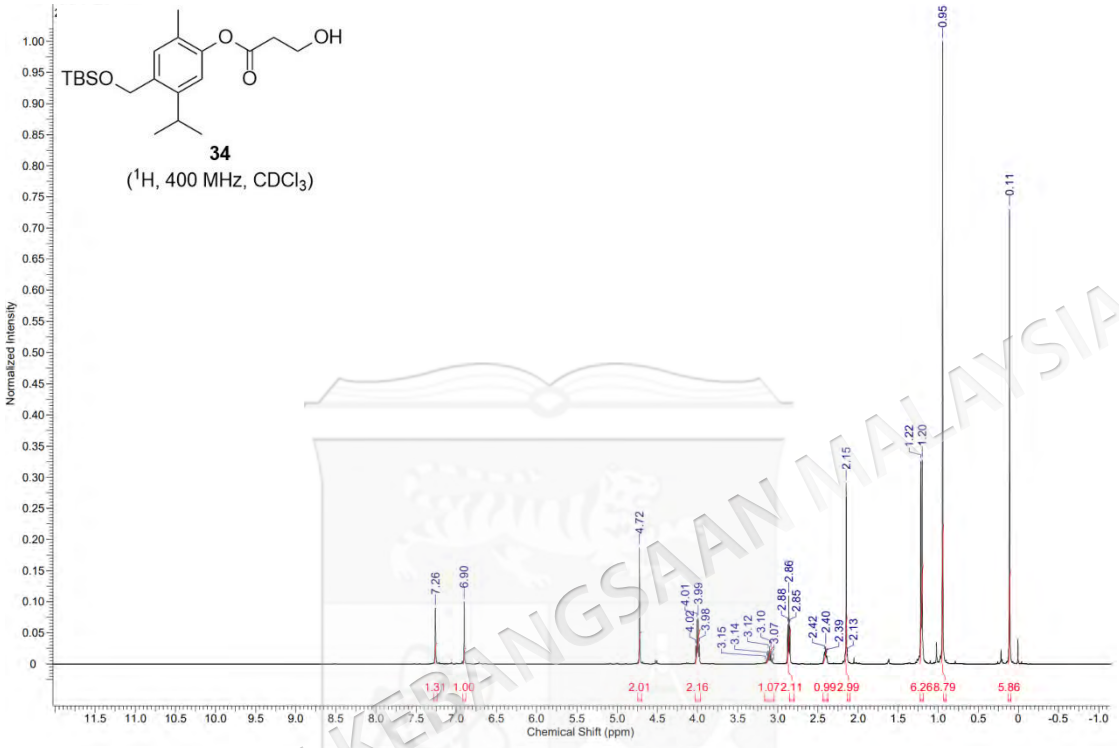

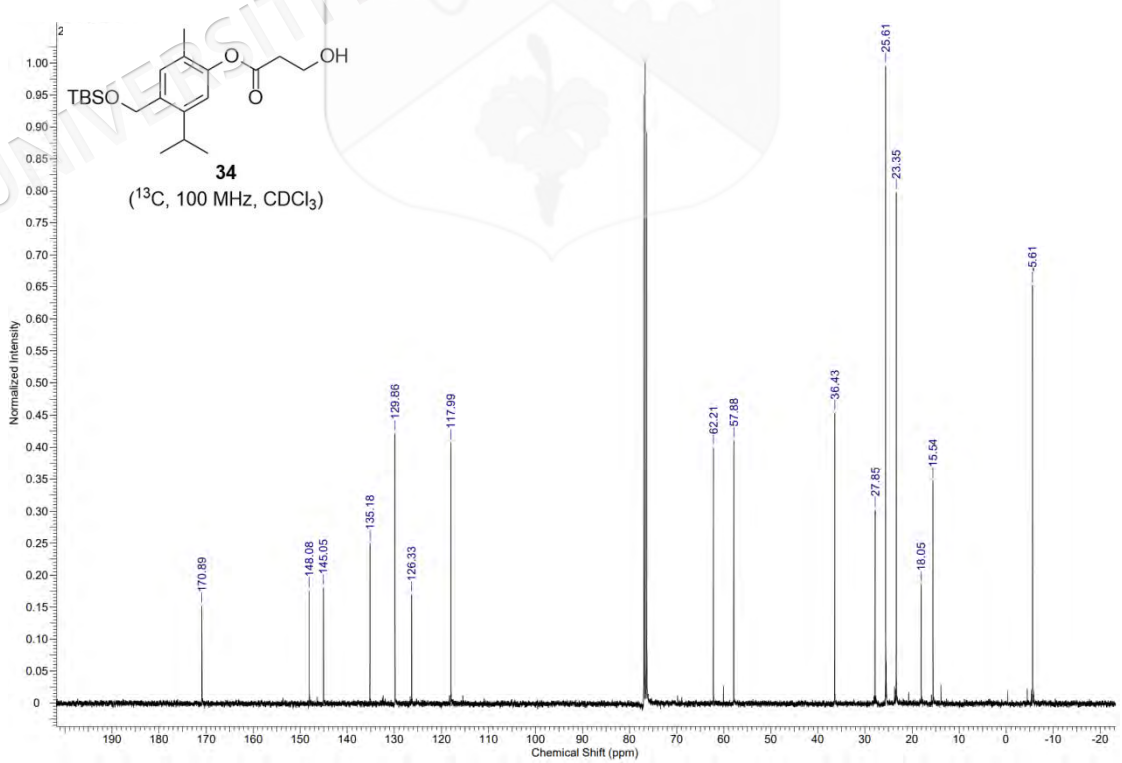

APPENDIX FF

^{1}H AND ^{13}C NMR SPECTRA OF 3-(4-(((TERT-BUTYLDIMETHYLSILYL)OXY)METHYL)-5-ISOPROPYL-2-METHYLPHENOXY)-3-OXOPROPYL 3-((TERT-BUTYLDIMETHYLSILYL)OXY)BENZOATE (35)

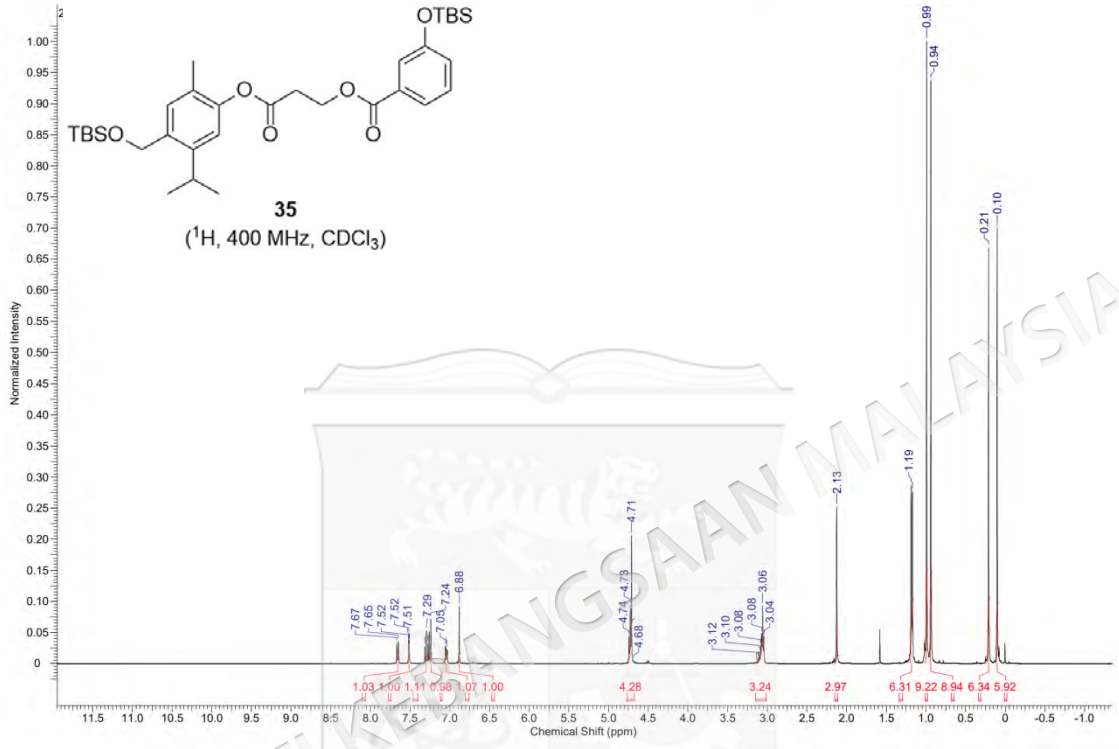

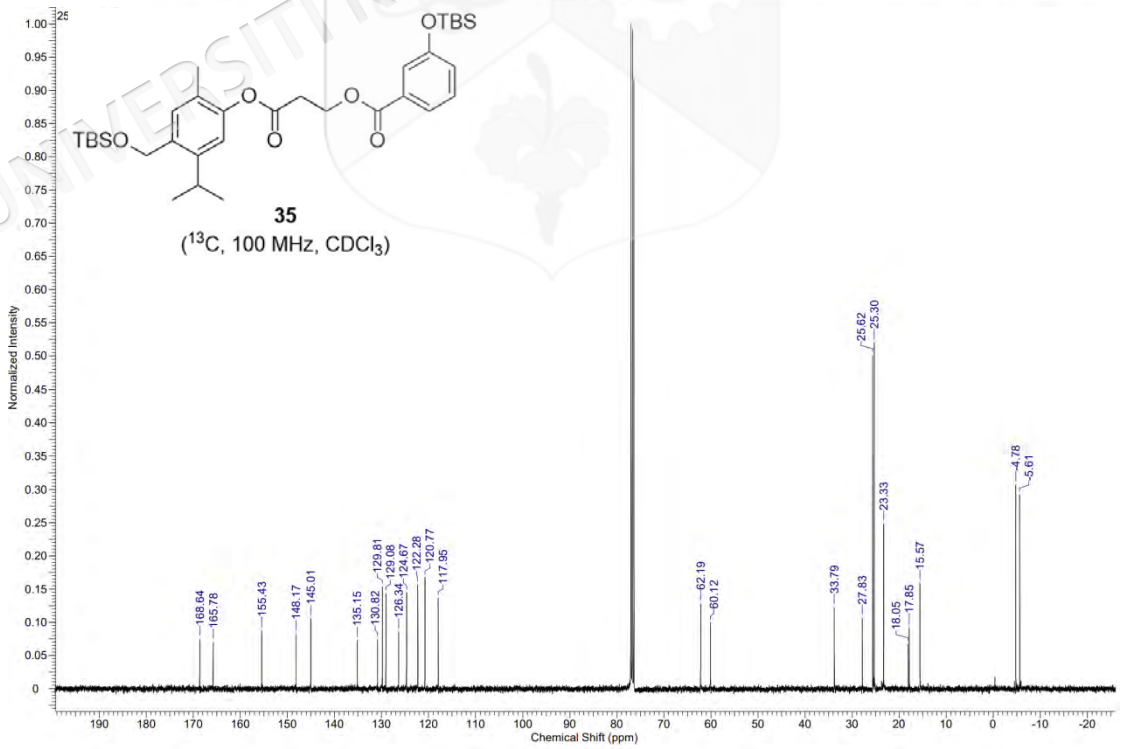

APPENDIX GG

^{1}H AND ^{13}C NMR SPECTRA OF 3-(4-(HYDROXYMETHYL)-5-ISOPROPYL-2-METHYLPHENOXY)-3-OXOPROPYL 3-HYDROXYBENZOATE (17)

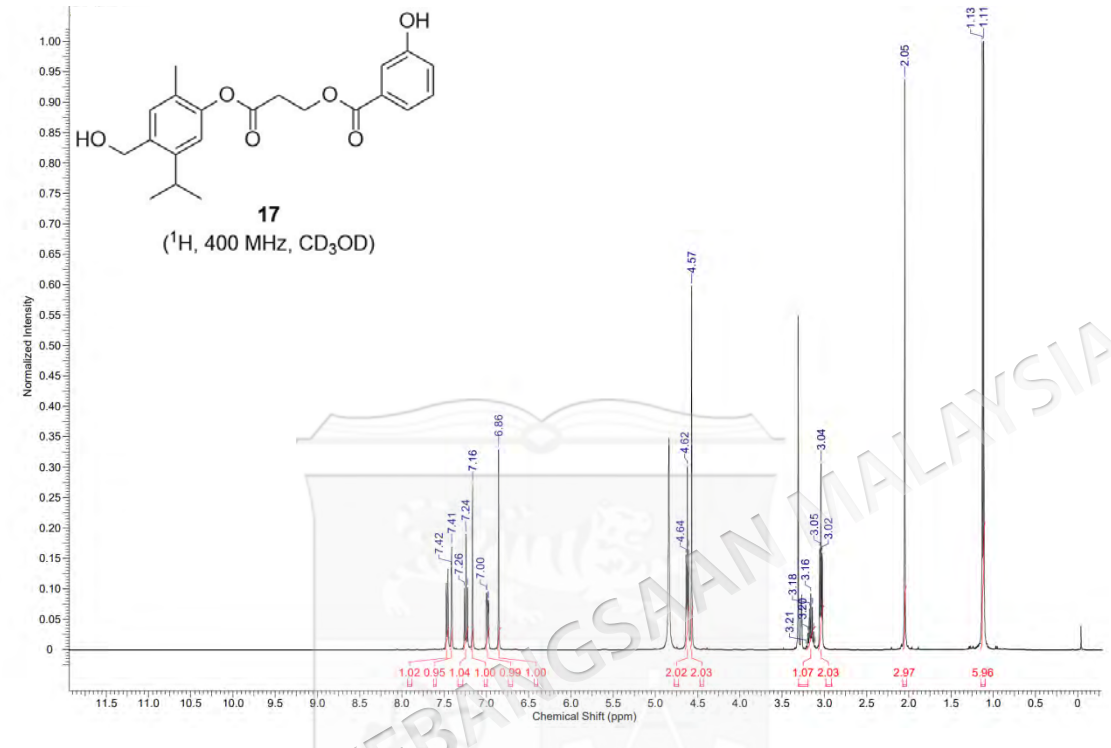

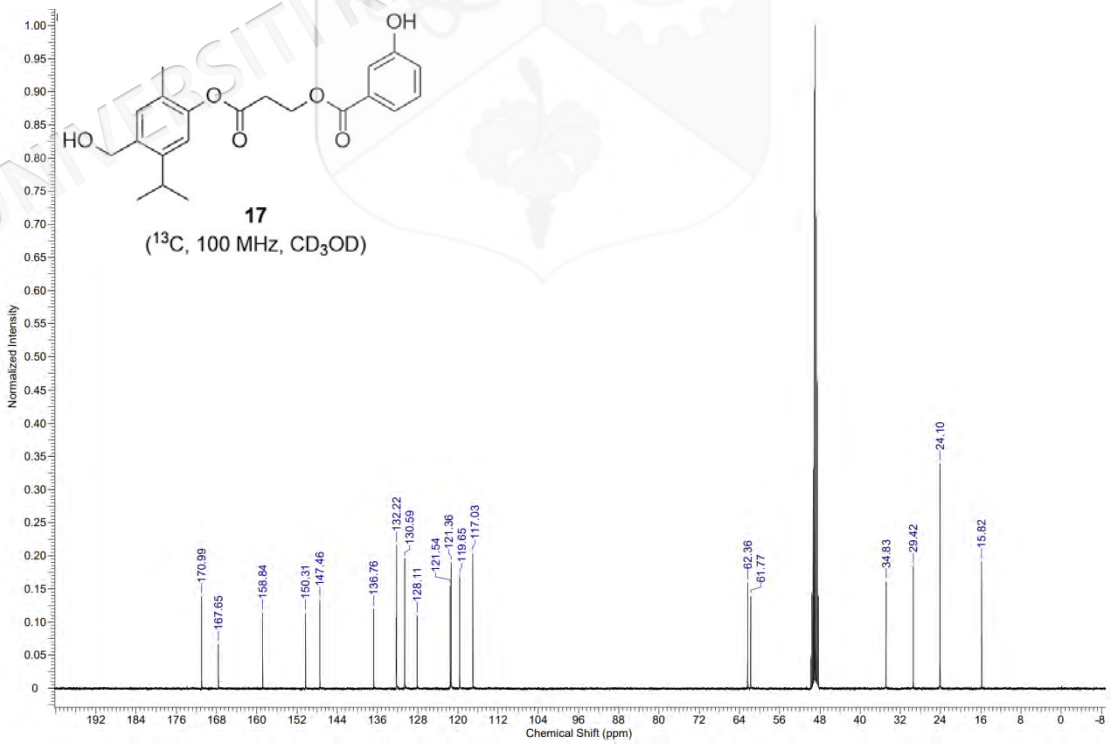

APPENDIX HH

^{1}H AND ^{13}C NMR SPECTRA OF 4-(((TERT-BUTYLDIMETHYLSILYL)OXY)METHYL)-5-ISOPROPYL-2-METHYLPHENYL 4-CHLOROBUTANOATE (31b)

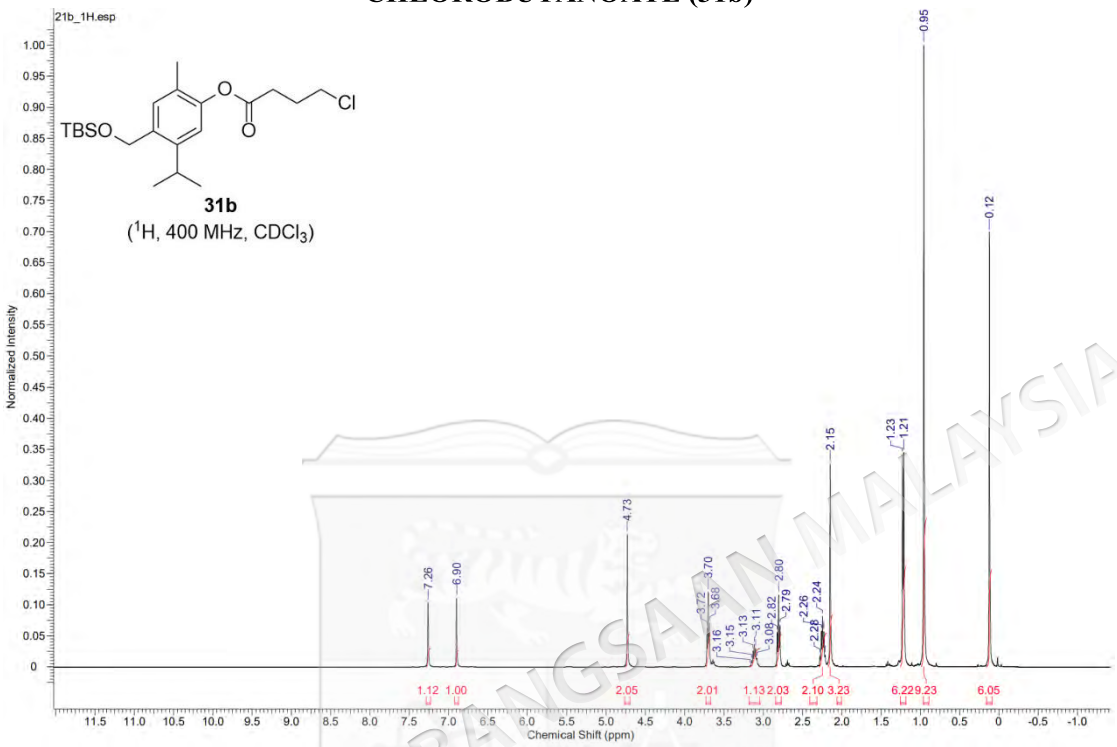

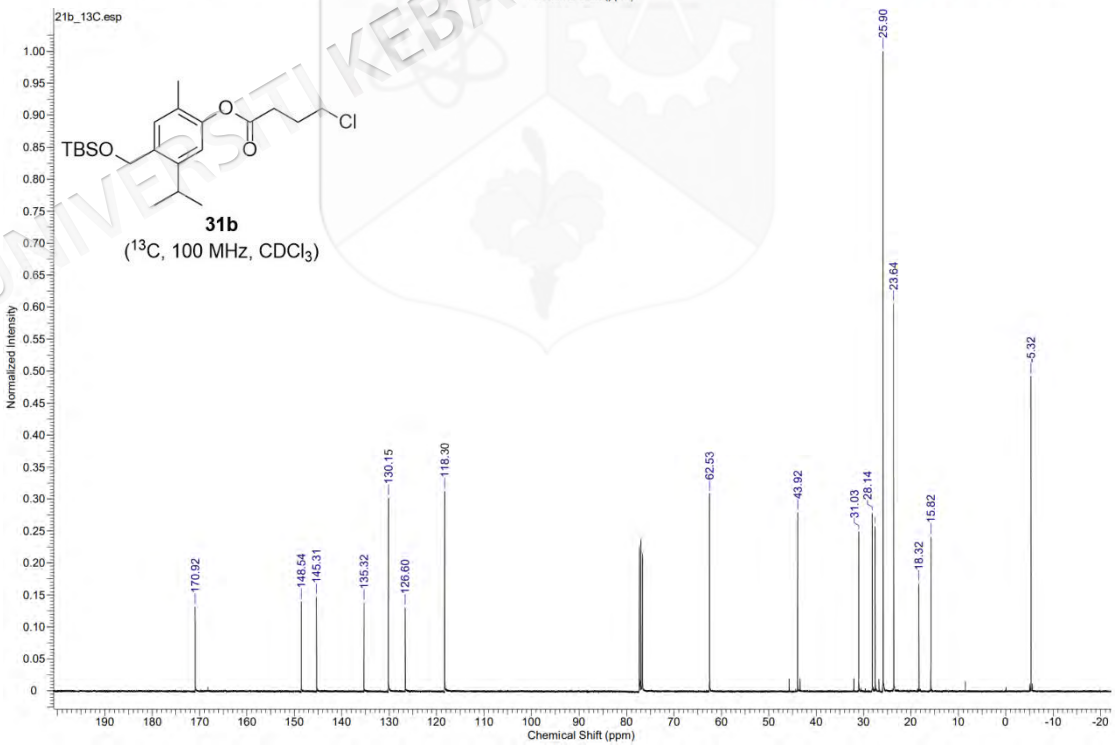

APPENDIX II

^{1}H AND ^{13}C NMR SPECTRA OF 4-(4-(((TERT-BUTYLDIMETHYLSILYL)OXY)METHYL)-5-ISOPROPYL-2-METHYLPHENOXY)-4-OXOBUTYL 3-HYDROXYBENZOATE) (32b)

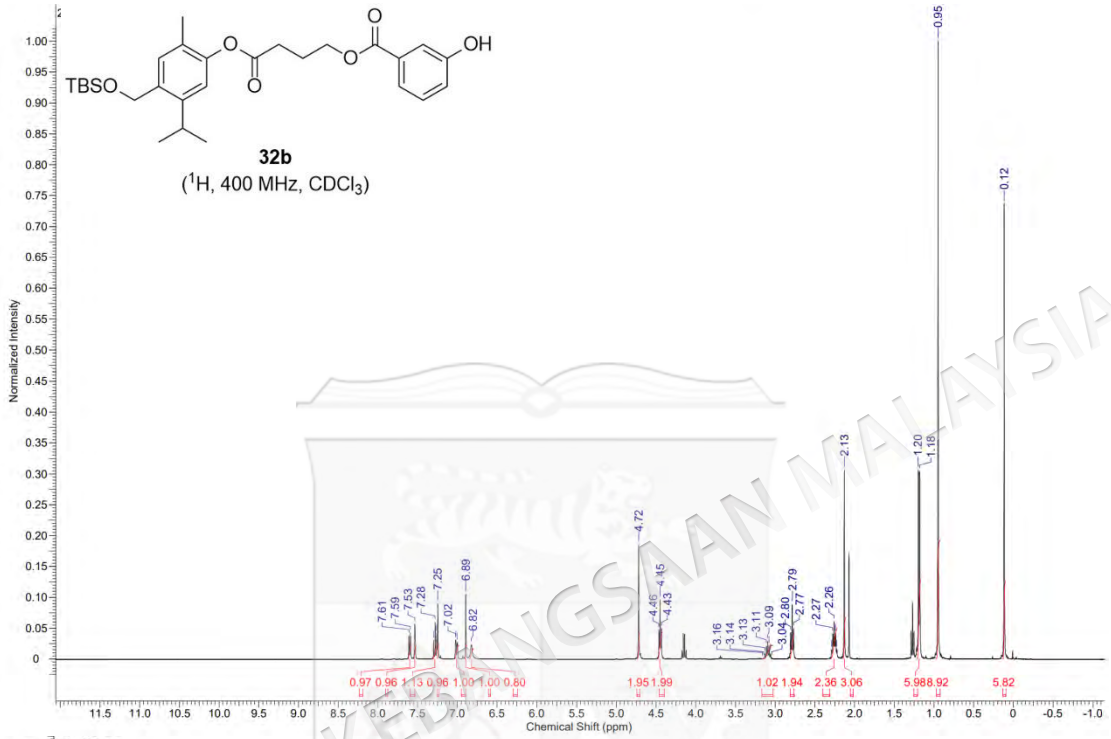

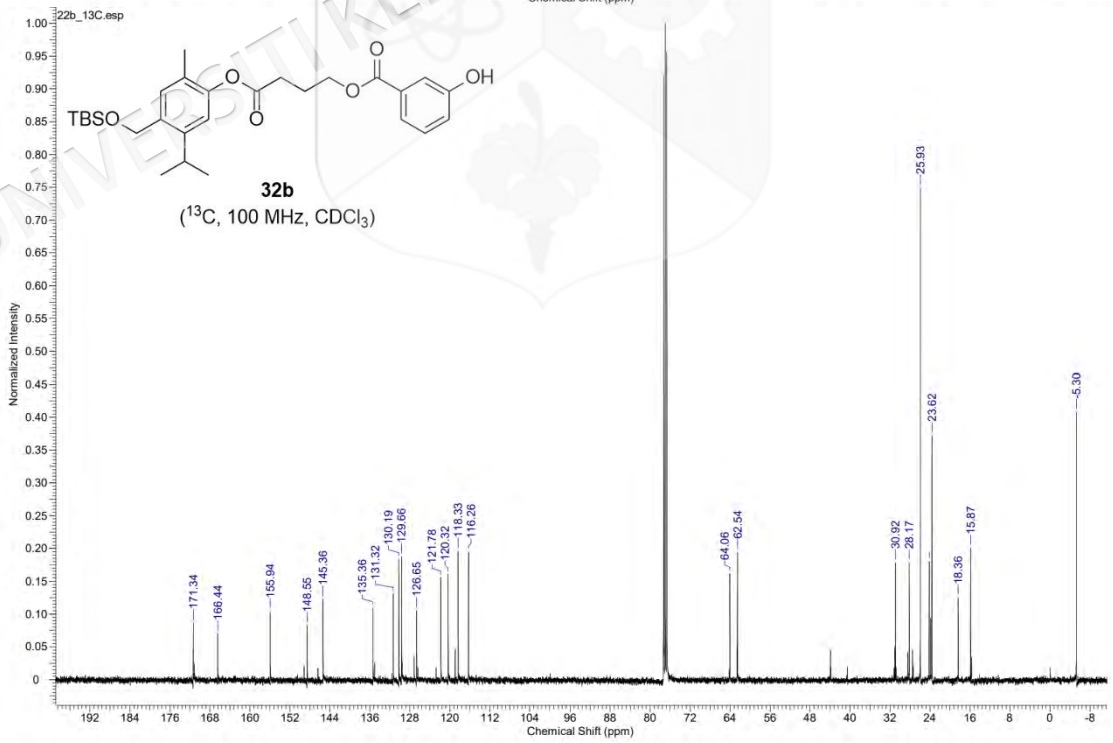

APPENDIX JJ

^{1}H AND ^{13}C NMR SPECTRA OF 4-(4-(HYDROXYMETHYL)-5-ISOPROPYL-2-METHYLPHENOXY)-4-OXOBUTYL 3-HYDROXYBENZOATE (18)

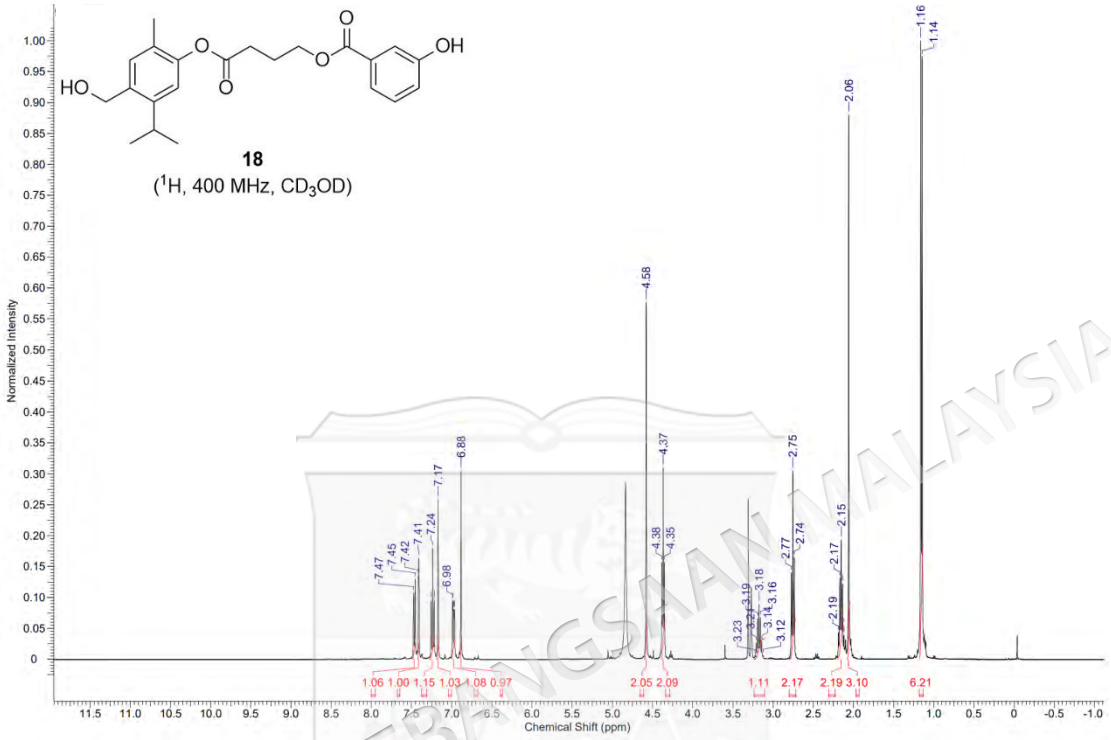

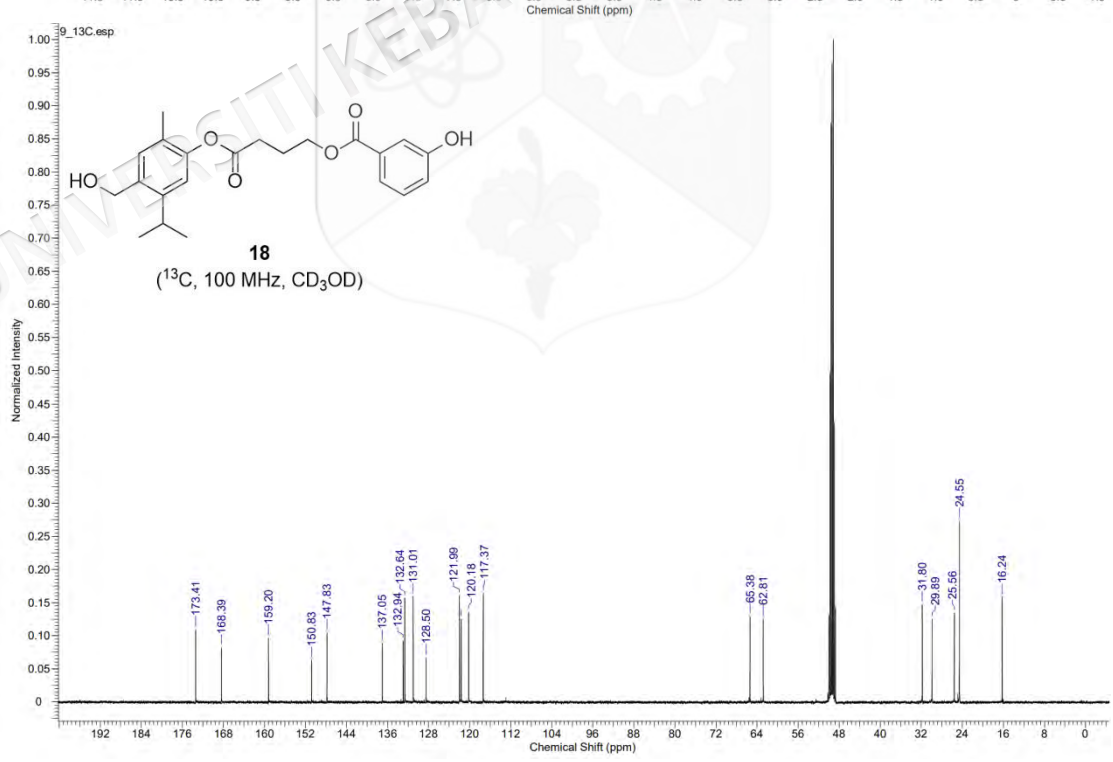

APPENDIX KK

^{1}H AND ^{13}C NMR SPECTRA OF ((4-(2-BROMOETHOXY)-2-ISOPROPYL-5-METHYLBENZYL)OXY)(TERT-BUTYL)DIMETHYLSILANE (36a)

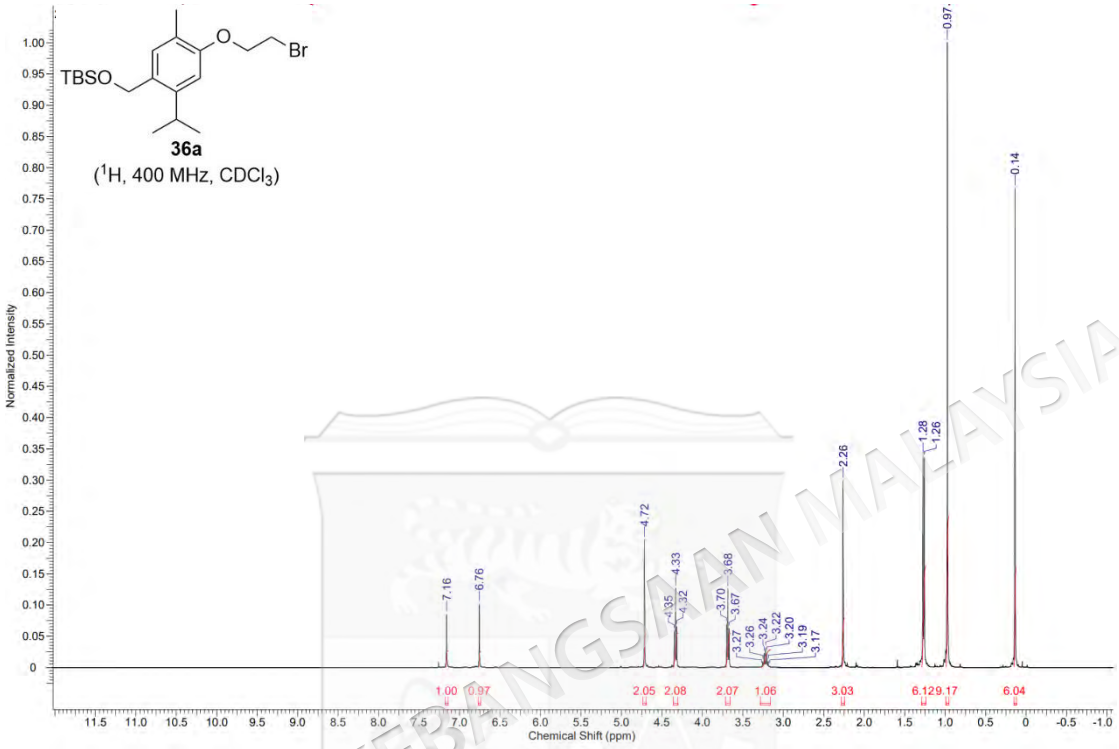

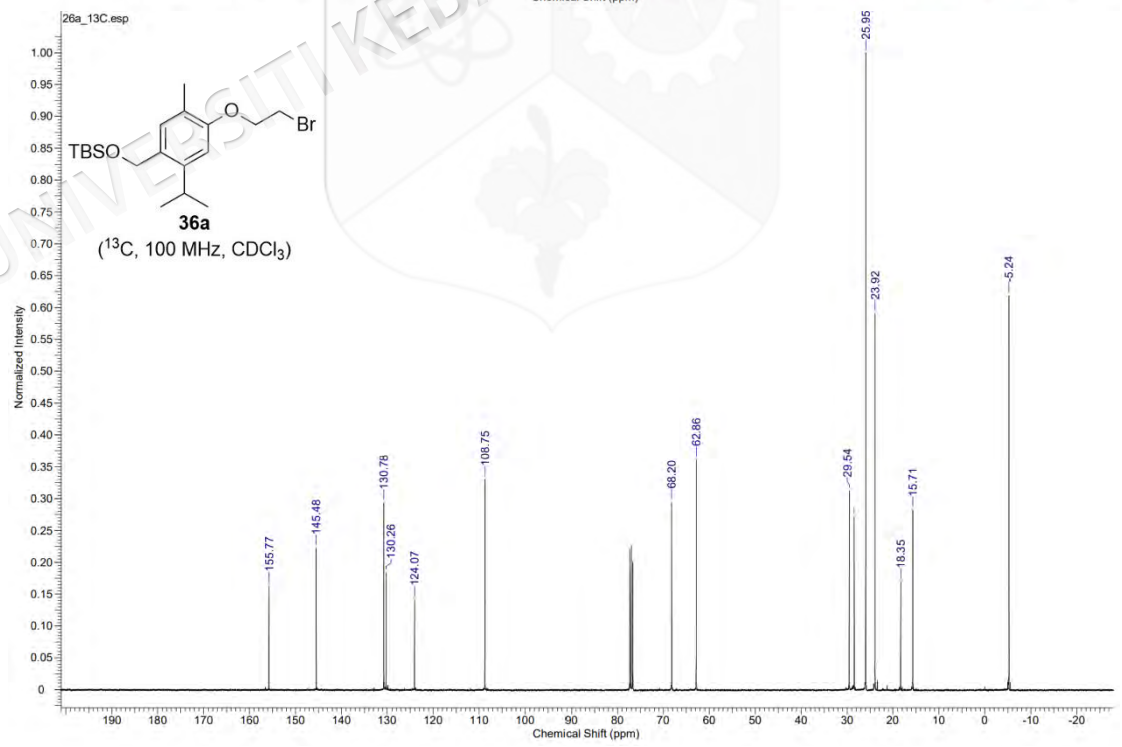

APPENDIX LL

^{1}H AND ^{13}C NMR SPECTRA OF 2-(4-(((TERT-BUTYLDIMETHYLSILYL) OXY)METHYL)-5-ISOPROPYL-2-METHYLPHENOXY)ETHYL 3-HYDROXYBENZOATE (37a)

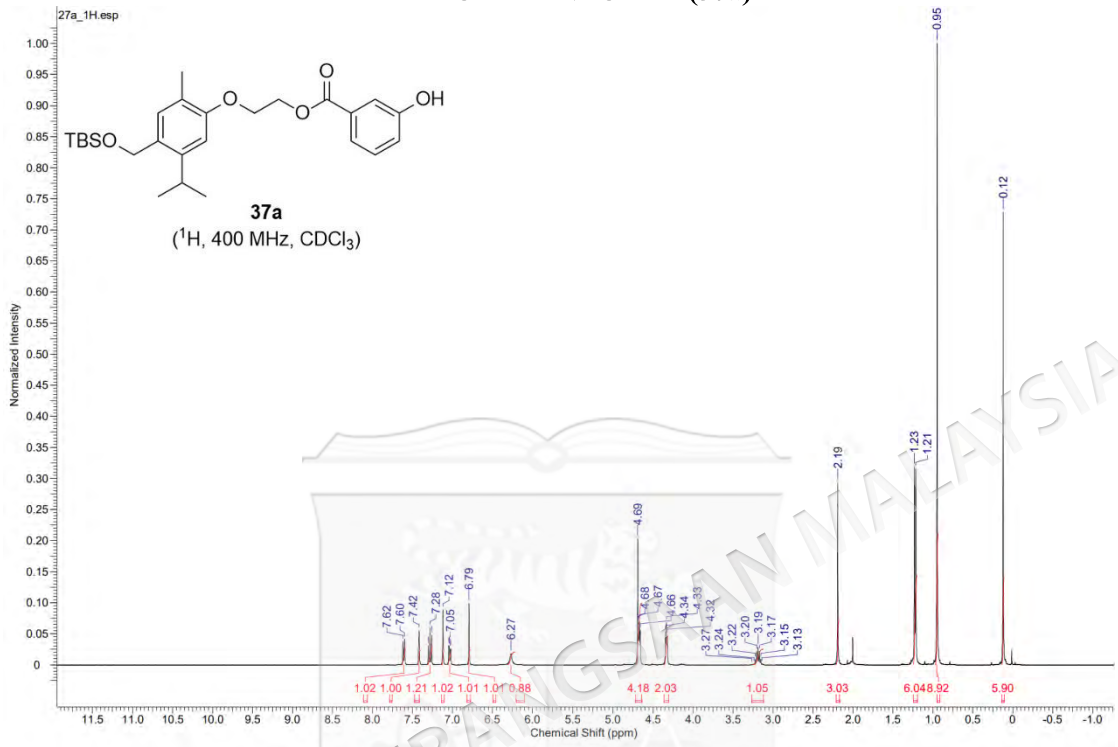

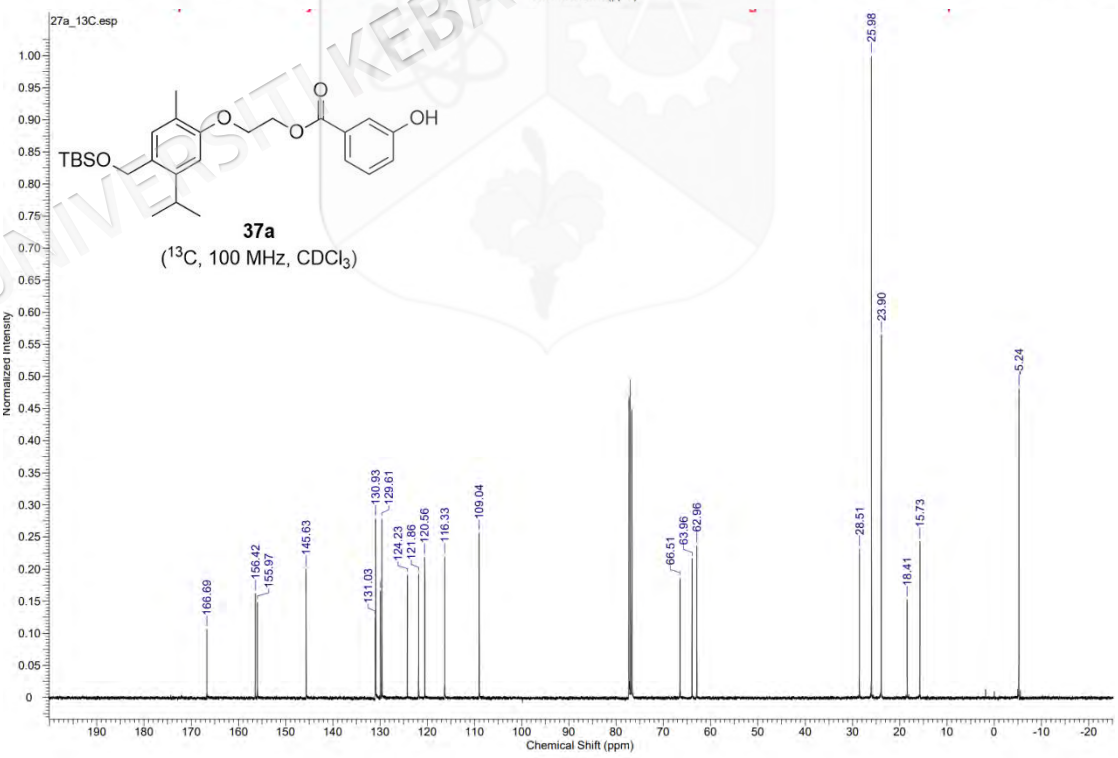

APPENDIX MM

^{1}H AND ^{13}C NMR SPECTRA OF 2-(4-(HYDROXYMETHYL)-5-ISOPROPYL-2-METHYLPHENOXY)ETHYL 3-HYDROXYBENZOATE (19)

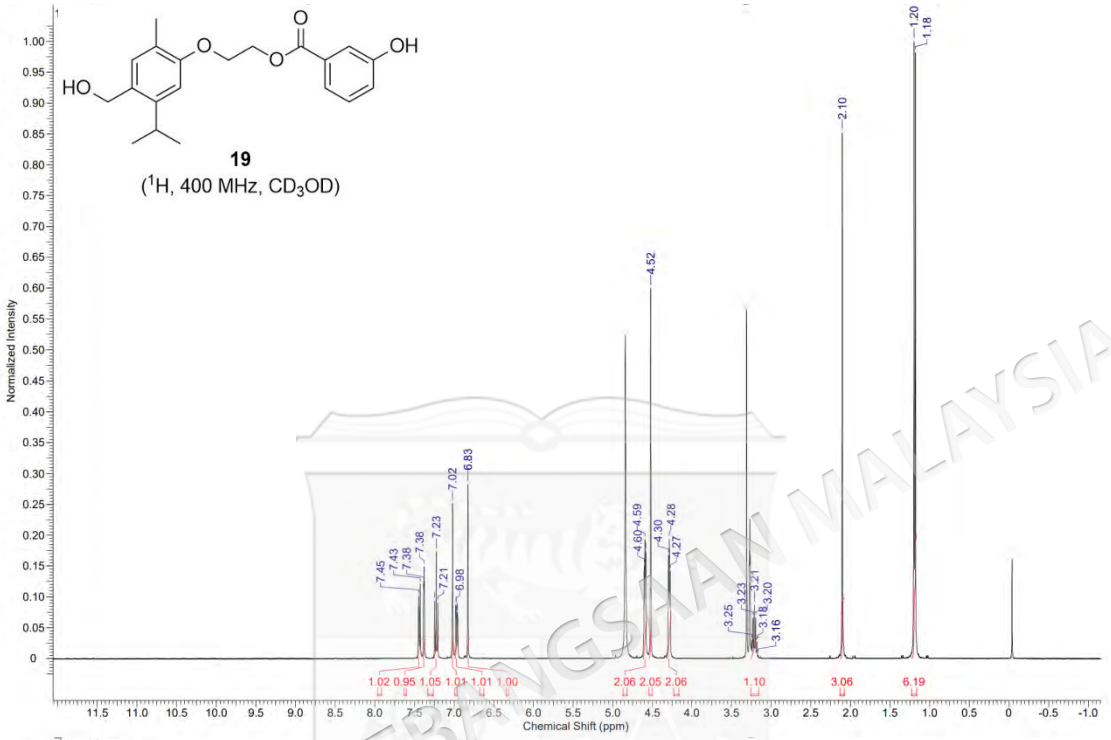

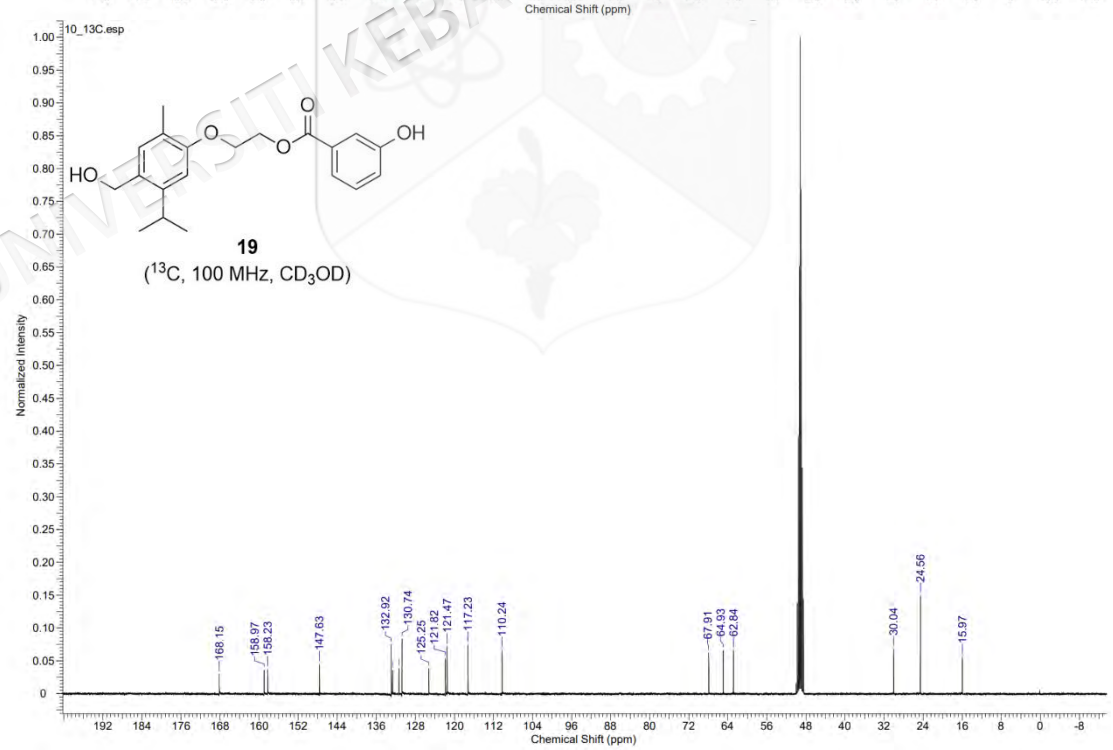

APPENDIX NN

^{1}H AND ^{13}C NMR SPECTRA OF ((4-(3-BROMOPROPOXY)-2-ISOPROPYL-5-METHYLBENZYL)OXY)(TERT-BUTYL)DIMETHYLSILANE (36b)

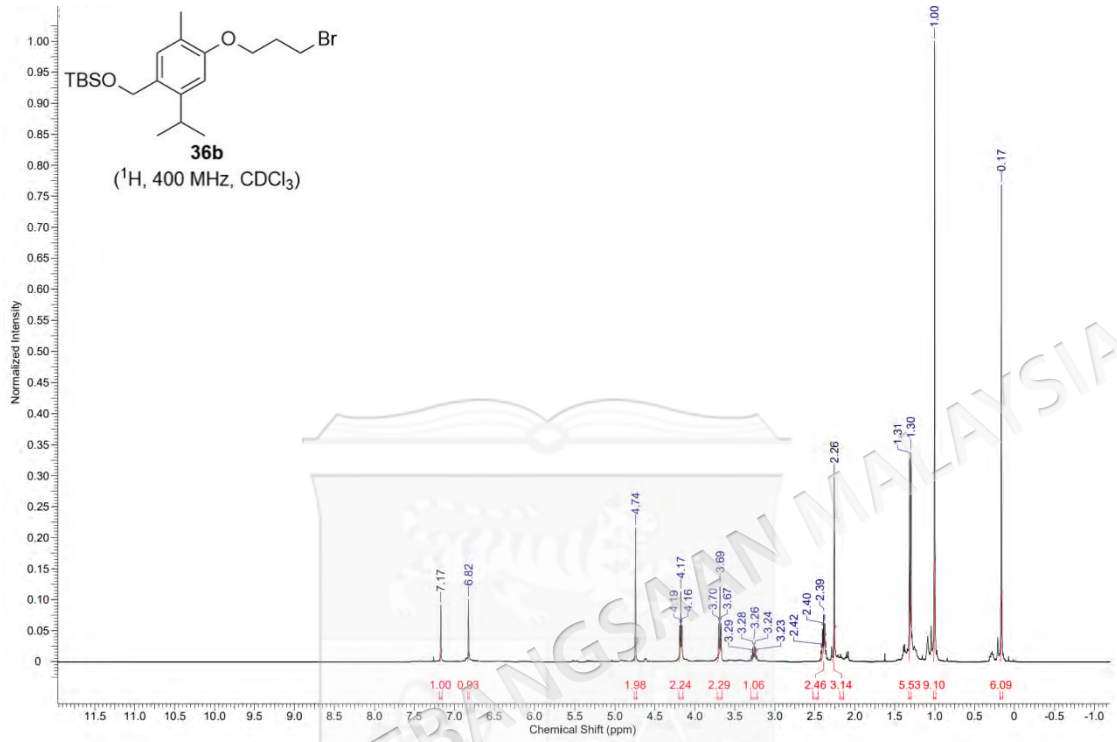

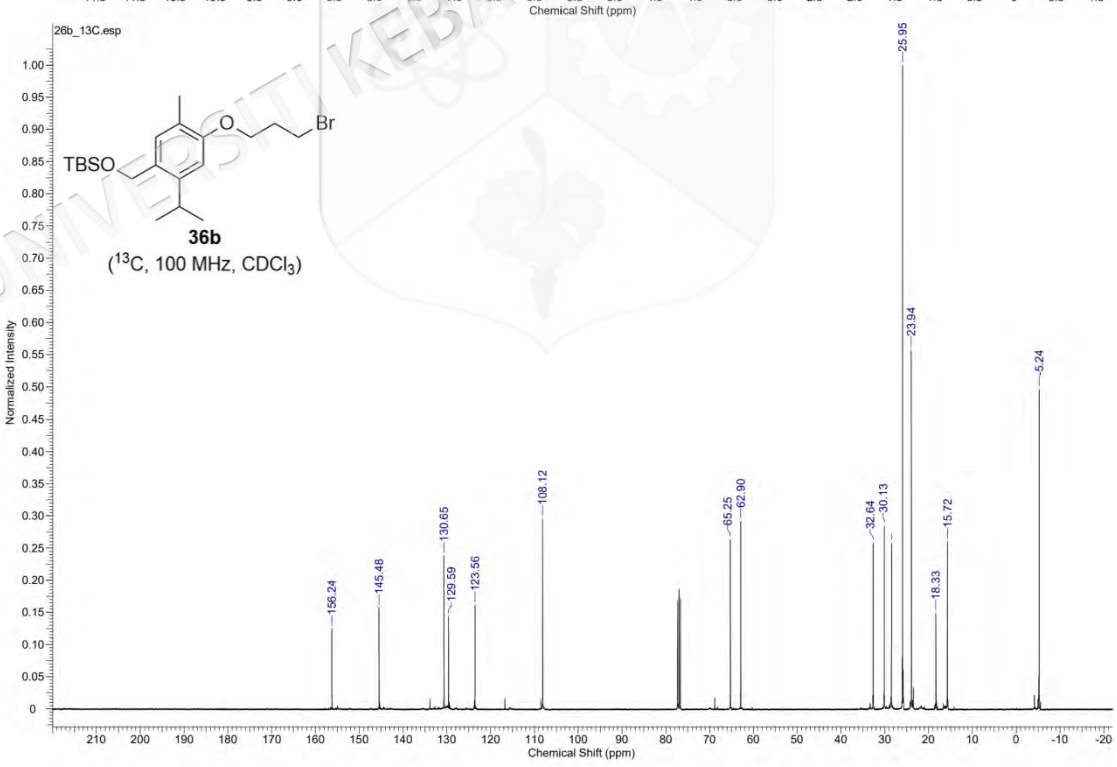

APPENDIX OO

^{1}H NMR AND ^{13}C NMR SPECTRA OF (3-(4-(((TERT-BUTYLDIMETHYLSILYL)OXY)METHYL)-5-ISOPROPYL-2-METHYLPHENOXY)PROPYL 3-HYDROXYBENZOATE) (37b)

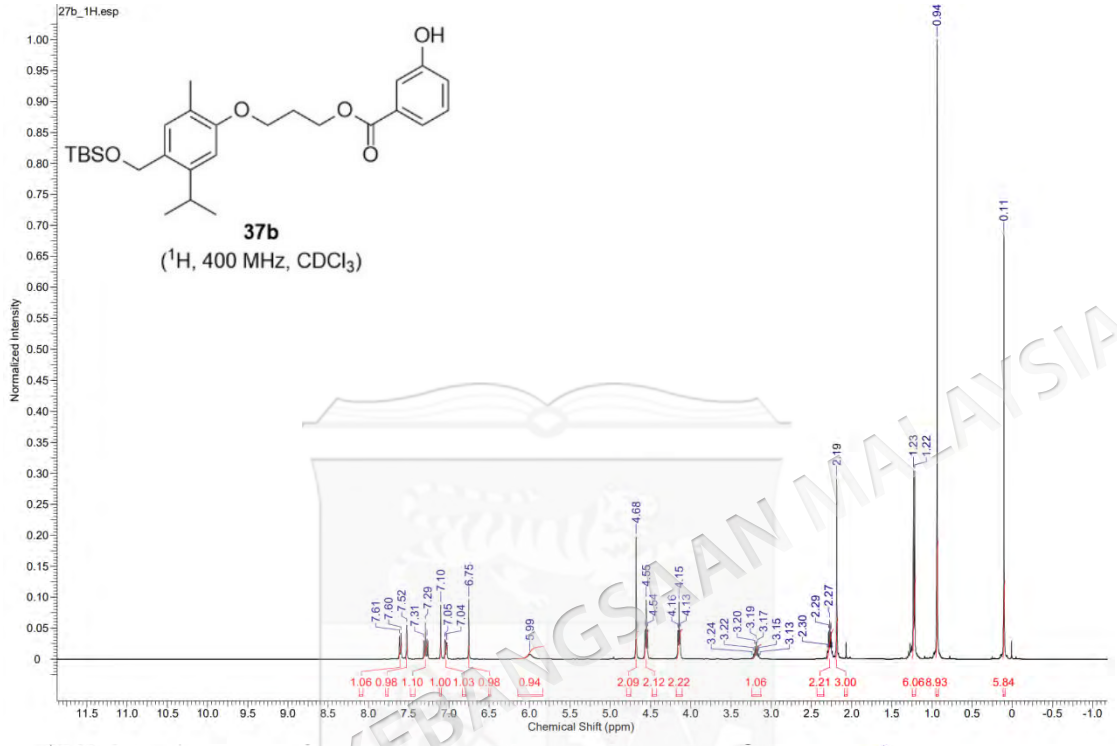

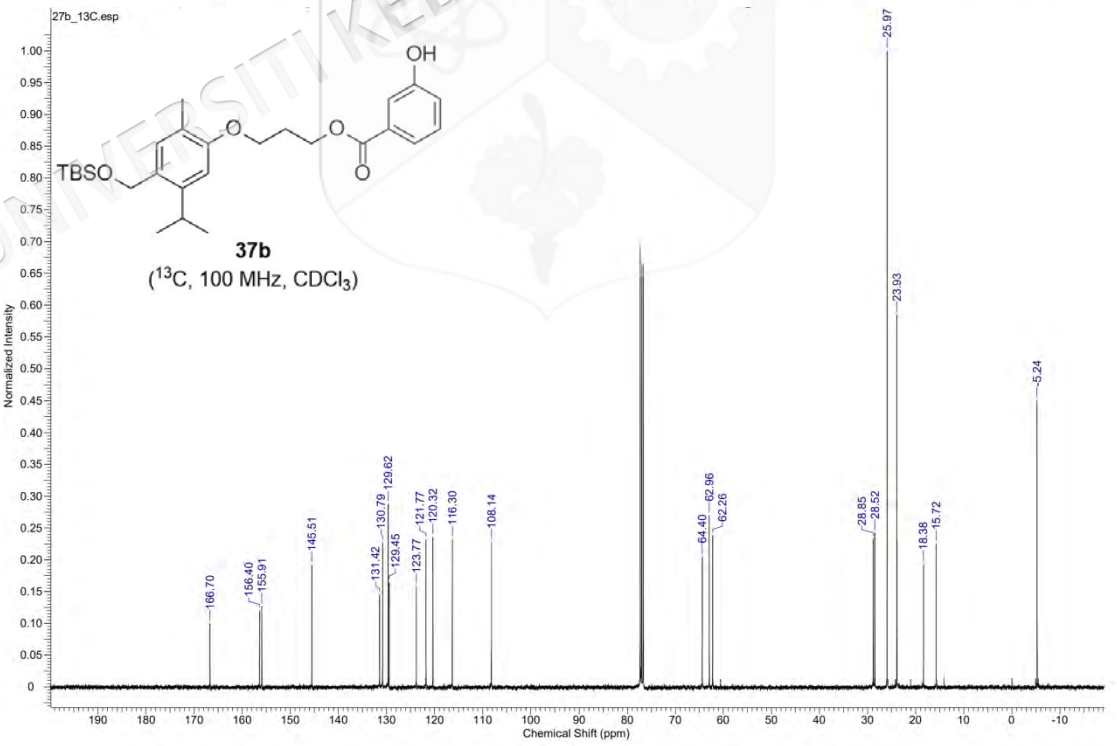

APPENDIX PP

^{1}H AND ^{13}C NMR SPECTRA OF 3-(4-(HYDROXYMETHYL)-5-ISOPROPYL-2-METHYLPHENOXY)PROPYL 3-HYDROXYBENZOATE (20)

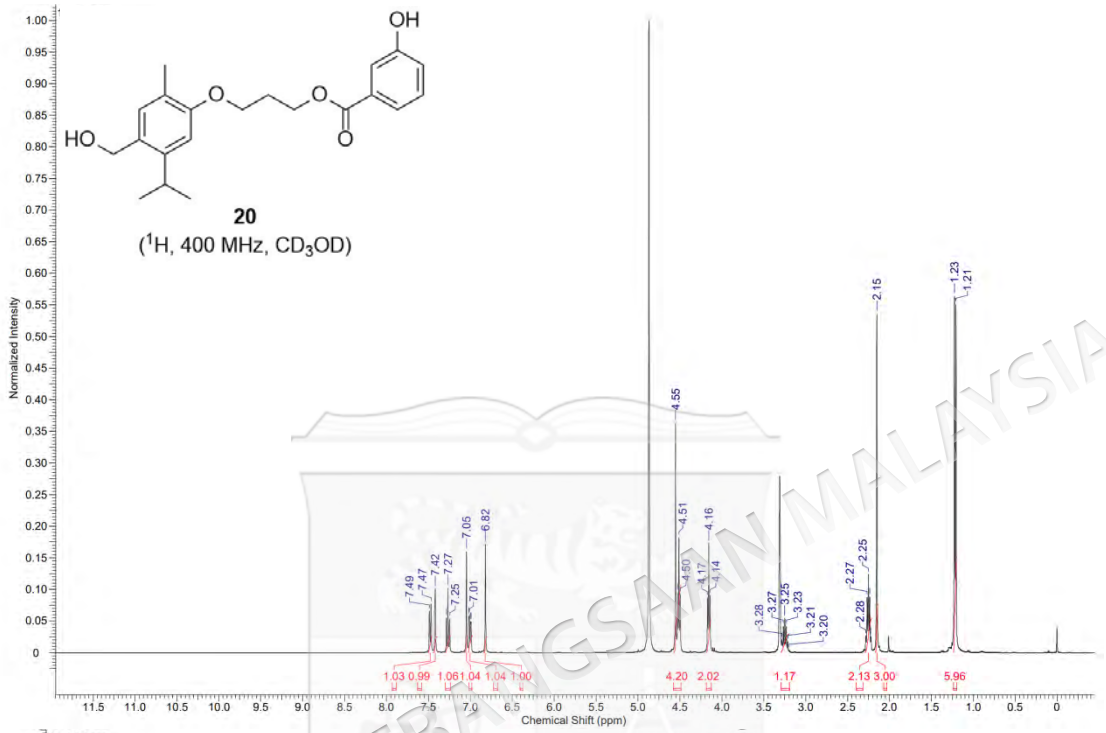

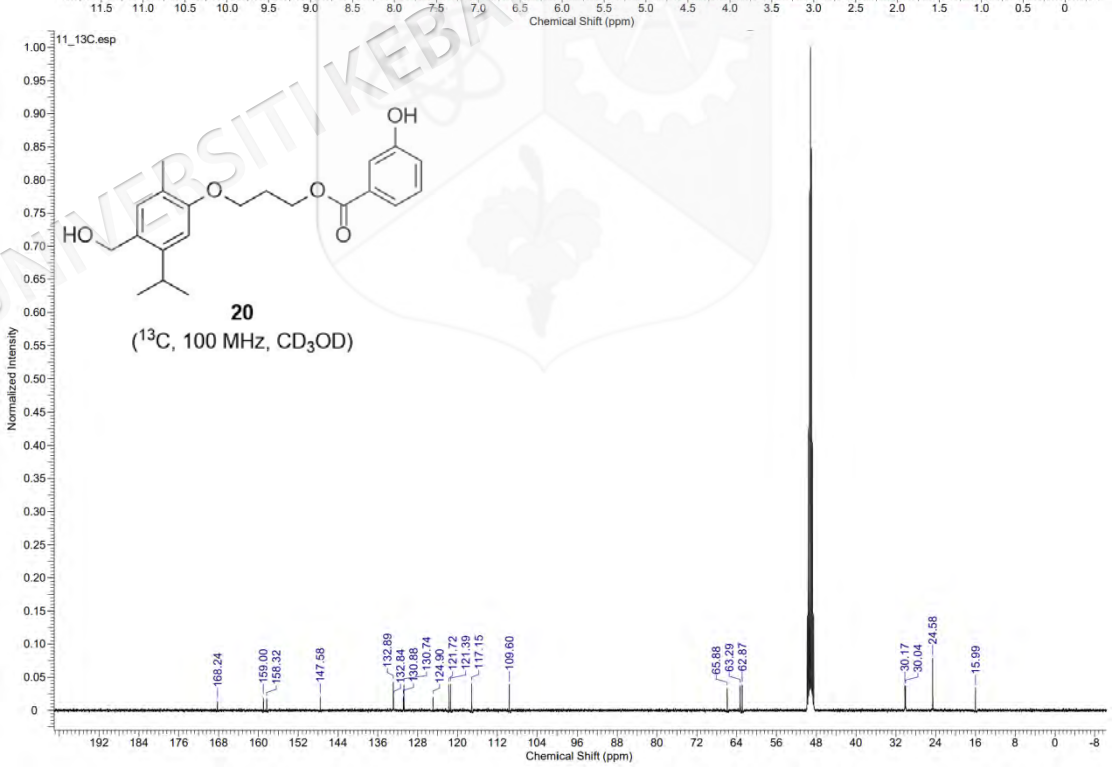

APPENDIX QQ

^{1}H AND ^{13}C NMR SPECTRA OF ((4-(4-BROMOBUTOXY)-2-ISOPROPYL-5-METHYLBENZYL)OXY)(TERT-BUTYL)DIMETHYLSILANE (36c)

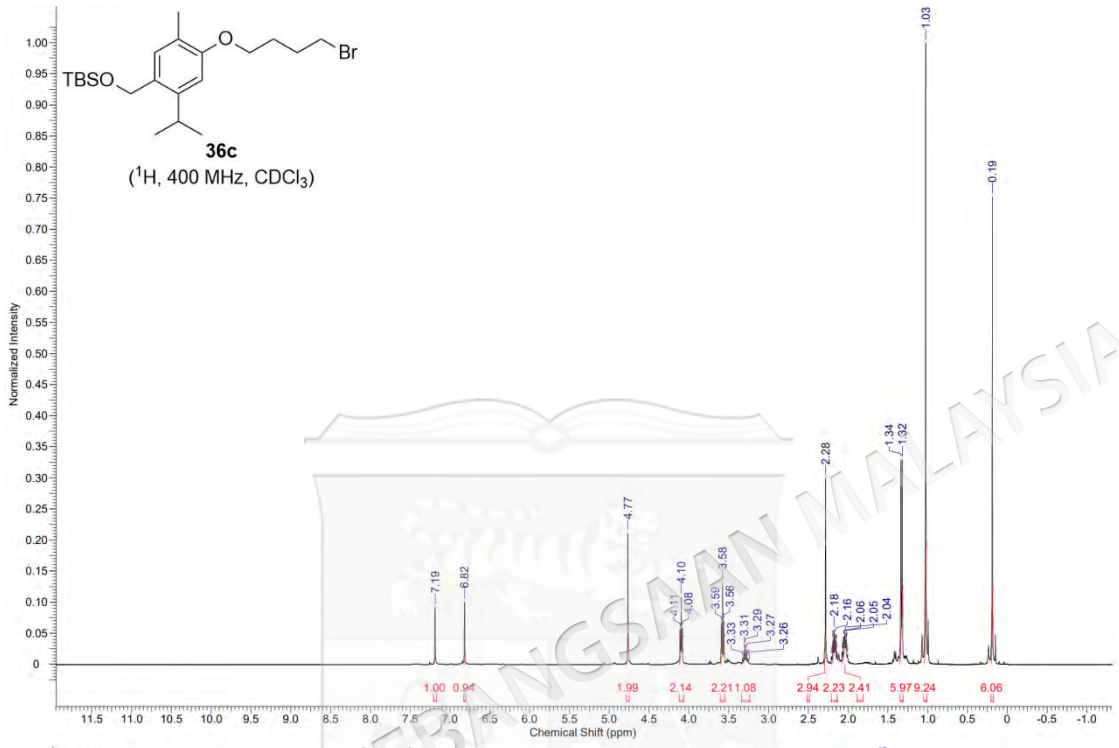

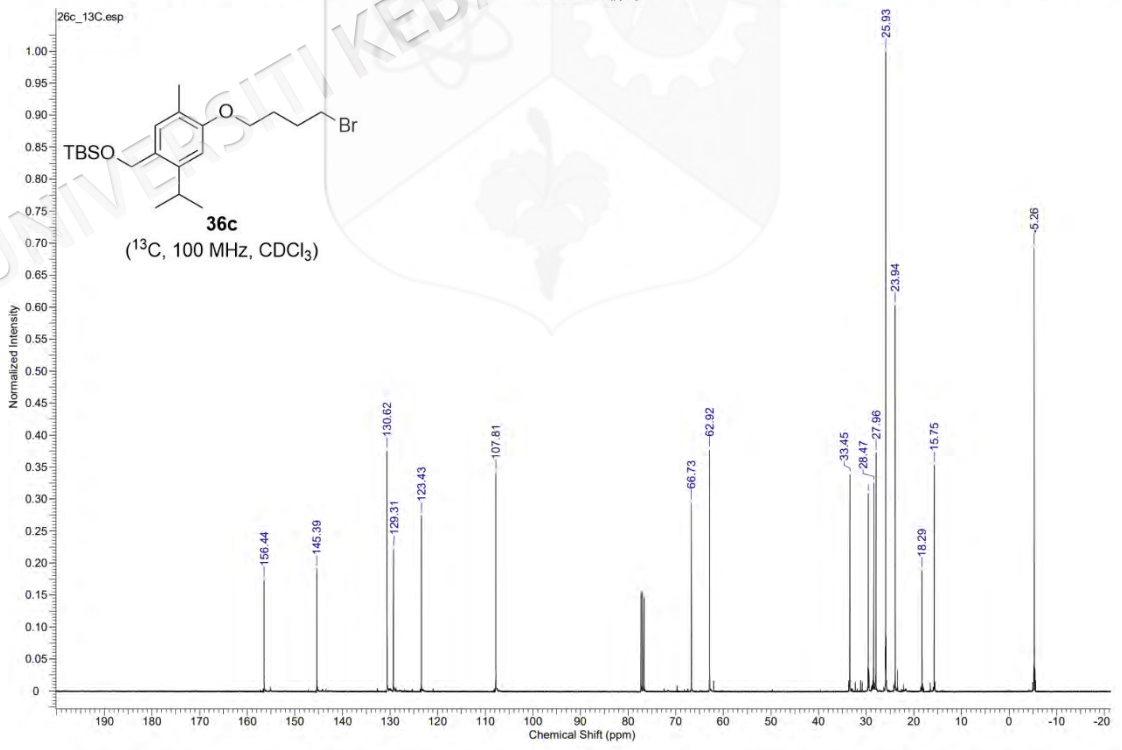

APPENDIX RR

^{1}H AND ^{13}C NMR SPECTRA OF 4-(4-(((TERT-BUTYLDIMETHYLSILYL)OXY)METHYL)-5-ISOPROPYL-2-METHYLPHENOXY)BUTYL 3-HYDROXYBENZOATE (37c)

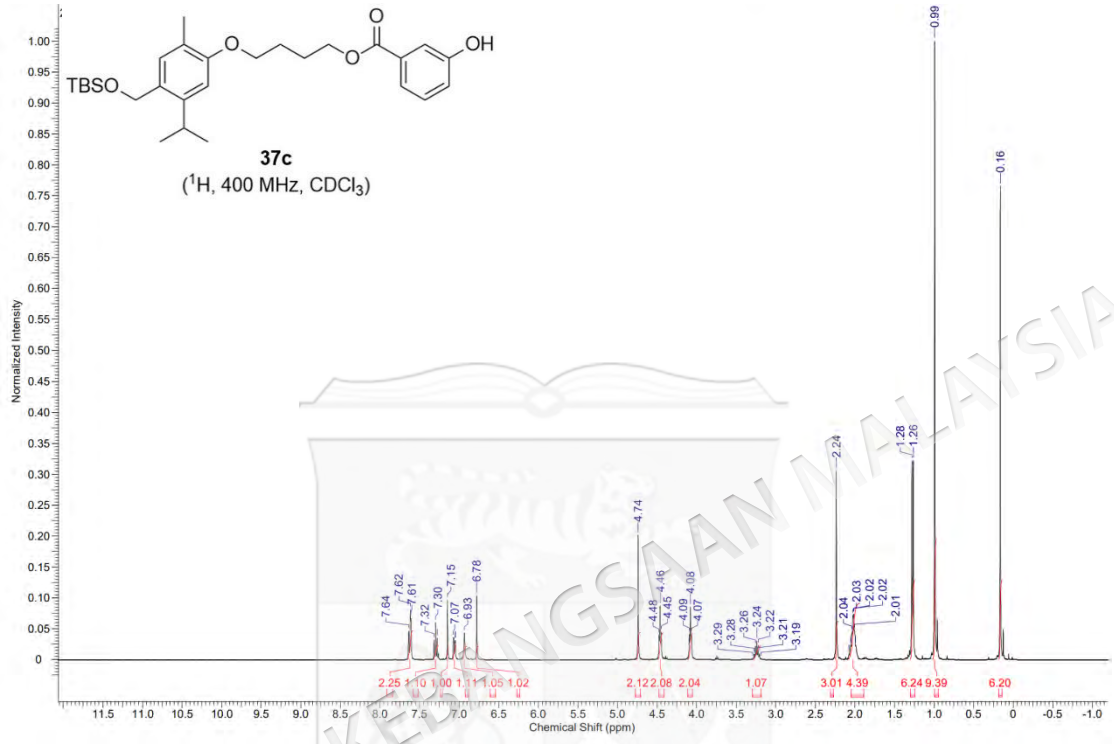

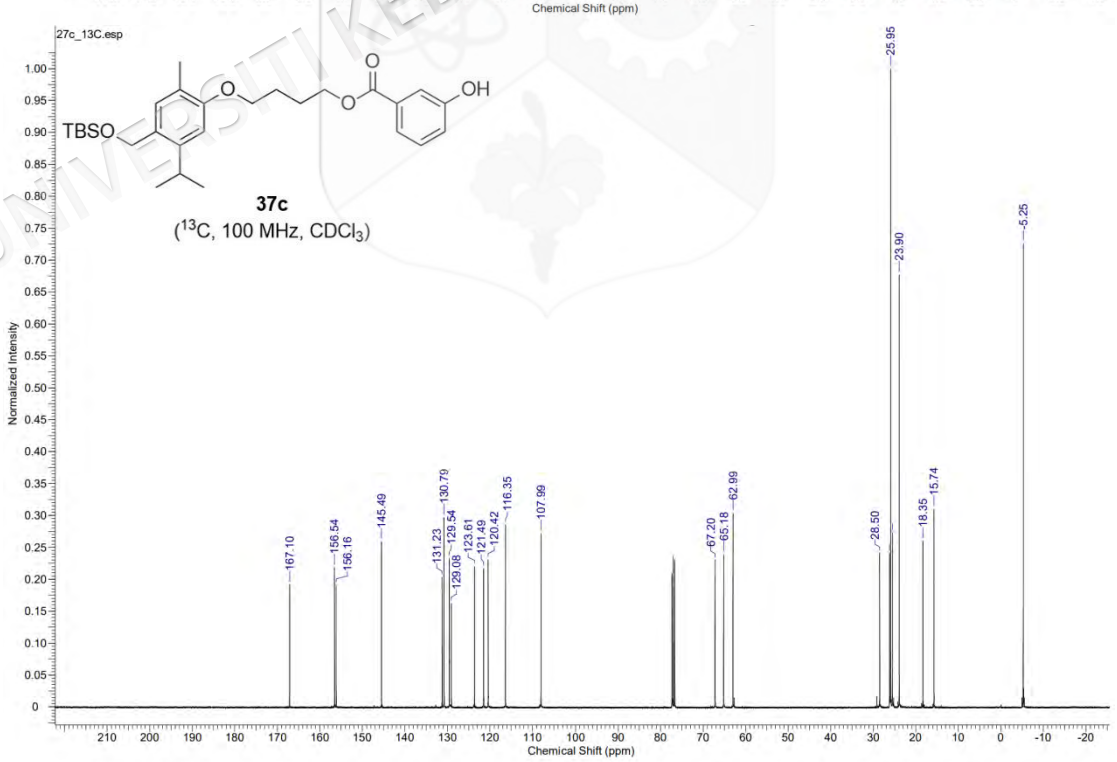

APPENDIX SS

^{1}H AND ^{13}C NMR SPECTRA OF 4-(4-(HYDROXYMETHYL)-5-ISOPROPYL-2-METHYLPHENOXY)BUTYL 3-HYDROXYBENZOATE (21)

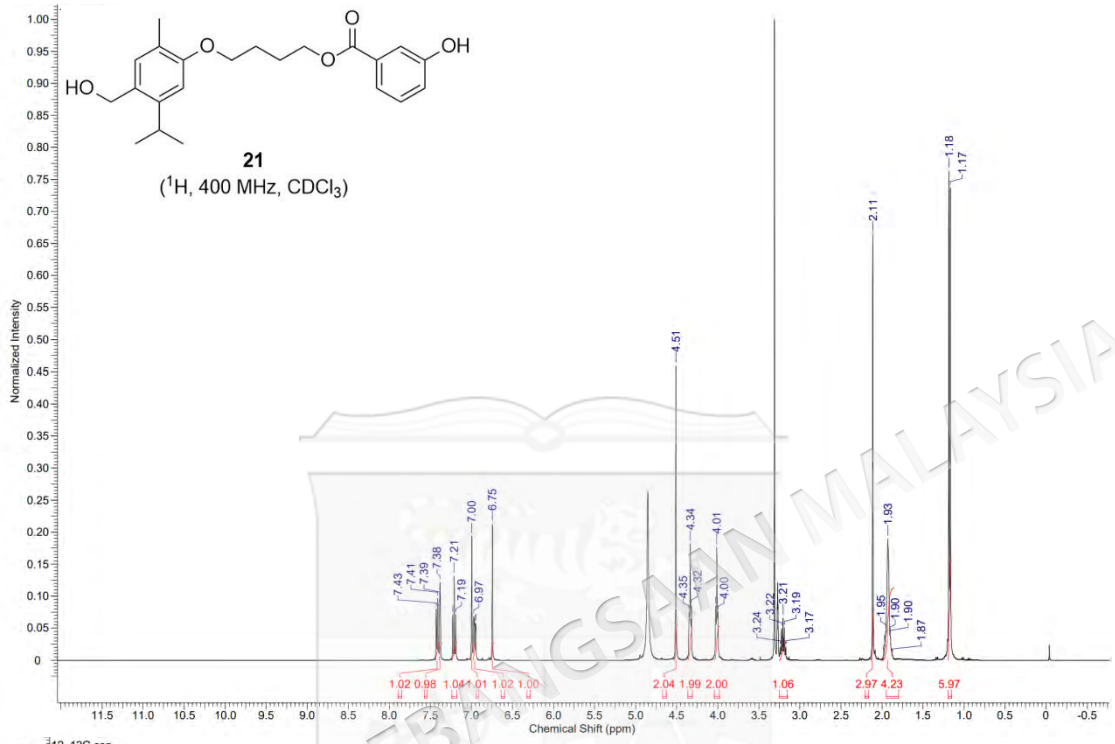

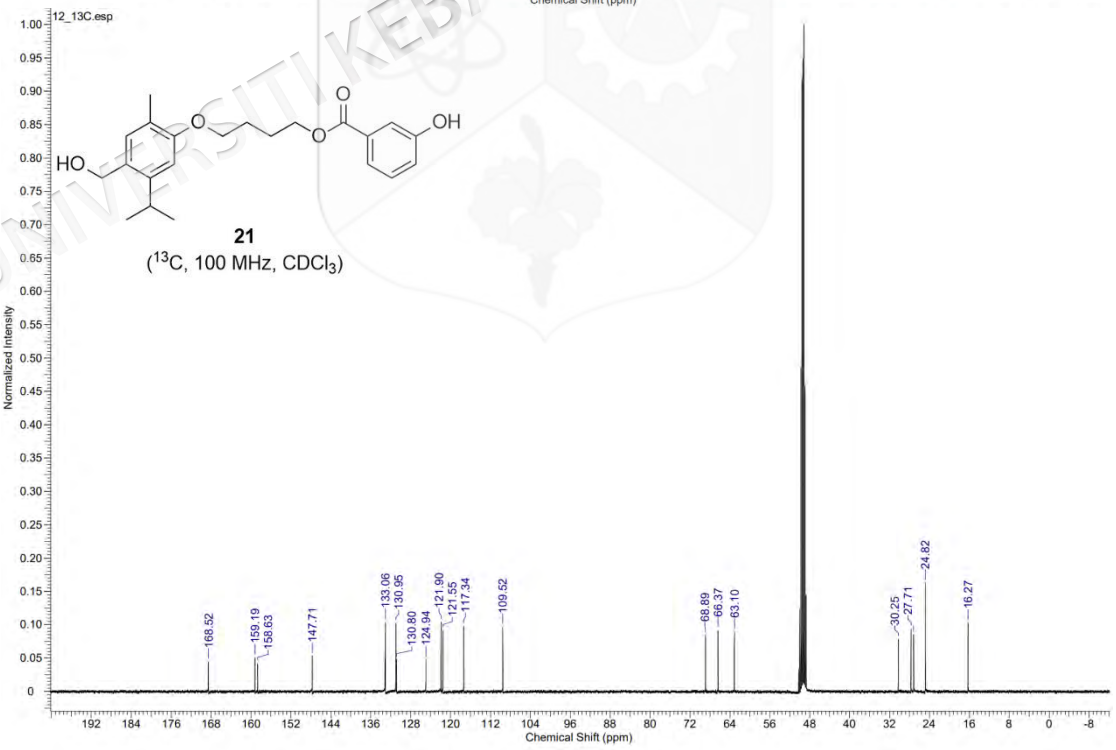

APPENDIX TT

LIST OF PUBLICATION AND CONFERENCES

Journal Publications:

1. **Retnosari, R.**, Ali, A.H., Zainalabidin, S., Ugusman, A., Oka, N.& Latip, J. 2024. The recent discovery of a promising pharmacological scaffold derived from carvacrol: a review.*Bioorg Med Chem Lett.* 109:129826. DOI: https://doi.org/10.1016/j.bmcl.2024.129826. (Published – Q2)
2. **Retnosari, R.**, Oh-hashi, K., Zainalabidin, S., Ugusman, A., Latip, J. & Oka, N. 2024. Carvacrol-conjugated 3-Hydroxybenzoic Acids: design, synthesis, cardioprotective potential against doxorubicin-induced cardiotoxicity, and ADMET study. *Bioorg Med Chem Lett.* 113:129973. DOI: https://doi.org/10.1016/j.bmcl.2024.129973. (Published – Q2)
3. **Retnosari, R.**, Ghani, M.A.A., Alkharji, M.M., Wan Nawi, W.N.I.S., Rushdan, A.S.A., Mahadi, M.K., Ugusman, A., Oka, N., Zainalabidin, S. & Latip, J. The protective effects of carvacrol against doxorubicin-induced cardiotoxicity in vitro and in vivo. *Cardiovasc Toxicol*. (in press). DOI: https://doi.org/10.1007/s12012-024-09940-8. (Published – Q2)
4. **Retnosari, R.**, Oka, N., Ugusman, A., Zainalabidin, S. & Latip, J. Carvacrol-phenolic acid hybrid (CPAH), a novel promising cardioprotector against doxorubicin-induced cardiotoxicity *in vitro* and *in vivo*. (In writing)

Conferences:

1. 3rd Science and Mathematics International Conference (SMIC) 2022 (7th September 2022, Online), Oral Presentation.